DISCLAIMER

This report was prepared as an account of work sponsored by an agency of the United States Government. Neither the United States Government nor any agency thereof, nor any of their employees, makes any warranty, express or implied, or assumes any legal liability or responsibility for the accuracy, completeness, or usefulness of any information, apparatus, product, or process disclosed, or represents that its use would not infringe privately owned rights. Reference herein to any specific commercial product, process, or service by trade name, trademark, manufacturer, or otherwise does not necessarily constitute or imply its endorsement, recommendation, or favoring by the United States Government or any agency thereof. The views and opinions of authors expressed herein do not necessarily state or reflect those of the United States Government or any agency thereof. Reference herein to any social initiative (including but not limited to Diversity, Equity, and Inclusion (DEI); Community Benefits Plans (CBP); Justice 40; etc.) is made by the Author independent of any current requirement by the United States Government and does not constitute or imply endorsement, recommendation, or support by the United States Government or any agency thereof.

IACMI/R002-2021/7.08

Next Generation Co-Molded One-Piece Automotive Parts

Author: Dr. Hendrik Mainka
Date: May 5, 2021

Final Technical Report
PA16-0349-7.8-01

Approved for Public Release.
Distribution is Unlimited.

The Institute for iacmi Advanced Composites Manufacturing Innovation
THE COMPOSITES INSTITUTE

U.S. DEPARTMENT OF ENERGY

The information, data, or work presented herein was funded in part by the Office of Energy Efficiency and Renewable Energy (EERE), U.S. Department of Energy, under Award DE-EE0006926

Project acknowledgement by authors (if any).

Next Generation Co-Molded One-Piece Automotive Parts

Principal Investigator: **Dr. Hendrik Mainka**

Organization: Volkswagen Group of America, Inc.

Address:

2704 Cherokee Farm Way
Knoxville, TN 37920

Phone: 1 (423) 596-9204

Email: hendrik.mainka@vw.com

Co-authors: Tom Skelskey, Ben Denos, Marton Kardos, Shane Skop, Ranjit Pacha, Edward Zenk

Date Published: (March 5, 2021)

Prepared by:
Institute for Advanced Composites Manufacturing Innovation
Knoxville, TN 37932
Managed by Collaborative Composite Solutions, Inc.
For the
U.S. DEPARTMENT OF ENERGY
Under contract DE- EE0006926

Project Period:
(Feb 2019 – Mar 2021)

Approved for Public Release

TABLE OF CONTENTS

List of Acronyms

List of Figures

List of Tables

1. EXECUTIVE SUMMARY

The purpose of this project was to determine the feasibility of co-molding Class A Sheet Molding Compound (SMC), structural SMC, and continuous fiber prepreg materials to produce a single piece co-molded automotive part, such as a hood. The combination of the three molding materials and the incorporation of selective design features (ribs, flanges, corrugations) was expected to eliminate the need for inner reinforcement panels, significantly reducing tooling costs and simplifying the manufacturing process. A multi-material solution would also result in significant weight savings.

The scope of this project included the material characterization of the three materials, development of cure and flow simulation models, and validation of the models against parts molded with different combinations of the materials on an 11"x11" plaque tool with rib features. The intent of this project was to apply the learnings obtained from co-molding a part with simplified geometry to a Phase 2 project that would produce a single piece hood, co-molded with the same materials.

Resins from INEOS Composites were provided to IDI to produce SMC and continuous fiber prepregs. Purdue University and INEOS Composites characterized the rheological and curing behavior of the different materials as well as the mechanical properties of the co-molded parts. This data was used by Purdue University to create simulation models. Models were created to predict both flow patterns and predict mechanical properties of different laminate constructions in and around the ribs. Michigan State University - Corktown validated Purdue's models by co-molding the three materials in different combinations on a tool containing rib features provided by Century Tool. The co-molded parts were evaluated against the simulation models by Purdue, Corktown and INEOS.

The project team demonstrated the following:

- The ability to obtain a cohesive co-molded structure made up of Class A SMC, Structural SMC, and continuous fiber prepreg.
- The ability to obtain a co-molded part with a Class A surface
- Modeling of flow and fiber orientation
- Modeling to predict mechanical properties of multi-material co-molded structures

The predicted flow behavior and fiber orientation from simulations were then compared with the molded samples. Exact local orientation state was difficult to compare between microscopy and flow simulation, but captured general trends. Multi-material flow behavior was generally modeled well with SMC materials, but the introduction of woven material sheets requires further model development. Purdue compared the predicted versus actual mechanical properties, and INEOS Composites evaluated the surface appearance of unpainted and painted co-molded parts. The models developed by Purdue demonstrated that the mechanical properties can be predicted for parts with varying material configurations. The resulting models can be applied to future co-molded part design, tooling design, and molding conditions.

2. INTRODUCTION

Depending on geometrical complexity and production volumes, sheet molding compounds can present a cost-efficient alternative to metals in many vehicle applications. This was proven with a sheet molding compound liftgate developed in a previous Institute for Advanced Composites Manufacturing (IACMI)

project, Project 3.7. (Mainka, 2020) The same team that tackled the complexities of Project 3.7 worked to solve the design, manufacturing and modeling issues in the present project. This project addressed a higher level of technological complexity by combining multiple material classes – such as multiple flowable molding compounds and local fiber reinforcement – in a single component. This required a thorough understanding of the manufacturing process, including the in-mold flow during the compression molding of a material mix. The experimental investigation was used to validate and fine-tune the computational models developed. It is important to note, that state-of-the-art simulation software are not capable of working with multiple molding compounds with varying rheological behavior in the same process.

The flow of sheet molding compounds during compression molding is fundamentally different from that of thermoplastics or fluids in general. The viscosity of SMCs is heavily influenced by temperature, as it decreases with increasing temperature. Since the charge placed into the heated mold is at room temperature, the bulk of the material is viscous and exhibits higher resistance against extensional flow. The thin layer of material in direct contact with the mold surface is heated rapidly, which in turn reduces its viscosity. This reduced viscosity layer of SMC acts as a lubricant for the bulk of the material, allowing the charge to extend in stable plug flow, without mixing the two sides: class-A surface and structural backside. An application-oriented result of the scientific experimentation was the understanding of the methods to control the molding challenges associated with the technology. For example, fiber preform movement during flow poses a risk to the successful manufacturing of multi-material components. The position of local reinforcing structures plays an important role in overall component stiffness, and therefore, their relocation during flow had to be minimized or controlled.

Another molding related challenge is the development of sink marks on the outer surface opposite rib structures. This effect is also known as rib read-through. Since the opposite side of these rib structures is on the to be painted class-A side, sink marks must be eliminated. This required a comprehensive experimental plan with varying relevant process parameters, e.g. molding pressure, curing temperature, substrate thickness, rib depth and thickness to name a few. Sink marks on the class-A side can also be caused by embedded prepreg underneath the class-A surface. These lead to unacceptable surface quality and therefore, need to be avoided. Similarly, to rib read-throughs, this was experimentally investigated within the project.

The one-piece hood is required to comply with pedestrian safety regulations, which limit the local stiffness of the component at given locations. Head Injury Criterion (HIC) simulation and testing is a major part of the proposed work. The issue is rooted in the conflicting mechanical requirements of component stiffness and pedestrian protection. Composite materials allow for their properties to be tailored through the application of localized reinforcements or through the implementation of specific design features such as varying wall thickness and smart rib design.

Due to the hybrid nature of the proposed material combination, pressure-temperature effects were investigated in order to prevent undesired out-of-plane deformation of the component due to changes in ambient temperature, i.e. warpage. This was influenced by tailoring the coefficient of thermal expansion of the individual materials, especially that of the SMCs. Furthermore, the manufacturing process and some of the molding parameters were also investigated in their effectiveness to control warpage and post-molding deformation.

3. BACKGROUND

Sheet molding compounds (SMC) present a promising alternative to metals in automotive body panel applications. SMC comprises of a thermoset resin, chopped reinforcement fibers, fillers and additives. Due to its heterogeneous nature, it can be tailored to specific applications through adjustments to its recipe. Therefore, there are established recipes for certain application, such as for Class-A body panels.

SMC has been used in body panel applications for decades, with its earliest series production applications being the third generation Chevrolet Corvette from 1973 and the Audi Quattro trunk lid from 1983. Commercial vehicles such as agricultural machines and semi-trailer trucks have a rich history in employing SMCs as well SMC parts usually consist of (at least) two major parts: an inner and an outer shell. (GM, 2012) This engineering technique allows for complex geometries and excellent mechanical performance on the inner shell, while ensuring a high quality surface on the outer panel, undisturbed by ribs and similar features. Other material solutions, such as thermoplastic systems or thermoplastic-thermoset-hybrids similarly consist of two shells. Typically, the structural shell employing SMC, utilizing its superior mechanical performance and a thermoplastic outer for superior paintability. (Editor, 2013)

Single-shell designs made of SMC are usually non-painted or non-class-A surfaces. (Malnati, 2017)

This study investigated a novel processing technique for sheet molding compounds to produce hybrid SMC parts in a single step, uniting the aforementioned inner and outer shells. The project consortium consisted of experts with multiple decades of total experience in the field, ranging from raw material manufacturing and SMC compounding to part molding and engineering services, to tackle the challenges along the way of developing this process.

4. RESULTS AND DISCUSSION

4.1. Material Characterization of SMC Pastes and Prepreg

In order to obtain inputs to accurately perform simulations and to gain a general understanding of the performance characteristics of the candidate materials in this project a large amount of characterization work was done. INEOS Composites performed a number of rheological and cure kinetics studies in order to characterize how the various SMCs behaved during their manufacturing curing cycles. Mechanical performance data was collected using samples from cured flat plaques containing single materials, or multi-material combinations. Three SMCs (Class A, ½" structural, and 1" structural) and one woven prepreg were the subjects of these studies.

4.1.1. SMC Paste Characterization: Rheology

The dynamic rheological properties as a function of frequency and temperature of the submitted SMC paste were measured on the TA Instruments ARES-RDA rheometer between 25 mm diameter parallel plates. The specimen was tested at 25°C as a function of frequency from 0.5 to 500 radians/second at a constant strain of 1%. Then the specimen was tested at a constant heating rate of 5°C/minute from 25°C to 175°C with a constant angular frequency of 10 Hz. For the frequency sweep test, the data was plotted as a function of test frequency at a constant temperature of 25°C. For the temperature sweep test, the data was plotted at a constant angular frequency of 10 Hz as a function of temperature. The measured smoothed properties include G' (Storage Shear Modulus), G'' (Loss Shear Modulus), Tan Delta, G*

(Complex Shear Modulus) and Eta* (Complex Viscosity). G' measures the stiffness of the specimen and represents the elastic nature of the material. G'' measures the amount of energy dissipated by the specimen as heat during oscillatory testing and represents the viscous nature of the material. Tan Delta is called the dissipation factor and is defined as G"/G'. G* is defined as the square root of $[(G')^2 + (G'')^2]$. Complex viscosity is defined as G*/angular frequency.

The minimum complex viscosity and the temperature at minimum complex viscosity or the Class A and Structural SMC pastes are given in Table 1.

Table 1 Rheology Temperature Sweep, Class A SMC Paste

Sample Id	Temperature at Minimum Viscosity (°C)	Minimum Viscosity (poise)
9130-94B (Class A SMC Paste) Spec #1	100.5	888.0
9130-94B (Class A SMC Paste) Spec #2	105.7	929.2
9130-94B (Class A SMC Paste) Spec #3	101.3	865.4
9130-94B (Class A SMC Paste) Spec #4	105.3	976.2
9130-94A (Structural SMC Paste) Spec #1	99.9	1066.0
9130-94A (Structural SMC Paste) Spec #2	100.2	1216.1
9130-94A (Structural SMC Paste) Spec #3	99.8	1126.2
9130-94A (Structural SMC Paste) Spec #4	100.2	1189.2

4.1.2. SMC Paste Characterization: Cure Kinetics,

The thermal transitions of the submitted samples were measured via the TA Instruments Q2000 Differential Scanning Calorimetry (DSC) using hermetically sealed aluminum pans. Each specimen was placed in a hot DSC cell at the required isothermal temperature and was held at that isothermal temperature until the reaction was complete. The specimen was then heated at 10°C/minute from -50°C to 250°C (2nd Scan). The DSC cell was purged with helium at a rate of 25mL/minute to prevent moisture condensation during cooling.

The thermal transitions of the submitted samples were measured by Modulated Differential Scanning Calorimetry (MDSC) on the TA Instruments Q2000 DSC using hermetically sealed aluminum pans. The sample was heated at a constant underlying heating rate of 2°C/minute with an oscillation amplitude of 0.318°C and an oscillation period of 60 seconds from -100°C to 225°C (1st Scan), cooled at 10°C/minute to 0°C, and was retested to 250°C (2nd Scan). The DSC cell was purged with helium at a rate of 25mL/minute to prevent moisture condensation during cooling. The reversing profiles identify the reversing thermal transitions (e.g., Tg). The non-reversing profiles identify non-reversing events (e.g., residual cure, volatilization, release of residual stress and/or molecular orientation, etc.).

Table 2 Dynamic DSC Results

Sample Identification	Heating Rate (°C/min)	Extrapolated Onset of Heat of Reaction (°C)	Total Heat of Reaction (J/g)	Peak Temperature (°C)
9130-94A MDSC (Spec #1)	2	102.92	229.0	108.09, 157.03
9130-94A MDSC (Spec #2)	2	100.18	238.8	105.14, 157.41
9130-94A (Spec #1)	5	111.21	253.43	117.59, 166.49
9130-94A (Spec #2)	5	110.22	242.42	116.13, 166.78
9130-94B MDSC (Spec #1)	2	105.44	99.04	109.00, 156.86
9130-94B MDSC (Spec #2)	2	108.62	107.1	113.38, 153.82
9130-94B (Spec #1)	5	115.81	109.45	119.82, 160.96
9130-94B (Spec #2)	5	114.89	109.85	118.53, 161.40

Table 3 Isothermal DSC Results

Sample Identification	Isothermal (°C)	Extrapolated Onset of Heat of Reaction (min)	Heat of Reaction (J/g)	Peak Time (min)	2nd Scan Extrapolated Onset of Heat of Reaction (°C)	2nd Scan Total Residual Heat of Reaction (J/g)	2nd Scan Peak Temperature (°C)
9130-94A (Spec #1)	80	67.81	109.8	87.90	109.14	64.13	135.24, 175.51
9130-94A (Spec #2)	80	60.48	100.5	83.23	106.49	60.86	132.10, 174.92
9130-94A (Spec #1)	90	18.36	113.9	25.12	109.42	50.81	136.16, 175.10
9130-94A (Spec #2)	90	27.07	103.1	35.55	109.15	61.34	136.20, 174.78
9130-94A (Spec #2)	90	23.31	114.3	34.36	111.08	59.69	138.70, 174.85
9130-94A (Spec #1)	100	5.79	147.8	8.84	115.01	41.21	144.60, 175.57
9130-94A (Spec #2)	100	6.61	143.4	10.72	120.44	37.20	149.66, 175.13
9130-94A (Spec #1)	110	1.81	124.9	3.24	113.82	46.62	143.04, 174.97
9130-94A (Spec #2)	110	1.62	115.8	3.17	120.24	40.41	150.56, 174.76
9130-94A (Spec #1)	120	0.64	118.1	1.12	119.65	45.07	152.71, 173.99
9130-94B (Spec #1)	80	123.90	40.72	145.43	109.84	24.62	138.94, 174.35
9130-94B	80	105.90	43.63	124.45	113.76	19.07	137.09,

(Spec #2)							173.32
9130-94B (Spec #1)	90	35.88	51.61	41.88	109.30	27.87	135.55, 174.42
9130-94B (Spec #2)	90	42.10	49.25	49.12	107.98	31.33	138.83, 174.13
9130-94B (Spec #1)	100	12.21	68.05	15.04	127.57	14.93	150.67, 175.01
9130-94B (Spec #2)	100	12.97	69.00	16.19	122.78	18.98	151.46, 172.83
9130-94B (Spec #1)	110	3.41	62.73	4.76	120.64	16.96	148.05, 174.83
9130-94B (Spec #2)	110	3.35	58.75	4.93	148.74	7.789	175.10
9130-94B (Spec #1)	120	1.14	68.77	1.86	130.46	16.66	155.66, 171.86
9130-94B (Spec #2)	120	1.14	67.08	1.90	132.22	13.41	155.81, 174.29
9130-94B (Spec #1)	130	--*	--*	0.79	131.96	18.04	155.94
9130-94B (Spec #2)	130	--*	--*	0.76	129.47	13.59	153.24, 173.42

4.1.3. SMC Paste Characterization, Cure Model

Using the cure kinetics experimental data provided by INEOS, a cure model was generated for both high and low rates of cure. The model had difficultly fitting both types of cure simultaneously; however, it successfully validated each type of cure individually. It was practically determined that only the high rates of cure were relevant for the rapid processing targeted in this project, so the poorer fit at low rates is disregarded here. The model fits for both Structural and Class A SMC pastes are shown in Figure 1.

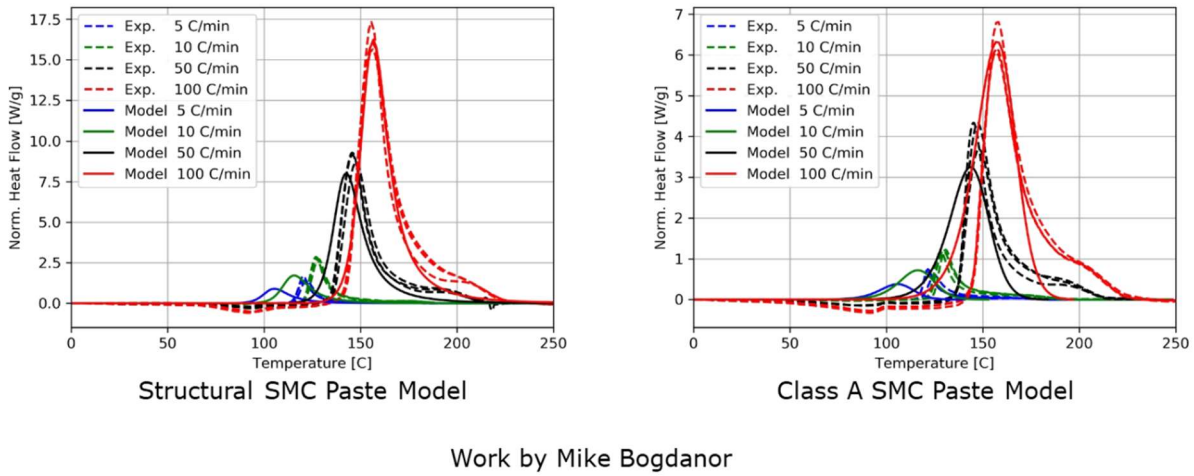

Figure 1. Cure Kinetics Model to DSC Experiments at Multiple Rates

In the present work, the cure kinetic behavior was not actively coupled to flow simulation viscosities. In other words, the analysis was performed but not directly developed into "live" simulation. Instead, viscosity at the time of forming was determined and a single value (i.e., the viscosity tensor) was applied

to simulations without considering degree of cure during the short time frame where material flowed. This coupling of cure kinetics and the changing viscosity is expected to more accurately capture the physics of the molding process.

4.1.4. Prepreg & SMC Mechanical Properties Characterization

Obtaining realistic material property inputs is critical to the success of finite element modeling and analysis. For this reason, the SMCs and prepreg were characterized individually and in various combinations listed below in Table 4.

Table 4. List of Single and Combined Materials Studied for Mechanical Properties

Batch Label	Material 1	Material 2	Material 3	Orientation
1A	Class A			Centered
1A-S	Class A			Axial
1A-S	Class A			Transverse
1B	1/2" Struct.			Centered
1B-S	1/2" Struct.			Axial
1B-S	1/2" Struct.			Transverse
1C	1" Struct.			Centered
1C-S	1" Struct.			Axial
1C-S	1" Struct.			Transverse
1D	Prepreg			Centered
2A	Class A	1/2" Struct.		Centered
2B	Class A	1" Struct.		Centered
2C	Class A	Prepreg		Centered
3A	Class A	Prepreg	1/2" Struct.	Centered
3B	Class A	Prepreg	1" Struct.	Centered

60% 3A

30% 3A

Directional Flow 3A

Knit 3A

Figure 2. Shows actual 3 component charge patterns, resulting plaques, and layer micrographs

Figure 2 shows the raw material forms as stacked in a charge pattern. The proposed material systems were selected to specifically target desired mechanical characteristics for specific automotive applications and their success in duplicating the desired traits used in the design of automotive hood and paneling. The materials selected were estimated by expert material manufacturers to approach the flexural and tensile stiffness needs and strength requirements that the OEM provided for hood design. Due to possible variations in geometry and manufacturing processes, the single-material properties were determined for charges oriented in the axial, transverse, and centered/random charge orientation states.

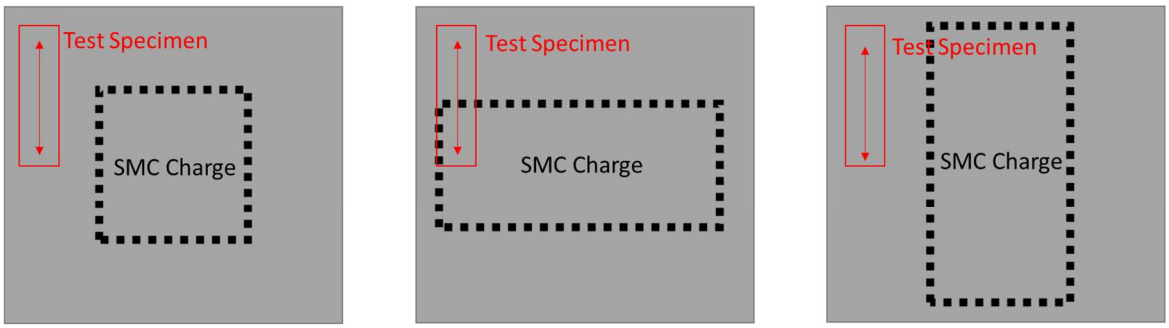

Figure 3. Single Material Charge Orientation and Mechanical Test Specimen Orientations

The charge orientations depicted in Figure 3 resulted in specifically oriented fiber states that provide analogous specimens to typical unidirectional CFRP 0, 90, and +/-45° samples. Multi-material samples were characterized only for centered charges that are assumed to result in statistically equal orientation states of the reinforcing fibers. The specific tests performed, and their ASTM and international testing standard equivalents are listed here.

Table 5. List of Primary Mechanical Characterization Tests Performed

	Testing Temperatures				
	23C	90C	-35C	Testing Standards	
Tensile Test	x	x	x	ASTM D638	DIN ISO 527
4-Point Bending (Flexure) Test	x	x	x	ASTM D6272	DIN ISO 14125
3-Point Bending (ILS) Test	x			ASTM D2344	DIN ISO 14130

These tests provide the most important mechanical performance data for most simulations. Three point tests were not used at all temperatures due to time constraints and resource limitations. The equations used to get material properties from experimental output are shown in Figure 4.

- Tensile, ASTM D638 (ISO 527 1B)
  - $\sigma = \frac{P}{bd}$
  - $E = \frac{\sigma}{\epsilon}$
  - $\nu = -\frac{\epsilon_{xx}}{\epsilon_{yy}}$

$\sigma = Stress,\quad P = Load,\quad b = width,\quad d = thickness,$
$E = Tensile\ Modulus,\quad \epsilon = Strain,\quad \nu = Poisson's\ Effective,$
$\epsilon_{xx} = Transverse\ Strain,\quad \epsilon_{yy} = Axial\ Strain$

- Flexure, ASTM D6272 (ISO 14125)
  - $\sigma = \frac{PS}{bd^2}\left[1 + \left(\frac{4.70D^2}{L^2}\right) - \left(\frac{7.04Dd}{L^2}\right)\right]$
  - $D = \frac{\delta_a}{4a}\frac{(3S^2-4a^2)}{(3S-4a)}$, *from 4pt simply supported beam*
  - $E_B = 0.21\frac{S^3 m}{bd^3}$
  - $\epsilon = \frac{4.70Dd}{S^2}$

$\sigma = Fiber\ Stress,\quad E_B = bending\ (tangent)\ modulus,\quad P = Load,$
$S = Support\ Span\ (80mm),\quad b = width,\quad d = thickness,$
$D = Maximum\ Deflection,\quad \delta_a = displacement\ at\ load\ point,$
$a = distance\ from\ support\ to\ load\ point\ (27.5mm),$
$m = slope\ of\ load\ deflection\ curve$

- Interlaminar Shear, ASTM D2344 (ISO 14130)
  - $ILSS = \frac{3P}{4bd}$

$ILSS = Interlaminar\ Shear\ Stress,\quad P = Load,$
$b = width,\quad d = thickness$

Figure 4. Equations for Mechanical Property Tests

These equations were used to make the necessary calculations to obtain resulting parameters. The averaged results derived from all the tests and in the different temperatures are listed in Table 6.

Table 6. Summary of Averaged Test Results

Group	Materials			Flow Alignment			Mean calculated values												
							Tension						Flexure 4PB						3PB
				Center	Axial	Transverse	23°C		90°C		-35°C		23°C		90°C		-35°C		23°C
							σ_{max}	E_x	σ_{max}	E_x	σ_{max}	E_x	σ_{max}	E_f	σ_{max}	E_f	σ_{max}	E_f	ILSS
							(MPa)	(GPa)	(MPa)	(GPa)	(MPa)	(GPa)	(MPa)	(GPa)	(MPa)	(GPa)	(MPa)	(GPa)	(MPa)
1A	Class A			X			92	10	76	8	107	15	179	11	117	7	209	14	30.2
1A	Class A				X		152	13	96	11	139	16	254	13	146	10	304	18	31.8
1A	Class A					X	51	9	47	5	73	13	225	10	90	5	163	12	25.1
1B	1/2" Struct.			X			130	10	92	8	143	13	231	11	126	7	254	13	35.2
1B	1/2" Struct.				X		180	15	92	10	126	14	328	16	150	10	285	14	26.5
1B*	1/2" Struct.					X	86	8	53	5	--	--	--	--	--	--	--	--	27.4
1C	1" Struct.			X			149	11	90	7	185	14	306	13	152	8	328	13	29.7
1C	1" Struct.				X		159	13	134	11	237	17	334	15	151	10	766	14	24.8
1C*	1" Struct.					X	89	8	--	--	100	11	203	8	97	5	172	10	28.7
1D	Prepreg			X			262	16	250	16	282	20	532	20	184	15	378	18	24.4
2A	Class A	1/2" Struct.		X			120	12	80	8	140	15	219	11	115	6	281	14	31.8
2B	Class A	1" Struct.		X			122	10	85	6	148	15	274	12	136	7	298	15	31.7
2C	Class A	Prepreg		X			153	13	112	10	154	16	237	12	148	10	345	16	30.6
3A	Class A	Prepreg	1/2" Struct.	X			139	12	88	8	146	15	207	10	110	6	309	16	26.1
3B	Class A	Prepreg	1" Struct.	X			159	12	96	8	146	15	249	11	113	7	282	15	30.6

Table 6 provides summarized results that were obtained from each of the tests performed and in the different temperature conditions. At least five replicates were performed for each average value shown above. Appendices 11.7, 11.8, and 11.9 contain more statistical data and individual specimen results. In the next few sections, we shall see results pertaining to the individual testing methods.

4.1.4.1.Tensile Test Results

Dog-bone shaped tensile samples were tested under tension until failure. At 23˚C, tests were carried out in the 22-kip MTS load-frame. The strain values were recorded using two Digital Image Correlation (DIC) stereo systems, with two 5 MP stereo cameras in each system, for each side of the sample. Only one system of cameras (Sys0) was used while testing single material samples (1A through 1D), while both systems (Sys0 and Sys1) were used while testing the multi-material samples (2A through 3B). Each system was separately calibrated prior to testing. The cameras served the purpose of continuously recording images during the test and synchronizing them with the load-frame loading. These images would later be used to perform DIC analysis using Vic3D software. Figure 55 shows the tensile test and DIC mechanism set-up.

Figure 5. 23°C Tensile Test DIC Mechanism Set-Up

At 90°C and -35°C, tensile tests were carried out using the 5-kip MTS load-frame and inside a series 651 MTS environmental chamber. Temperature control command was used to ramp up and/or hold at certain temperatures. Liquid nitrogen was fed into the chamber through the solenoid valve connection to bring temperatures down to -35°C. Due to the reflective and refractive effects of the environmental chamber's glass window, coupled with the fog created on its inside during low-temperature (-35°C) testing, we were unable to set up DIC mechanism. Hence, an extensometer was attached to the samples during testing to record strain values. A thermocouple inside the environmental chamber was attached to each sample loaded at 90°C and -35°C, these temperatures are generally understood to provide an accurate temperature reading. Figure 6 shows the environmental chamber and extensometer set-up. All tests were carried out at a constant load-frame displacement rate of 2mm/min.

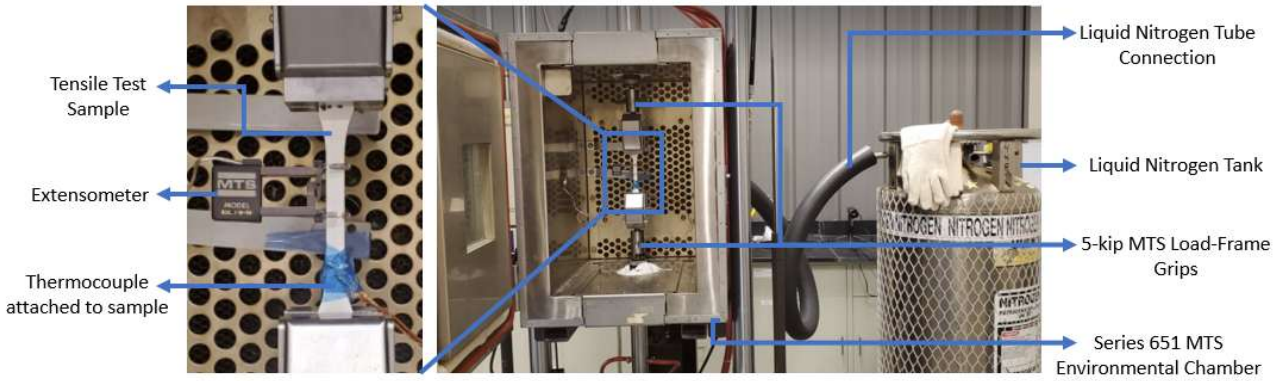

Figure 6. 90°C and -35°C Tensile Test Environmental Chamber and Extensometer Set-Up

After testing, the individual sample stress-strain curves were obtained as well as their respective tensile properties. The equations in Figure 4 were then used to calculate a combination of averages used to summarize the data. Figures 7-9 below are the bar charts and box plots depicting average tensile strength, tensile modulus and maximum strains of all the samples. The results in green correspond to test data obtained from tensile tests conducted at 23°C. Red and blue correspond to tests conducted at 90°C and -35°C, respectively.

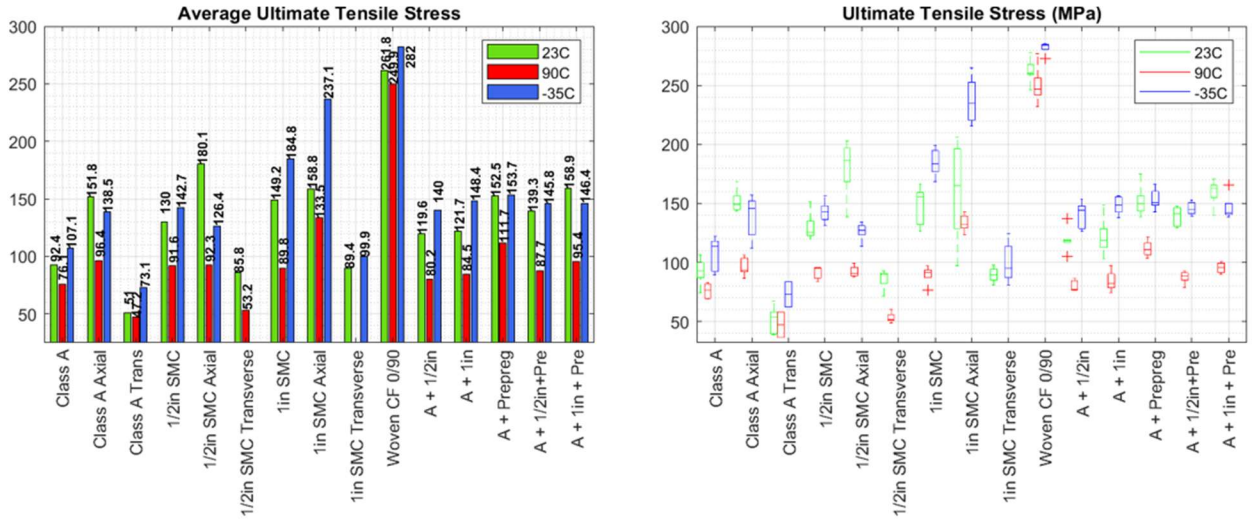

Figure 7. Ultimate Tensile Stress at Different Temperatures, Bar Chart and Box Plot

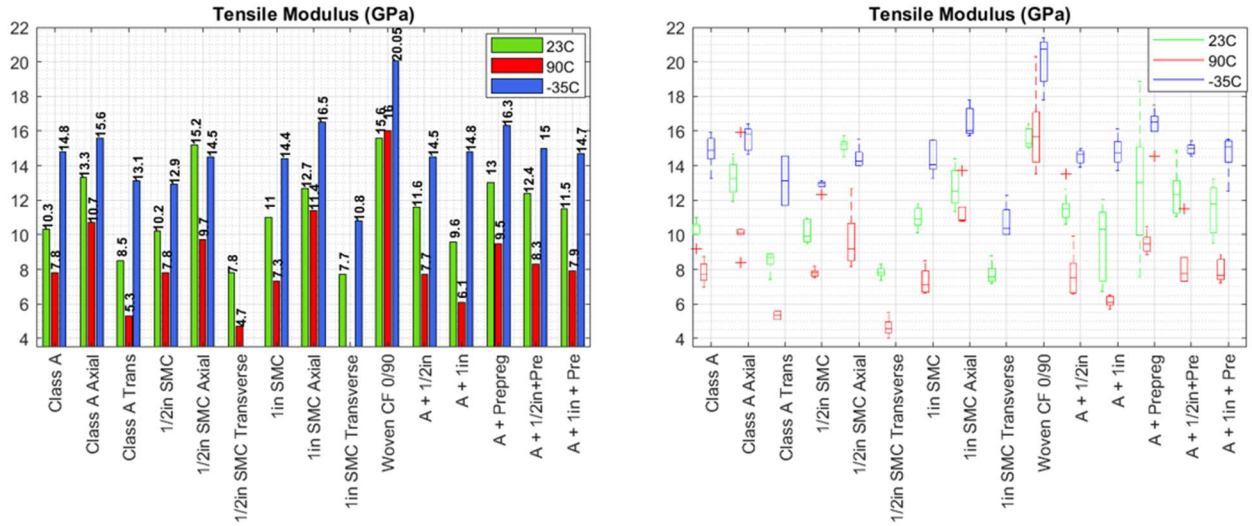

Figure 8. Tensile Modulus at Different Temperatures, Bar Chart and Box Plot

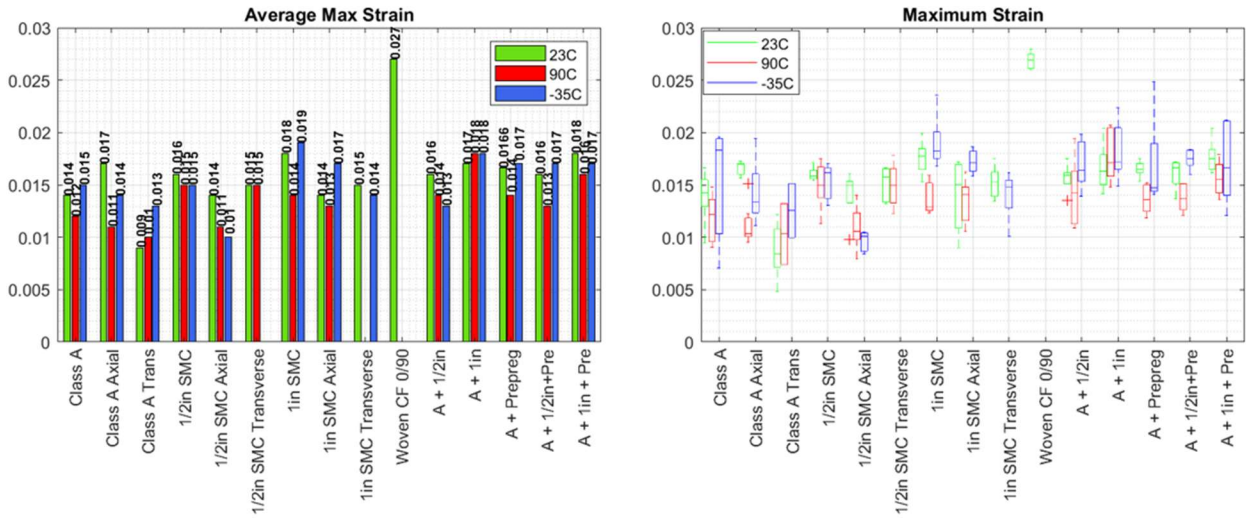

Figure 9. Maximum Strain under Tensile Loading at Different Temperatures, Bar Chart and Box Plot

An important note to make is that there is ½" SMC (1B) Transverse test data at -35°C, and 1" SMC (1C) Transverse data at 90°C are absent. This is due to a lack of enough transverse samples for both 1B and 1C. Furthermore, we observed that the transverse data for both 1B and 1C at 23°C showed similar results. Hence, we made the decision to test all the available 1B transverse samples at 90°C and all the 1C transverse samples at -35°C. It was assumed that these transverse high and low temperature results are interchangeable for ½" and 1" SMCs.

Furthermore, we have not recorded ultimate strain values for the woven continuous fiber (1D) samples. This is because during the 90°C and -35°C tests, the failure of individual tows caused large vibration impulses that moved the extensometer. Hence, the strain data after the first jump is bad, so we could not get a good ultimate strain. The modulus (which depends on very early strains) and ultimate stress (which doesn't depend on the extensometer data) were still good.

As a general trend, we see that the samples show high strength and modulus value, i.e., they become stiffer at -35°C. The individual sample stress-strain curves and test results are presented in Appendix 11.7.

4.1.4.2.Flexure (4-Point Bending) Test Results

For the 4-point bending tests, rectangular samples of length 100mm and width 25mm were extracted from the plates. As shown in Figure 10. Schematic of 4-Point Bending Test Set-Up, flexure loading points were adjusted to be 25mm apart (L_S) and support points were 80mm apart (L_A), according to test requirements. The support and loading points (R_A and R_S) were of radius 3.175 mm, each.

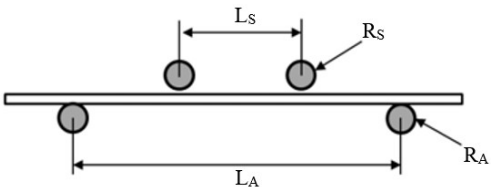

Figure 10. Schematic of 4-Point Bending Test Set-Up

Loading for samples with axial fiber orientation was performed at 15mm/min displacement rate. All other samples were loaded at 10mm/min displacement rate. All tests were carried out in the 5-kip MTS Load-Frame. The 90°C and -35°C tests were conducted inside the Series 651 MTS Environmental Chamber. A

thermocouple inside the environmental chamber was attached to a spare sample throughout the testing in order to accurately read temperatures.

After testing, we obtained the individual flexural stress-strain curves and resulting flexural properties, along with combined averages using the equations shown in Equations for Mechanical Property Tests. Figures 11 and 12 are bar charts and box plots of average flexural strength and modulus of all samples. The results in green correspond to test data obtained from tensile tests conducted at 23°C. Red and blue correspond to tests conducted at 90°C and -35°C, respectively.

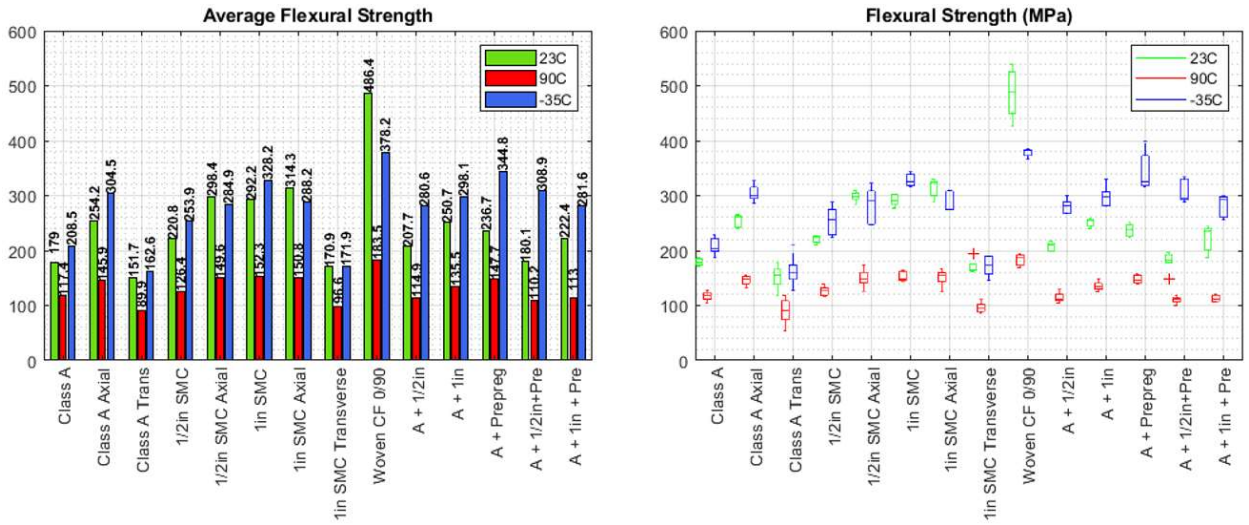

Figure 11. Flexural Strength at Different Temperatures, Bar Chart and Box Plot

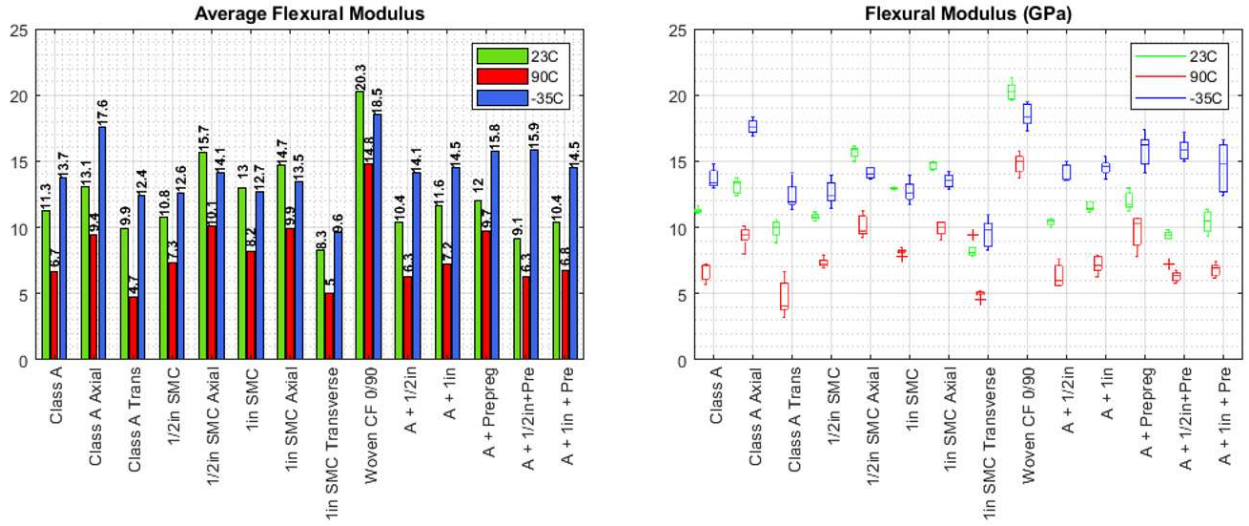

Figure 12. Flexural Modulus at Different Temperatures, Bar Chart and Box Plot

The "Woven CF 0/90" samples were the only ones to have statistically higher performance at room temperature than at -35°C. As continuous material sheets, perhaps they are more subject to interlaminar effects where there is likely a discrete resin-only layer between plies. Cold temperatures (and humid condensating air in the environmental chamber) may have had a unique effect on this different microstructure that does not occur for the SMC materials that lack such a clear interlaminar

mesostructure. The individual sample stress-strain curves, test results and failure analysis data are presented in the appendix 11.8.

4.1.4.3.Interlaminar Shear (ILS) 3 Point Bend Test Results

In the case of 3-point bending (interlaminar shear) tests, the samples were 20mm in length (l) and 25mm in width (b). As shown in the schematic in Figure 13, the support points were 10mm apart (L_A), as per the ASTM D2344 standard. The support and loading points (R_A and R_S) were of radius 3.175 mm, each. The samples were placed such that their lengths (l) spanned across the two support points (x-axis), while the length spanned along the z-axis.

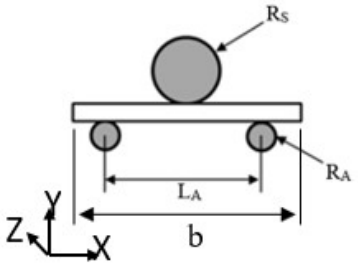

Figure 13. Schematic of 3-Point Bending Test Set-Up

The 3-point bending tests were conducted solely at 23°C and at a constant loading rate of 10mm/min, as per ASTM D2344 standard, and due to time and resource restrictions. Loading for each sample continued until a load drop of 30% of peak load, at which point the test was stopped. Figure 14 shows the variation of ILS test results for samples in each plate series.

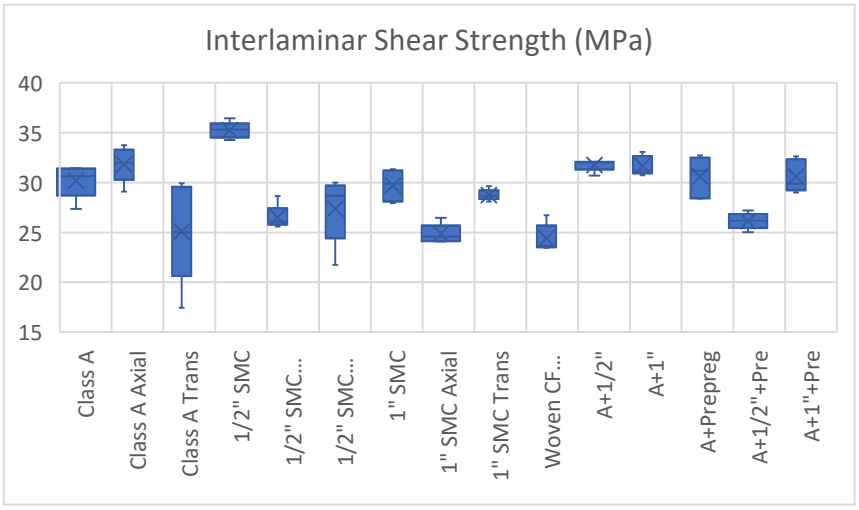

Figure 14. Interlaminar Shear Strength at Room Temperatures, Box Plot

An important note to make is that during the first four test sets, i.e., Class A Centered, Axial, Transverse and ½" SMC Centered, the samples were erroneously oriented such that their 20mm side spanned across the support points (x-axis) while the 25mm side spanned along the z-axis, as opposed what was stated in the test standard and requirements. Hence, the ILSS for these samples were calculated with the width being 20mm in the equation shown in Figure 4. For the subsequent tests, we corrected the sample orientation, now making the width equal to 25mm in the same equation. Hence, we observe slightly heightened Interlaminar Shear Strength values for the first four sets of tests, as seen in Figure 14.

The individual sample load-displacement curves, test results and failure analysis data are presented in the appendix 11.9.

4.1.4.4.Coefficient of Thermal Expansion (CTE) Test Results

The coefficient of thermal expansion was measured through CTE analysis. This analysis was performed for single-material series only 1) because it was deemed sufficient to study the isolated CTEs for any simulation material characterization and 2) because the measurement apparatus measures one side of a flat sample and the unbalanced, unsymmetric material combinations in this study would all result in sample curvature, invalidating the measurements. Figure 15 shows the experimental set-up required to perform this test.

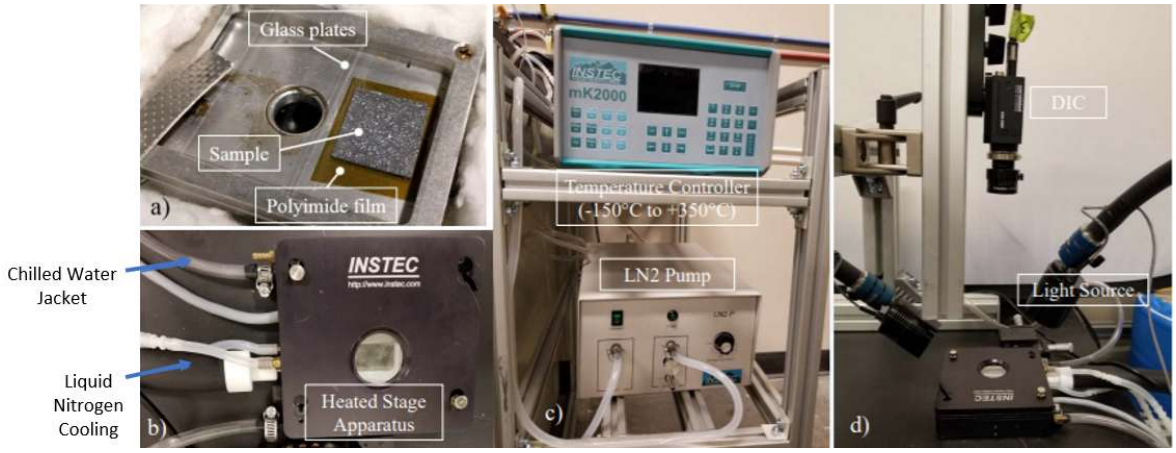

Figure 15. CTE Analysis Experimental Set-Up (Karmarkar, 2018)

The samples used to accomplish CTE analysis were of the same size and dimension as those used for Interlaminar Shear (3-point bending) tests, i.e., 20 mm in length and 25 mm in width. Prior to CTE analysis, the samples were speckled with paint for measurement of strain field using the DIC system. Since our tests had to run between temperatures -35˚C and 90˚C, the heated stage apparatus was equipped with liquid nitrogen cooling system to bring the temperature down to -35˚C. Then, the temperature was set to ramp up to 90˚C, hold, and finally ramp down to room temperature before stopping. This was controlled by the Instec mK2000 temperature controller, which has a sensitivity 0.001˚C. The focus and aperture for the DIC camera was set and the temperature control command was given. The DIC camera captured images at 5 seconds frequency. After the test, the captured images were used to calculate average Lagrangian strain as a function of temperature. Figure 16 shows an example of DIC analysis performed for the region of interest on one of the 1D-8 samples along with their Lagrangian x-direction strain range. Figures 17 through 19 show results of analysis.

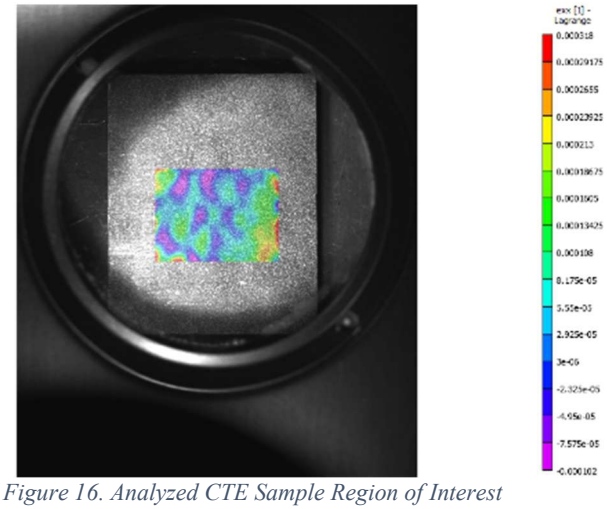

Figure 16. Analyzed CTE Sample Region of Interest

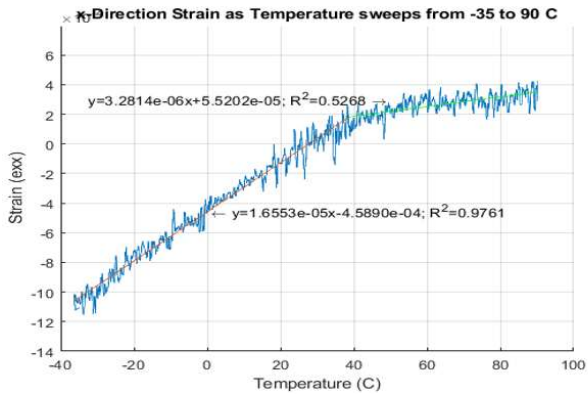

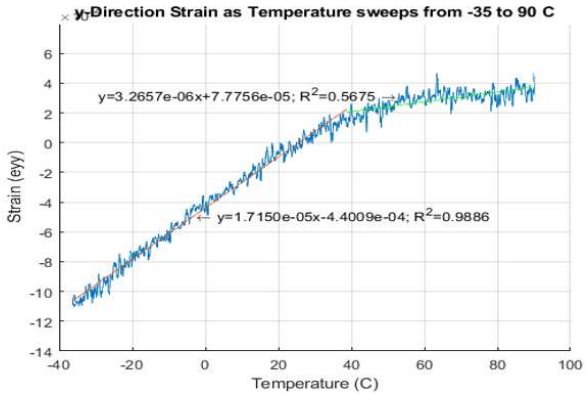

Figure 17. X and Y direction strain from the 1A test

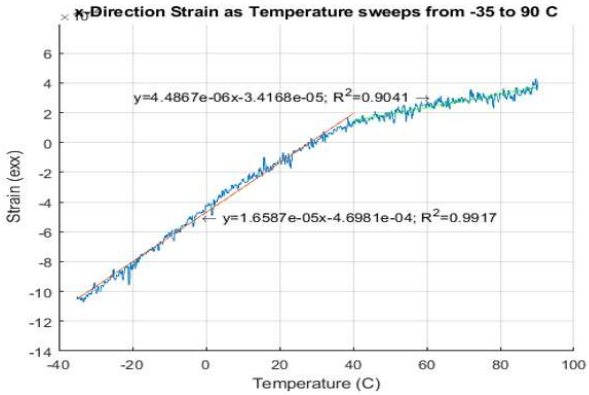

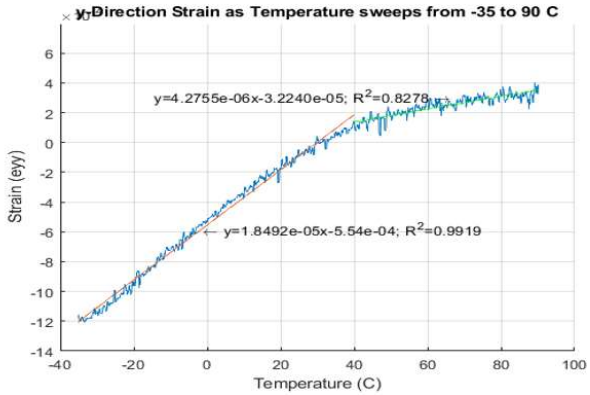

Figure 18. X and Y direction strain from the 1B test

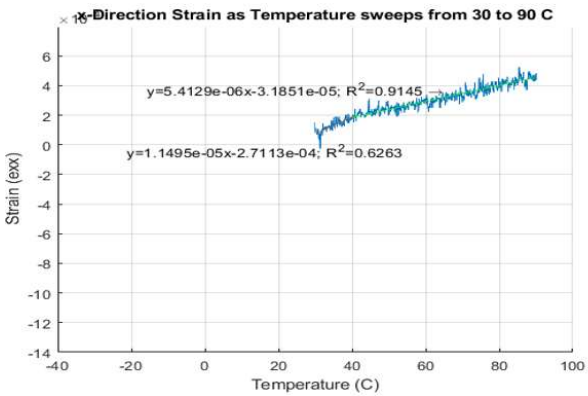

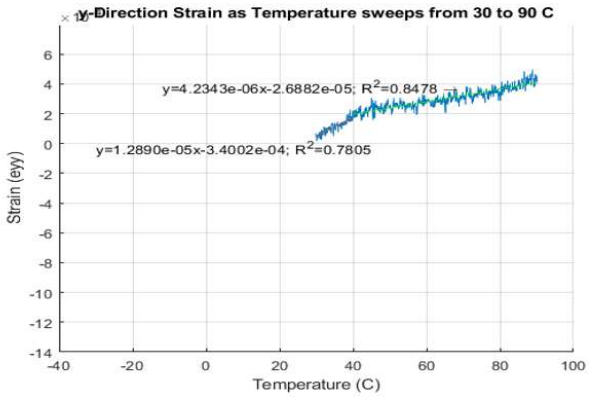

Figure 19. X and Y direction strain from the 1C test

It is important to note that due to lack of availability of the 1" SMC (1C) CTE test data from temperatures -35˚C to 30˚C, we were unable to perform analysis and plot the data. Hence, the strain plot for 1C in Figure 1920 shows data from 30˚C to 90˚C.

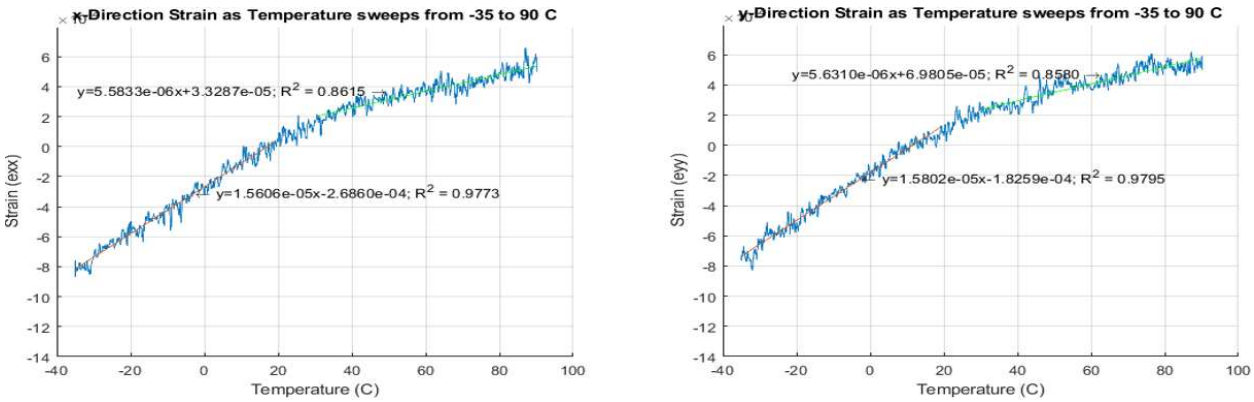

Figure 20. X and Y direction strain from the 1D test

The results for coefficients of thermal expansions along the x- and y-directions for the single material center-charged samples are summarized in Table 7.

Table 7. Summary results of single-material center-charge CTE Test samples

		CTE 1: -35°C to 40°C [10^{-6} °C^{-1}]	CTE 2: 50°C to 90°C [10^{-6} °C^{-1}]
1A	x-axis	16.553	3.281
	y-axis	17.15	3.266
1B	x-axis	16.587	4.487
	y-axis	18.492	4.276
1C	x-axis	14.495	5.413
	y-axis	12.89	4.234
1D	x-axis	15.606	5.583
	y-axis	15.802	5.631

4.2. Tooling Development

The current design of a one-piece hood utilizes heavily ribbed sections to provide correct stiffness levels in the part to meet desired load cases. This presents a major hurdle to the appearance aspect of the part, which is an automotive Class "A" surface. There exists a major problem with rib-read through on the A-surface of the part due to A-side "sink" on the rib sections. In order to begin developing solutions to the rib-read through issue a development tool was needed to simulate rib-read through on a Class "A" surface. The development tool would also allow for the design team to begin modeling the material flow in rib-sections with single and multi-component systems.

4.2.1. Ribbed Plaque Tool Development

The ribbed plaque development tool was modeled to utilize an existing 11"x11" flat plaque tool located at the Michigan State University Scale-up Research Facility (MSU-SuRF) in order to reduce overall project costs. The existing flat plaque tool has a class "A" surface finish on the core side (male half of mold providing internal molded shape), which needed to be maintained for appearance/surface measurements during the study. A new cavity (female half of mold providing external molded shape) was proposed

utilizing industry best practices for rib design in order to reduce A-surface read through. Figure 211 below, highlights the initial proposed cavity and rib design.

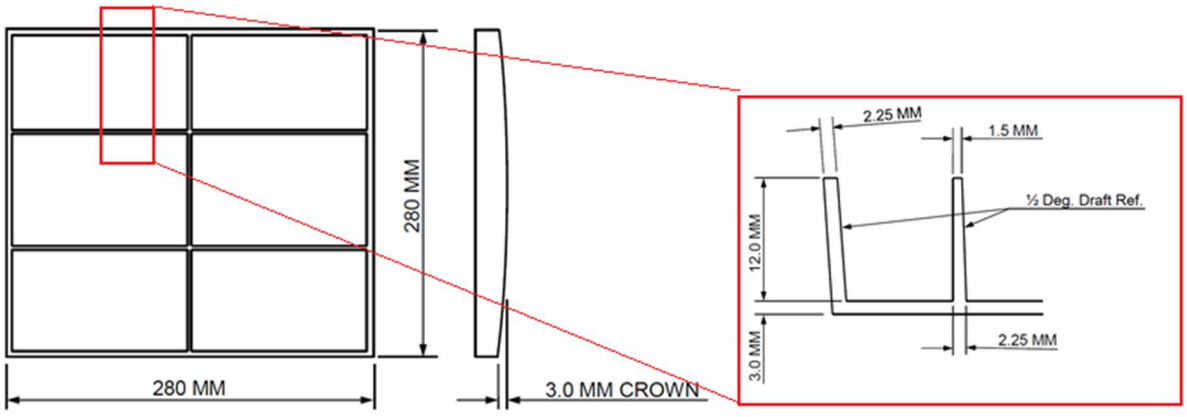

Figure 21 Initial proposed cavity rib pattern and rib geometry.

Upon review by the project team, changes were made to the rib pattern in order to ease design costs and to allow for better working space within the press working area. The modifications to the cavity design can be seen below in Figure 22, showing the initial cavity design provided by the tooling supplier (WesTool). The first major change to the rib pattern were the removal of the border rib along the edges of the plaque, this design change was suggested by the tooling supplier in order to reduce the cavity dimensions to allow for a reasonable working area in the press, as well as reducing the cost to cut the new cavity. The second major change being the rib pattern, which was switched from a 6-panel design to a nine panel design, to allow for a centralized air-poppet to be installed in the cavity to aid in part removal. The nine panel design also factored better into potential experimental designs for the tool.

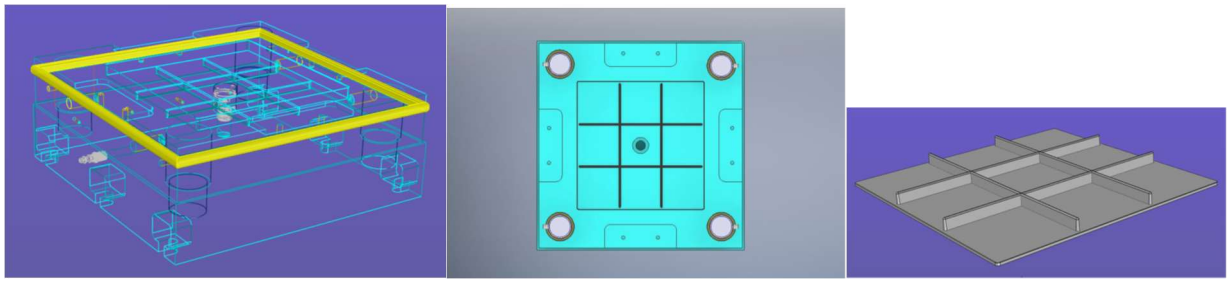

Figure 22 Initial cavity design provided by tooling supplier (WesTool)

Upon review of the initial design, scrutiny was placed on the rib design and the effect that design would play on the A-Surface of the panel.

Figure 233 highlights the rib design as provided by the supplier and 2 options for improved rib designs provided based on industry best practices.

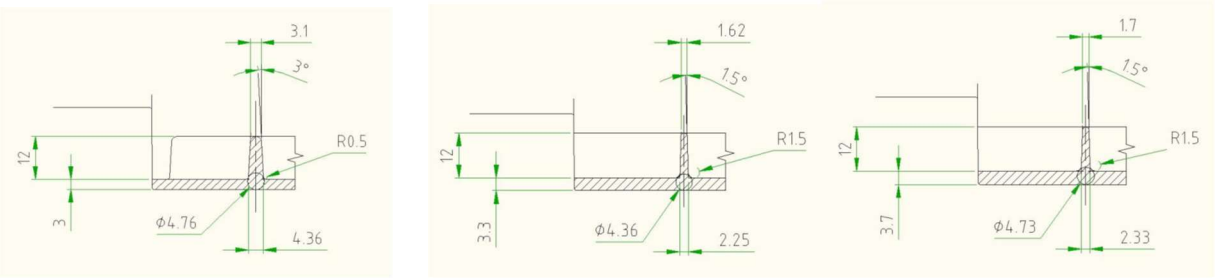

Tooling Design | Option A: 3.3mm plaque | Option B: 3.7mm plaque

Figure 23 Highlights the initial rib design provided by the tooling supplier as well as two improved designs provided by Magna, based on improved rib radii vs panel thickness

It was decided to move forward with Option A by the project team in order to maintain a reasonable panel thickness (3.3mm vs 3.7mm), consistent with light-weighting efforts for the project. The radii/draft angle of the ribs was also increased to 1.5° in order to reduce the amount of material at the rib root to reduce the sinking effect on the A-surface caused by shrinkage in the rib.

The cavity design was approved and built by WesTool to begin development trials at the MSU-SuRF.

4.3. Molding Trials

Experimental molding for the project focused on two Class "A" molds located at the MSU-SuRF in order to begin evaluating the molded properties of multi-material systems. All trials utilized three types of SMC produced by IDI International (Class "A" SMC, ½" Glass Structural SMC, 1" Glass Structural SMC) and a woven glass prepreg material, also provided by IDI International.

4.3.1. Flat Plaque Trial

The first iteration molding trial on the flat plaque tool was designed to examine differing charge pattern lay-outs and the effect SMC flow plays on woven prepreg. The molding conditions were held constant for all charge and material iterations at a standard temp 295/305F (Core/Cavity) with a max pressure of 65 tons (~1,000psi) for 2 min dwell. Table 8 below provides the material combination matrix that was used for the flat plaque study and the naming convention used for experimental designs. Single component panels were molded of each material that would be molded as multi-material systems i.e. Class "A" SMC (1A), ½" GF Structural SMC (1B), 1"GF Structural SMC (1C), and a woven glass pre-preg (1D). Two component systems were developed utilizing a Class "A" SMC on the A-surface of the tool with a 2nd structural layer (1/2" GF Structural SMC, 1" GF Structural SMC, or a woven pre-preg layer) i.e. 2A has constituent materials of Class "A" SMC and ½" Structural SMC . Three component systems were molded as a sandwich structure with the top layer (Class A side) composed of Class "A" SMC, a middle layer of woven pre-preg and a bottom layer of either ½" GF structural SMC or 1" GF structural SMC i.e. 3A has a Class "A" SMC layer, woven pre-preg layer, and ½" structural SMC layer.

A total of 10 panels of each material combination were molded utilizing ~60% mold coverage of SMC and 95% mold coverage of prepreg (where applicable) in order to collect material characterization properties. Additional panels were molded with directional flow of SMC in order to obtain transverse and axial flow properties as well.

Table 8. The material combinations utilized for the first iteration flat plaque study

1-Component	1A: Class "A"	1B: 1/2" Structural	1C: 1" Structural	1D: Woven Glass Pre-preg
2-Component	2A: 1A + 1B	2B: 1A + 1C	2C: 1A + 1D	
3-Component	3A: 1A + 1D + 1B	3B: 1A + 1D + 1C		

Flow studies were conducted on the flat plaque tool in order to characterize the flow associated with co-molded multi-material systems. Figure 24 below highlights the charge patterns utilized for the initial flat plaque flow study, all press parameters were kept constant. The baseline charge pattern was developed to simulate a traditional SMC charge pattern representing 60% tool coverage with the addition of a woven pre-preg patch centrally located on the SMC charge, both 0/90 and +/-45 pre-preg orientations were studied. Several iterations were developed to simulate relationships between the flow characteristics of SMC and woven pre-preg patches. The "fabric deformation" pattern shown in Figure 24 looks to highlight the effects of directional flow on a centrally located woven pre-preg patch, again 0/90 and +/-45 pre-preg orientations were studied. In order to assess flow effects on smaller patches, the "influence of flow direction" charges were developed to identify effects of uniform (A), perpendicular (B) and parallel (C) SMC flow directions on pre-preg patches. Additional charges were developed to simulate SMC short shots (incomplete part filling in the tool), to study fabric deformation in "end of flow" situations. Lastly, a "realistic" reinforcement approach utilizing a window structure was studied as a real-world analog to look at the effects of bound patches with different patch lay-ups i.e. as a single piece (A), as individual strips (B) and as an over-laid "L" pattern (C).

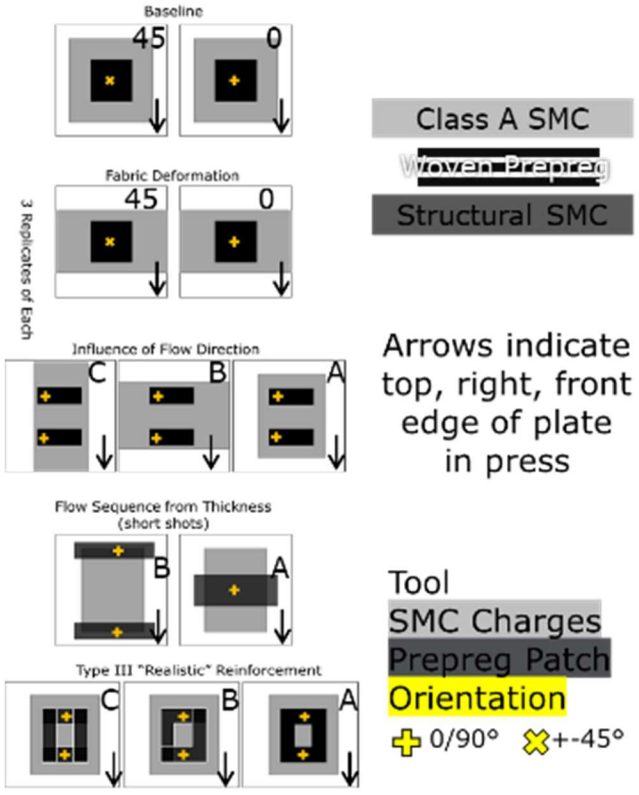

Figure 24. Highlights the flow scenarios of interest for the first flow molding trial. Charge cavity boundary in white, SMC in gray, Woven prepreg in black, orientation indicated with yellow symbols.

All molded plaques were distributed to project partners for visual inspection followed by a battery of destructive and non-destructive testing and compared against simulated panels provided by Purdue University.

4.3.2. Ribbed Plaque Trial

The first iteration molding trial on the ribbed plaque tool was designed to examine flow patterns of fibers under different flow situations i.e. flow distance, co-flow and knitting. The same molding conditions were utilized as with the flat plaque study, but the rib tool included the addition of vacuum. The material combinations were down selected from the flat plaque study to the 1A (Class "A" SMC), 2A (Class "A" SMC/1/2" GF Structural SMC), 2B (Class "A" SMC/1" GF Structural SMC), 3A (Class "A" SMC/ GF Woven Pre-preg/1/2" Structural SMC), 3B (Class"A" SMC/GF Woven Pre-preg/1" Structural SMC) systems. Four charge patterns were developed for the study to simulate desired flow scenarios, Figure 255 below shows the representative charge patterns for the 1, 2, and 3 component systems to simulate a 60% standard charge coverage, 30% centered high flow charge pattern, 30% directional/aligned flow and 30% knitting flow. Five replicates of each variety were molded and used for characterization

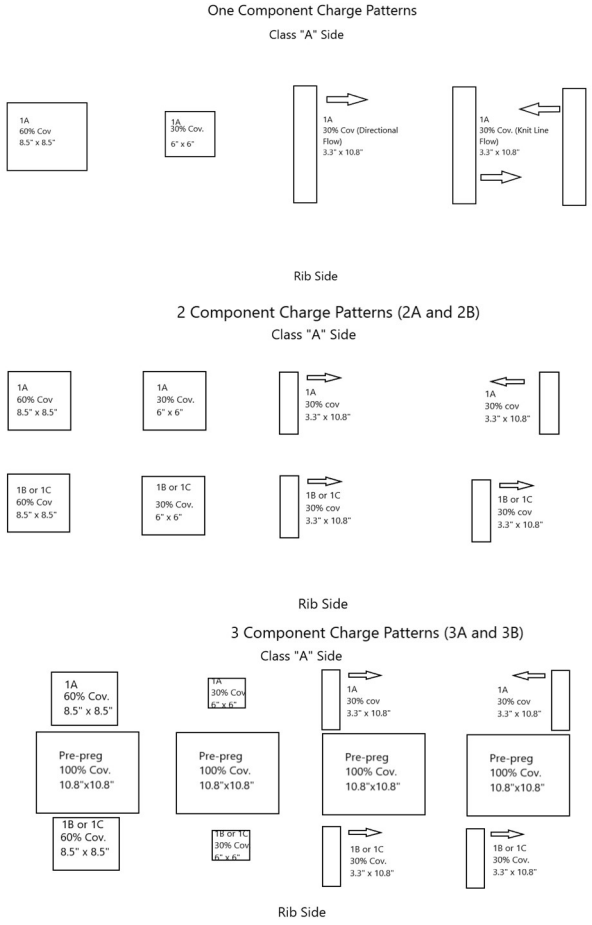

Figure 25. Highlights the representative charge patterns developed to simulate the desired flow scenarios for single component (Top), two component (Middle), and three component (Bottom)

Single component systems were down-selected to include only Class "A" SMC to utilize as a baseline for the studies. The top image in Figure 25, highlights the ply dimensions used in the study, with Figure 26 showing actually cut charges prior to molding. The 60% charge coverage pattern consisted of three plies of 8.5"x8.5" SMC, centered on the tool cavity, this pattern represents a standard charge coverage and orientation. The 30% charge coverage pattern consists of five plies at 6"x 6" SMC, centered on the tool cavity, representing a higher flow situation. The directional flow pattern consists of four plies at 3.3" x 10.8" and set flush to the left shear edge of the tool (arrows in Figure 25 elements signify flow direction) simulating a high directional flow situation. The Knit line pattern represents four plies at 3.3" x 10.8" separated into two stacks placed on opposite shear edges of the cavity surface (arrows in Figure 25 elements signify flow direction) simulating an undesirable knit line situation in the molded panel.

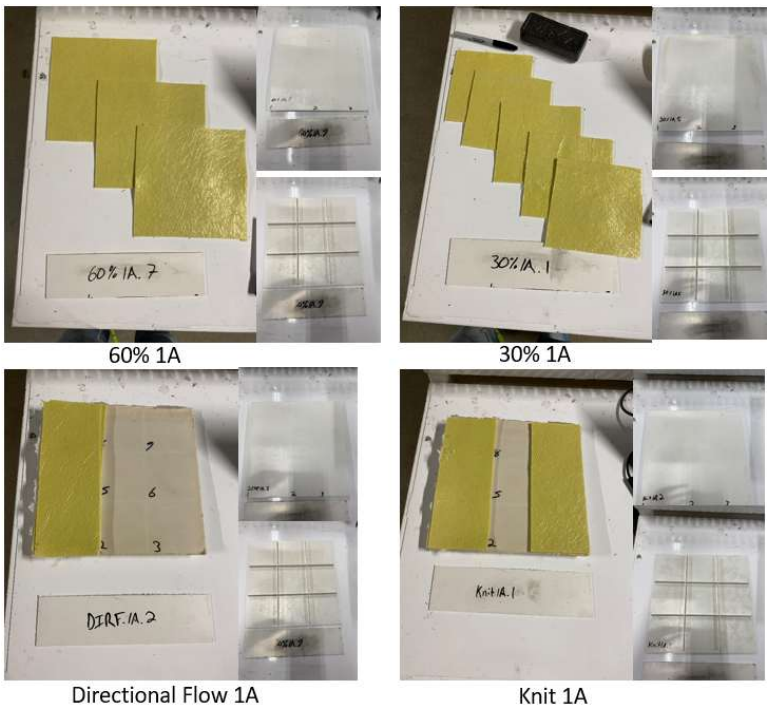

Figure 26. Shows actual 1 component charge patterns and resulting plaques

Two component systems were down-selected with the 2C combination (Class "A" SMC/Woven GF Pre-preg) being removed to save material for 3 component options. The two component charge patterns were developed to mimic the single component charges, with the number of plies evenly split between the two SMC materials i.e. 60% charge coverage was composed of two plies of Class "A" SMC and 1 ply of structural SMC, 30% coverage three plies of Class "A" SMC and 2 plies of Structural SMC, directional flow and knit line flow patterns consisted of 2 plies of Class "A" SMC and 2 plies of Structural SMC. All charges maintained the same placement as the single component systems, with the exception of the knit line charge patterns, which separated the two material types placing them on either end (See bottom photo in Figure 26). Micrographs were taken of each panel of the 3x3 squares of the rib plaque as well as the separating ribs, the resultant micrographs can be seen in Figure 27.

60% 2A

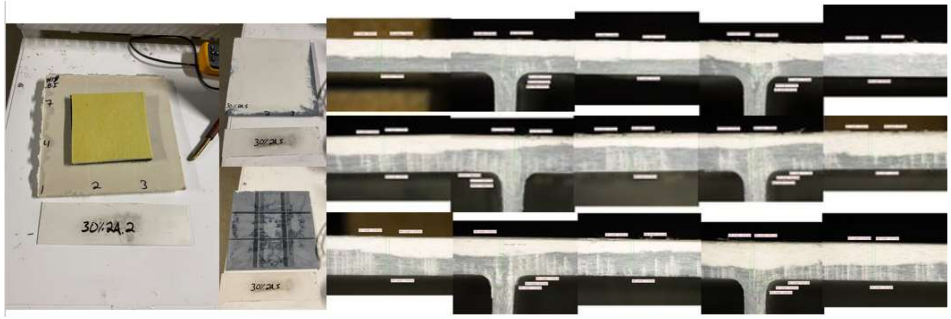

30% 2A

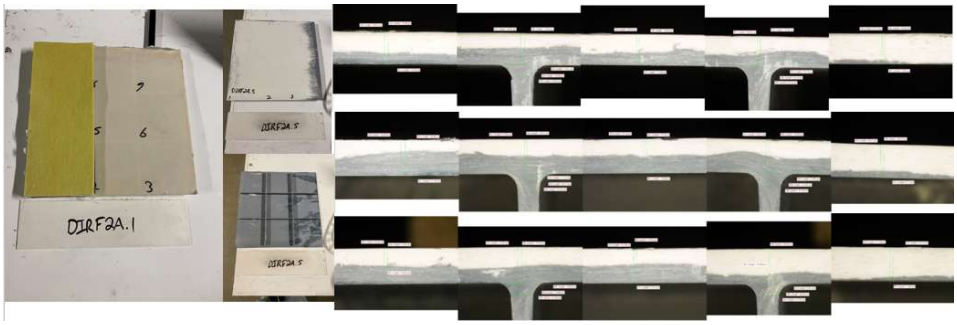

Directional Flow 2A

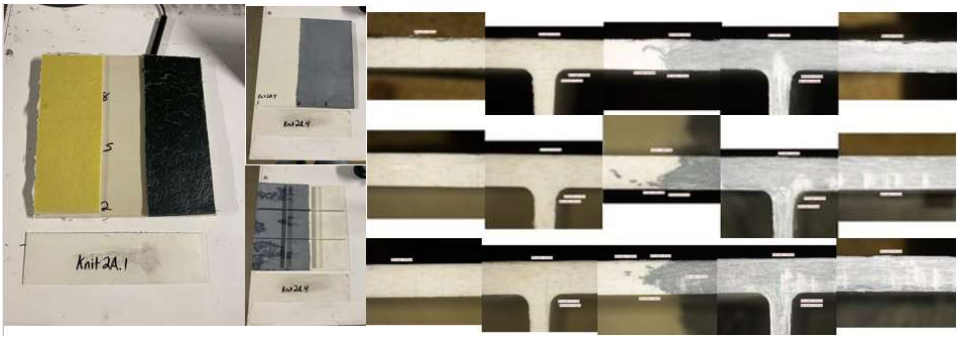

Knit 2A

Figure 27 Shows actual 2 component charge patterns, resulting plaques and layer micrographs

Both three component systems were included for study on the ribbed plaque tool to simulate the fiber distortion effects of flowing SMC over a woven pre-preg material. Figure 28 highlights the cut charges prior to being loaded into the mold. Due to woven glass fiber pre-preg's inability to flow, all pre-preg plies were cut for full coverage or 10.8" x 10.8" (allowing for fit in mold). SMC charges used in the three component systems were kept the same as the two component systems. Micrographs were then taken of each of the 3x3 squares of the rib plaque, as well as the separating ribs, resultant micrographs can be found in Figure 28.

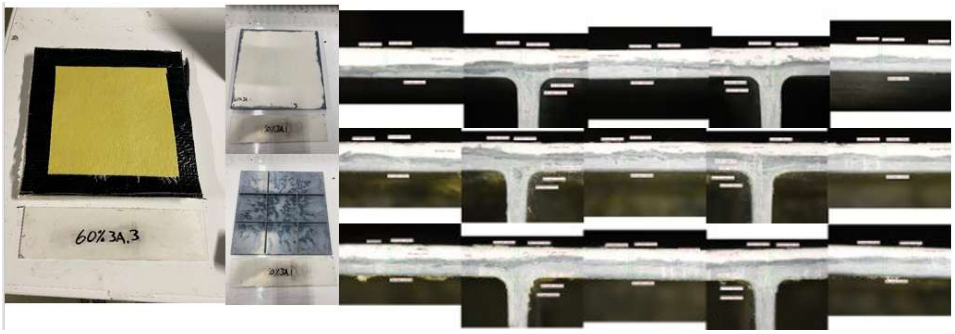

60% 3A

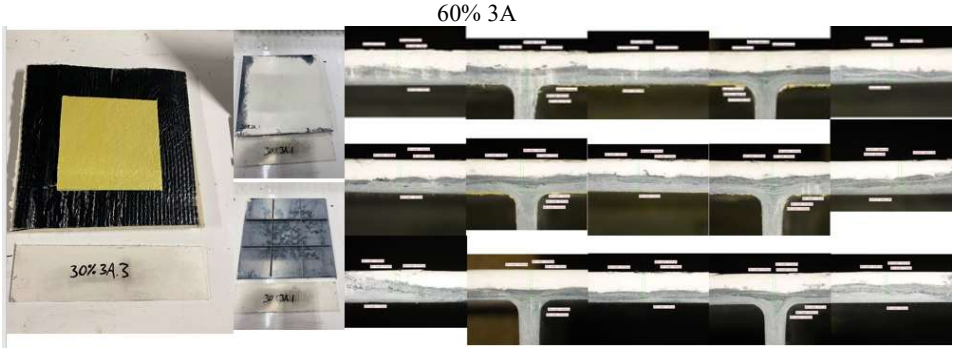

30% 3A

Directional Flow 3A

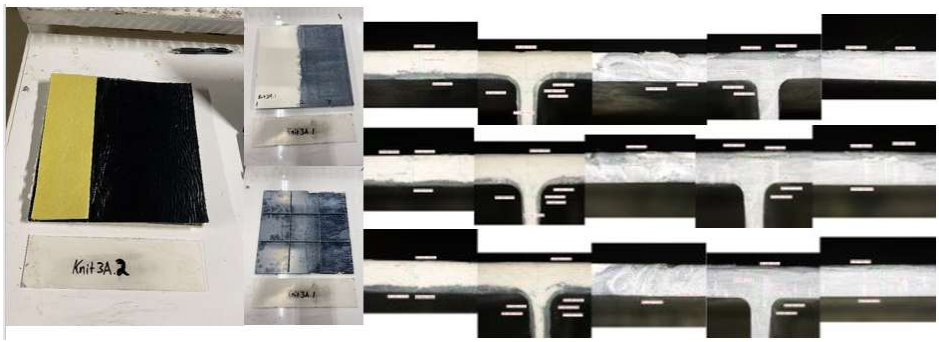

Knit 3A

Figure 28. Shows actual 3 component charge patterns, resulting plaques, and layer micrographs

All molded panels were shipped to project partners upon completion of molding operations to undergo a battery of destructive and non-destructive testing and compared against simulated panels from Purdue.

4.4. Simulation and Modeling

Simulation was used in this project to capture the material charge flow phenomena of the manufacturing process, to determine if the simulation could act as a predictor of the final material performance. This specifically includes flow front development of each material and final orientation state predictions. This was increasingly challenging due to the unique multi-material flow being analyzed, a characteristic not available for analysis using common commercial software. However, using Purdue University's existing molding simulation solution [1,2] built in Abaqus/Explicit, utilizing the Smoothed Particle Hydrodynamics method, multi-material simulations were performed. In this simulation framework, each material domain could have a uniquely effective viscosity definition. The materials vary in effective viscosity due to both their innate properties (e.g., fiber bundle length) but also their thermal history in the actual manufacturing process.

4.4.1. Use of SMC Paste Characterization

The flow of bi-material moldings on a flat plate tool was observed for both Class A and Structural SMC layers. The Class A SMC layers appeared to experience less flow; however, due to the innate material characteristics of Structural SMC layers, its structural soundness generally correlates with a higher viscosity and difficulty in processing. This conclusion from our observations was rather unexpected. However, in the physical manufacturing process, the Structural + Class A SMC charge was placed directly on the tooling surface, with the structural side in immediate contact with the heated tooling surface, resulting in a clear difference in thermal history and viscosity development of each material. Using a video recording of the process, the following process was observed:

- Top platen set to 325°F.
    - Top platen actually achieves 280-314°F.
    - This targets the top tooling surface to be 295-300°F.
- Bottom platen set to 350°F.
    - Bottom platen actually achieves 325-370°F.
    - This targets the bottom tooling surface to be 305-310°F.
- Place charge on bottom tool surface.
- Raise bottom platen and tool.
- Top tool contact with full 65-ton force.
    - There is about 16 seconds between the material charge being placed on bottom tool surface and contact with top tooling surface.
- Hold 65 ton for 2 minutes.
- Lower bottom platen and tool.

This information was used to create a simple 1D heat flow model, which could be combined with INEOS' cure kinetics and rheology data to determine effective viscosity at the time of pressing. The 1D heat transfer model considered a total 5.4 mm thick charge (2.7 mm representing a layer of Structural SMC and 2.7 mm representing a layer of Class A SMC). The material charge was initially 20°C (68°F). The lower boundary condition was a fixed temperature at 151.67°C (305°F). The upper boundary condition was set to free convection and radiation to an ambient temperature of 20°C (68°F).

As thermal material characterization was not performed on the studied materials, reference material properties were obtained for similar materials from MatWeb. From the reference ranges, we chose the low end of the specific heat range (1.10-1.51 J/g-°C) and high end of the conductivity range (0.25-0.70 W/m-K). This gave the fastest estimate of heat transfer from the lower tooling surface through the material charge. (MatWeb Material Property Data, n.d.)
(

The simulation considered the 16 second delay between the charge being placed onto the bottom tooling surface before pressure is applied. From the simulation, in these 16 seconds, the lower half of the charge (Structural SMC) experiences an average heating rate of 350 K/min, while the upper half of the charge (Class A SMC) experiences an average heating rate of 150 K/min. At the time of applied pressure, the average temperature of the lower half of the charge is 112.5°C, and the average temperature of the upper half of the charge is 60°C.

These heating rates are not obtained by any of the experimental characterization. However, in referencing the DSC data for the rates characterized and obtained by INEOS, these heating rates indicate that curing has not yet begun. Similarly, the temperature sweep rheology data was obtained at a 5 K/min rate which is quite slow compared to the thermal model predictions. At 60°C, the temperature sweep rheology for Class A SMC paste indicates a viscosity of $\sim 3 \times 10^3$ P. At 112.5°C, the temperature sweep rheology for Structural SMC paste is already experiencing the effects of curing (due to the lower temperature rate of the test). Therefore, we look at the minimum viscosity of the Structural SMC which is $\sim 1 \times 10^3$ P. Thus, from this simple investigation, we see that at the time of molding, the Structural SMC paste is at a lower viscosity than the Class A SMC paste due to the experienced thermal history. This difference will be exacerbated for thicker material charges or lower thermal conductivity. The thermal conductivity of a similar IDI material is only reported to be 0.35 W/m-K (see Figure 29).

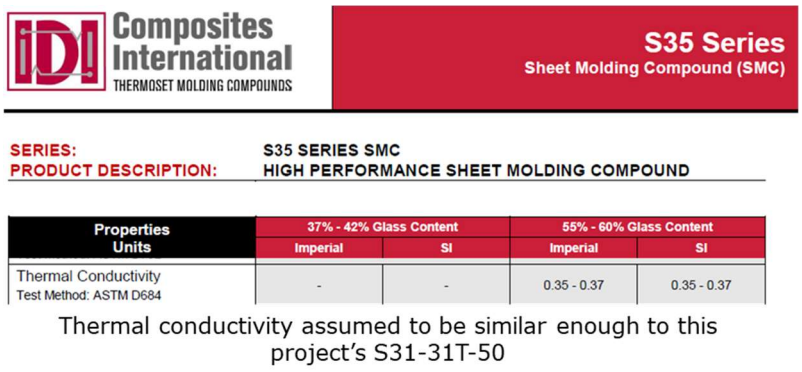

Figure 29. Thermal Conductivity Estimate from Similar Material System

4.4.2. Multi-material Flow Simulation

The goal of this project is to use manufacturing process simulation on multiple SMC materials co-molded together. In current popular flow simulations codes, simulating the flow of multiple materials each with their own respective anisotropic viscosity is not possible. Therefore, in order to perform this task, Abaqus with a VUMAT was implemented in a way to track and update local material orientation (fiber orientation) and orientation-dependent viscosity. The VUMAT tracks 9 variables related to the current material state: 3 variables represent the fiber orientation vector $\mathbf{p}$, 3 variables represent a secondary orientation vector $\hat{\mathbf{q}}$ initially transverse to $\mathbf{p}$, and 3 variables representing the stretch ratios s, w, h in the directions $\mathbf{p}$, $\mathbf{q}$, and $\mathbf{r}$ respectively where $\mathbf{r} = \frac{\mathbf{p}\times\hat{\mathbf{q}}}{\|\mathbf{p}\times\hat{\mathbf{q}}\|}$ and $\mathbf{q} = \frac{\mathbf{r}\times\mathbf{p}}{\|\mathbf{r}\times\mathbf{p}\|}$. These variables are updated in response to the deformation of each increment of the simulation and are used in the constitutive relationship that can be applied for an SMC layer or continuous fiber layer. The constitutive relationship is given as:

$$\boldsymbol{\sigma} = 2\eta\mathbf{D} + 4\eta(R_1 - 1)\mathrm{dev}(\mathbf{pppp}:\mathbf{D}) + 4\eta(R_2 - 1)\mathrm{dev}(\hat{\mathbf{q}}\hat{\mathbf{q}}\hat{\mathbf{q}}\hat{\mathbf{q}}:\mathbf{D})$$
$$+E_1(s-1)\mathrm{dev}(\mathbf{pp}) + E_2(w-1)\mathrm{dev}(\hat{\mathbf{q}}\hat{\mathbf{q}}) + K(\det(\mathbf{F}) - 1)\mathbf{I}$$

where $\mathbf{D} = \mathrm{dev}(\Delta\boldsymbol{\epsilon}/\Delta t)$. The materials parameters are the isotropic portion of the viscosity η, the anisotropic contribution to viscosity of the primary fiber direction R_1, the anisotropic contribution to viscosity of the secondary fiber direction R_2, a penalizing elastic modulus in the primary fiber direction E_1, a penalizing elastic modulus in the secondary fiber direction E_2, and a penalizing bulk modulus K. For an SMC layer, only η, R_1, and K are non-zero, while all parameters are used for a fabric layer. Typically, R_1 is set to 100 to resist extensional flow in the fiber direction, and K is adjusted so that negligible volumetric strain occurs in the simulation.

Initial simulations were performed considering a bi-material plate with a single layer of Structural SMC and single layer of Class A SMC. They were initialized with 3 particles per layer thickness and with an initial viscosity ratio from the minimum viscosities observed for each paste. The Class A paste reaches a minimum of $\sim$900 P while the Structural paste reaches a minimum of $\sim$1100 P. This provides about a 1.2:1 viscosity ratio between the two material charges. This simulation showed nearly equal flow of each layer with the Class A progressing slightly faster than the Structural as expected by the input viscosity ratio. However, this was the opposite behavior as witnessed in experimentation. Following the initial simulation, a trial simulation was performed with a viscosity ratio of 1:2 as an investigation of if observed behavior would result from this ratio. More relative material flow was seen and in a consistent manner with the experimental observations with some of the lower viscosity charge reaching the edges of the part sooner and becoming viewable from the upper surface (edge bleed-through). These results are shown in Figure 30.

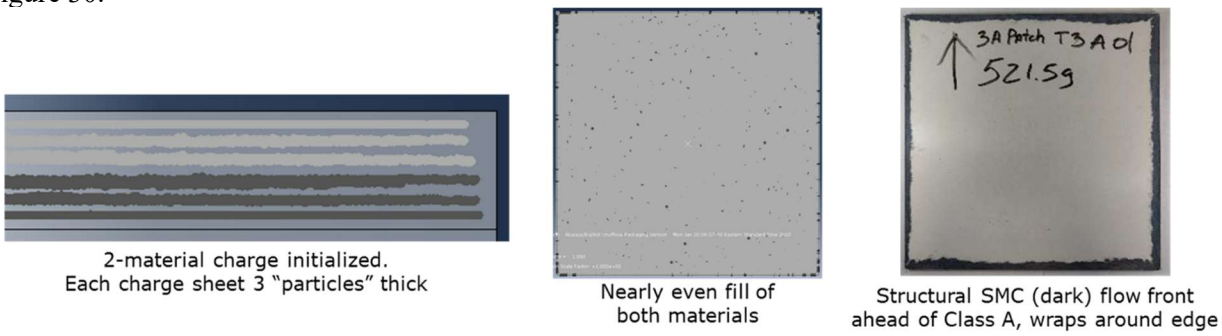

Figure 30. Multi-Material Flat Plate Molding Simulation with Matching Material Interface in Final Plates

Following the flat plate molding-modeling iteration, the thermal investigation of Section 4.4.1 was performed revealing a likely viscosity ratio exceeding 3 to 1 (Structural to Class A) under two SMC sheet processing conditions with a larger viscosity ratio for thicker charges.

An initial ribbed plate molding simulation was performed considering 1 layer of Structural SMC (on the ribbed side) and 1 layer of Class A SMC (on the flat side) and the 1:3 viscosity ratio determined by the heat transfer investigation. The resulting filling pattern is shown in Figure 31. An equivalent molding trial was not conducted, but the initial results demonstrate the potential for edge bleed of the structural visible from the Class A side and the Class A showing near the rib roots due to the ribs requiring more material to fill than the flat sections.

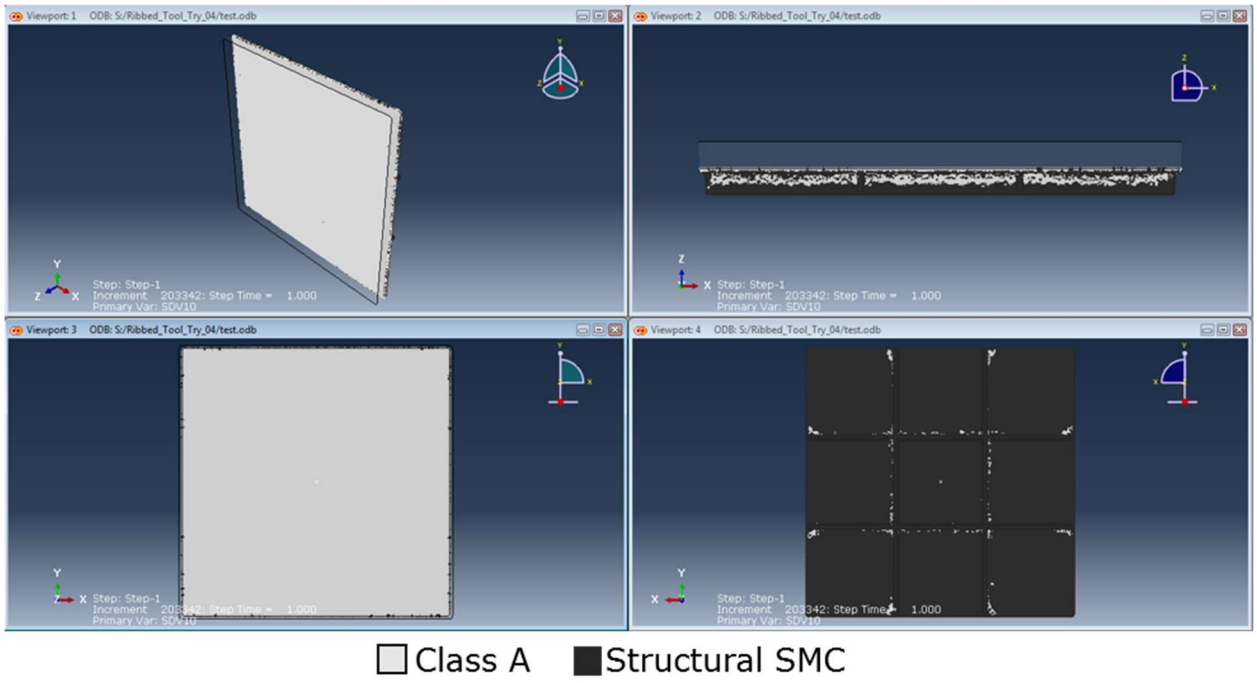

Figure 31. Ribbed Plate Molding Simulation with Class A and Structural SMC Properties. Charge cavity transparent, ribs seen in bottom right.

A subsequent ribbed plate molding simulation was performed intending to replicate the 30% charge coverage, 2A material combination series of molding trials. This series had 3 layers of ½" Structural SMC and 2 layers of Class A SMC. Here, we used a viscosity ratio of 1:10 due to the larger thickness of the charge. The resulting material distribution can be seen in Figure 32 showing good comparison with the edge bleed seen in the experiment.

An equivalent simulation was performed to replicate the 60% charge coverage, 2A material combination series of molding trials. This series had 2 layers of ½" Structural SMC and 1 layer of Class A SMC. The resulting material distribution can be seen in Figure 33. In the 30% coverage case, 60% of the material is Structural SMC, while in the 60% coverage case ~67% of the material is Structural SMC. Due to this fact alone, it may be suspected that there will be more edge bleed of Structural SMC. Nevertheless, due to the experiencing less total flow, the relative flow of the separate materials is less extreme and less edge bleed is seen in the 60% coverage case as compared to the 30% coverage case in both the simulations and experiments.

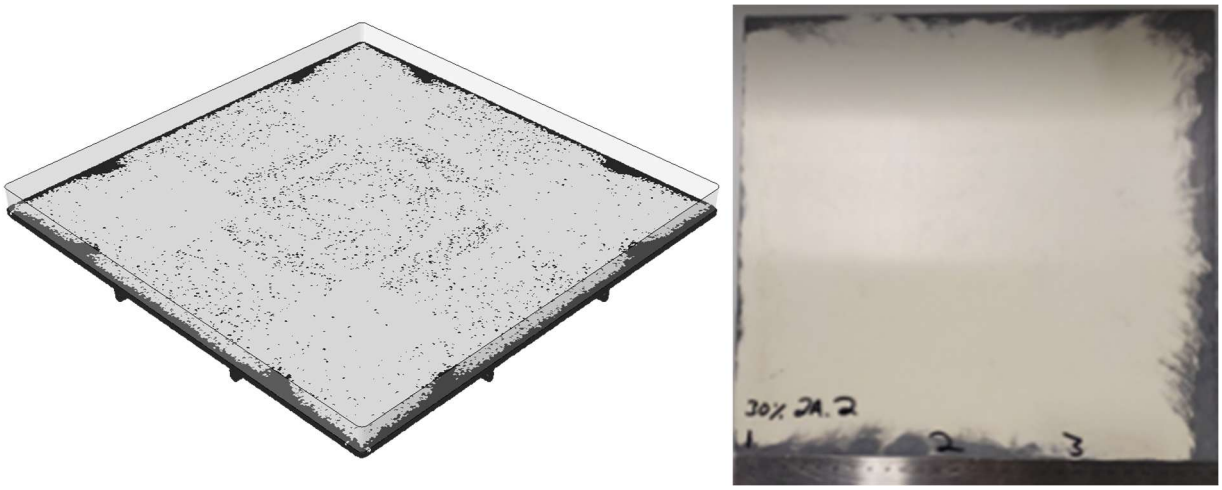

Figure 32. Ribbed Plate Molding Simulation Result for Class A + ½" Structural SMC and Photo of Actual Molded Plate. 30% Coverage. 2A Material Combination.

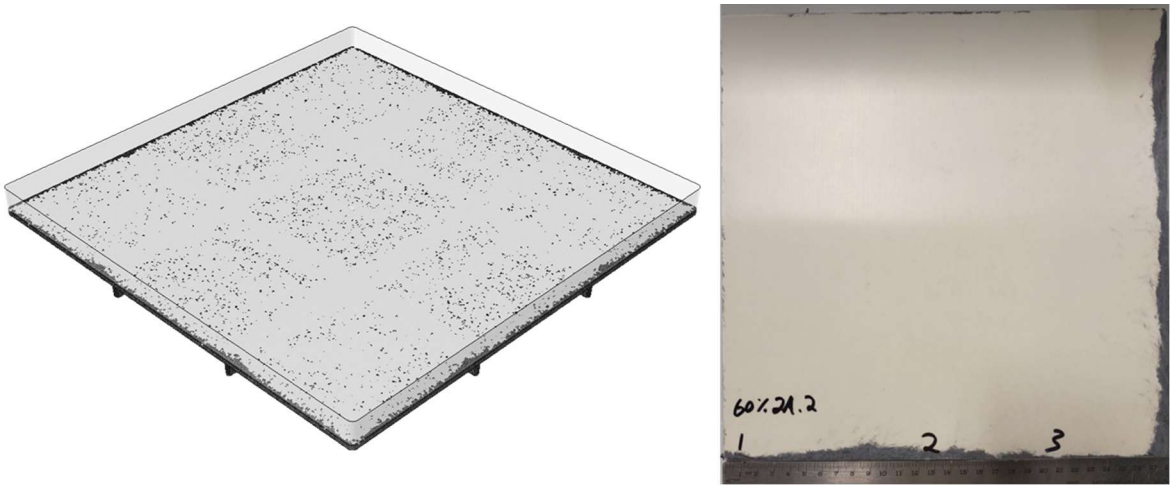

Figure 33. Ribbed Plate Molding Simulation Result for Class A + ½" Structural SMC and Photo of Actual Molded Plate. 60% Coverage. 2A Material Combination.

Theoretically, the anisotropic contribution to viscosity due to a fiber bundle increases with the square of the fiber bundle aspect ratio. To this end, a simulation for comparison with the 30% coverage, 2B material combination was performed with the same 1:10 viscosity ratio (η) but increasing the anisotropy ratio of the Structural SMC from $R_\eta = 100$ in the previous simulation to $R_\eta = 400$ due to the increased bundle length moving from the ½" Structural SMC to the 1" Structural SMC. The resulting fill is shown in Figure 34. Here, we see the edge bleed is reduced as compared to the 2A simulation. However, the experimental observation shows a completely reversed trend where the edge bleed occurs in the opposite direction. This indicates that a further increase in viscosity is seen when moving from the ½" to 1" Structural SMC than supposed.

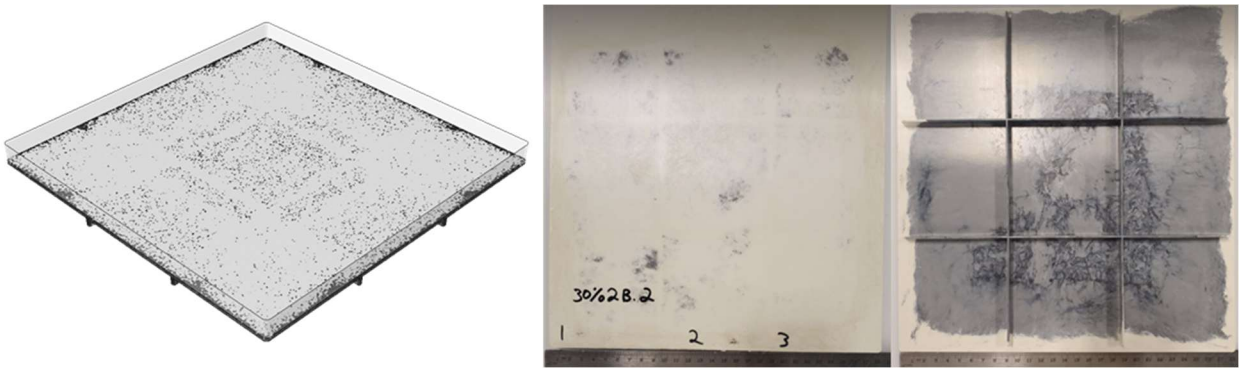

Figure 34. Ribbed Plate Molding Simulation Result for Class A + 1" Structural SMC and Photo of Actual Molded Plate. 30% Coverage. 2B Material Combination.

A final investigation was performed considering the 3A material combination and the 60% coverage setup. This simulation required the full constitutive model discussed previously for a single fabric layer between one layer of Class A SMC and one layer of ½" Structural SMC. Due to the thinness of the fabric layer, only a single layer of Smoothed Particle Hydrodynamics (SPH) particle elements could be used to represent the fabric without excessively increasing the model size. The prepreg layer was modeled with $R_1 = R_2 = 100$ and $E_1 = E_2$ treated as penalties to prevent extension in the fiber direction. Unfortunately, the simulation encounters errors once the fabric layer must start slightly entering the rib sections. The inextensible and incompressible penalty imposed upon the fabric layer provides significant numerical difficulty. Figure 35 shows the state of the simulation at the time of encountering numerical errors. The entire upper surface has reached its near final configuration, while the ribbed sections have yet to complete filling. Figure 36 shows the top view of the corresponding molding trial. Clearly, the simulation is capturing the effect of the fabric layer in greatly limiting the amount of flow of the upper SMC layer. Further study is required to determine the root of the encountered numerical issues including mesh refinement, solver parameters, and potentially modeling the fabric layer as shell elements with contact with the SPH modeled SMC layers.

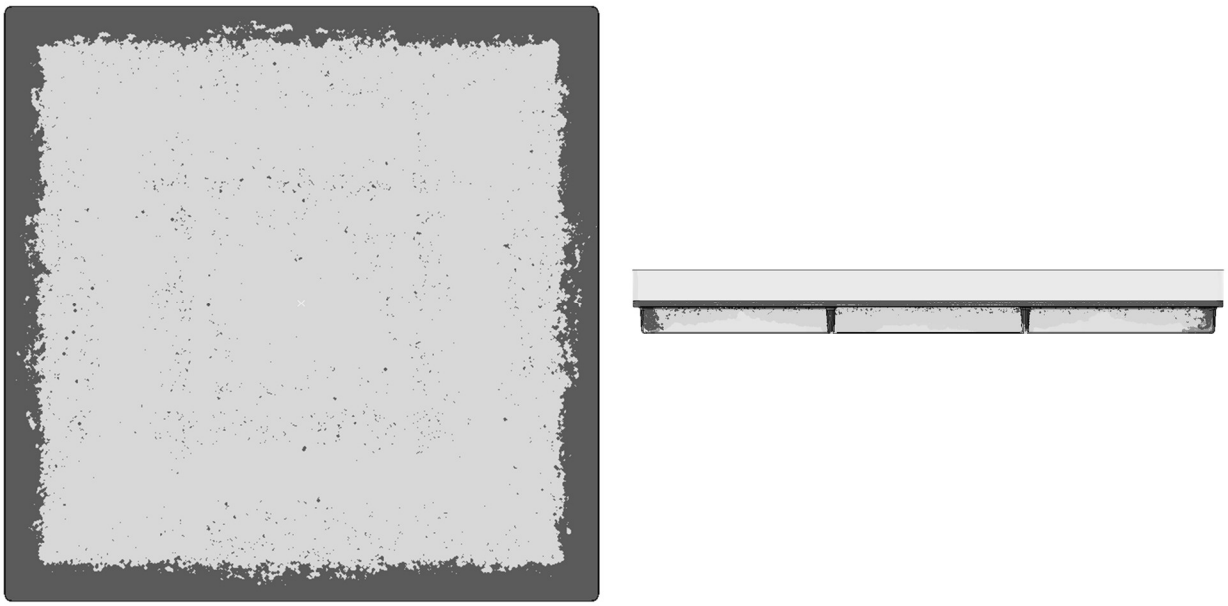

Figure 35. Ribbed Plate Molding Simulation Intermediate Result for 3A Material Combination (SMC layers in White, Fabric Layer in Black). Top view Left. Side view Right.

Figure 36. Top View of Ribbed Plate 60% Coverage with 3A Material Combination.

The diagonals of the orientation tensor were extracted for simulation results of 1A 30%, 1A 60%, 2A 30%, and 2A 60% as an average from the 75% to 85% of the plaque from the flat portion and ribs as diagramed in Figure 37. The resulting tensor components are shown in
Table 9. Here, we see the expected result for a center charge in that $\mathbf{A}_{xx}$ and $\mathbf{A}_{yy}$ are approximately equal in the flat section but with slight preference for the **x**-direction in the region chosen likely due to the influence of the ribs in acting as flow channels allowing easier **x**-directional flow than **y**-directional flow. Additionally, we see the **z**-directional alignment increases and **y**-directional alignment decreases steeply when moving from the flat section into the ribs.

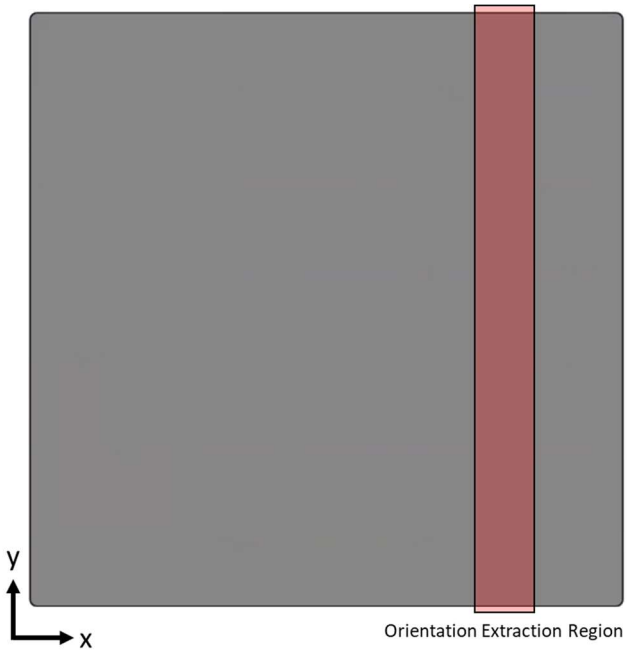

Figure 37. Diagram of Orientation Extraction Region

Table 9. Average Orientation Results from Modeling

		1A 30%	*1A 60%*	*2A 30%*	*2A 60%*
Flat	$\mathbf{A}_{xx}$	0.488	0.501	0.496	0.495
	$\mathbf{A}_{yy}$	0.488	0.488	0.470	0.488
	$\mathbf{A}_{zz}$	0.024	0.011	0.034	0.018
Ribs	$\mathbf{A}_{xx}$	0.615	0.580	0.596	0.627
	$\mathbf{A}_{yy}$	0.135	0.132	0.165	0.139
	$\mathbf{A}_{zz}$	0.250	0.289	0.239	0.234

The results here do not compare perfectly with the inspection performed in Section 4.5.2.1 Microscopy. That microscopy was performed at very localized sites, which considering the fiber bundle nature of the composite contain local snapshots of only a few bundle mesostructures. Very broadly, both the microscopy and flow simulation show low Aij diagonal terms in the through thickness direction of the local microstructure as expected. For a better validation exercise, even more microscopy would have to be performed to homogenize orientation state over a comparable inspection region to the simulation analysis above.

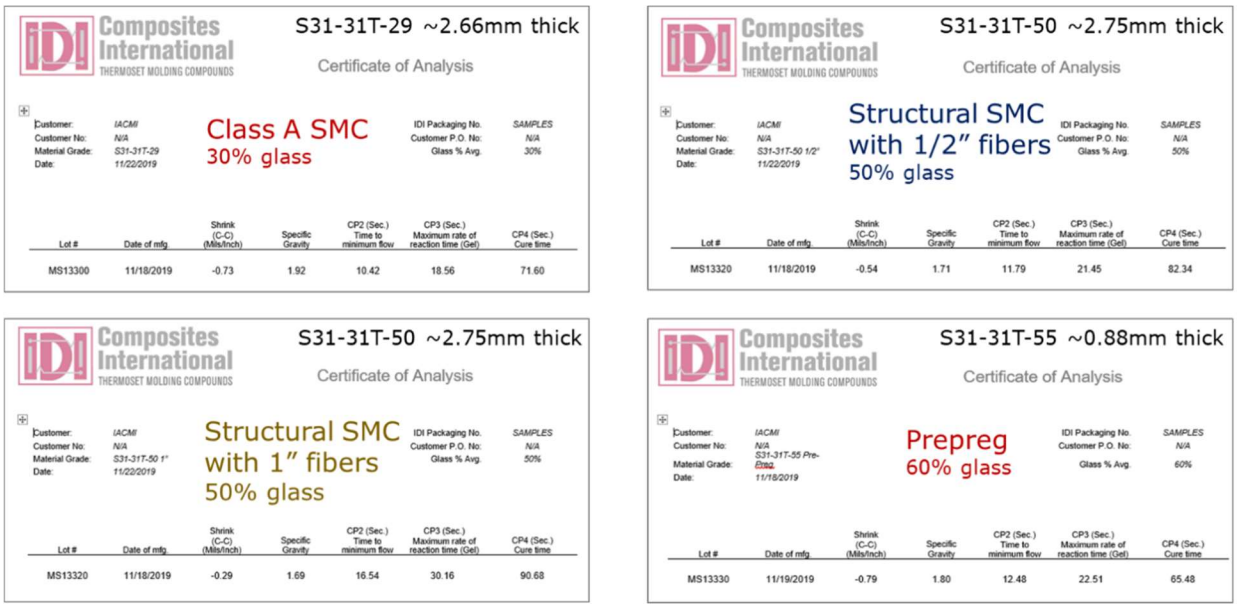

Figure 38. Basic Properties of Four Candidate Materials for this Study

Georgian Bay Reinforcement Fabrics

WOVEN ROVING
PRODUCT SPECIFICATION

Issued: August, 2002
Revised: April, 2014

Product:		**R24-A01** Can be made with E glass of ECR Glass		
		Metric	SAE	
Style:		R24	R24	
Finish:		A01 (Polyester, Vinyl Ester, Epoxy and Acrylic Resin Compatible)	A01	
Weave:		Plain	Plain	
Construction	Warp: Weft:	19.7 /10cm (+/- 1) 16.8 /10cm (+/- 1)	5.0 /inch (+/- 0.3) 4.3 /inch (+/- 0.3)	ASTM D-3775
Yarn	Warp: Weft:	2200 tex 2200 tex	225 yield 225 yield	
Weight		813 g/m² (+/-5%)	24 oz/yd² (+/-5%)	ASTM D-3776
Thickness:		0.75 mm (+/-0.3)	0.030 inches (+/-0.004)	ASTM D-1777
Packaging Core:		77.01 mm ID Core	3.0 inch ID Core	
Available Widths:		76 mm to 1980 mm	3 inch to 78 inch	

All values above are nominal and are to be used as guidelines.
Although all statements are believed to be accurate and reliable, they are presented without guarantee or responsibility on our part.

Georgian Bay Reinforcement Fabrics

Figure 39. Woven Fiber Architecture Details Matching the Woven Prepreg Studied

(Favaloro, 2017; Favaloro AJ, 2018)

4.5. Characterization of Molded Parts

Other than the mechanical characterization of flat plates in Section 4.1.4 that was used to determine effective properties for single and combined materials, a number of other non-destructive and destructive methods were used to investigate the results of multi-material molding. Some methods were investigated as options for future studies, some for validation of flow simulations, and some to investigate manufacturability with different charge designs.

One of the manufacturing studies involved placing undersized prepreg “patches” between class A and structural SMC charge sheets. These patches were in various configurations shown in Figure 40, and represented the possibility that a hood or other component would require only local reinforcement with continuous fiber materials.

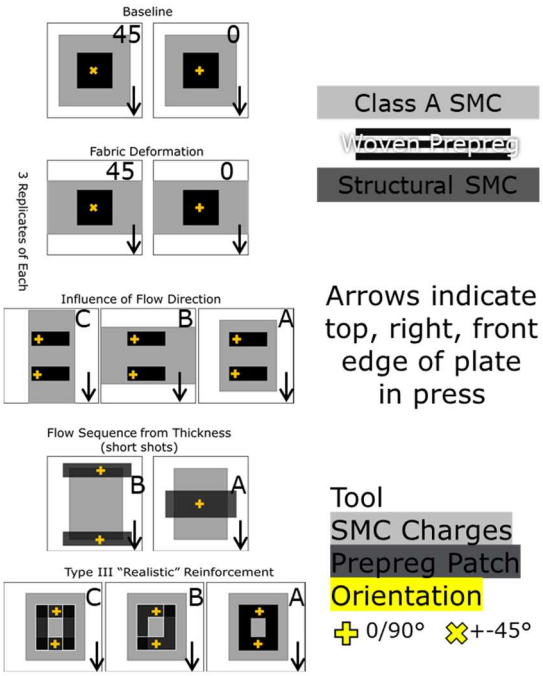

Figure 40. Prepreg Patch Molding Experiment Charge Diagrams

It was of interest to see how the SMCs would flow around the patches, how the patches might deform or translate with flow, and whether a class A surface could be maintained. While describing the various inspection methods employed, this study may be used as an example case.

4.5.1. Non-Destructive Methods

Wherever possible, non-destructive inspection methods are employed to characterize molded parts. Some of these methods utilize qualitative observations, and some lend themselves more easily to quantified measurements. The purpose here was to investigate various methods of inspection that could be used on development or final parts in order to assess the part geometry, surface quality, and boundaries of visible or embedded constituent materials. Ultrasonic, X-ray, and surface quality analysis showed some success while the thermographic methods here were very limited.

4.5.1.1. Visual Inspection

Photographs and direct observations were insightful in many cases to determine how the co-molded materials behaved as they transitioned from their charge positions to final, filled states. Figure 41 shows one example of an intentional short-shot where the tool was prevented from closing entirely in order to see how the flow front develops. This can be very useful for comparison with flow simulations. In this specific case the charge was already covering much of the tool surface and the flow front development is not as meaningful as it might be for a 30% area coverage charge. However, there is some apparent interaction at the boundary of the SMC and continuous fiber prepreg patch.

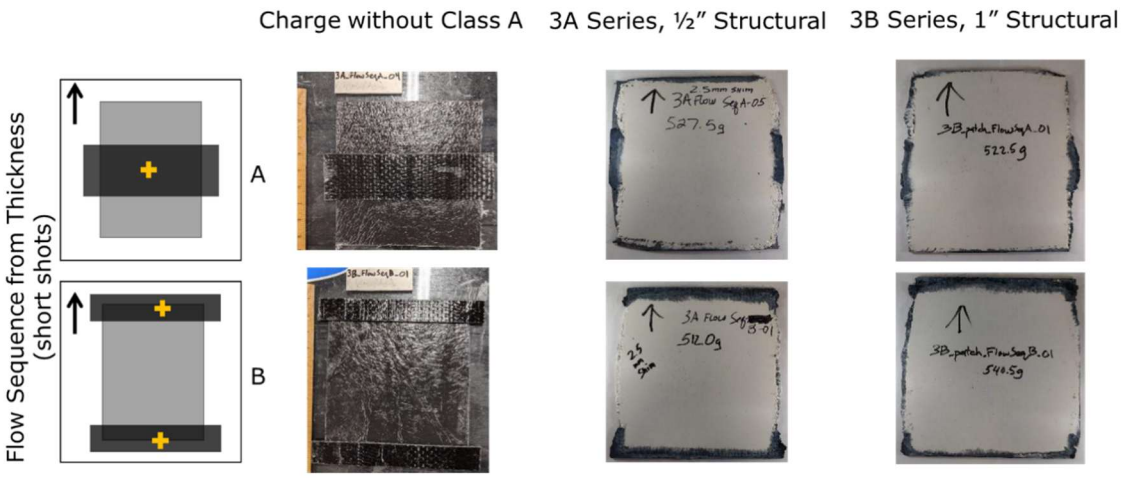

Figure 41. Prepreg Patch Experiment Short Shot Charge and Results

Figure 42 shows another continuous fiber patch case where "window frames" were created with one, two, or four pieces of prepreg and placed in the center of the SMC charge area. In all of these cases the structural (darker) SMC with ½" long fibers appear to have flowed earlier and reached the tool boundaries before the class A SMC, resulting in edges dominated by the structural material.

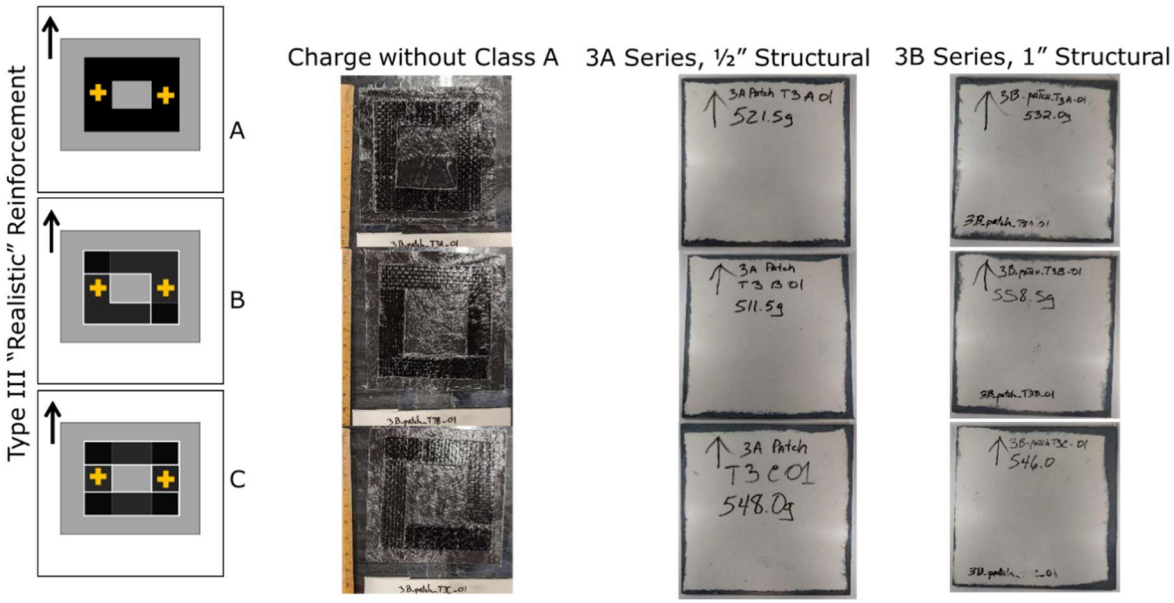

Figure 42. "Window Frame" Prepreg Patch Molding Experiment and Results

Variations in the size of that structural SMC bleed-through indicate variability that may need to be accounted for in production, where the class A surface should not have any material other than the class A SMC visible. Because the cure profiles of both class A and structural SMC pastes were very similar, the likely culprit behind this difference in flow is thermal history. This observation encouraged investigation to see if the structural material was going through a drop in viscosity earlier than the class A, which it was.

4.5.1.2. Micrometer Measurement

As part of cataloging all of the plates manufactured, caliper or micrometer measurements of edge thickness were taken at MSU-SuRF and Purdue. For the flat plate molding series that was used in material characterization, all plates received by Purdue were measured at eight points around their perimeter with a digital micrometer. That data is manipulated in two ways to create the plots in Figure 43; first using the average thickness of each plate and then using all the individual measurements.

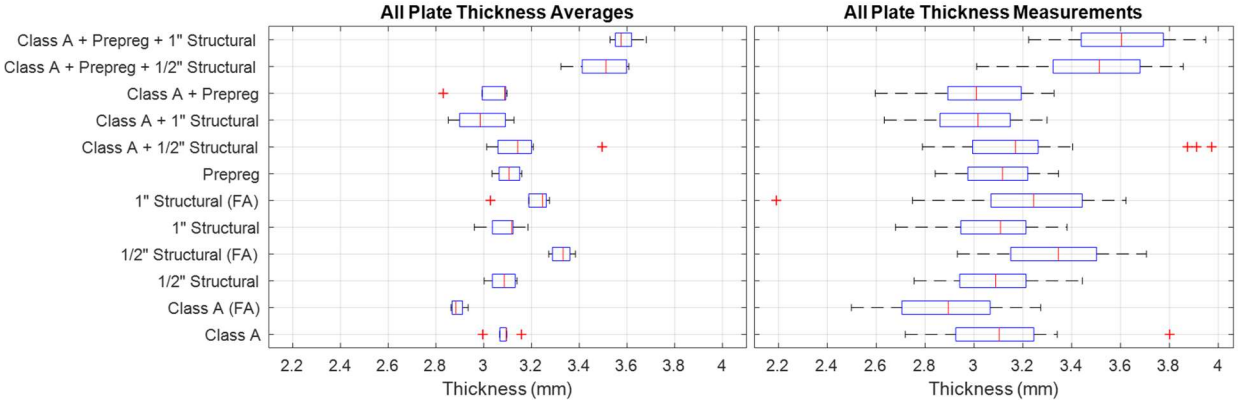

Figure 43. Flat Multi-Material Plate Thicknesses and Distributions for Plate Averages and All Individual Measurements

The difference in the two box plots illustrates how variable the thickness within each plate could be. Out of 69 center-charge plates, the average standard deviation in thickness was 0.18mm and for the 15 flow aligned plates it was 0.24mm. It is not too surprising that with increased material deformation, the flow aligned plates have slightly higher thickness deviations.

4.5.1.3. Ultrasonic

Non-destructive inspection or evaluation typically infers more than just external observation. Four inspection methods were used to try to determine the location of the prepreg continuous fiber patch material inside of molded SMC plates. The first discussed is ultrasonic C-scans performed by University of Tennessee Knoxville (UTK) with the guidance of Dr. Vaidya and Dr. Penumadu' s labs.

It was proven that the excitation signal passed through the molded plates was altered sufficiently to outline the position of prepreg patches as shown in Figure 44.

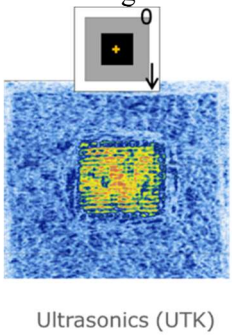

Figure 44. Ultrasonic C-Scan Image from UTK Showing Prepreg Patch at Center of Flat Plate

Performing this analysis on non-flat geometries would likely require a surface-normal-following ultrasonic transducer. This method does show promise if it is desirable to investigate the final position of any internal reinforcements having sufficiently different micro- and meso-structures from the SMCs.

4.5.1.4. 2D X-Ray

UTK also assisted with some x-ray scan time and provided the results for a centered prepreg patch and a "window frame" prepreg patch seen in Figure 45.

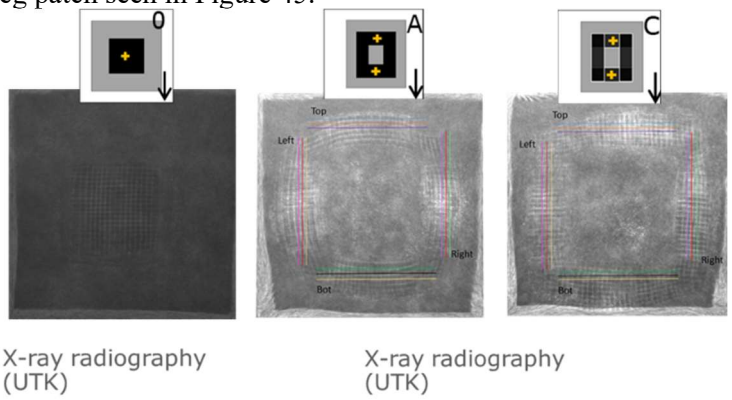

Figure 45. 2D X-Ray Images of Prepreg Patches in Flat Plates with Patch at Center (left) and Window Frame Patch (right 2)

The contrast of the images is inherently a function of the material density and x-ray equipment but can be altered for easier visualization via normal image processing. This will not create new information that does not exist, but may make it easier for a viewer to observe the internal structures. The displacement of the window frame patches was investigated. Pattern A was made from a single continuous piece of woven prepreg, while pattern C was made from four separate pieces of prepreg. Figure 46 shows the slight differences in the flow-deformed final patch locations.

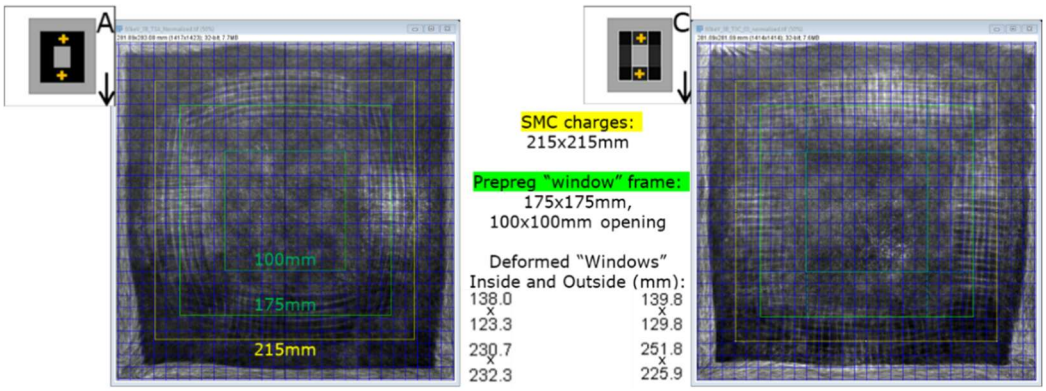

Figure 46. 2D X-Ray of Flat Plates with Window Frame Prepreg Patches Showing Initial and Final Patch Locations

The initial prepreg charge locations are shown in green lines, while the yellow shows the initial SMC charge edges. The final maximum deformed widths and heights are shown in Figure 46 as well as in Table 10.

Table 10. Initial and Final Dimensions of Window Frame Prepreg Patches for Two Patch Patterns

		W_0 (mm)	H_0 (mm)	W_1 (mm)	H_1 (mm)	ΔW (mm)	ΔH (mm)
Frame Pattern A	Class A SMC	215	215	267	268	+52	+53
	Struct. SMC	215	215	280	280	+65	+65
	Prepreg (outer)	175	175	231	232	+56	+57
	Prepreg (inner)	100	100	123	138	+23	+38
Frame Pattern C	Class A SMC	215	215	265	267	+50	+52
	Struct. SMC	215	215	280	280	+65	+65
	Prepreg (outer)	175	175	225	252	+50	+77
	Prepreg (inner)	100	100	130	140	+30	+40

These measurements were taken at the points of greatest deformation. The quantified changes in width and height show that SMC deformations were very repeatable, as expected because they end at the tool cavity edge. The prepreg deformations were less consistent. The same is seen visually in the bar chart of Figure 47.

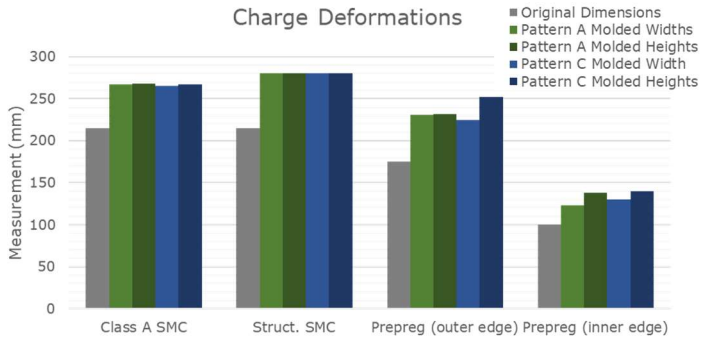

Figure 47. Displacements of Two Window Frame Pattern Prepreg Patch Charge Materials

The X-ray seems to clearly show the internal prepreg structure, successfully identifying the orientation of the tows within the prepreg, therefore supporting this method for non-destructive inspection of panels. The method may also work well for panels with some curvature such as an automotive hood, however the object must be able to be positioned in front of a large sensor panel, to record a proper reading.

4.5.1.5. Thermography Attempt

There was hope that non-destructive thermography would be able to capture the internal structure of a three-material plate containing continuous fiber prepreg. At the recommendation of more experienced thermography users, two 1200W/s flash sources were purchased and used to investigate. The first test had three carbon fiber with polyetherketoneketone (PEKK) plies taped to the outside of one of the co-molded panels to provide a baseline of effectiveness with the Forward Looking Infrared (FLIR) camera. Figure 48 shows the initial test setup.

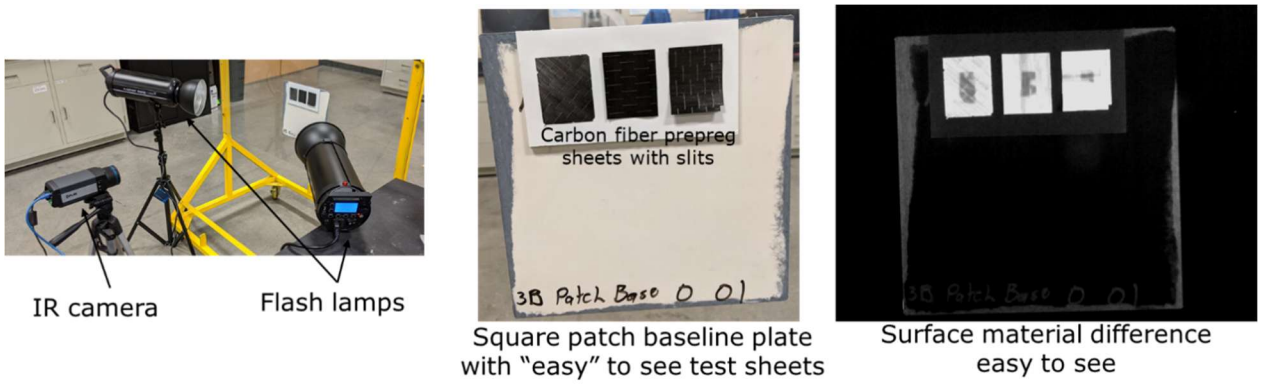

Figure 48. Flash Thermography Setup and Baseline Example with External CFRP Rectangles

The thermal contrast between the carbon fiber squares, the class A SMC, and the structural SMC was very clear, but offered no improvement over what could be seen with the eye or normal photography. Next the panel was imaged alone, and analysis was attempted with default visualization and other image analysis methods. As seen in Figure 49 none of the attempted methods were very successful in showing internal features.

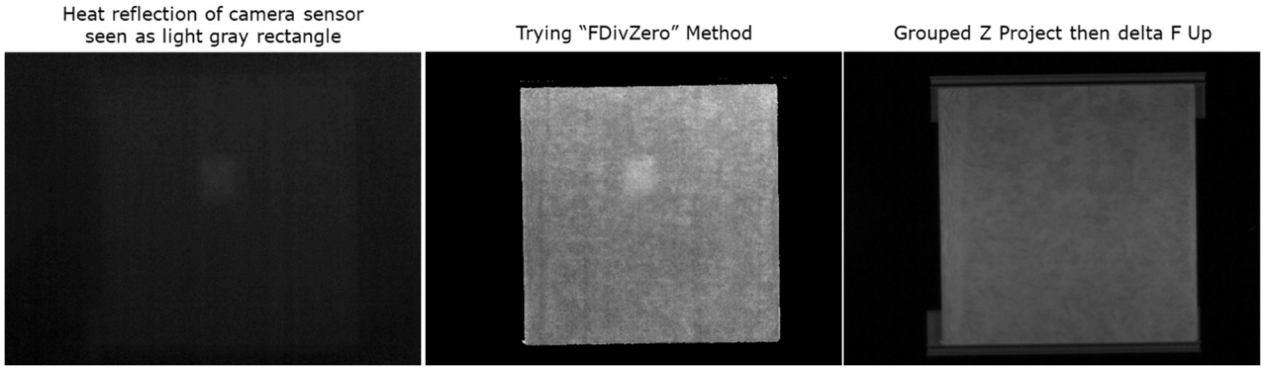

Figure 49. Three Thermography Attempts to Discern Prepreg Patches Inside Flat Plates

The lighter rectangle seen on two of the three attempts was a reflection of the camera lens/sensor. It was decided that flash thermography did not induce sufficient thermal energy into the sample plate to see "inside" the relatively thick panels. Also, the heterogeneous nature of the SMC also made distinct feature detection difficult. Obviously, thermography has been used successfully, especially in highly ordered Carbon Fiber Reinforced Polymer (CFRP) laminate systems, where a flaw such as a crack or large void may have an extremely different thermal "signature" than the surrounding material. Here it was not successful.

4.5.1.6. Surface Quality

Surface appearance was evaluated by measuring the curvature of the surface of the molded panels. INEOS Composites measured the curvature utilizing their QualiSensor test plaque inspection system. The QualiSensor utilizes the Snell-Descartes law of light reflection. The law states that the angle of incidence and the angle of reflection are equal. An imperfect surface will change the angle of reflection. The QualiSensor system projects a periodic pattern of alternating horizontal and vertical black and white stripes on to a plaque. The reflection is then captured by a camera and the system calculates curvature profiles. The standard deviation of the slope curves is used to evaluate the flatness of the surface. A perfect surface would have a standard deviation of zero. The QualiSensor system also filters the surface

curvature maps into five different wavelengths. The filters are as follows:

- A wavelength: 0.1 mm – 0.3 mm
- B wavelength: 0.3 mm – 1.0 mm
- C wavelength: 1.0 mm – 3.0 mm
- D wavelength: 3.0 mm – 10.0 mm
- E wavelength: 10.0 mm – 30.0 mm

The shorter wavelengths, A and B, give an indication of the amount of short-term waviness, often referred to as orange peel. The C and D wavelengths give an indication of the longer-term waviness and the E wavelength is an indication of part shape and warp. The standard deviations of the curvature maps are measured and reported for each of the wavelengths.

Three series of test were performed to evaluate the effect of the different materials on the surface appearance. First, MSU-SuRF molded 9 combinations of materials on a flat plaque tool. The following combinations were molded:

- 1A: 1 component, Class A
- 1B: 1 component, ½" fiberglass structural SMC
- 1C: 1 component, 1" fiberglass structural SMC
- 1D: 1 component, continuous fiber prepreg
- 2A: 2 component, Class A + ½" structural SMC
- 2B: 2 component, Class A + 1" structural SMC
- 2C: 2 component, Class A + continuous fiber prepreg
- 3A: 3 component, Class A + continuous fiber prepreg + ½" structural SMC
- 3B: 3 component, Class A + continuous fiber prepreg + 1" structural SMC

The standard deviations from the C and D wavelength curvature profiles are given in Table 11 and Figure 50. The results indicate that all samples with a Class A component (1A, 2A, 2B, 2C, 3A, 3B) were statistically the same and had better surface appearance than the samples without a Class A component. The one component prepreg sample (1D) had the worst overall surface appearance.

Table 11. Surface appearance of flat plaques with different combinations of materials.

Description	N	Mean Curvature SD C wavelength (1/m)	Mean Curvature SD D wavelength (1/m)
Class A	5	1.8698	0.3941
Class A/ structural 1/2"	5	1.7972	0.4049
Class A/Prepreg	5	1.7036	0.3689
Class A/Prepreg/Structural 1"	9	1.9161	0.6297
Class A/Prepreg/Structural 1/2"	5	1.9194	0.4405
Class A/Structural 1"	5	1.8554	0.3841
Prepreg	4	2.6755	1.4312
Structural 1"	5	2.2460	0.6504
Structural 1/2"	5	2.1872	0.5869

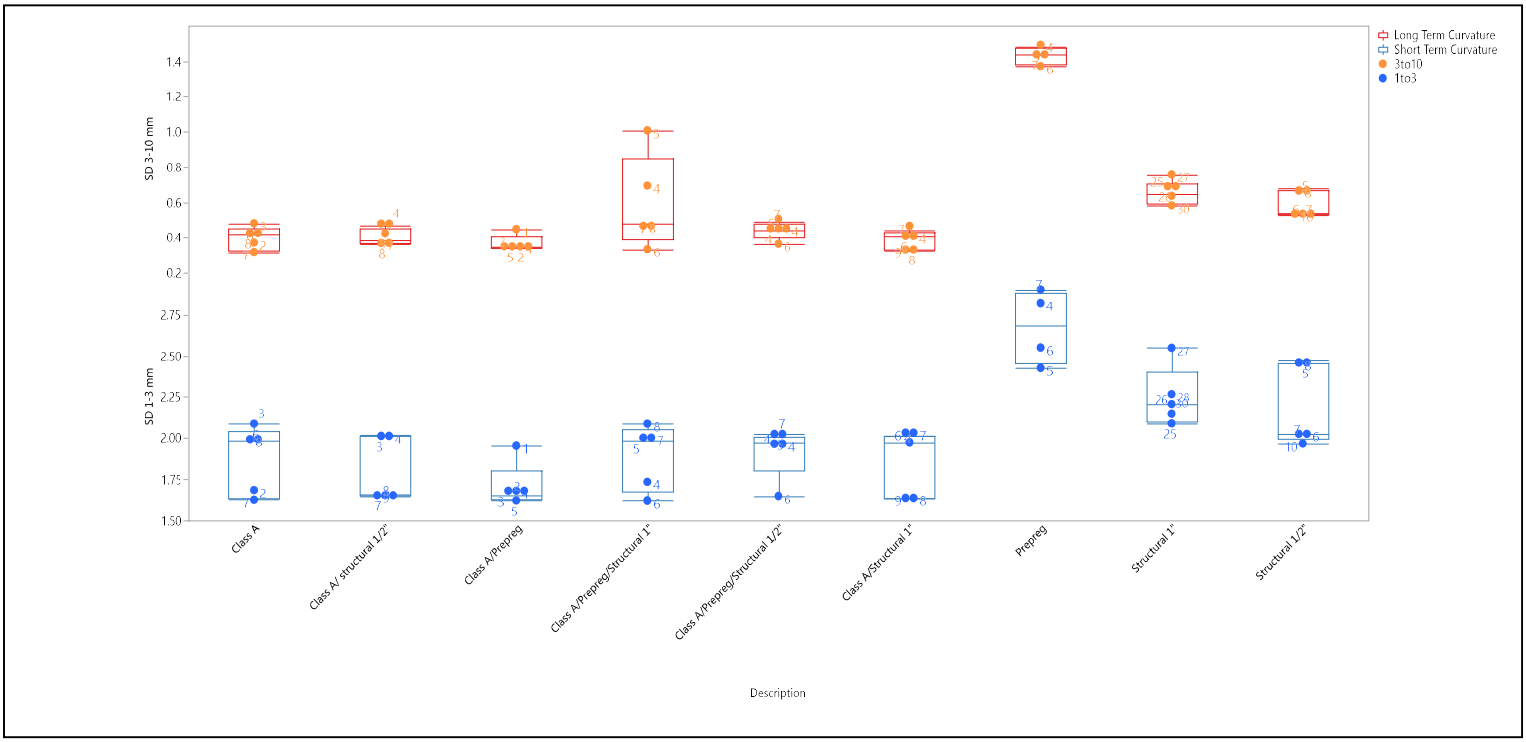

Figure 50. Surface appearance of flat plaques molded with different combinations of materials.

The single component Class A plaques, 2 component plaques containing Class A SMC and the Class A + Continuous Prepreg + ½" Structural SMC were primed and painted. The QualiSensor was used to evaluate the surface appearance after priming and after the final paint was applied. The results of the primed samples are shown in Table 12.

Table 12. Surface appearance of primed flat plaques molded with different combinations of materials.

Description	N	Mean Curvature SD A wavelength (1/m)	Mean Curvature SD B wavelength (1/m)	Mean Curvature SD C wavelength (1/m)	Mean Curvature SD D wavelength (1/m)	Mean Curvature SD E wavelength (1/m)
Class A	4	2.531	3.5233	2.3075	0.5085	0.1350
Class A/1" Structural	4	2.5068	3.3348	2.0768	0.5788	0.2111
Class A/1/2" Structural	5	2.7432	3.6716	2.2390	0.5793	0.1679
Class A/Continuous Prepreg/1/2" Structural	3	2.5727	3.4967	2.3320	0.5847	0.1712

The following is a summary of the conclusions when conducting an analysis of means against the overall mean at each of the wavelengths.

- A wavelength: The Class A/ ½" Structural SMC have a higher mean (worse appearance) than the overall mean of the plaques.

- B wavelength: The Class A/ 1" Structural SMC has a lower mean (better appearance) than the overall mean and the Class A/ ½" Structural SMC has a higher mean (worse appearance) than the overall mean.
- C, D, E wavelengths: There are no statistical differences between the means of the plaques at these wavelengths.

The final surface analysis was completed on the parts after final painting. The results from the Qualisensor are given in Table 13.

Table 13. Surface appearance of primed and painted plaques molded with different combinations of materials.

Description	N	Mean Curvature SD A wavelength (1/m)	Mean Curvature SD B wavelength (1/m)	Mean Curvature SD C wavelength (1/m)	Mean Curvature SD D wavelength (1/m)	Mean Curvature SD E wavelength (1/m)
Class A	2	1.0279	1.3405	1.4425	0.6608	0.1927
Class A/1" Structural	6	1.0045	1.1922	1.1826	0.5830	0.1850
Class A/1/2" Structural	5	0.9160	1.0999	1.1628	0.5718	0.1521
Class A/Continuous Prepreg/1/2" Structural	6	1.0478	1.3425	1.5677	1.0402	0.2922

The following is a summary of the conclusions when conducting an analysis of means against the overall mean at each of the wavelengths.

- A,B,C wavelengths: There are no statistical differences between the means of the plaques at these wavelengths.
- D wavelength: The Class A/Continuous Prepreg/ ½" Structural SMC has a higher mean (worse appearance) than the overall mean.
- E wavelengths: There were statistical differences in the means at the E wavelength. The Class A/Continuous Prepreg/ ½" Structural SMC had the highest mean (worse appearance) than the overall mean. The next highest mean was the Class A system. The Class A system had better appearance than the 3-part system but worse than the two Class A/structural systems. There was no statistical difference between the Class A/1/2" Structural plaques and the Class A/1" Structural plaques.

The Qualisensor deflectometer is capable of distinguishing differences in smoothness of molded parts when compared against each other. The final determination of whether the surface is an acceptable Class A surface must be made by the stakeholders and compared to acceptable standards.

4.5.2.Destructive Methods

4.5.2.1. Microscopy

Initial microscopy was performed by INEOS to determine how clearly the layers of Class A SMC, continuous fiber prepreg, and structural SMC could be delineated. Figure 51 captures some of this preliminary characterization.

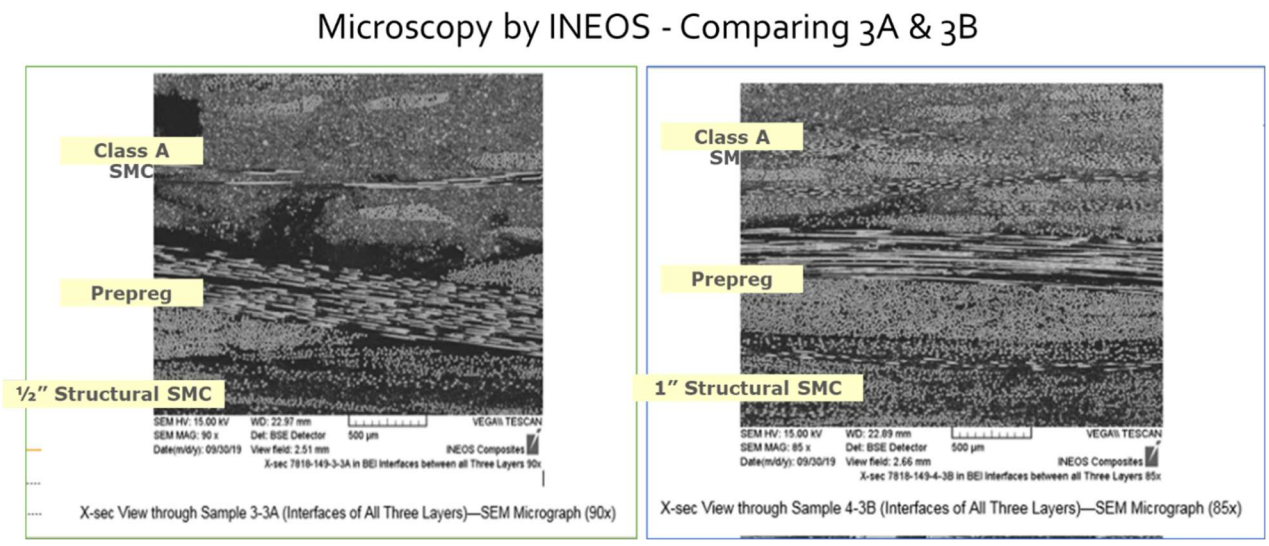

Figure 51. Micrographs of Three-Material Flat Plates Showing Relative Thicknesses and Indicating Fiber Orientations

Microscopy was also used near the end of the project to ascertain approximate fiber orientation states in the ribbed plates. This inspection was meant to be performed for samples with four different material flow types – 30%, 60%, DIRF and Knit. "30%" and "60%" depicts centered placement of charge with 30% and 60% of area coverage, respectively. "DIRF" suggests that the charge was placed on one side of the mold and the material flowed to the other side, while "Knit" depicts placement of two charges at two opposite sides and the material flows towards the center.

Time constraints required careful selection of the location of inspection on the plate. Ultimately, for center-charged plates, one 1" wide inspection location with a rib was chosen outside of the initial charge area and for flow aligned plates ("DIRF"), two locations were chosen along the same rib to compare the relative alignment of fibers as the flow progresses. The knit charge plates were not slated for initial inspection but may be investigated later if time permits. The approximate inspection locations are shown in red and rib locations in black in Figure 52.

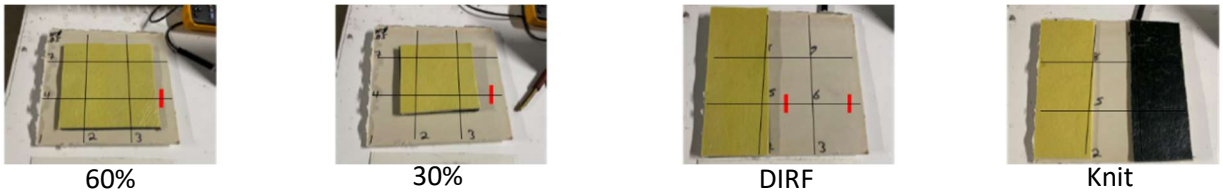

Figure 52. Microscopy Inspection Locations Shown in Red on Charge Placement Images

With four 1" microscopy samples to inspect per material system and five material combinations, there were twenty relatively large fiber orientation investigations to perform. Each sample was investigated in three locations; one through the plate thickness away from the rib, then two at different depths in the rib. One example micrograph is shown to illustrate the investigated locations in Figure 54. The inspection plane was always normal to the red "X".

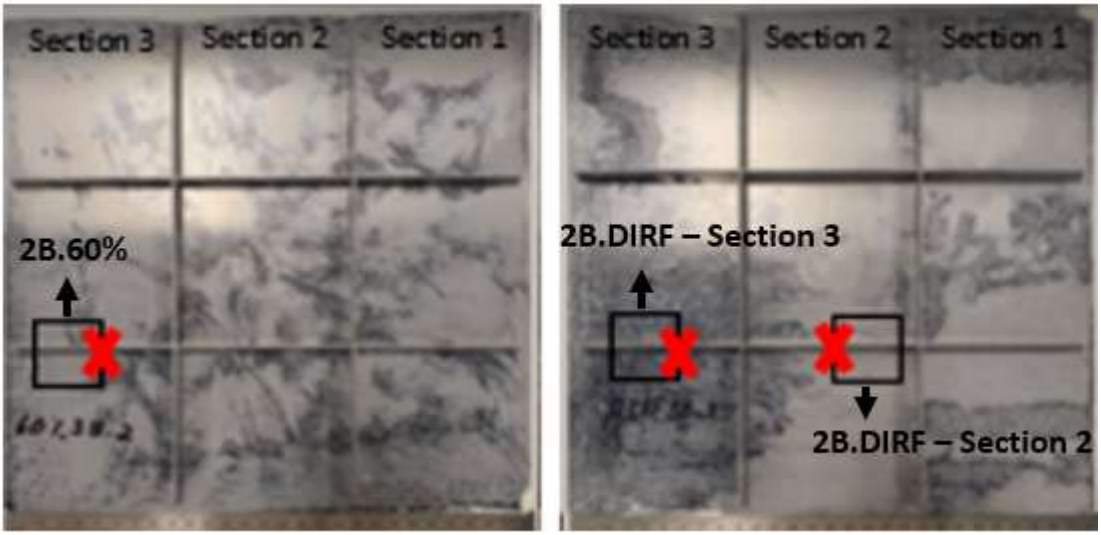

Figure 53. Microscopy sample location on ribbed plates – one sample from center-charged (left) and two samples from DIRF (right)

After extraction, these samples were potted, polished and cleaned. Microscopy was achieved using a Leica inverted microscope with a 10x magnification lens. Following is the resulting image of microscopy of one sample cross sections (Figure 54). The fiber ellipse inspection was done along lines across rib widths and through plane thicknesses, as shown in the image.

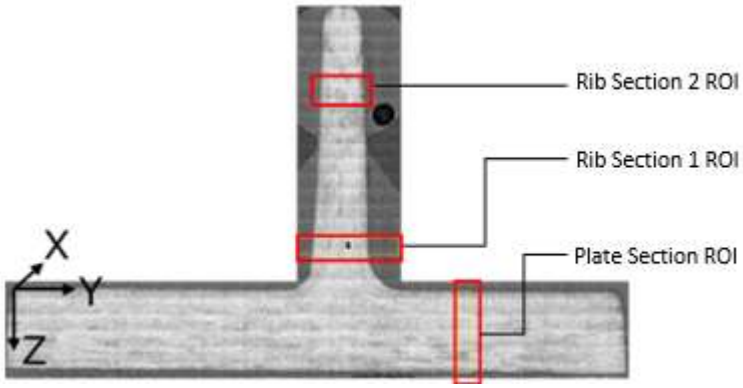

Figure 54. Plate and Rib Section ROIs for Fiber Ellipse Inspection

Using ImageJ, fiber ellipses along an inspection line were captured and their major and minor axis, centroid, and in-image angle from x=0 (horizontal) were used to make a plot of fiber orientation relative to position in the examined area. It was also desirable to present the local orientation states using their orientation tensor terms. The fiber direction angle (θ) and the orientation tensor (A) for each fiber were calculated as follows:

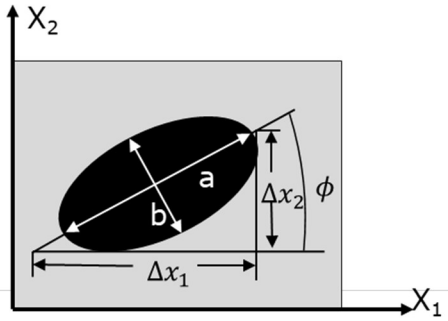

Fiber Orientation angle: $\cos(\theta) = \frac{b}{a}$

In-Plane Fiber Angle: $\tan(\phi) = \frac{\Delta x_2}{\Delta x_1}$

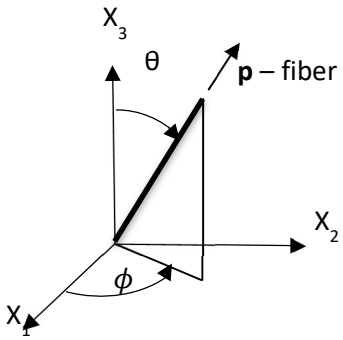

Fiber Vector Equations:

$$\boldsymbol{p} = -\boldsymbol{p}$$
$$p_1 = \sin\theta\cos\varphi$$
$$p_2 = \sin\theta\sin\varphi$$
$$p_3 = \cos\theta$$

Orientation Tensor Equations:

For single fiber,

$$A_{ij} = p_i p_j = \begin{bmatrix} p_X p_X & p_X p_Y & p_X p_Z \\ p_Y p_X & p_Y p_Y & p_Y p_Z \\ p_Z p_X & p_Z p_Y & p_Z p_Z \end{bmatrix}$$

$\mathbf{A}_{ij}$ is symmetric, and

$$a_{XX} + a_{YY} + a_{ZZ} = 1$$
$$0 \leq a_{ii} \leq 1$$

For our inspection, the diagonal orientation tensor values were of utmost importance, since they represented fiber orientations in the x-, y- and z-axes. The resulting average values of A_{xx}, A_{yy} and A_{zz} are summarized in Table 14.

Table 14. Average Diagonal Fiber Orientation Tensor Results

		1A 30%	1A 60%	1A DIRF Sec2	1A DIRF Sec3	2A 30%	2A 60%	2A DIRF Sec2	2A DIRF Sec3	2B 30%	2B 60%	2B DIRF Sec 2	2B DIRF Sec 3		3A 30%		3A 60%		3A DIRF Sec 2		3A DIRF Sec 3		3B 30%	3B 60%		3B DIRF Sec 2		3B DIRF Sec 3
Plate	Axx	0.43	0.26	0.36	0.35	0.27	0.35	0.35	0.39	0.28	0.20	0.48	0.48		0.49		0.52		0.66		0.46		0.44	0.61		0.64		0.40
	Ayy	0.52	0.70	0.51	0.51	0.67	0.58	0.56	0.46	0.69	0.79	0.44	0.49		0.19		0.43		0.25		0.48		0.52	0.36		0.33		0.57
	Azz	0.05	0.03	0.14	0.14	0.06	0.06	0.10	0.15	0.03	0.02	0.08	0.03		0.32		0.05		0.09		0.07		0.04	0.03		0.03		0.03
Rib	Axx	0.41	0.43	0.32	0.34	0.30	0.33	0.42	0.31	0.38	0.44	0.39	0.22	0.38	0.61	0.60	0.57	0.47	0.64	0.74	0.56	0.67	0.55	0.50	0.58	0.47	0.60	0.56
	Ayy	0.06	0.11	0.03	0.05	0.06	0.20	0.08	0.06	0.06	0.06	0.06	0.05	0.03	0.17	0.14	0.09	0.09	0.03	0.04	0.04	0.04	0.08	0.03	0.03	0.03	0.03	0.07
	Azz	0.53	0.46	0.65	0.61	0.65	0.46	0.50	0.64	0.56	0.51	0.55	0.73	0.60	0.22	0.26	0.35	0.44	0.34	0.21	0.40	0.29	0.38	0.48	0.39	0.50	0.37	0.37

In the "plate" sections of samples, the fiber directions are perpendicular to the z-direction. Hence, A_{zz} for those are close to zero. Given that the summation of A_{ij} is 1, one can approximately determine the A_{yy} values for plates if the A_{xx} information is available. Additionally, the fibers in the rib sections of the samples run approximately perpendicular to the y-direction, bringing the A_{yy} values for the same close to 0. Hence, A_{zz} values for fibers in the rib sections can be approximately extrapolated, given the A_{xx} values for the same. Hence, overall, A_{xx} values are of most importance.

The average fiber orientation tensor diagonal term, A_{ii}, values for each plate and material flow type were

plotted on bar charts as shown below (Figure 55-56). These approximately represent how much fiber orientation is along each coordinate axis, X, Y, and Z.

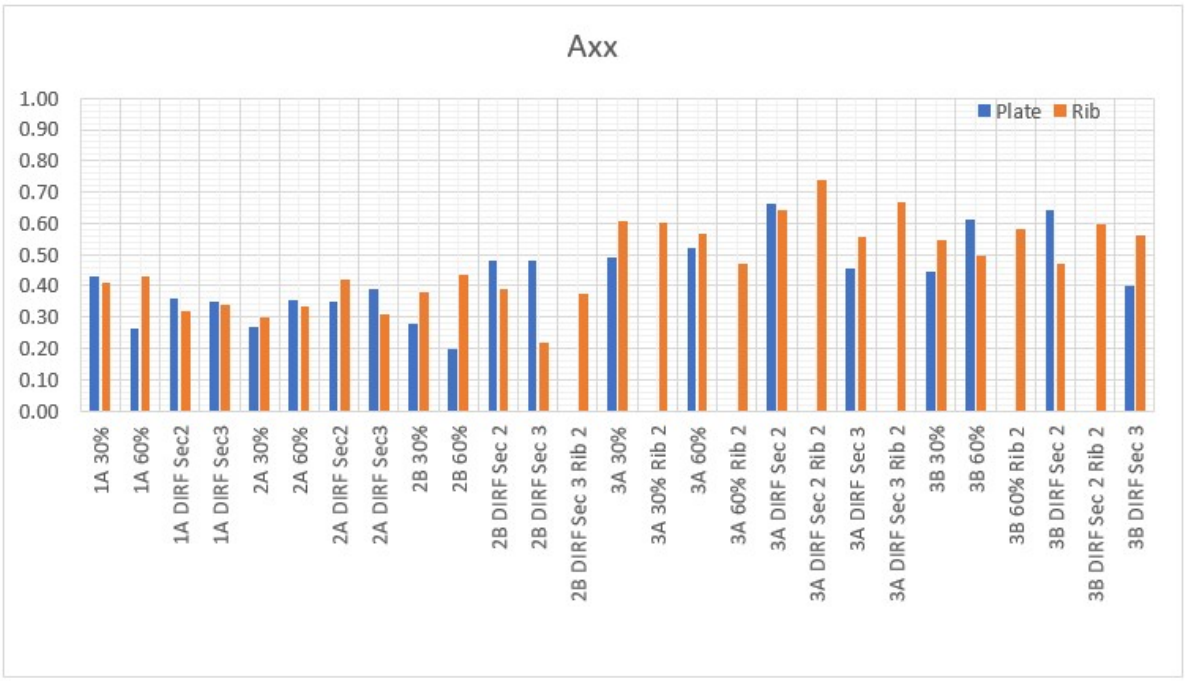

Figure 55. x-Direction Fiber Orientation Tensor Results, A_{xx}, Bar Chart

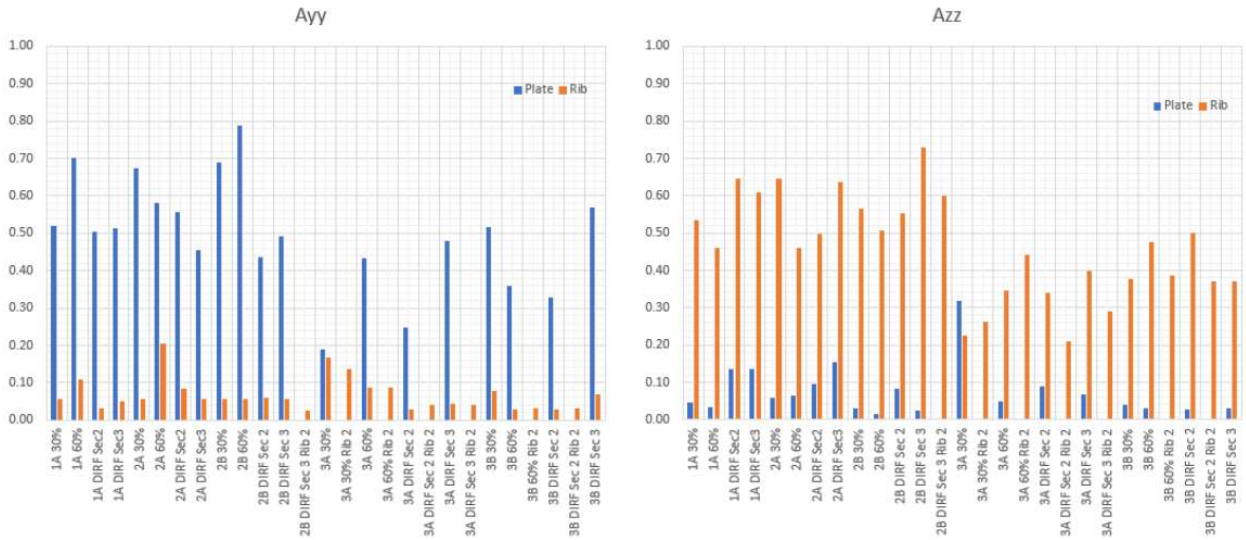

Figure 56. y-Direction (A_{yy}) and z-Direction (A_{zz}) Fiber Orientation Tensor Results Bar Chart

The blue bars represent the plate sections, and the orange ones represent the rib sections. In general, we see that A_{yy} values for fibers in the plate sections, and A_{zz} values for fibers in the rib sections, reduce as we move from single material to multi-material series. This is due to the possibility that the woven continuous fibers in the multi-material plates restrict the flow of materials in the y- and z-directions, respectively.

Since A_{xx} values are expected to be non-zero for both plate and rib sections, they were plotted against

fiber locations for each plate and material flow type. An example of such plotting, along with the fiber inspection, for one of the plate series is shown below in Figure 57. The detailed inspection and plotting procedure for all the samples is presented in the Microscopy Results.

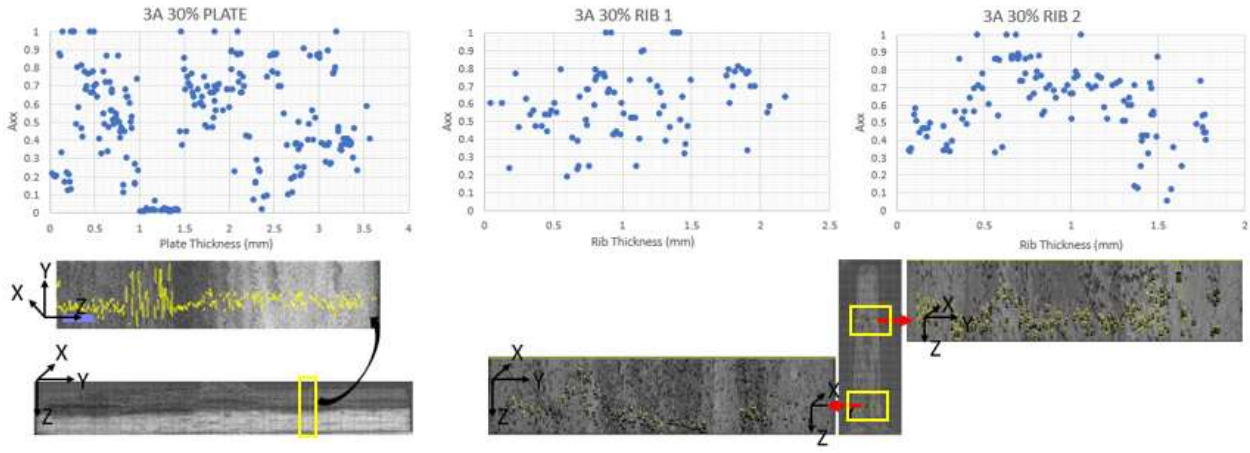

Figure 57. Fiber Ellipse ROI and Inspection - 3A Plate Series

Here, we see one region of interest in the plate section and two in the rib sections selected and magnified for fiber ellipse inspection. Once selected, ellipses were drawn around the fibers, following a single inspection line along the vertical z-direction (or the horizontal y- direction, in the case of rib sections). Once all ellipses were detected along the line through the entire width of the region of interest, the measurements (in mm) were recorded in excel format. The plots show A_{xx} values against the fiber centroid locations.

It is worth noting that no measurement weighting scheme was used to adjust the A_{ij} calculated from the fiber cross section ellipses, even though it is apparent that a fiber with an elongated cross section will take up more area, and thus result in a lower count of that measurement overall. By following a single inspection line perpendicular to the largest fiber orientation components instead of measuring all fibers in a given area, the need for weighting was somewhat minimized anyway. Furthermore, this is a very rough estimate of local orientation state because the number of fibers sampled is less than desirable and certain orientations are more visible, and thus easier to add to the data sample set.

In this exercise, the microscopy-based orientation were extremely localized, which is difficult to directly compare with "regional" simulation orientation results. Nevertheless, matching locations from the flow simulations were interrogated for predicted orientation states and the results are presented in section 4.4.

4.5.2.2. Burn Off

Full panel burn-offs were performed on select ribbed panels to visually/qualitatively examine the fiber orientation as a result of multi-material flow. Due to time constraints with the project, only six ribbed panels were chosen to undergo destructive burn-off testing. Panels chosen for evaluation were 30 and 60% 1A panels (Single comp. Class "A" SMC) and all four charge variations of the 3A material combination (Class "A", Prepreg, ½" Structural SMC).

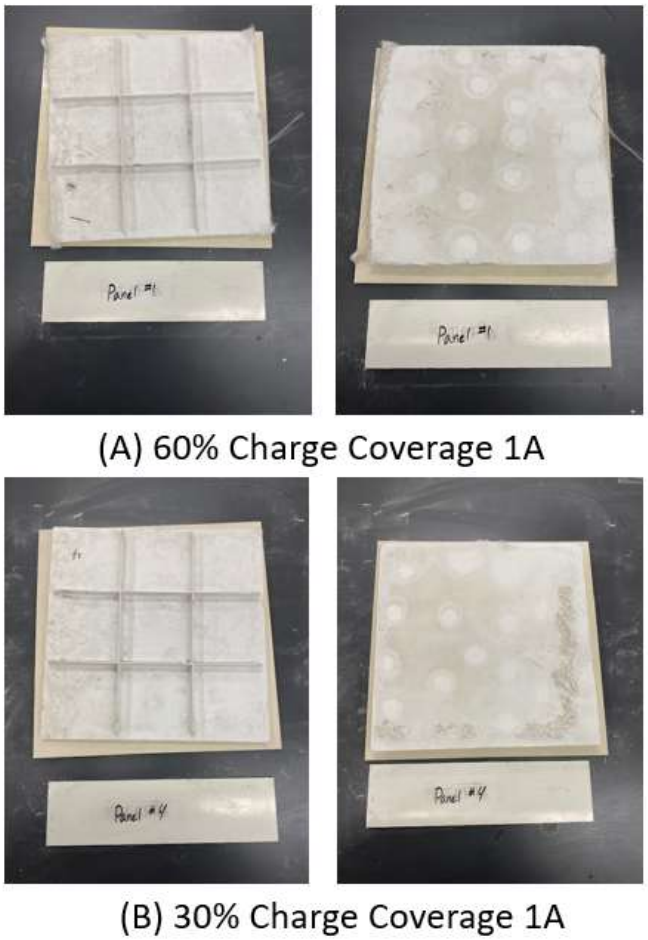

Figure 58. Shows "A" and "B" side images of the 60% 1A and 30% 1A burn-off-panels

The single component samples were run to provide a reference to a standard single component system charge pattern. 30 and 60% charge coverage had similar fiber orientations, with the exception of a slightly increased fiber read-through on the surface of to 30% panel as can be seen on the A-surface picture (Figure 58). The additional flow associated with lower mold coverage (30%) appear to cause a slight separation to occur between fiber and filler leading to the appearance of loose fibers on the A-surface of the panel.

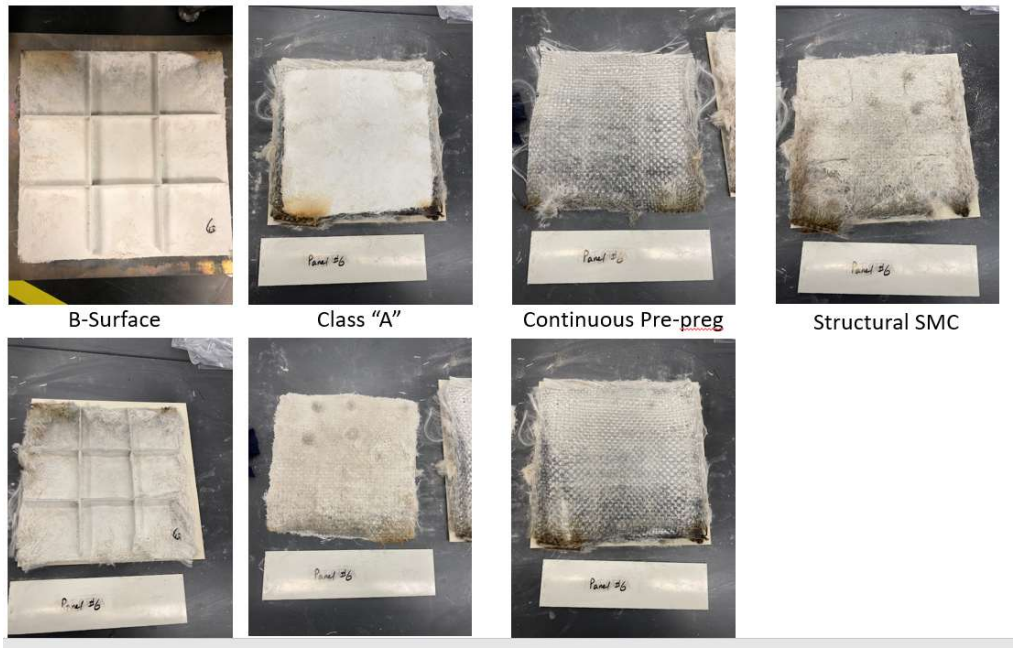

Figure 59. Highlights the material layer break-down of the 60% 3A burn-off panel

As can be seen in Figure 59 above, the break-down for the 60% three component system, highlights the three distinct material layers in the panel. Starting with the Class "A" layer, shows the material is hindered from fully filling the A-surface of the panel, as noted by the ~one-inch gap between the Class "A" material and the edge of the panel. The Structural SMC on the B-surface appears to completely fill the B-side of the panel. Fiber distortion in the continuous prepreg layer appears minimal with the exception of the outer edges of the panel.

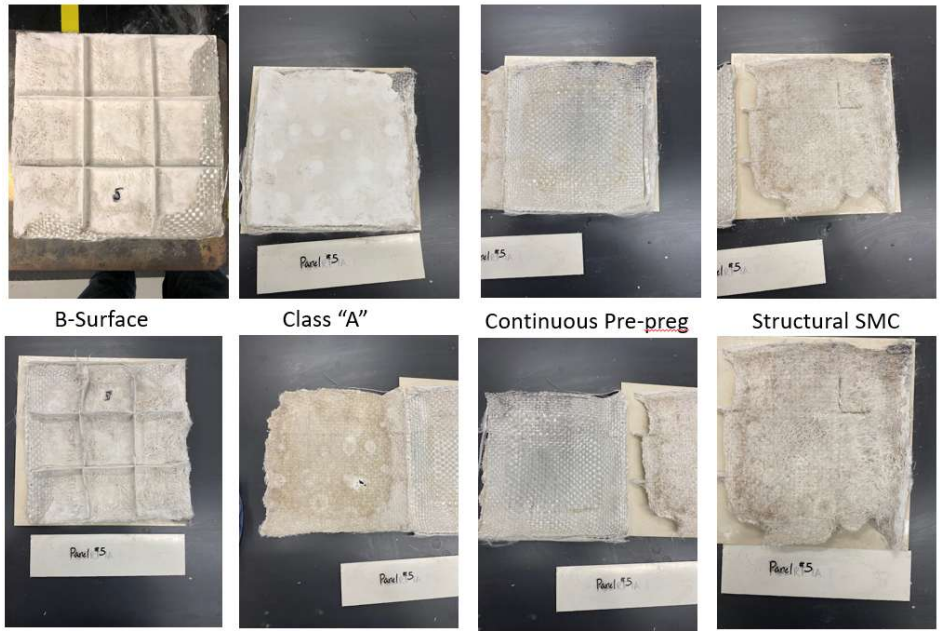

Figure 60 Highlights the material layer break-down of the 30% 3A burn-off panel

Figure 60 above, shows the break-down of the 30% 3A component panel, of note is the fill pattern of the two SMC materials. Both SMCs show flow heading into opposite corners of the tool leaving shorts/uneven material distribution in the panel. This will require additional studies to mitigate as an

uneven flow between the two SMC materials will lead to inconsistent parts in production. Also of note is the distortion pattern of the continuous prepreg layer, the 30% SMC charges can be clearly seen in the undisrupted center of the prepreg, with orientation disruptions fanning out in a circular pattern following the flow of the SMC materials. Again, this type of distortion will lead to additional variability in part properties heading into production and needs to be mitigated/optimized moving forward.

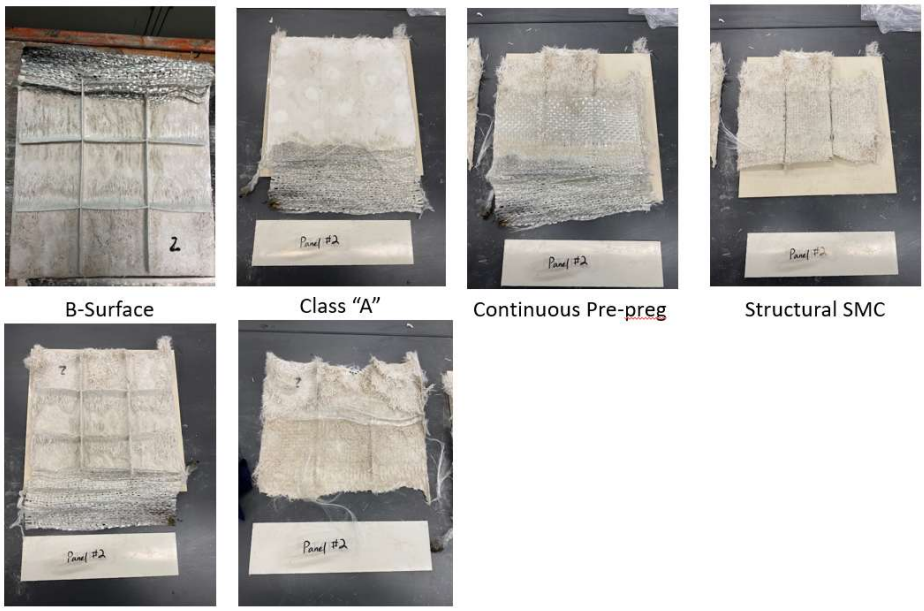

Figure 61. Highlights the material break-down of the 3A directional flow burn-off panel

As shown in above Figure 61 the addition of a directional flow charge pattern critically disrupts the continuous prepreg layer between the two SMC layers. The continuous prepreg patch migrated with the flowing material approximately three inches from its starting location causing the ripple section at the edge of flow.

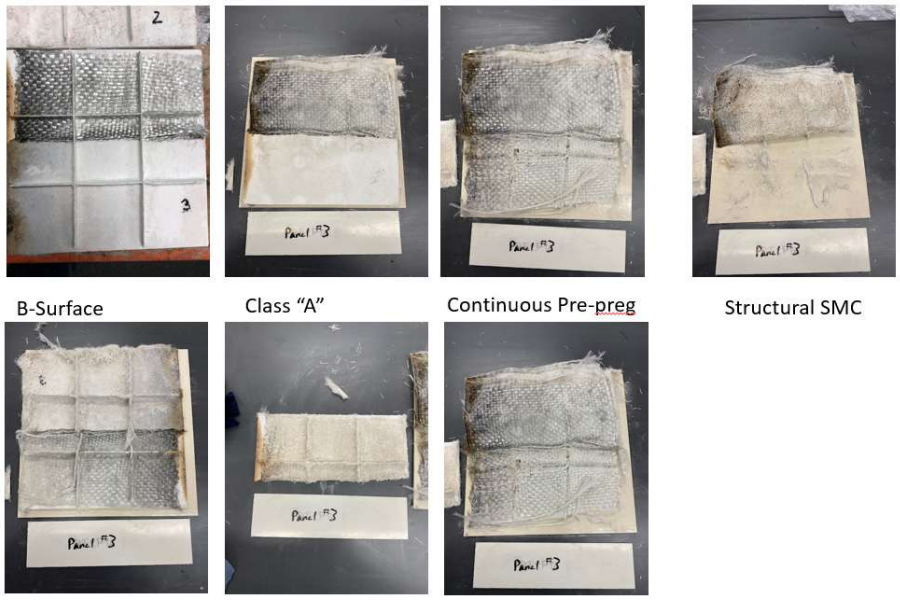

Figure 62. Highlights the material layer break-down for the Knit 3A burn-off panel

Similar to the three component directional flow panel the Knit panel has a significant ripple at the center where the SMC flow fronts come together at the knit line (See Figure 62).

4.6. One Piece Hood Specifications

The demonstrator hood has to fulfill the OEM-specific mechanical requirements. These are defined and discussed in the form of component load cases, describing loading setup, forces and permissible deflections at pre-defined measurement locations. A set of critical load cases was compiled to provide a basis for the preliminary design:

- Bending stiffness along longitudinal axis of vehicle
- Torsional Stiffness
- Transverse bending stiffness at latch
- Transverse bending stiffness at hinge

The one-piece hood has to comply with pedestrian safety regulations, which limit the local stiffness of the component at given locations. HIC requirements served as a major part of the specification book. The HIC indicators are derived from the deceleration curve of the headform tester and the peak thereof. The deceleration peak of the headform tester is an excellent indicator to predict– in case of an actual collision with a passenger – if the crash victim would suffer serious head injury. Designing a single-piece hood structure for HIC is a challenging task. The issue is rooted in the conflicting mechanical requirements of component stiffness and pedestrian protection. Composite materials allow their properties to be tailored through the application of localized reinforcements or through the implementation of specific design features such as varying wall thickness and smart rib design. Computational topology optimization was utilized in the preliminary design of the demonstrator part to guide designers in providing reinforcing elements and substructures at the most effective locations and balancing the stiffness and compliance requirements of the structure. Topology optimization results were taken into account along with manufacturability considerations to design the preliminary part geometry. Pedestrian safety regulations differ between given regions of the world. In the scope of this project, the European standards were taken into consideration, as defined by the European New Car Assessment Programme shown graphically in Figure 63 (Version 8.4, November 2017).

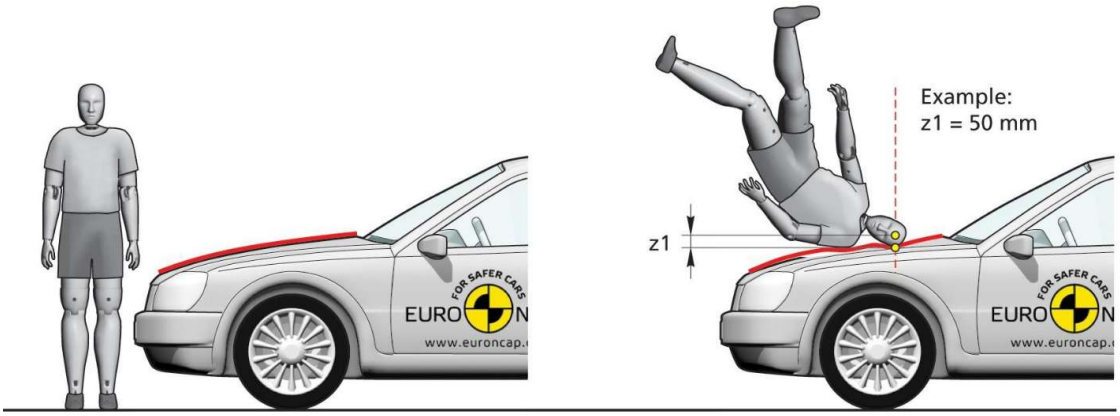

Figure 63: Simulated accident involving a pedestrian in walking posture, with a head impact on the hood. (Source: European New Car Assessment Programme, Version 8.4, November 2017.)

Due to the hybrid nature of the proposed material combination pressure-temperature effects are necessary to be investigated in order to prevent undesired out-of-plane deformation of the component due to changes in ambient temperature, i.e. warpage. This can be influenced by tailoring the coefficient of thermal expansion of the individual materials, especially that of the SMCs. Furthermore, the manufacturing process and some of the molding parameters can also help the controlling of warpage and post-molding deformation.

The hood demonstrator has to fulfill class-A requirements, including painted surface waviness. This poses a challenge, i.e. the development of sink marks on the backside of rib structures. This effect is also known as rib read-through. Since the backside of these structures is on the to-be-painted class-A side, it is crucial to avoid sink marks and other surface disturbances. Parameters such as molding pressure, curing temperature, substrate thickness, rib depth and thickness have to be set up in a way to mitigate the evolution of such surface defects. Sink marks or local changes in the surface morphology map of the substrate can also be caused by prepregs underneath the class-A surface. These lead to unacceptable surface quality and therefore, have to be avoided as well.

Furthermore, the demonstrator had to fit to the vehicle body form which the baseline version stems. This provides the framework for the design of the demonstrator part and will be further discussed in the next chapter.

4.7. Preliminary Design

The initial target application for this co-molding technology was for an automotive hood. A preliminary design model was created to follow the geometry and attachment points of an aluminum hood provided by an OEM. Also, several realistic loading cases were provided, allowing for initial targets to be assumed for the maximum load and deflection of an automotive hood.

The preliminary design was based on the original benchmark geometry. The outer surface and the perimeter area was defined by the vehicle body the demonstrator parts have to fit to. Therefore, design flexibility was only allowed on the inner side of the hood component. The original metal reinforcements were adopted to serve as force transmissions points. The project goals allow for these metal parts to be substituted or altered, their inclusion in the preliminary design served the purpose of simplification.

A single-shell design was investigated with several rib configurations, based on the mechanical characterization results of the base materials and their hybrids. The aforementioned load cases define major load paths along which these rib structures have to be located, as shown in Figure 64.

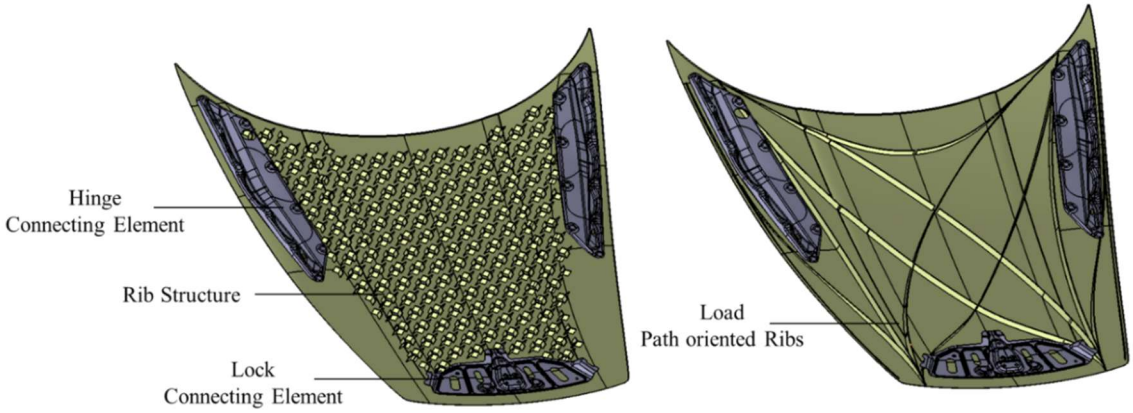

Figure 64: Design sketches of the one-piece hood (1400 mm x 1250 mm) demonstrating the versatile rib and reinforcement structures included in the investigation and development

Some of the rib designs investigated were path oriented, long structures while other designs were comprised of the repetition of smaller structures. This latter design was deemed to be better tailorable for head impact and crash requirements. A combination of such structures is also possible, as long as rib read-through is avoided. Furthermore, a topology optimization was also performed, to serve as the basis for defining rib locations at the preliminary design stage.

4.7.1. Metallic Hood Baseline

An initial model was created using the aluminum hood geometry to ensure loads, contacts, and boundary conditions were being created correctly in the finite element model. The components and their masses are shown in Figure 65.

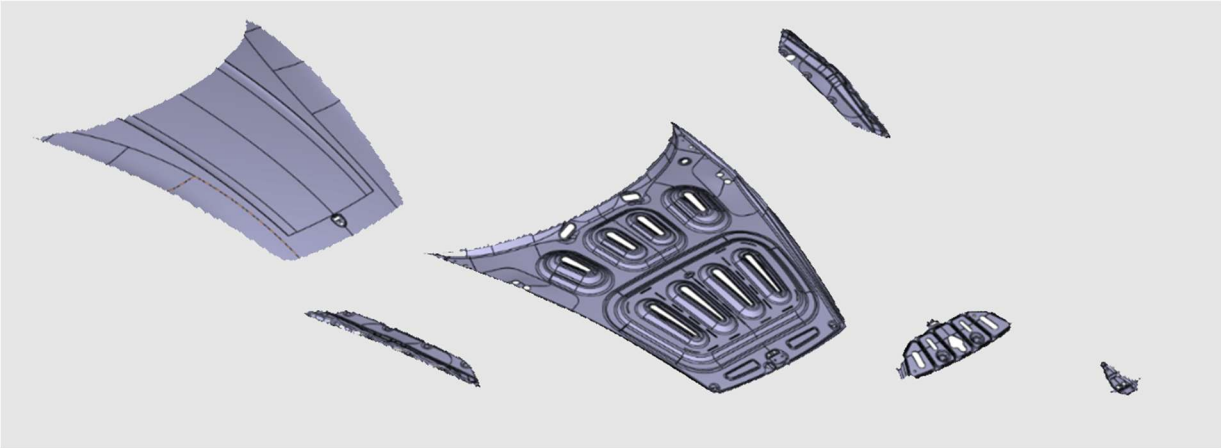

Figure 65. Aluminum Hood Baseline Model Components and Masses

The total aluminum hood mass is 8.7kg using the model volume and a density of 2.7g/cm^3. There are four loading conditions that are considered when modeling the performance of this aluminum hood model and for the later composite model. The first approximately captures the bending stiffness of the hood and will be called LC1. LC1 is shown in Figure 66.

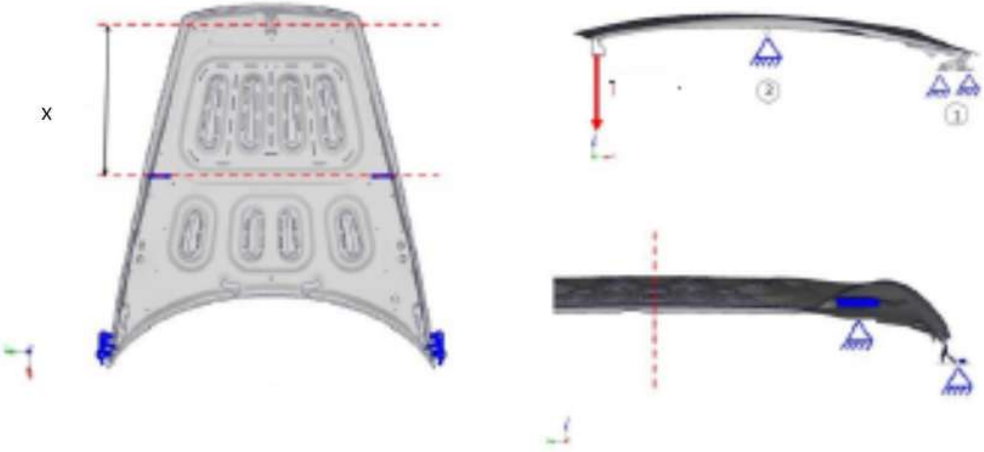

Figure 66. Load Condition 1 (LC1) for Bending Stiffness

LC1 is set up with pins at the hood hinges, rollers at the mid-support, and force applied to the hood latch. The total deflection in Z should be <20mm at the front center of the hood. Load case 2 (LC2) is shown in Figure 67 and captures torsional rigidity.

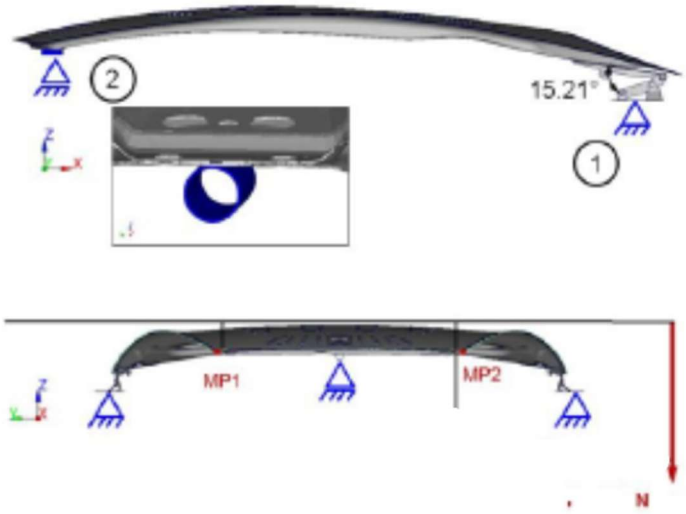

Figure 67. LC2 for Torsional Rigidity

LC2 is modeled with pins at the hinges, a pin at the latch, and has a moment applied using the two front corners of the hood as load application points. The vertical, Z, offset between the two front hood corners should be less than 54.2mm. LC3 tests the transverse flexural stiffness and is shown in Figure 68.

Figure 68. LC3 Transverse Flexural Stiffness about Latch

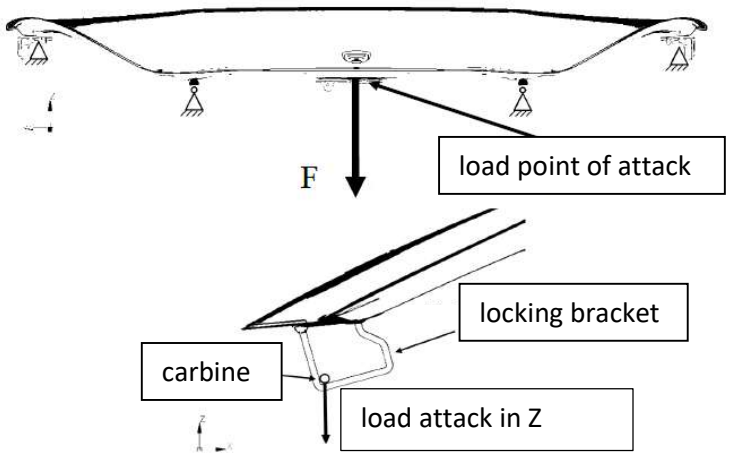

LC3 has pins at the hinges, a Z-direction support where hood bumpers are, and a 500N load on the latch carabiner itself. The deflection at the latch must be <1.3mm. LC4 highlights the transverse flexural stiffness at the hinges and is shown in Figure 69.

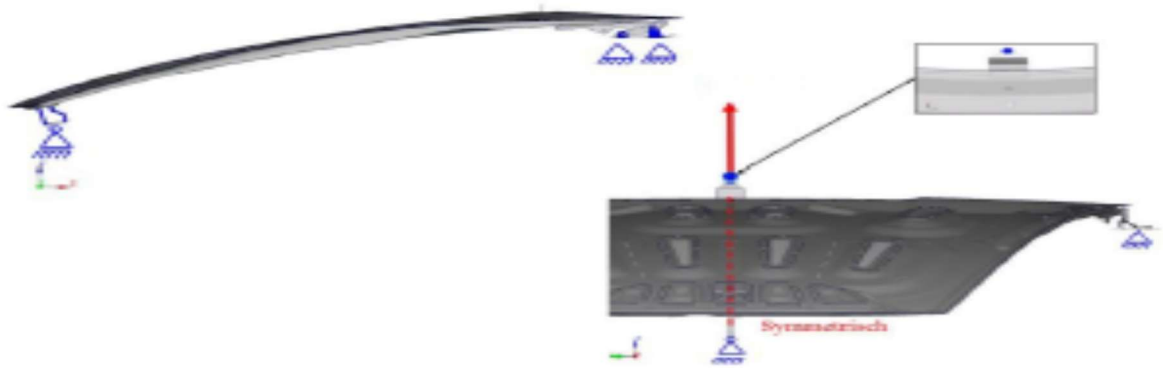

Figure 69. LC4 Transverse Flexural Stiffness at the Hinges

LC4 again has pins at the hinges, Z-direction support at the hood bumper locations, and an upward (+Z) load at the back-center edge of the hood between the hinges. Deflection near the load point must be less than 5mm.

With all of these load conditions in mind, the aluminum hood geometry was modeled with C3D10 quadratic tetrahedron elements, each sub-geometry was connected by tie constraints at rivet points and along the hem flange, MPCs and reference points were created to allow load and boundary condition introductions, and contact between sub-geometry surfaces was enabled. The meshed model is seen in Figure 70.

Figure 70. Meshed Aluminum Hood Geometry with All Components and Reference Points

The hem flanges, rivets and regions with contact enabled are shown in more detail in Figure 71.

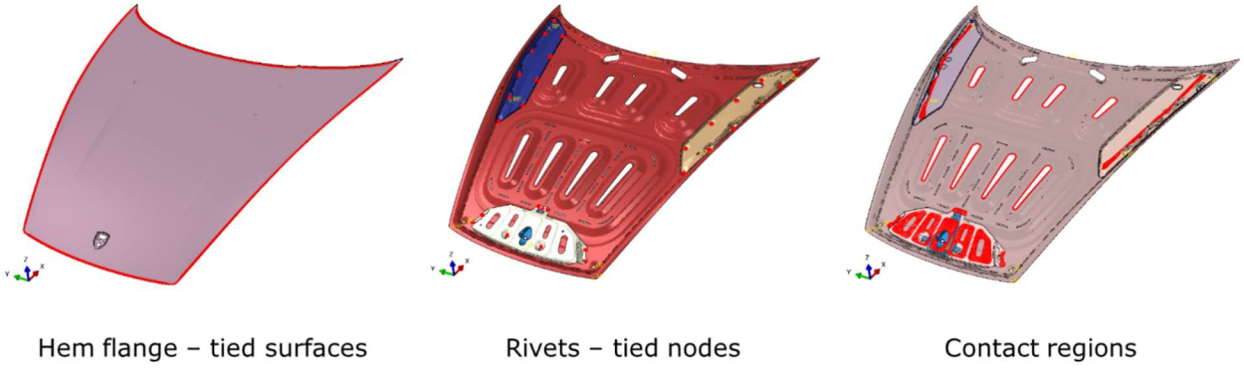

Figure 71. Hem Flange, Rivet, and Contact Region Definitions

For more efficient analysis, contact is only enabled in the regions where it is likely. With the model set up and load conditions defined, the analysis can be run and results are presented in Figure 72.

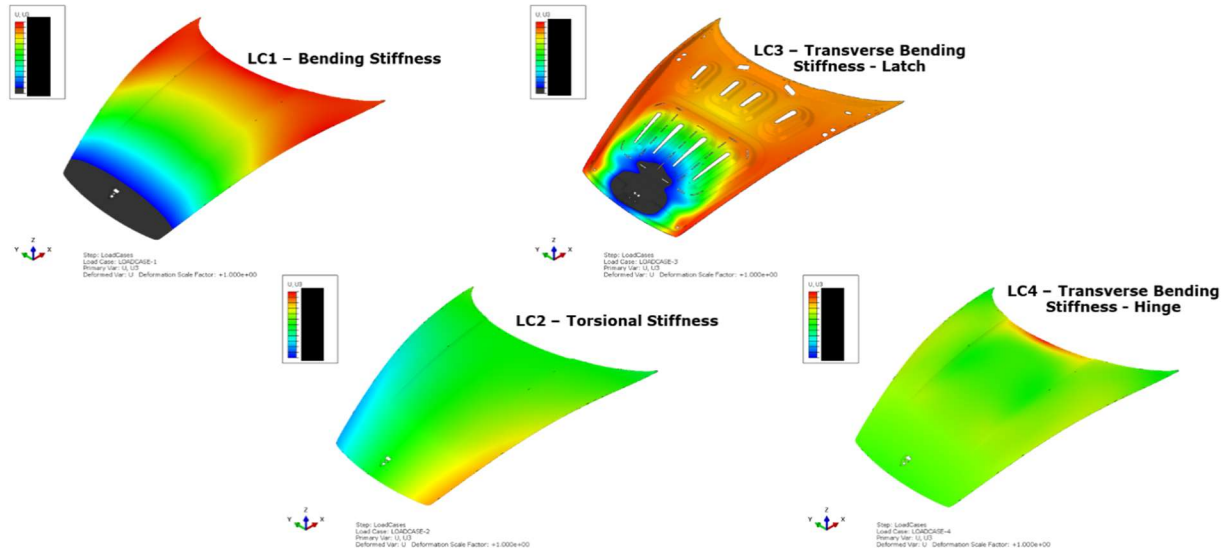

Figure 72. Results of Each Isolated Load Case on the Aluminum Hood Relative to Defined Target Displacements

It is apparent that LC1 and LC3 are the most critical for this two-piece aluminum hood geometry because there are deflections exceeding the defined displacement limits

Now that the effectiveness of the 8.7kg aluminum hood model can be qualitatively assessed, it is time to review the same load cases for a reduced component count SMC hood.

4.7.2. Multi-Material SMC Design and Optimization Effort

The ultimate desired outcome for this composite co-molding work is a one-piece hood design that meets all discussed load cases, has equal or lesser mass than the aluminum version, and reduces part count from six components down to one. As a first design and simulation step to assess the feasibility of these desires, a composite hood model was created using outer shell geometry that matches that of the aluminum hood studied above. Because of the very high local load effects, separate SMC hinge and latch reinforcements are retained at this stage, making this study a four-piece design. So, any design

optimization here is attempting to combine the previously stamped hood inner and outer shells into a single multi-material SMC design containing Class A SMC at the outer surface, a layer of continuous fiber prepreg below that, and a structural SMC lower rib structure.

Topology optimization was implemented to decrease the mass (volume) of the underlying reinforcements rib structures of this model, but the model began as a very thick approximate hood seen in Figure 73.

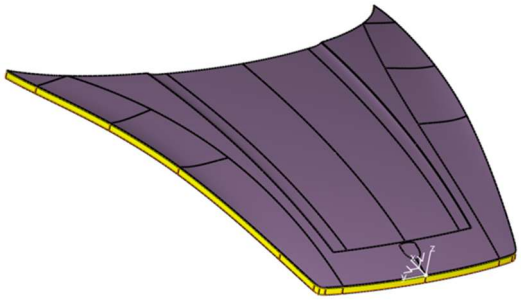

Figure 73. SMC Hood Geometry with Gray Outer (Class A + Fabric) and Yellow Inner (Structural SMC)

The purpose of this initial study was to determine the primary load paths under the two most demanding load cases, LC1 and LC3. So, the gray outer just needs to be an isotropic surrogate material representing the Class A + woven prepreg and the yellow inner is an isotropic surrogate for the structural SMC. Load case 1 results in a topology that attempts to prevent bending from the front to back of the hood as seen in Figure 74.

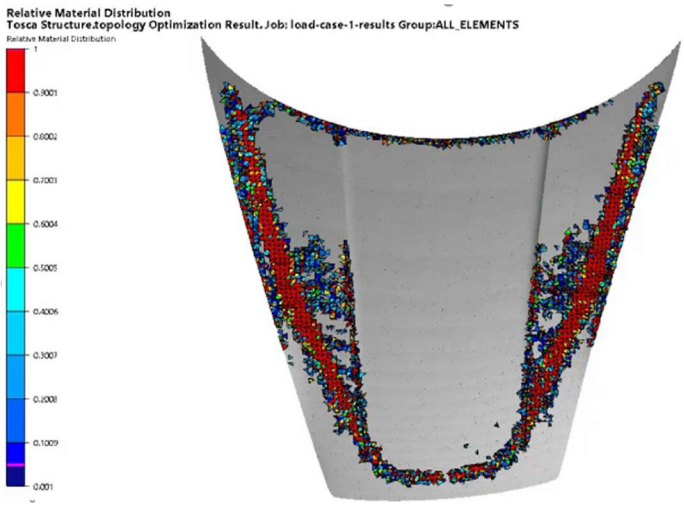

Figure 74. Structural SMC Topology Optimization Under Load Case 1 (Bending Front to Back)

LC1 shows that some ribs must be aligned to carry this bending load from the hinges to the latch area. LC3 is the other load case used to determine a general rib design pattern. A need for some cross bracing of the hood and reinforcement around the entire perimeter seems to be the result shown in Figure 75.

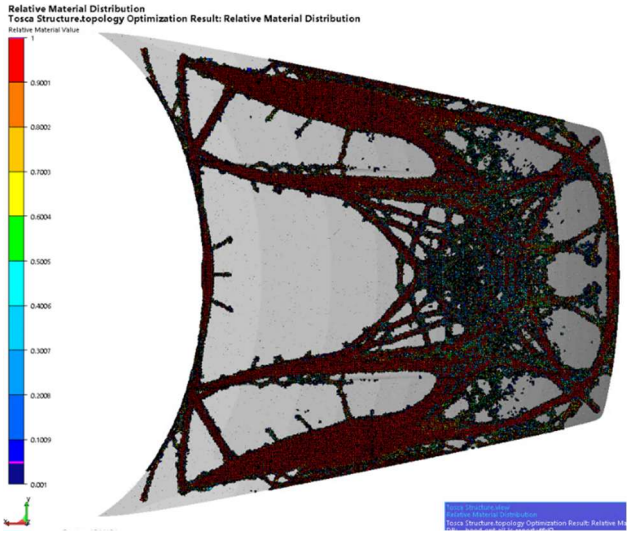

Figure 75. Structural SMC Topology Optimization Under Load Case 3 (Transverse Bending from Latch Load)

Both volume minimizing topology optimizations are useful for determining a general reinforcement pattern that will handle the provided load cases well. As with most topology optimizations, some engineering interpretation must be applied.

The "one-piece" hood design with ribs was created with a maximal number of ribs that could be reduced during a further design optimization trial. It has separate SMC hinge and latch reinforcements to handle higher local loads in those areas, as seen in Figure 76.

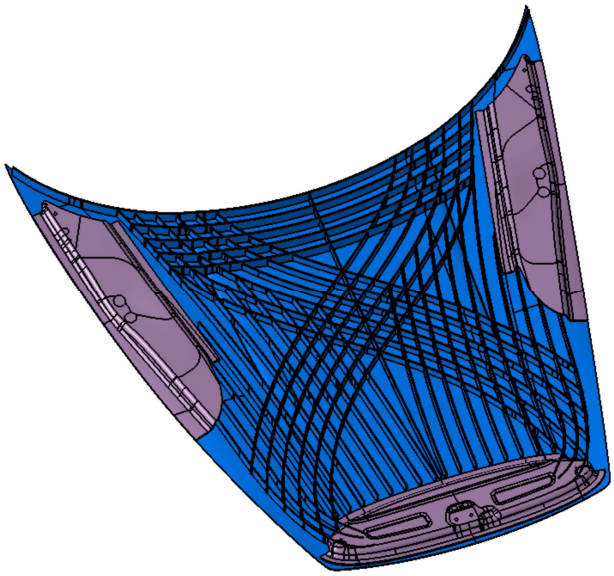

Figure 76. Rib Optimization Design Space

The single main panel shown in blue contains Class A SMC at the outer surface (E=10.3GPa), structural SMC in the ribs (E=11.3GPa), and a prepreg fabric layer in between (E=19.8GPa). Those isotropic moduli used are close enough to the experimentally measured values to be functional for this preliminary design study. The outer panel is 2.75mm thick and the ribs have a 3x25mm profile. The design optimization run went through 24 iterations starting with no ribs and ending with almost all the ribs that

were “available” as shown in Figure 77.

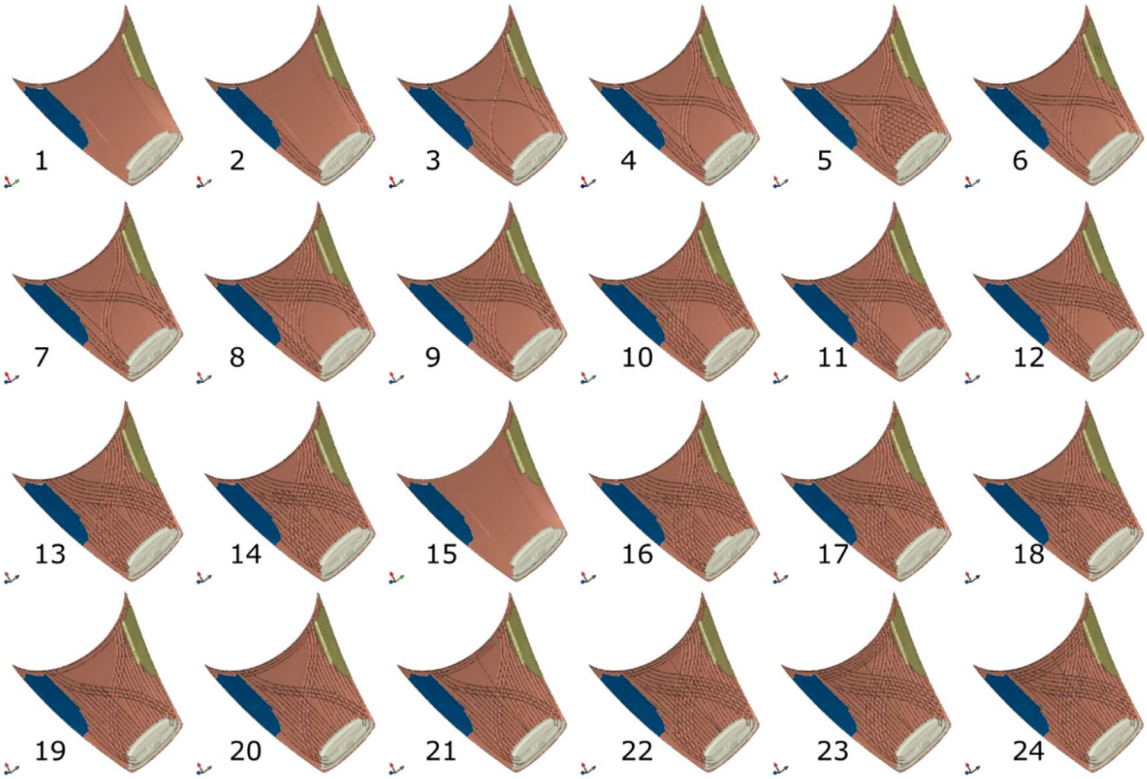

Figure 77. Rib Optimization Iterations to Meet Load Cases 1-4

Each iteration also could have a layer of continuous fabric as a part of the outer panel, each hinge, and/or the front latch reinforcement. For each iteration, the four load cases were run and their failure/success metric was quantified and added to Figure 78. Results are shown in bands because of the different combinations of additional fabric properties that could be added to each design.

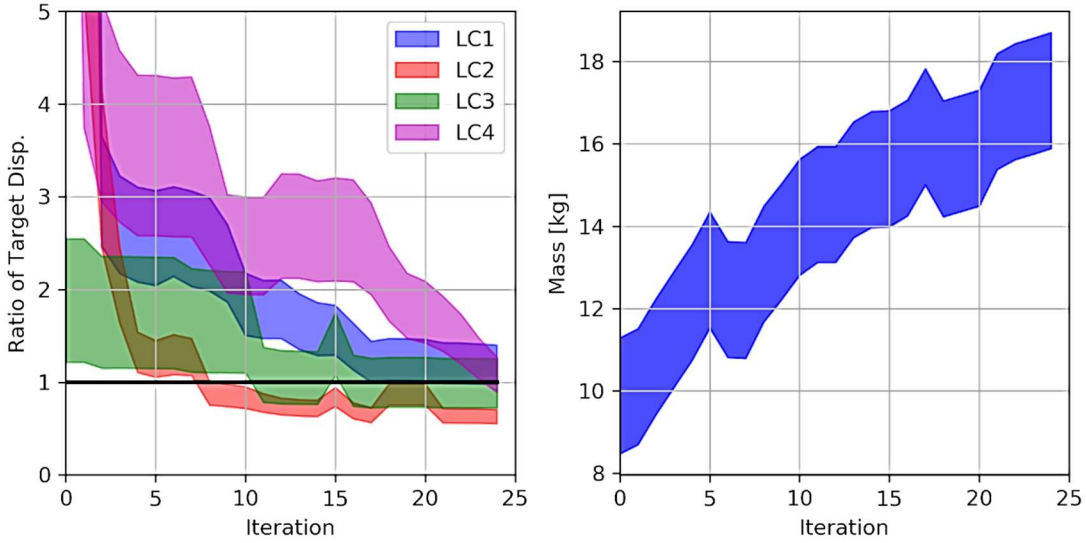

Figure 78. Rib Optimization Improving to Satisfy Load Cases, but Mass Increases

As the iteration designs (and sub-design fabric reinforcement combinations) progressed toward satisfying the four explored load cases, the mass of the hood increased. After achieving a design that satisfied all load cases the total assembled mass was 16-18kg. This is twice the mass of the aluminum baseline model (8.7kg). The metallic design being two stamped pieces joined together gives it an extremely efficient bending stiffness or area moment of inertia.

Perhaps further rib design and optimization could derive a more efficient molded one-piece design. If the benefits of lowering part count, decreasing manufacturing steps, decreasing tooling cost, or other considerations for SMC manufacturing outweigh the mass trade-off, then this may be a feasible solution. There may also be other automotive panels that are more obvious applications of this manufacturing method.

4.8. Priming and Painting

Primer application was conducted at Red spot Paint.

Primer Material: Red spot Gray 2K SMC primer- UBP9762JANB
Spray Equipment: Binks 610 Automatic Conventional spray gun
Number of Passes: 2
Gun Traverse Speed: 1700 IPM
Index Distance: 2 inches
Atomization Pressure: 50 PSI (triggered)

After application of the primer(s), the panels were flashed 10 minutes at ambient temperature (68 – 72F) in a horizontal position and then baked for 30 minutes @ 270F in a horizontal position
Dry film thickness is attached in Table 15. Applications parameters are shown in Figure 79

Basecoat-BASF Medium Solids Solvent borne, E138KU502PPOP NEGRO BIC
Clearcoat-BASF 2K Low bake, E42CU029P CLEAR JP 71-0312

Application Parameters

VARIABLES

BOOTH

CATEGORY	BC1	BC2	CC1	CC2
HUMIDITY	60±3.0			
TEMPERATURE	24C±2.0			
VELOCITY	0.6±0.05			

ATOMIZER

CATEGORY	BC1	BC2	CC1	CC2
ATOM AIR PRESSURE AT CAP (PSI)				
ATOMIZER	ECOBELL	ECOBELL	ECO BELL	ECO BELL
BELL SPEED LOADED (RPM)	50000	46000	40000	40000
EVERGLOSS 3F71-0312 HARDENER				
FAN AIR PRESSURE AT CAP (PSI)				
FILM BUILD TOTAL (MICRON)		12.5 +- 2.5		37.5± 2.5
FLASH TEMP (C)	23	23	23	23
FLASH TIME (MIN)	1	10	1	8
FLOW RATE	250	100	180	180
FURTHER INSTRUCTION	400 pot	400 pot	400 POT	400 POT
FURTHER INSTRUCTIONS 1				
GUN-TARGET DISTANCE (CM)	30	30	30	30
LINE SPEED (CM/SEC)	0.0	0.0	0.0	0.0
NUMBER OF COATS	1	1	1	1
PANEL ATM0064 TPO 4X 12				
SHAPING AIR PRESSURE (SLPM)	30	20	20	20
STROKE SPEED (CM/SEC)			0.0	0.0
VOLTAGE 1 (KV)	60	45	70	70

OVEN

CATEGORY	BC1	BC2	CC1	CC2
2ND BAKE TEMP (C)				85
2ND BAKE TIME (MIN)				45

Figure 79 Primer and Paint Applications Parameters

Table 15 Dry Film Thicknesses

Panel Number	Primer	DFT (mils)	Clicks	Date Sprayed
2A-1	UBP2C	1.1	28/34	2/6/2020
2A-2	UBP9762HG	1.45	32/30	2/6/2020
3B-2	UBP9762JANB	1.1	27/27	2/7/2020
3B-1	UBP9762JANB	1.1	27/27	2/7/2020
2C-5	UBP9762JANB	1.1	27/27	2/7/2020
2C-3	UBP9762JANB	1.1	27/27	2/7/2020
2C-4	UBP9762JANB	1.1	27/27	2/7/2020
2C-2	UBP9762JANB	1.1	27/27	2/7/2020
2B-15	UBP9762JANB	1.1	27/27	2/7/2020
2C-1	UBP9762JANB	1.1	27/27	2/7/2020
3A-7	UBP9762JANB	1.1	27/27	2/17/2020
3A-10	UBP9762JANB	1	27/27	2/17/2020
2B-11	UBP9762JANB	1	27/27	2/17/2020
2B-12	UBP9762JANB	1	27/27	2/17/2020
2B-9	UBP9762JANB	1	27/27	2/17/2020
2B-13	UBP9762JANB	1	27/27	2/17/2020
2B-14	UBP9762JANB	1	27/27	2/17/2020
3A-8	UBP9762JANB	1	27/27	2/17/2020
2B-10	UBP9762JANB	1	27/27	2/17/2020
3A-4	UBP9762JANB	1	27/27	2/17/2020
3A-2	UBP9762JANB	1.05	27/27	2/17/2020
2B-9	UBP9762JANB	1.05	27/27	2/17/2020
2B-8	UBP9762JANB	1.05	27/27	2/17/2020
2B-7	UBP9762JANB	1.05	27/27	2/17/2020
3A-10	UBP9762JANB	1.05	27/27	2/17/2020
3A-5	UBP9762JANB	1.05	27/27	2/17/2020
3A-3	UBP9762JANB	1.05	27/27	2/17/2020
2B-5	UBP9762JANB	1.2	27/27	2/18/2020
2B-4	UBP9762JANB	1.2	27/27	2/18/2020
2B-3	UBP9762JANB	1.2	27/27	2/18/2020
2B-2	UBP9762JANB	1.2	27/27	2/18/2020
2B-6	UBP9762JANB	1.2	27/27	2/18/2020
2B-1	UBP9762JANB	1.2	27/27	2/18/2020
2A-10	UBP9762JANB	1.2	27/27	2/18/2020
2A-9	UBP9762JANB	1.2	27/27	2/18/2020
2A-8	UBP9762JANB	1.2	27/27	2/18/2020
2A-4	UBP9762JANB	1.05	26/26	2/18/2020

2A-5	UBP9762JANB	1.05	26/26	2/18/2020
2A-6	UBP9762JANB	1.05	26/26	2/18/2020
2A-7	UBP9762JANB	1.05	26/26	2/18/2020
1A-6	UBP9762JANB	1.05	26/26	2/18/2020
1A-7	UBP9762JANB	1.05	26/26	2/18/2020
1A-9	UBP9762JANB	1.05	26/26	2/18/2020
1A-10	UBP9762JANB	1.05	26/26	2/18/2020
2A-3	UBP9762JANB	1.05	26/26	2/18/2020
1A-5	UBP9762JANB	1.05	26/26	2/18/2020
1A-10	UBP9762JANB	1.05	26/26	2/18/2020
1A-4	UBP9762JANB	1.05	26/26	2/18/2020
1A-3	UBP9762JANB	1.05	26/26	2/18/2020
1A-2	UBP9762JANB	1.05	26/26	2/18/2020

5. BENEFITS ASSESSMENT

Vehicle curb weight is directly proportional to the fuel economy of vehicles, therefore light-weighting is crucial for fuel efficiency. This also holds true for battery electric vehicles, which inherently tend to be heavier than conventional powertrains. Therefore, employing lightweight materials translates to lower greenhouse gas and particulate emissions during the vehicle use phase. Glass fiber reinforced composites, especially molding compounds, allow for cost-efficient lightweight components. Working with SMC enables a significant reduction in tooling costs due to the single-step manufacturing process, as opposed to the multi-step forming of sheet metal. Furthermore, SMC allows for a substantial part count reduction, leading to simplified manufacturing and assembly processes. The technology developed in this work combines two or more functionalized materials to further reduce part count and process complexity. This is expected to lead to over 80% lower tooling expenses in the case of a big area component, such as the demonstrator part.

As opposed to metallic materials, glass fiber reinforced SMC does not interfere with electromagnetic radiation, enabling the integration of antenna systems, radars and sensors. Apart from the clear design advantage, this also entails new solution approaches to the equipment necessary for connected vehicles.

The developed technology can be implemented in other application cases and industry sectors. Otherwise functionalized materials can be molded into hybrid part with the demonstrated technology, as long as their rheological behavior is compatible. General understanding for this was also achieved in the scope of this work

6. COMMERCIALIZATION

Founded in 1955, Volkswagen Group of America, Inc., with its principal place of business in Herndon, Virginia, is a wholly owned subsidiary of Volkswagen AG, one of the world's leading automobile manufacturers and the largest carmaker in Europe. Volkswagen AG comprises of over 12 brands, offering products not only on the spectrum of vehicles – from motorcycles to heavy-duty commercial vehicles – but also mobility as a service. The University of Tennessee, Knoxville has recently become the site of Volkswagen's first innovation hub in North America. This collaboration will focus on developing lighter vehicle components made from composite materials, the electrification of vehicles, and other automotive innovations. This hub marks the culmination of years of collaboration since Volkswagen opened its

Chattanooga assembly plant in 2011, which assembles the Volkswagen Passat, as well as the Atlas and Atlas Cross Sport, two sport utility vehicles (SUV), while currently being extended to house the manufacturing line of Volkswagen's first all-electric SUV built on the Modular Electric Drive Matrix (MEB) platform, the ID.4.

The project partners will utilize their connections arching over several industry branches to find alternative applications for the developed materials and technology. Since the demonstrator part has to fulfill a highly complex set of requirements with conflicting mechanical load cases, the project already addresses many relevant questions and concerns for vehicle applications, enabling the direct application in other parts. Closures systems such as doors and liftgates, fenders and other parts of passenger cars, light duty vehicles and trucks can directly utilize the outcomes of this work. Other applications in different industry branches might require the materials or the manufacturing process to be tuned and altered.

The developed simulation software can be readily employed for other compression molding scenarios, by adjusting the material cards and the simulation code as needed. The simulation of multi-material compression molding is a scarcely studied field. The work performed in the scope of this project can serve as the basis of similar computational tasks.

7. ACCOMPLISHMENTS

Using the manufacturing methods and simulations available, the team determined that automotive hood geometry mass-to-performance ratio probably doesn't benefit from a single-panel co-molding of SMCs. A design optimization tool for one specific geometry was developed to explore the parameter space. The simulation methods for multi-material flow front and orientation prediction were developed to a new level. A number of non-destructive investigation methods were evaluated for future use on co-molded panels.

8. CONCLUSIONS

As presented in the details of this report, the team was able to develop modelling tools to predict flow patterns and mechanical properties of co-mold molded materials of different laminate configurations. The remaining challenge is determining if these results can be transferred to an actual automotive part. The tooling costs for a full size hood is a barrier to demonstrating the full potentials of the project.

9. RECOMMENDATIONS

The recommendation of the team is to proceed with a second phase of the project to develop a unique manufacturing process, along with the required material intermediates, enabling the cost-efficient production of a one-piece automotive hood.

10. REFERENCES AND/OR BIBLIOGRAPHY

Mainka, Hendrik, Laduch, Thomas, Kardos, Marton, Penumadu, Dayakar, Vaidya, Uday, Bogdanor, Michael, Skop, Shane, & Hassen, Ahmed Arabi. Reduction of CO2 Emissions Through Lightweight Body Panels (Project Final Report). United States. https://doi.org/10.2172/1769017

Editor. (2013). Retrieved from plastics.gl: https://www.plastics.gl/automotive/improved-styling-freedom/

Favaloro AJ, S. D. (2018). Simulation of prepreg platelet compression molding: Method and orientation validation. (N. Y. Y, Ed.) *Journal of Rheology, 62*(6), 1443-1455. doi:10.1122/1.5044533

Favaloro, A. (2017). *Rheological Behavior and Manufacturing Simulation of Prepreg Platelet Molding Systems. Ph.D. Thesis.* Purdue University.

GM. (2012, 8 16). *GM Corporate Newsroom*. Retrieved from media.gm.com: https://media.gm.com/media/us/en/gm/news.detail.html/content/Pages/news/us/en/2012/Aug/0816_corvette.html

Karmarkar, S. (2018). *Extrusion Deposition Additive Manufacturing For High Temperature Tooling.* West Lafayette: Purdue University.

Malnati, P. (2017, 9 18). *Composites World*. Retrieved from CompositesWorld.com: https://www.compositesworld.com/articles/smc-d-lft-a-hybrid-box-for-the-gen-2-ridgeline-

MatWeb Material Property Data. (n.d.). Retrieved from MatWeb: http://www.matweb.com/search/datasheet.aspx?matguid=36ff812971894f88a6c5f9af35826dcc&ckck=1

Nassar, A., & Nassar, E. (2020). Effect of fiber orientation on the mechanical properties of multi layers laminate nanocomposites. *Heliyon*. Retrieved from https://www.sciencedirect.com/science/article/pii/S2405844020300128?via%3Dihub

11. APPENDICES

11.1. Frequency Sweep Rheology Curves

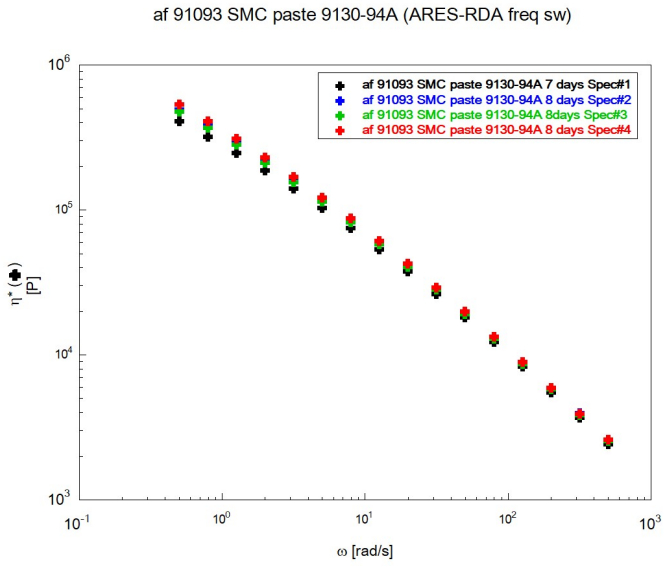

3

af 91093 SMC paste 9130-94A 7 days Spec#1 (ARES-RDA temp sw) (SeqTest 2)

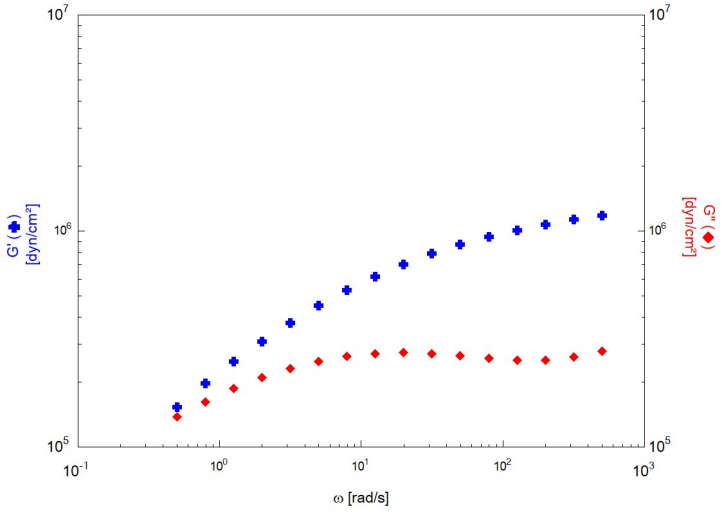

af 91093 SMC paste 9130-94A 8 days Spec#2 (ARES-RDA temp sw) (SeqTest 2)

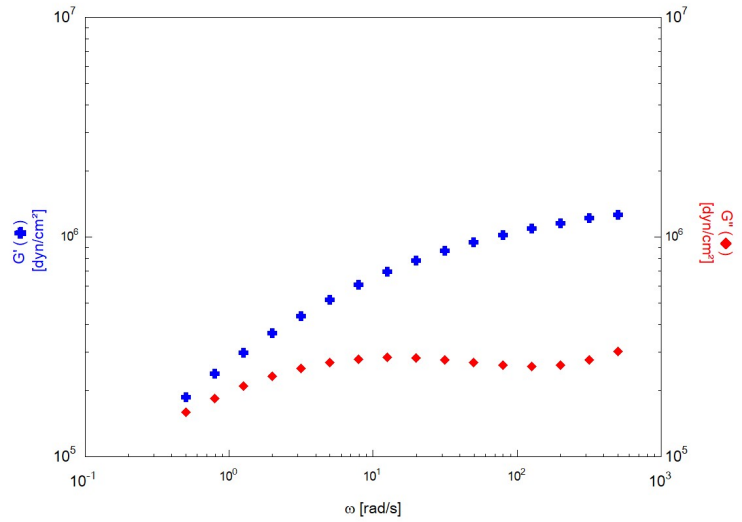

af 91093 SMC paste 9130-94A 8days Spec#3 (ARES-RDA temp sw) (SeqTest 2)

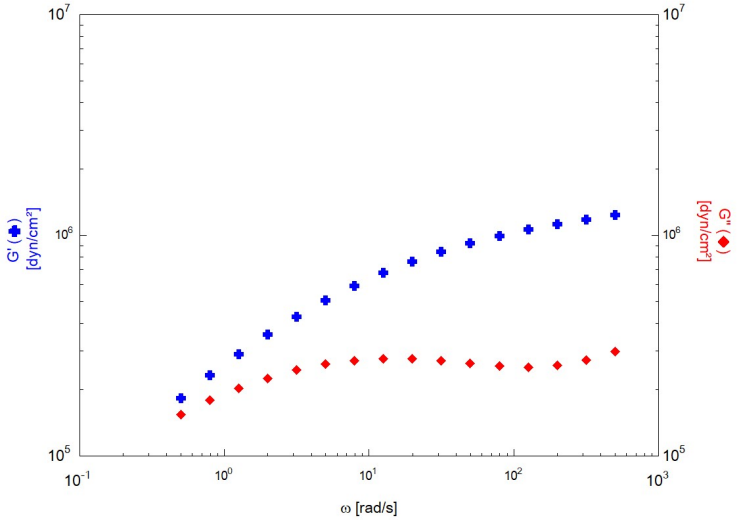

af 91093 SMC paste 9130-94A 8 days Spec#4 (ARES-RDA temp sw) (SeqTest 2)

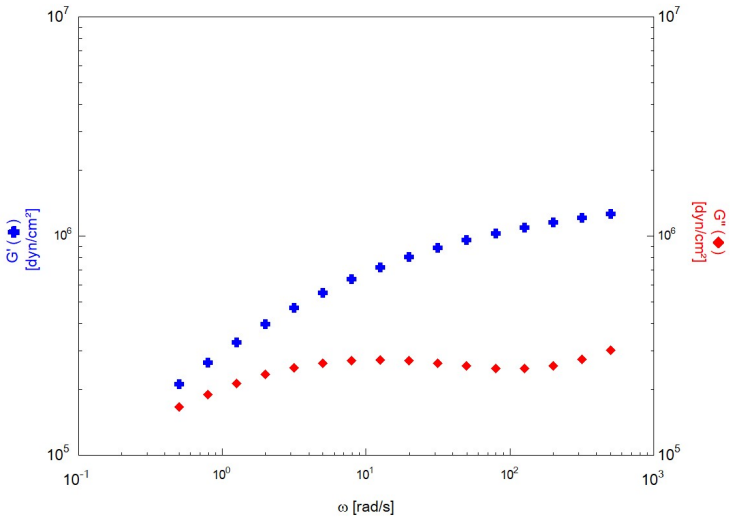

af 91093 SMC Class A Paste 9130-94B (ARES-RDA temp sw) (SeqTest 2)

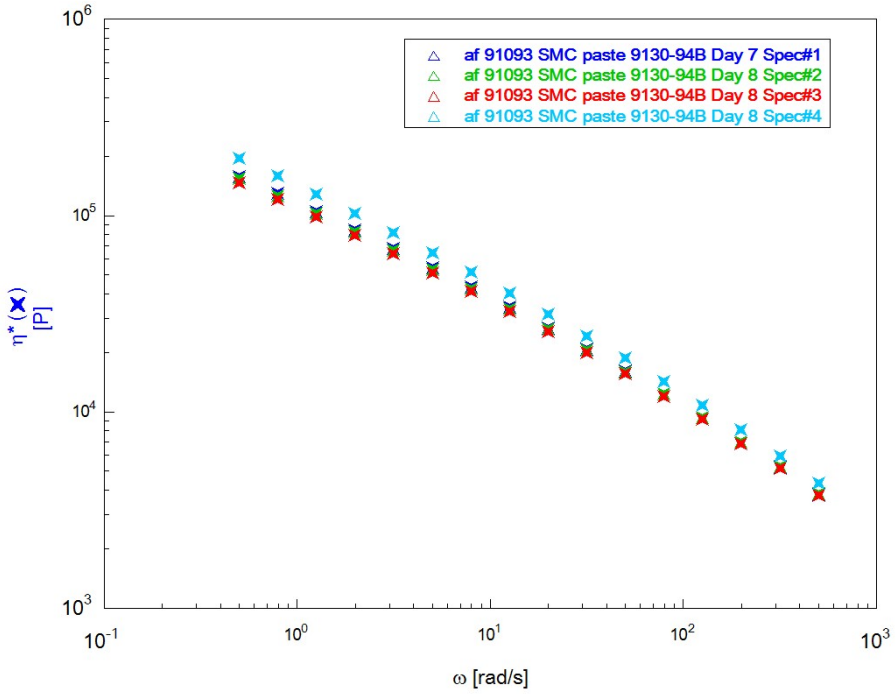

af 91093 SMC paste 9130-94B Day 7 Spec#1 (ARES-RDA temp sw) (SeqTest 2)

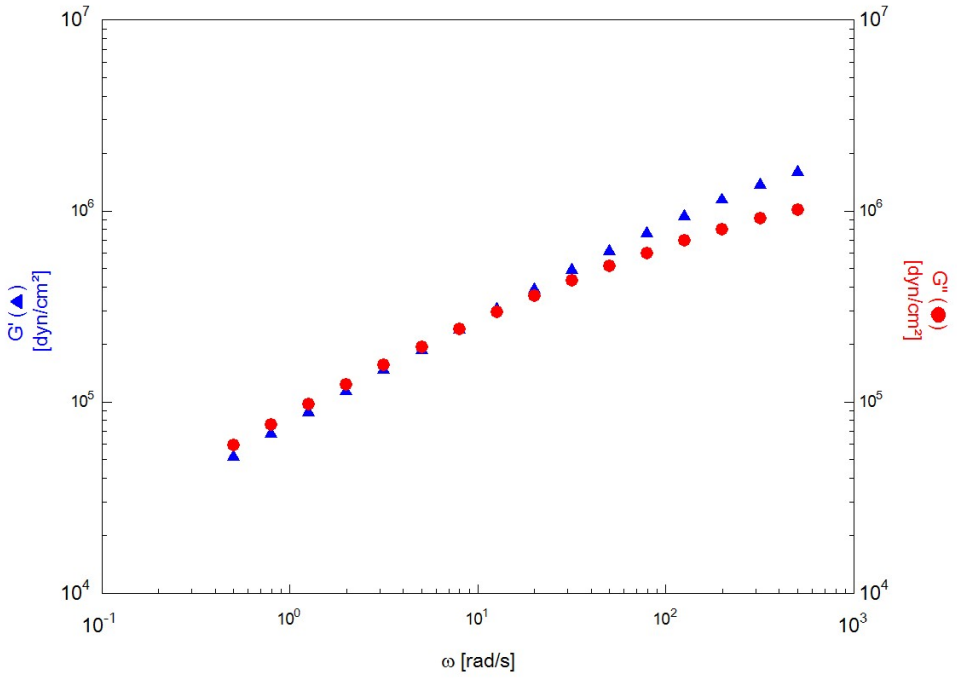

af 91093 SMC paste 9130-94B Day 8 Spec#2 (ARES-RDA temp sw) (SeqTest 2)

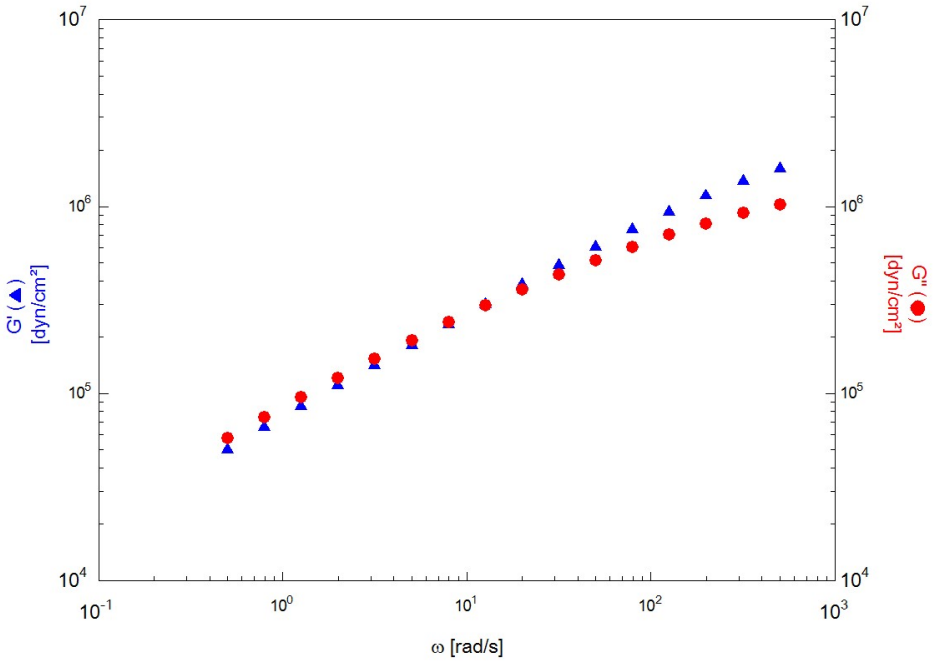

af 91093 SMC paste 9130-94B Day 8 Spec#3 (ARES-RDA temp sw) (SeqTest 2)

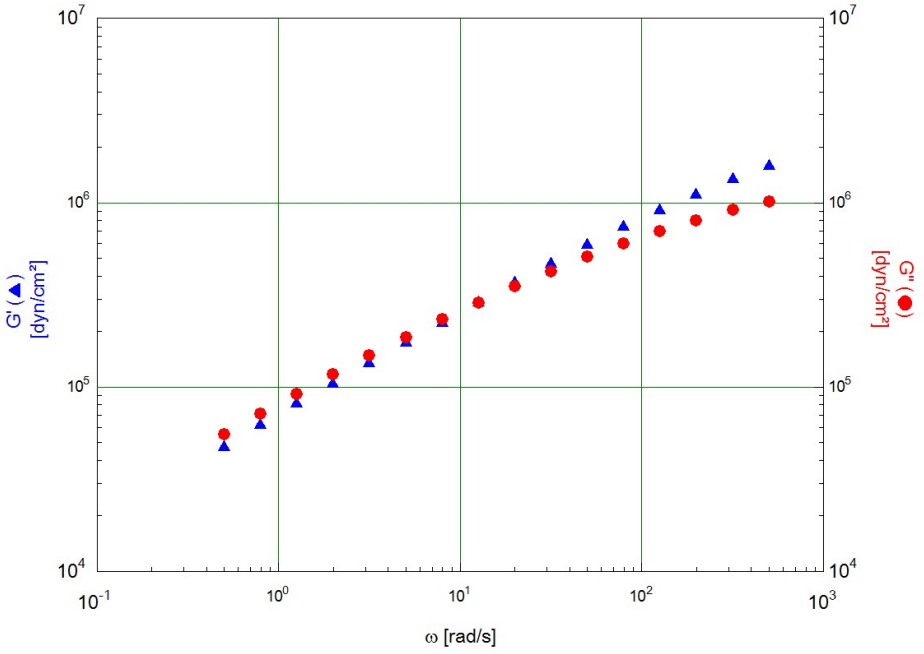

af 91093 SMC paste 9130-94B Day 8 Spec#4 (ARES-RDA temp sw) (SeqTest 2)

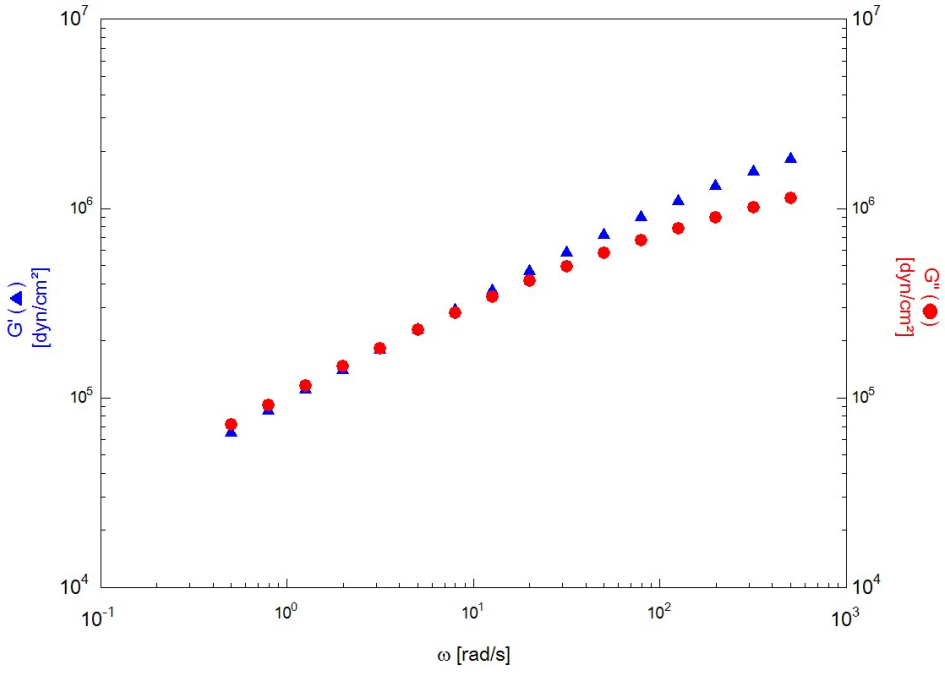

11.2. Temperature Sweep Rheology Curves

af 91093 SMC paste 9130-94A (ARES-RDA temp sw)

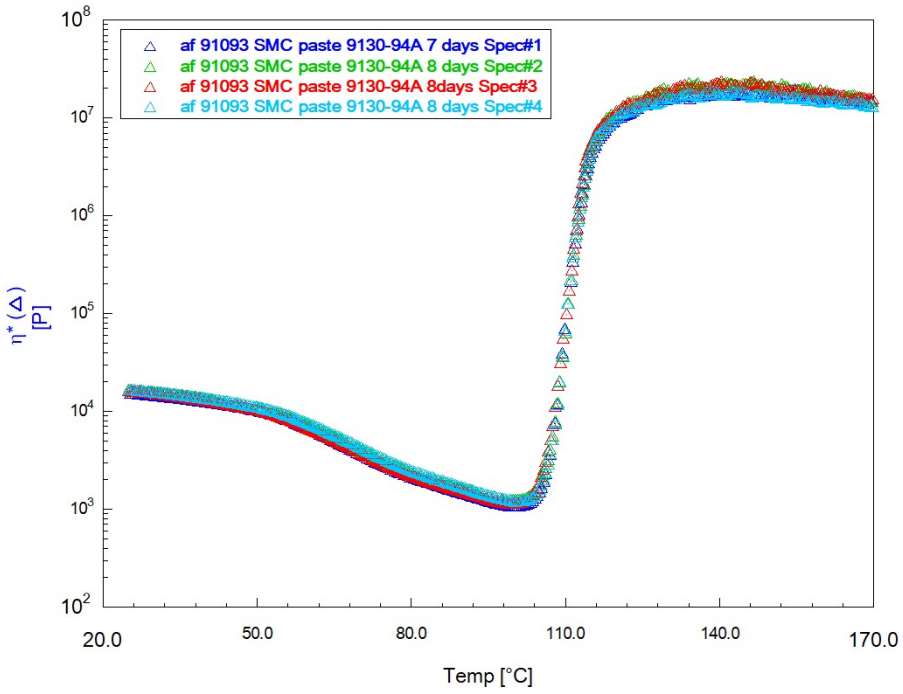

af 91093 SMC paste 9130-94A 7 days Spec#1 (ARES-RDA temp sw) (SeqTest 4)

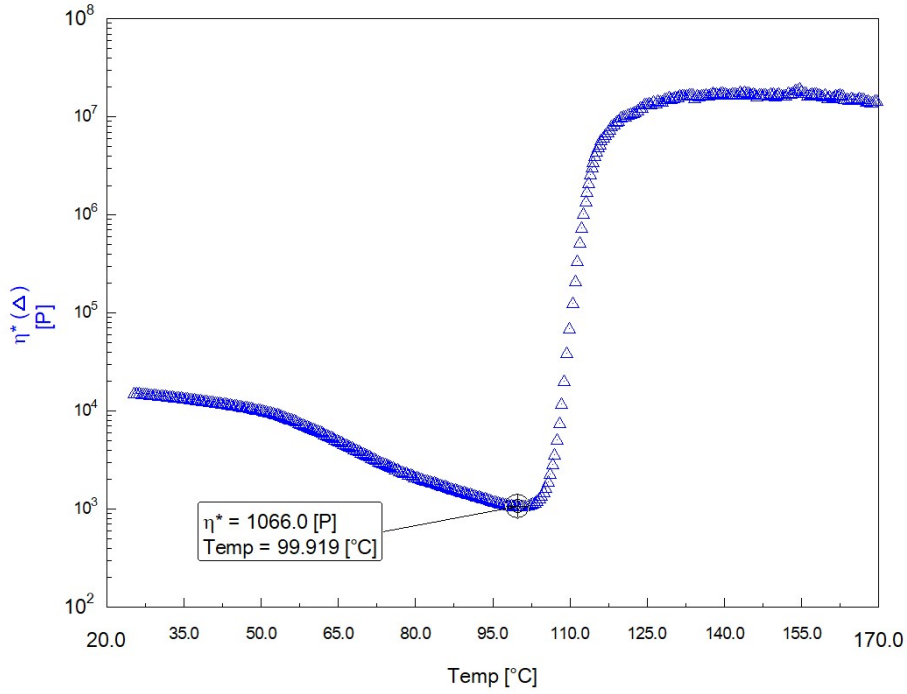

af 91093 SMC paste 9130-94A 8 days Spec#2 (ARES-RDA temp sw) (SeqTest 4)

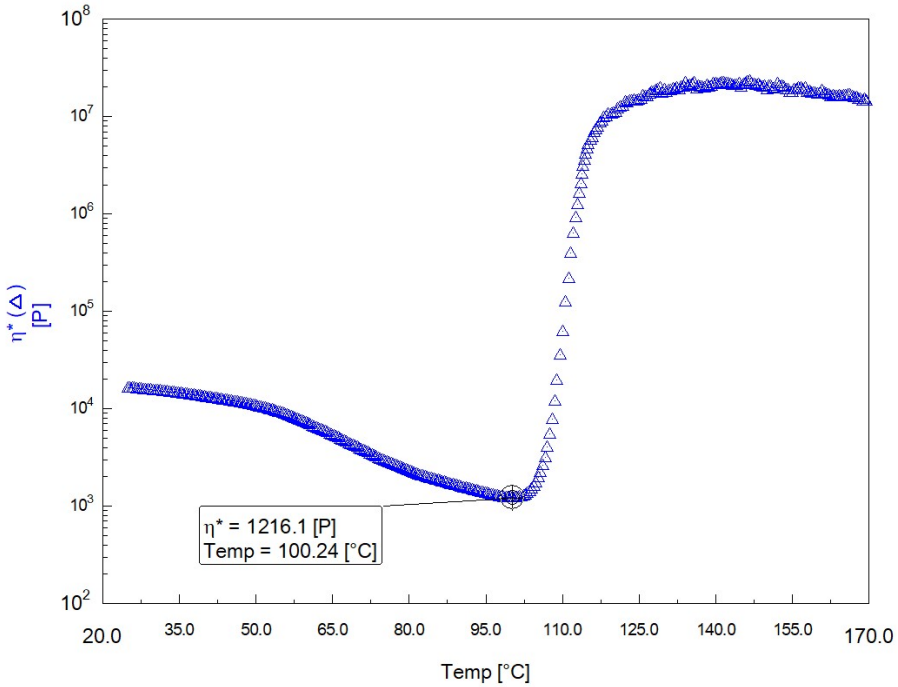

af 91093 SMC paste 9130-94A 8days Spec#3 (ARES-RDA temp sw) (SeqTest 4)

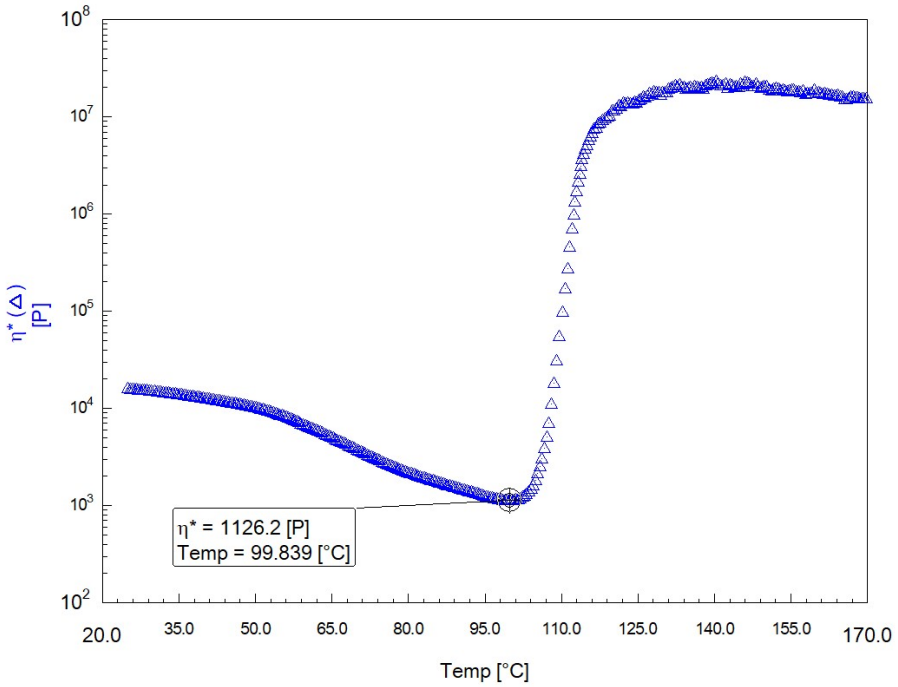

af 91093 SMC paste 9130-94A 8 days Spec#4 (ARES-RDA temp sw) (SeqTest 4)

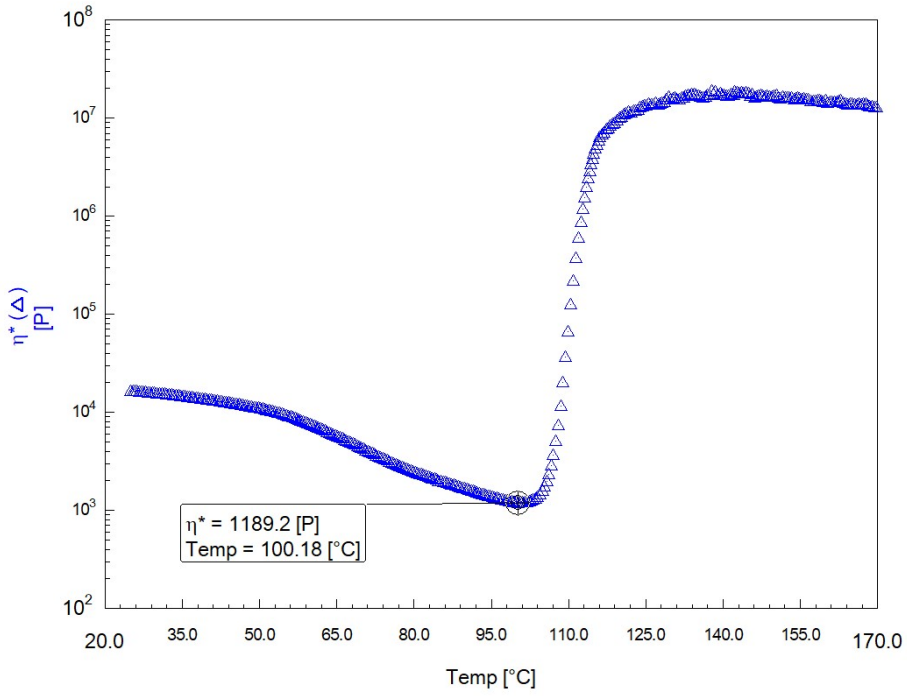

af 91093 SMC paste 9130-94A 7 days Spec#1 (ARES-RDA temp sw) (SeqTest 4)

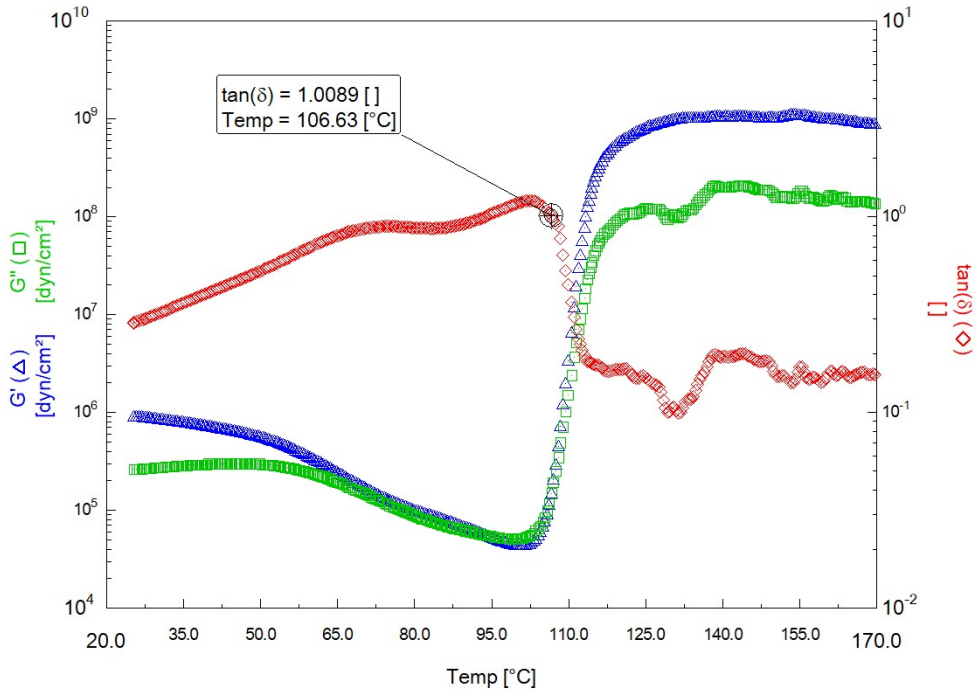

af 91093 SMC Class A paste 9130-94B (ARES-RDA temp sw)

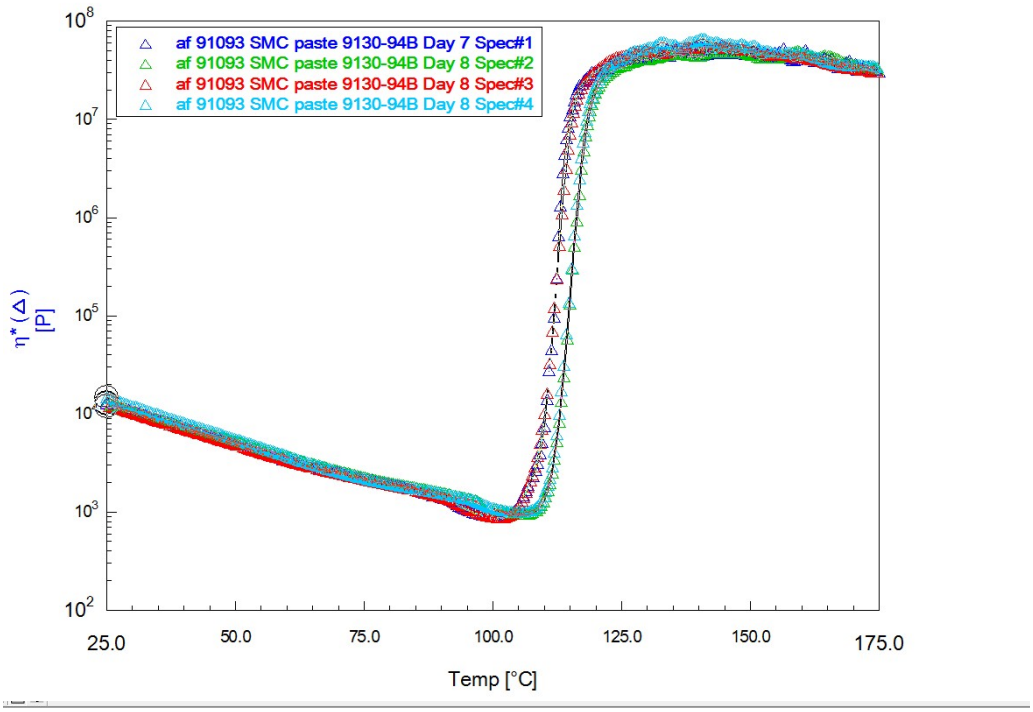

af 91093 SMC paste 9130-94B Day 7 Spec#1 (ARES-RDA temp sw) (SeqTest 4)

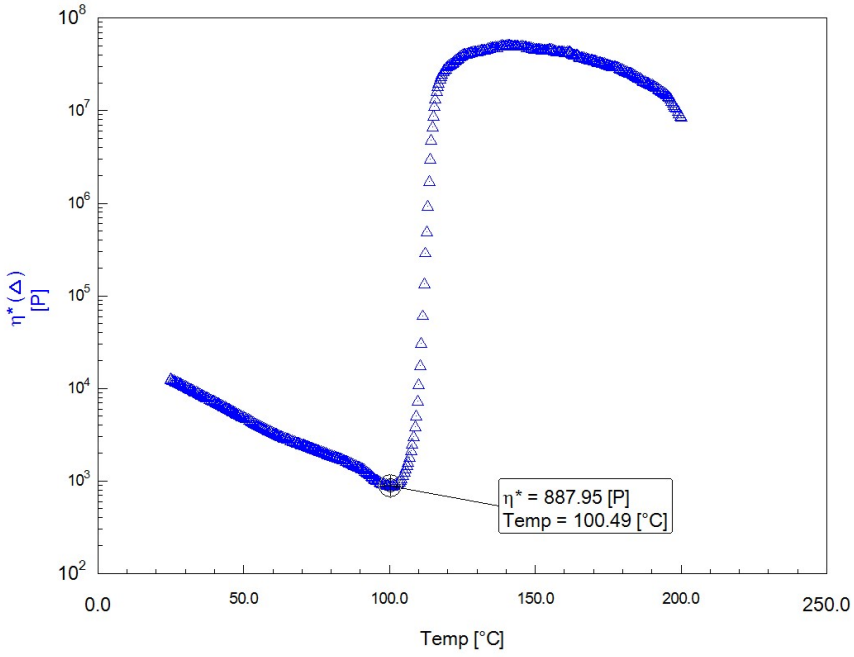

af 91093 SMC paste 9130-94B Day 8 Spec#2 (ARES-RDA temp sw) (SeqTest 4)

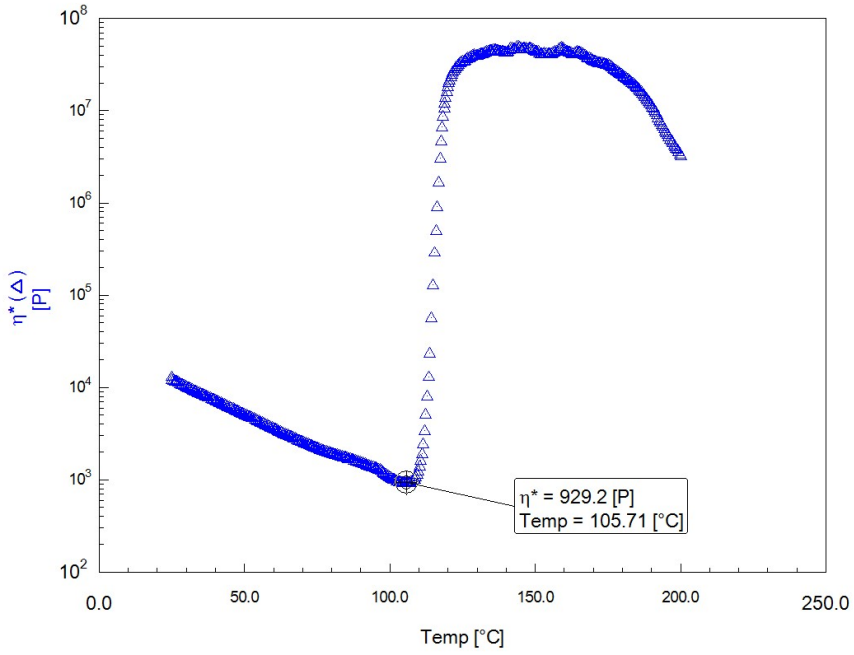

af 91093 SMC paste 9130-94B Day 8 Spec#3 (ARES-RDA temp sw) (SeqTest 4)

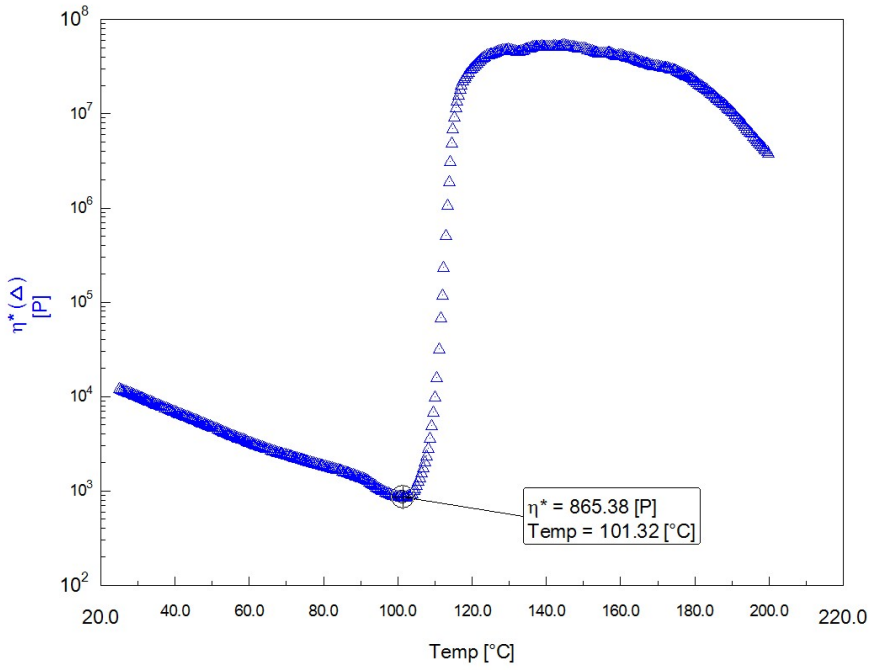

af 91093 SMC paste 9130-94B Day 8 Spec#4 (ARES-RDA temp sw) (SeqTest 4)

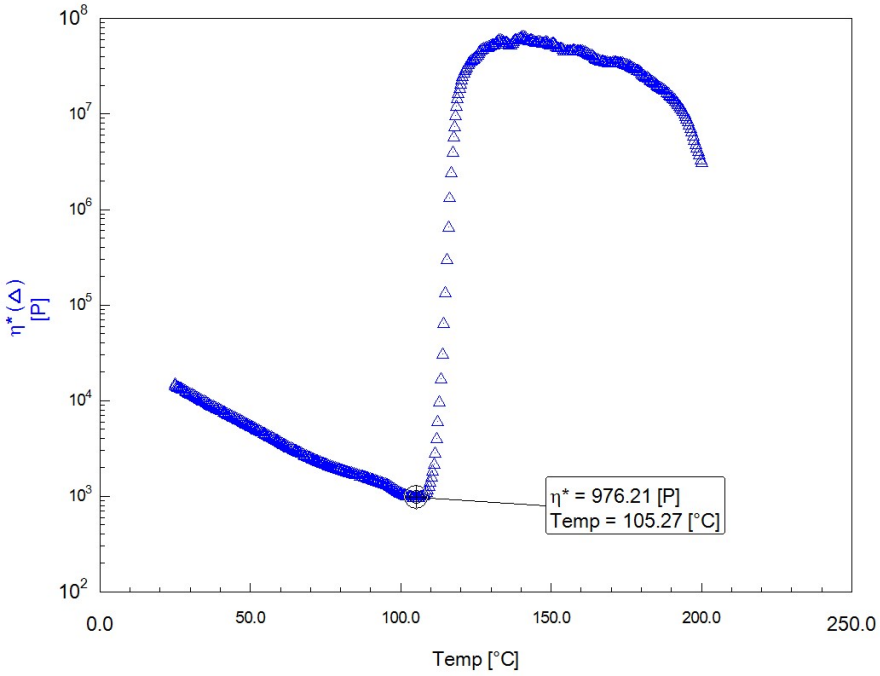

af 91093 SMC paste 9130-94B Day 7 Spec#1 (ARES-RDA temp sw) (SeqTest 4)

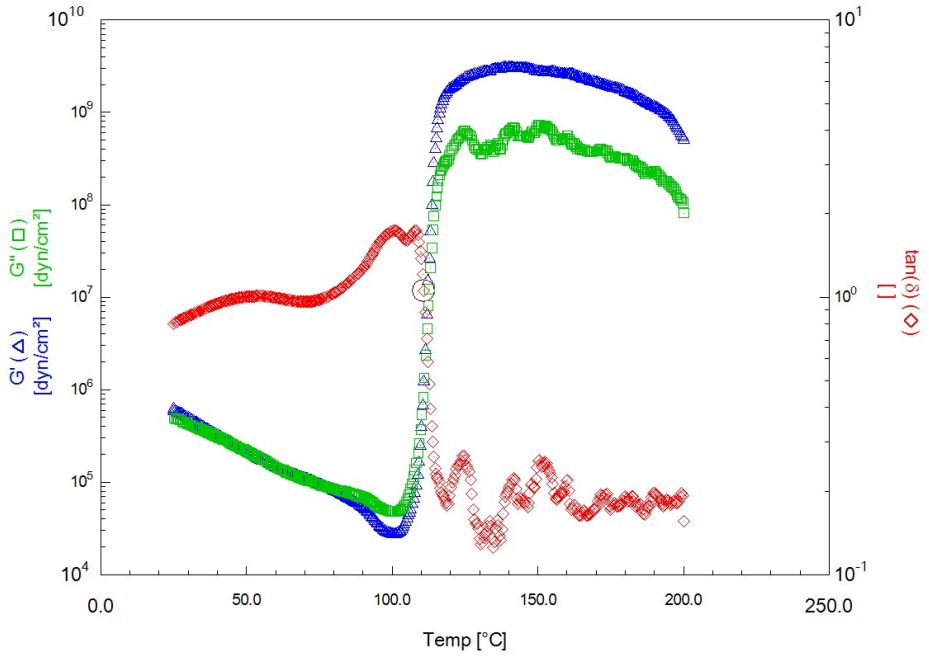

11.3. Isothermal Rheology Curves at 90 C

af 91093 SMC paste 9130-94A Structural (ARES-RDA iso 90c) 11-6-19

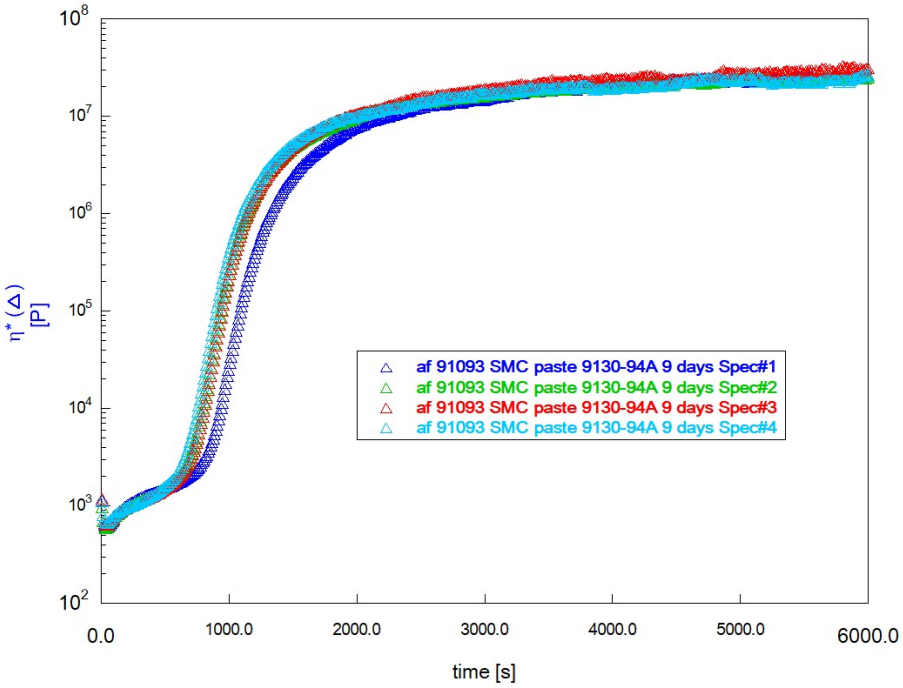

af 91093 SMC Class A paste 9130-94B Day 9 (ARES-RDA iso 90c) 10-10-19

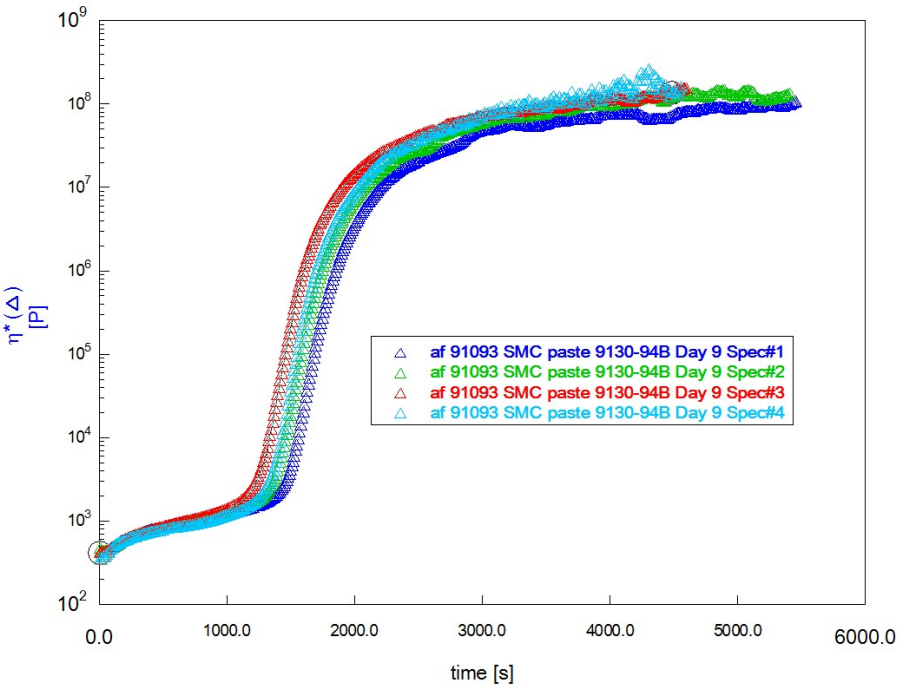

11.4. DSC Overlays

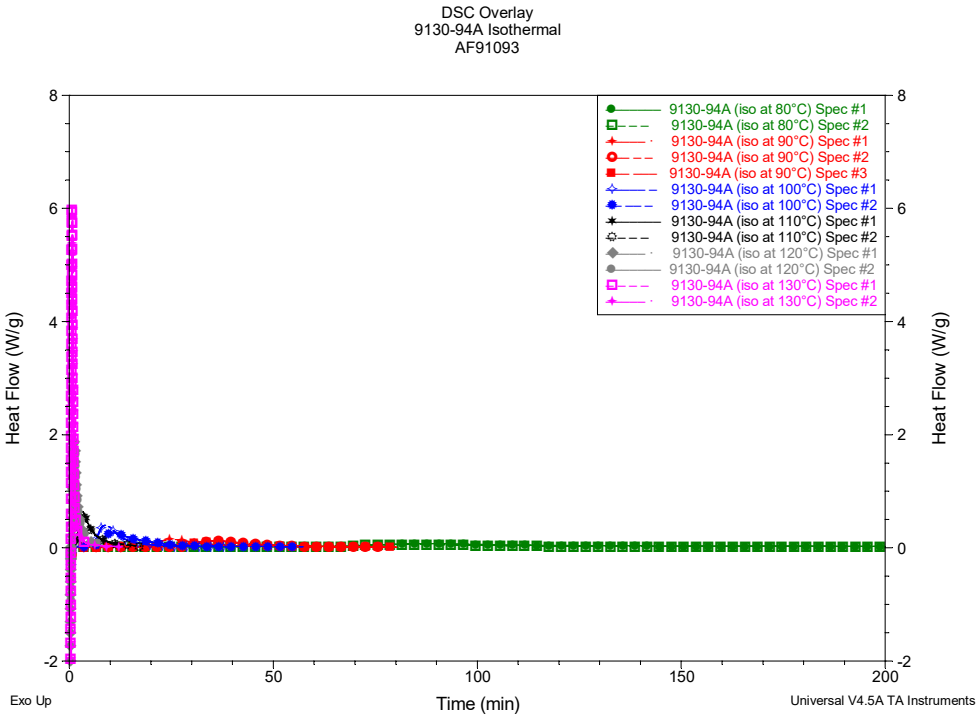

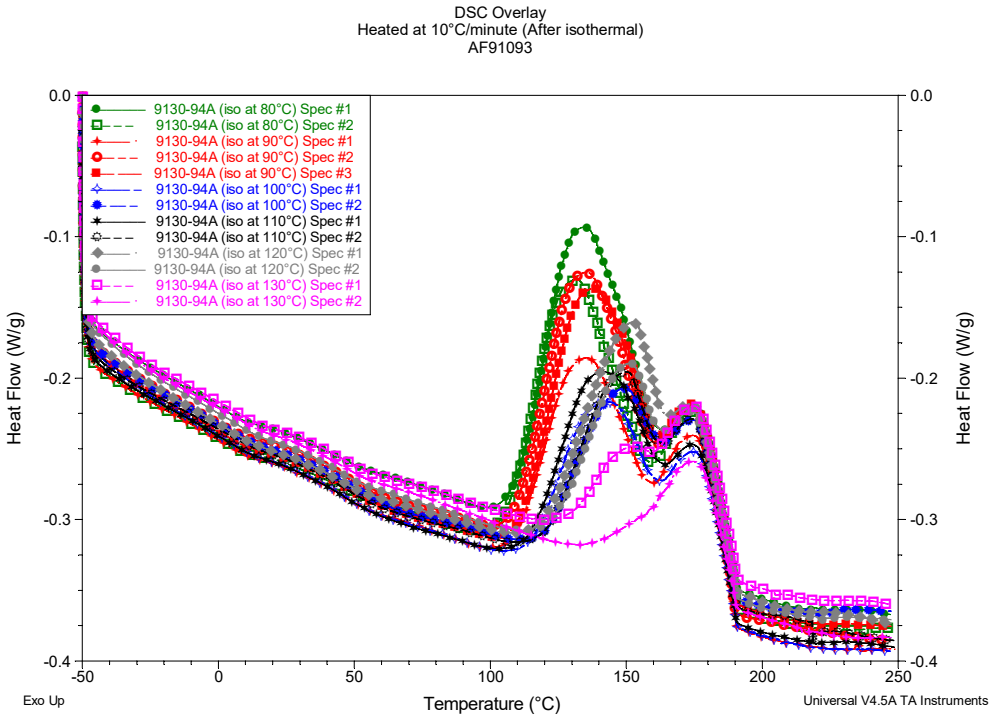

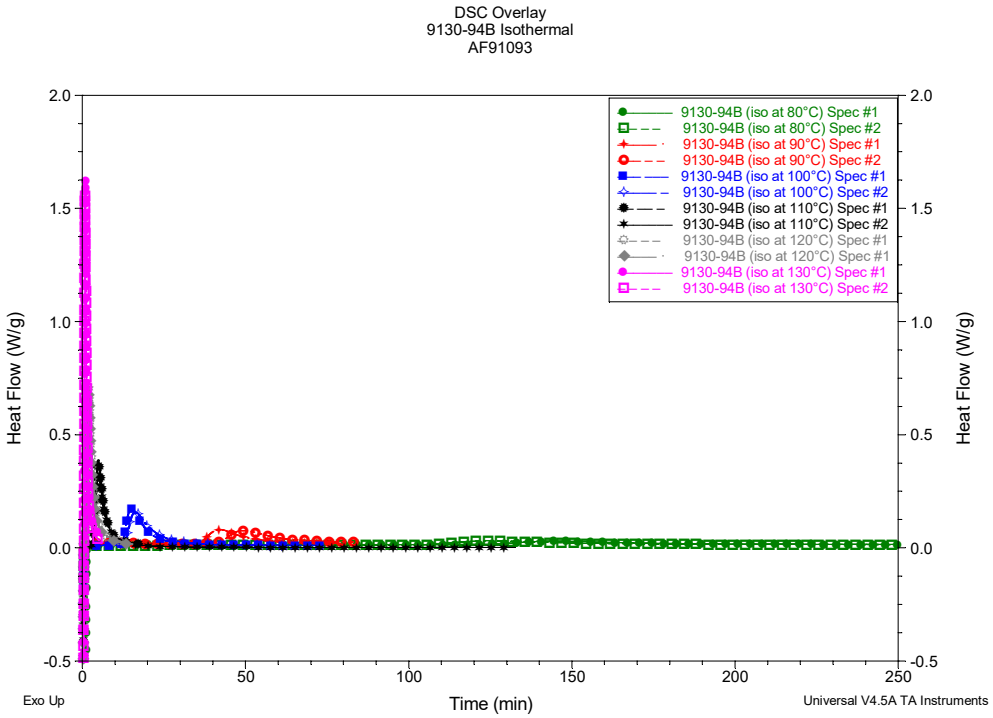
DSC Overlay
9130-94B Isothermal
AF91093
9130-94B (iso at 80°C) Spec #1
9130-94B (iso at 80°C) Spec #2
9130-94B (iso at 90°C) Spec #1
9130-94B (iso at 90°C) Spec #2
9130-94B (iso at 100°C) Spec #1
9130-94B (iso at 100°C) Spec #2
9130-94B (iso at 110°C) Spec #1
9130-94B (iso at 110°C) Spec #2
9130-94B (iso at 120°C) Spec #1
9130-94B (iso at 120°C) Spec #2
9130-94B (iso at 130°C) Spec #1
9130-94B (iso at 130°C) Spec #2
Heat Flow (W/g)
Time (min)
Exo Up
Universal V4.5A TA Instruments

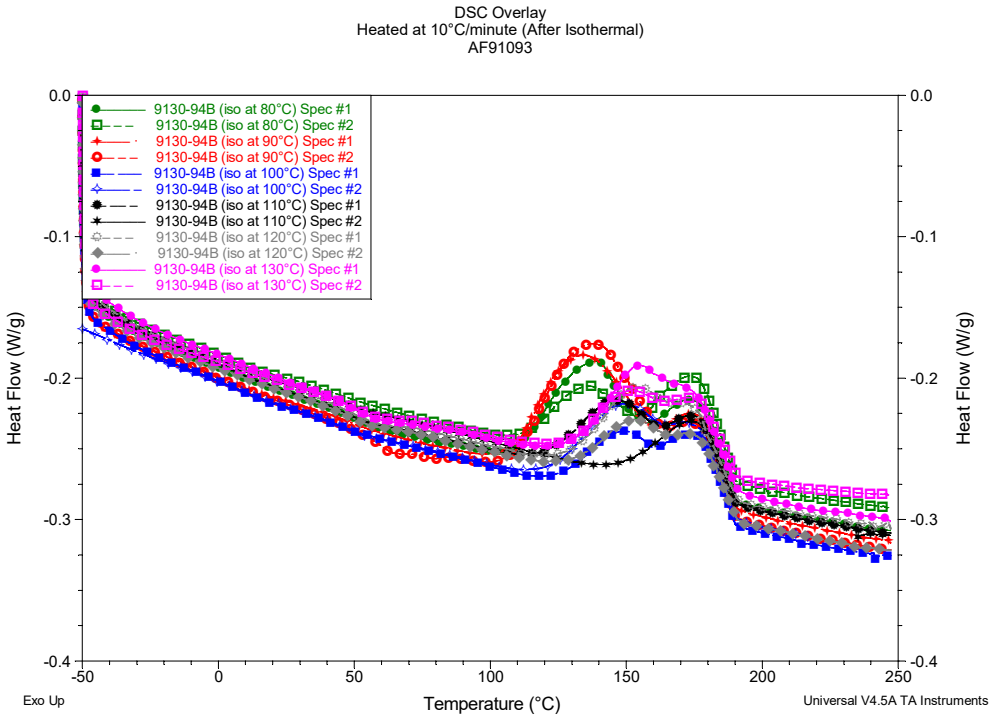
DSC Overlay
Heated at 10°C/minute (After Isothermal)
AF91093
9130-94B (iso at 80°C) Spec #1
9130-94B (iso at 80°C) Spec #2
9130-94B (iso at 90°C) Spec #1
9130-94B (iso at 90°C) Spec #2
9130-94B (iso at 100°C) Spec #1
9130-94B (iso at 100°C) Spec #2
9130-94B (iso at 110°C) Spec #1
9130-94B (iso at 110°C) Spec #2
9130-94B (iso at 120°C) Spec #1
9130-94B (iso at 120°C) Spec #2
9130-94B (iso at 130°C) Spec #1
9130-94B (iso at 130°C) Spec #2
Heat Flow (W/g)
Temperature (°C)
Exo Up
Universal V4.5A TA Instruments

11.5. MDSC Profiles

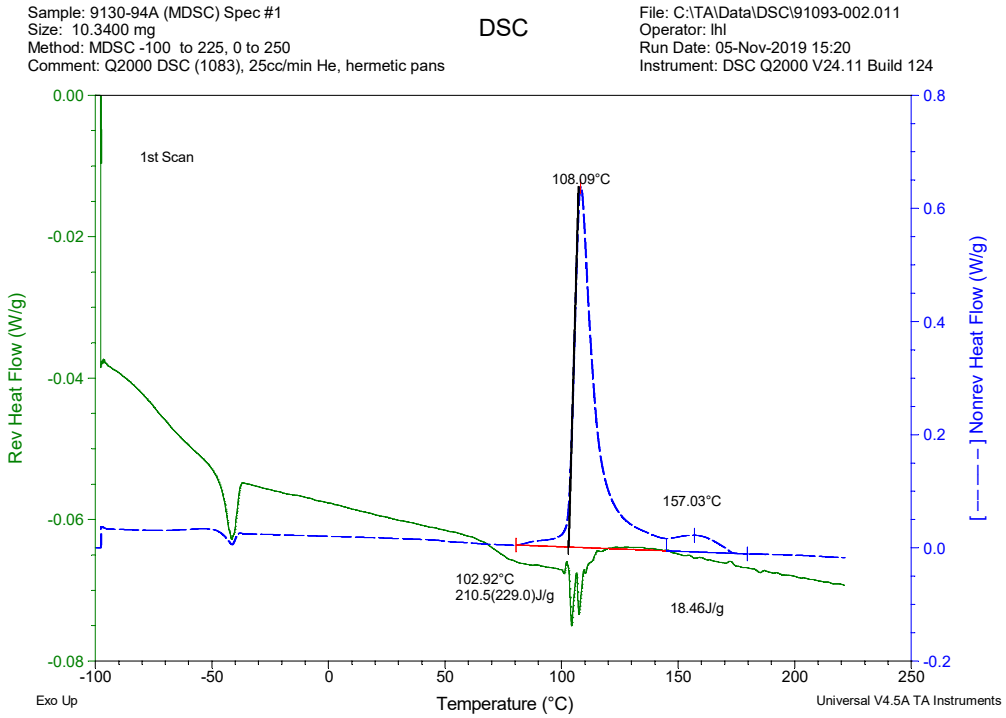

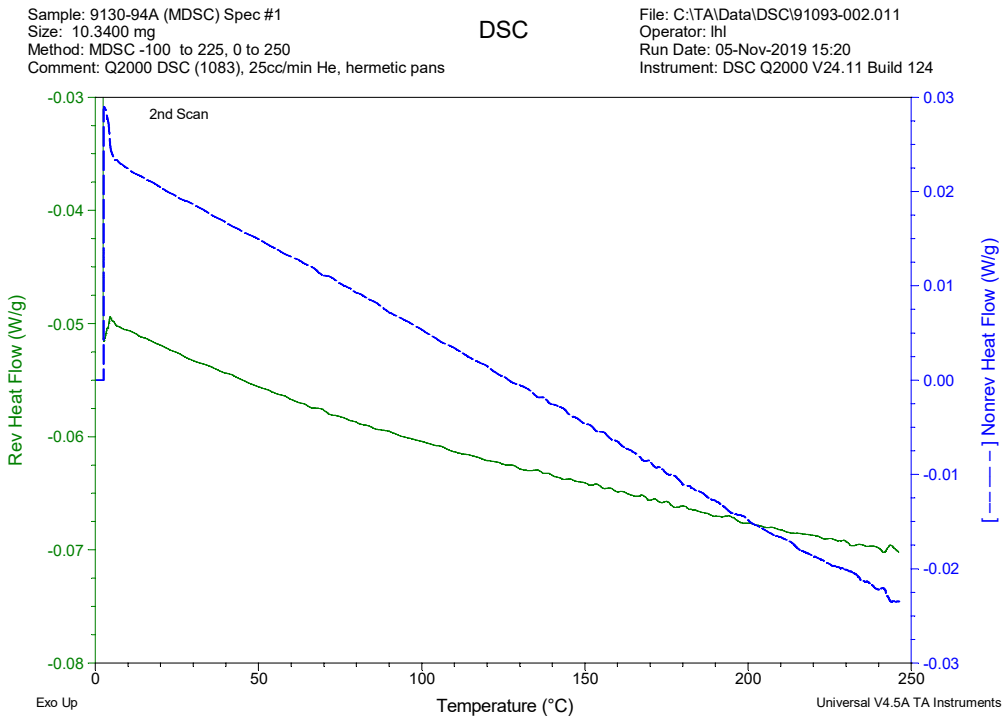

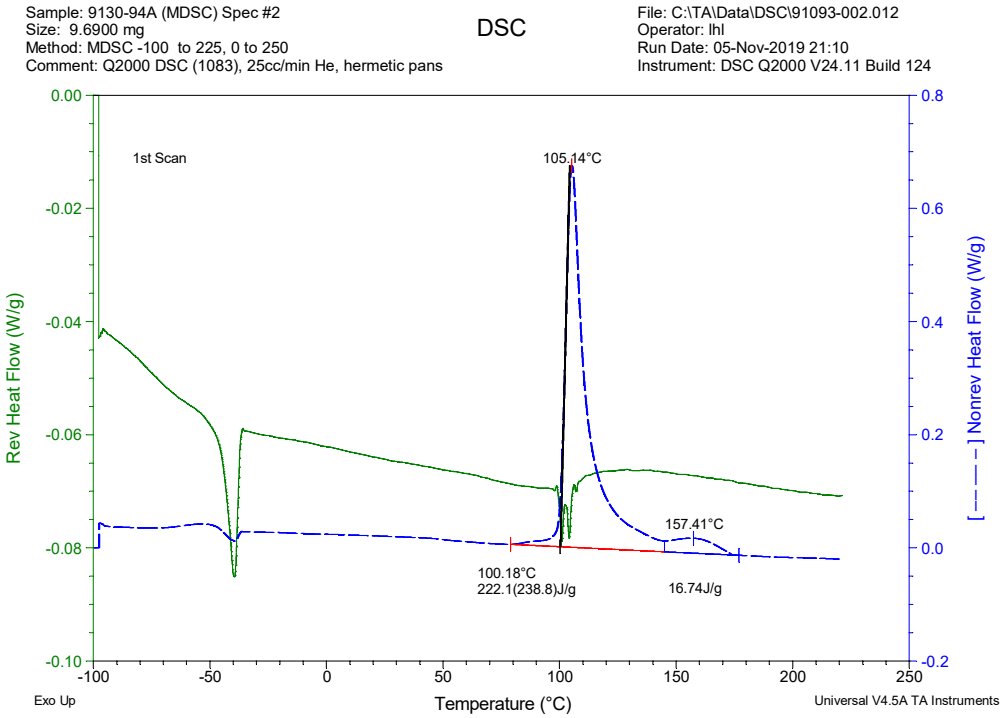
Sample: 9130-94A (MDSC) Spec #2
Size: 9.6900 mg
Method: MDSC -100 to 225, 0 to 250
Comment: Q2000 DSC (1083), 25cc/min He, hermetic pans
DSC
File: C:\TA\Data\DSC\91093-002.012
Operator: lhl
Run Date: 05-Nov-2019 21:10
Instrument: DSC Q2000 V24.11 Build 124
1st Scan
105.14°C
157.41°C
100.18°C
222.1(238.8)J/g
16.74J/g
Rev Heat Flow (W/g)
[— — —] Nonrev Heat Flow (W/g)
Temperature (°C)
Exo Up
Universal V4.5A TA Instruments

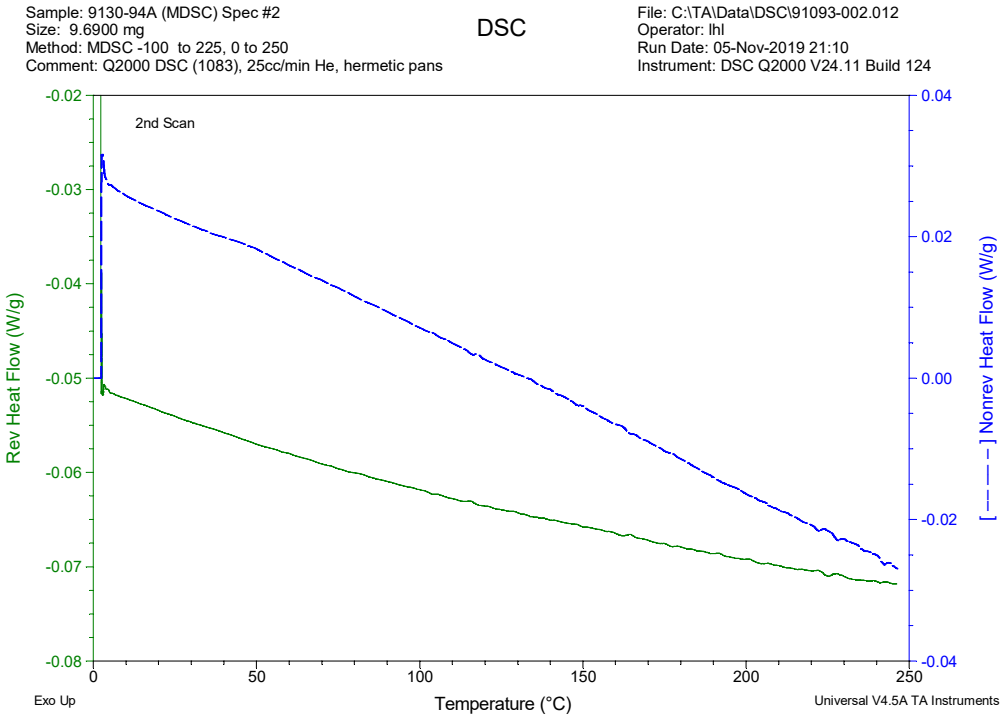
Sample: 9130-94A (MDSC) Spec #2
Size: 9.6900 mg
Method: MDSC -100 to 225, 0 to 250
Comment: Q2000 DSC (1083), 25cc/min He, hermetic pans
DSC
File: C:\TA\Data\DSC\91093-002.012
Operator: lhl
Run Date: 05-Nov-2019 21:10
Instrument: DSC Q2000 V24.11 Build 124
2nd Scan
Rev Heat Flow (W/g)
[— — —] Nonrev Heat Flow (W/g)
Temperature (°C)
Exo Up
Universal V4.5A TA Instruments

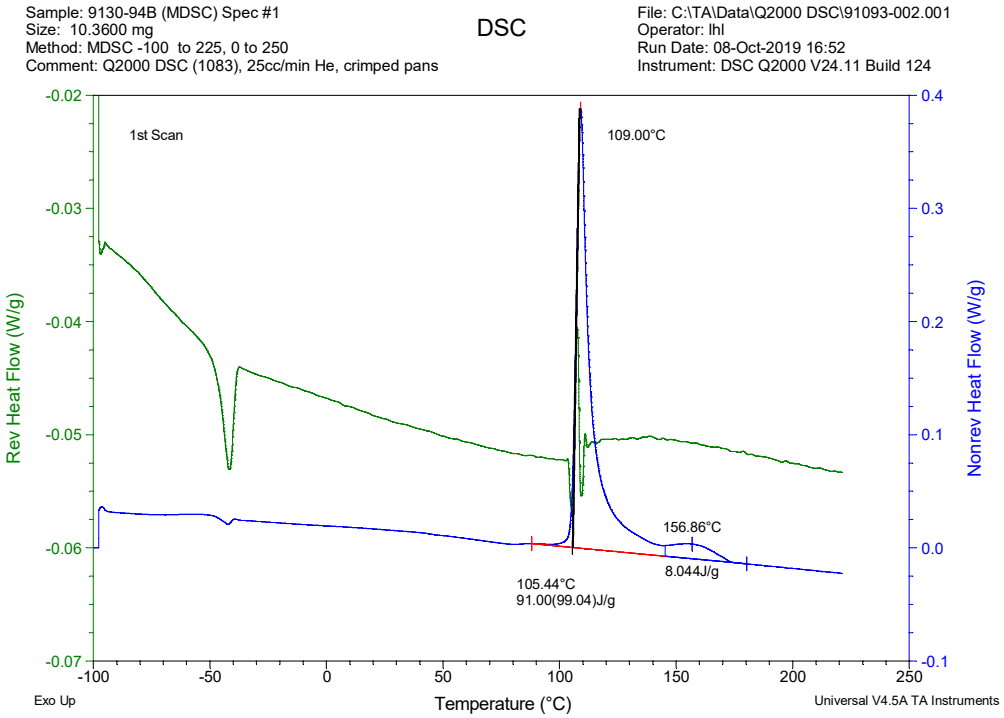
Sample: 9130-94B (MDSC) Spec #1
Size: 10.3600 mg
Method: MDSC -100 to 225, 0 to 250
Comment: Q2000 DSC (1083), 25cc/min He, crimped pans
DSC
File: C:\TA\Data\Q2000 DSC\91093-002.001
Operator: lhl
Run Date: 08-Oct-2019 16:52
Instrument: DSC Q2000 V24.11 Build 124
1st Scan
109.00°C
156.86°C
8.044J/g
105.44°C
91.00(99.04)J/g
Rev Heat Flow (W/g)
Nonrev Heat Flow (W/g)
Temperature (°C)
Exo Up
Universal V4.5A TA Instruments

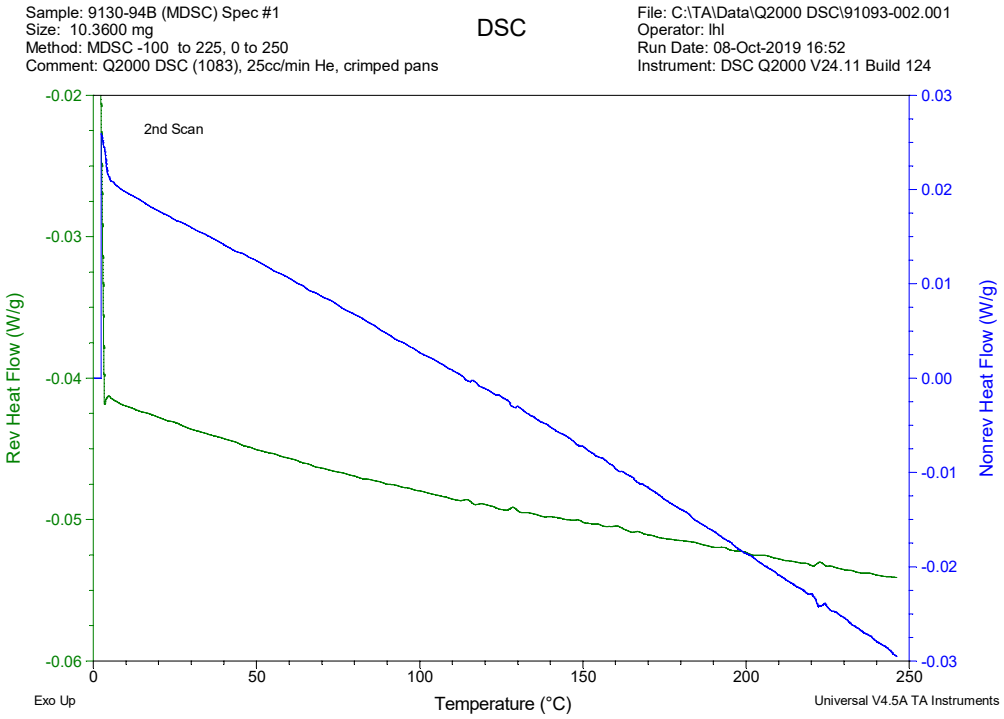
Sample: 9130-94B (MDSC) Spec #1
Size: 10.3600 mg
Method: MDSC -100 to 225, 0 to 250
Comment: Q2000 DSC (1083), 25cc/min He, crimped pans
DSC
File: C:\TA\Data\Q2000 DSC\91093-002.001
Operator: lhl
Run Date: 08-Oct-2019 16:52
Instrument: DSC Q2000 V24.11 Build 124
2nd Scan
Rev Heat Flow (W/g)
Nonrev Heat Flow (W/g)
Temperature (°C)
Exo Up
Universal V4.5A TA Instruments

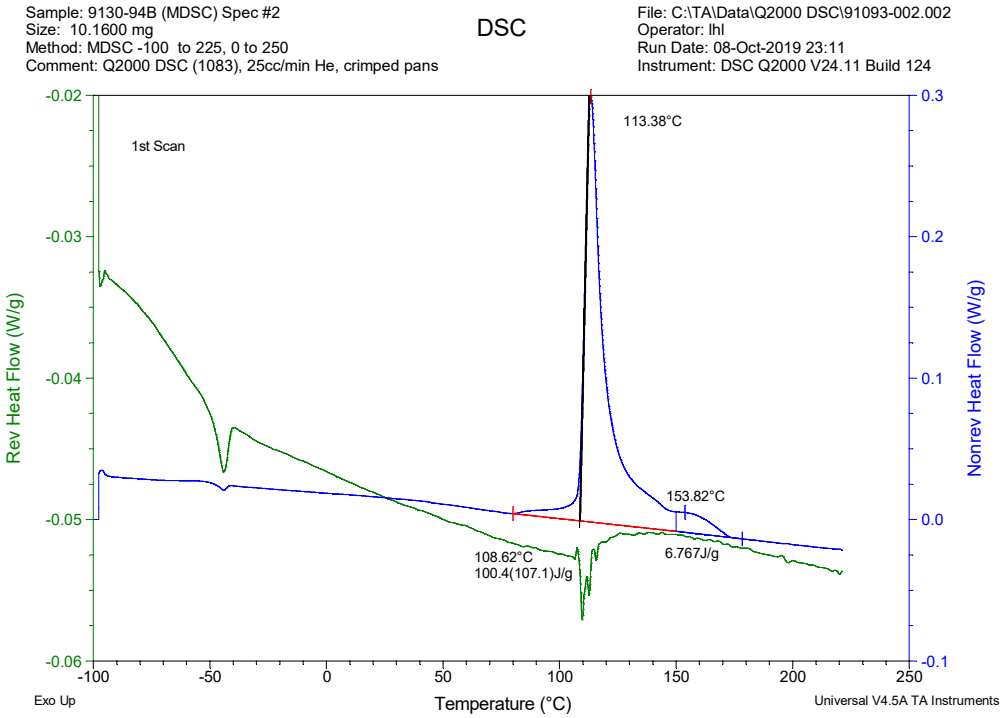
Sample: 9130-94B (MDSC) Spec #2
Size: 10.1600 mg
Method: MDSC -100 to 225, 0 to 250
Comment: Q2000 DSC (1083), 25cc/min He, crimped pans
DSC
File: C:\TA\Data\Q2000 DSC\91093-002.002
Operator: lhl
Run Date: 08-Oct-2019 23:11
Instrument: DSC Q2000 V24.11 Build 124
1st Scan
113.38°C
153.82°C
108.62°C
100.4(107.1)J/g
6.767J/g
Rev Heat Flow (W/g)
Nonrev Heat Flow (W/g)
Temperature (°C)
Exo Up
Universal V4.5A TA Instruments

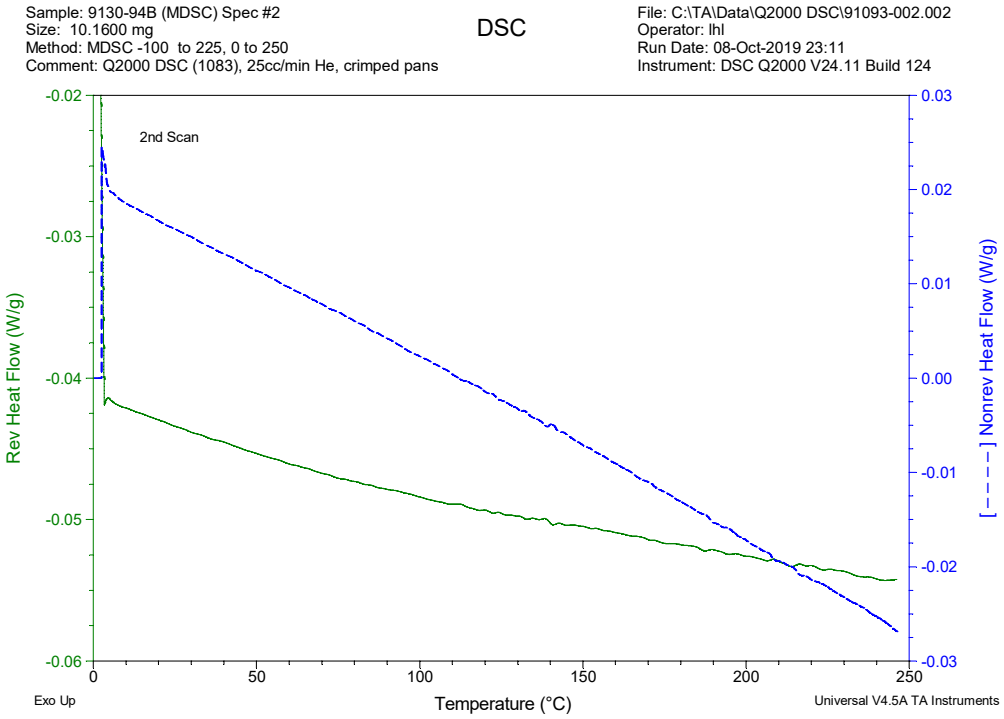
Sample: 9130-94B (MDSC) Spec #2
Size: 10.1600 mg
Method: MDSC -100 to 225, 0 to 250
Comment: Q2000 DSC (1083), 25cc/min He, crimped pans
DSC
File: C:\TA\Data\Q2000 DSC\91093-002.002
Operator: lhl
Run Date: 08-Oct-2019 23:11
Instrument: DSC Q2000 V24.11 Build 124
2nd Scan
Rev Heat Flow (W/g)
[- - - -] Nonrev Heat Flow (W/g)
Temperature (°C)
Exo Up
Universal V4.5A TA Instruments

11.6. DSC Profiles

Sample: 9130-94A (Spec #1) 5°C/min 7 days
Comment: 50ml/minute nitrogen
Method: -50 to 250 (5°C/min)
Operator: lhl
File: C:\TA\Data\Discovery DSC\91093 9130-94A (Spec #1) 5°Cmin 7 days -50 to 250 (5°Cmin) .tri

Instrument/Date: DSC2500,11/5/2019 8:46:10 AM
Sample Mass: 9.81000 mg
Pan type: Aluminum Hermetic
Project: 91093

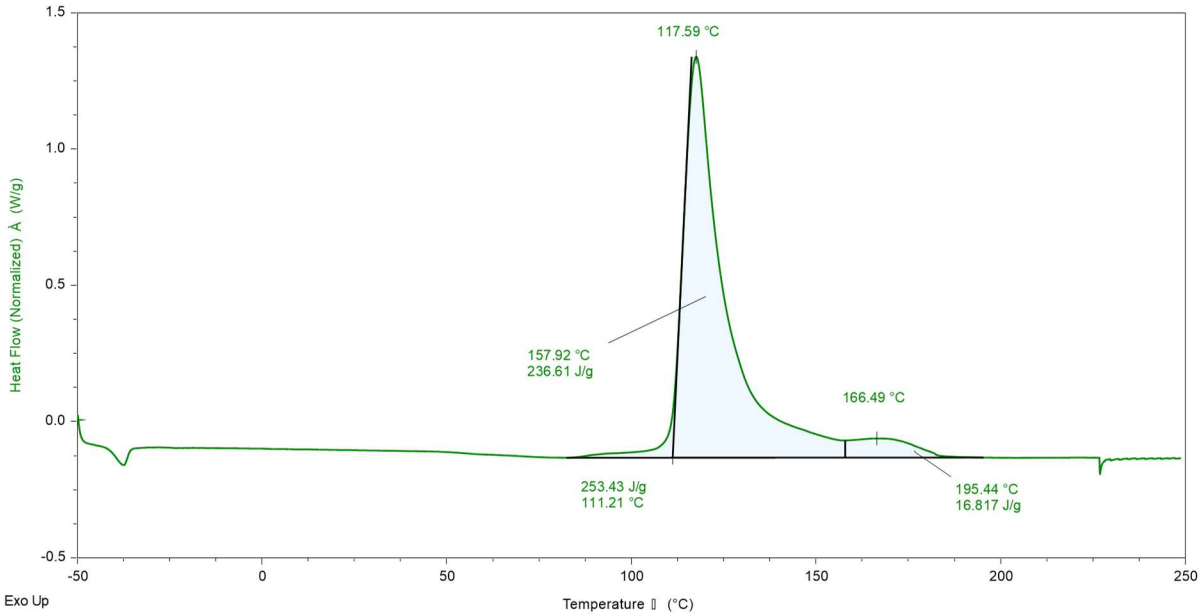

Sample: 9130-94A (Spec #2) 5°C/min 7 days
Comment: 50ml/minute nitrogen
Method: -50 to 250 (5°C/min)
Operator: lhl
File: C:\TA\Data\Discovery DSC\91093 9130-94A (Spec #2) 5°Cmin 7 days -50 to 250 (5°Cmin) .tri

Instrument/Date: DSC2500,11/5/2019 10:00:08 AM
Sample Mass: 9.88000 mg
Pan type: Aluminum Hermetic
Project: 91093

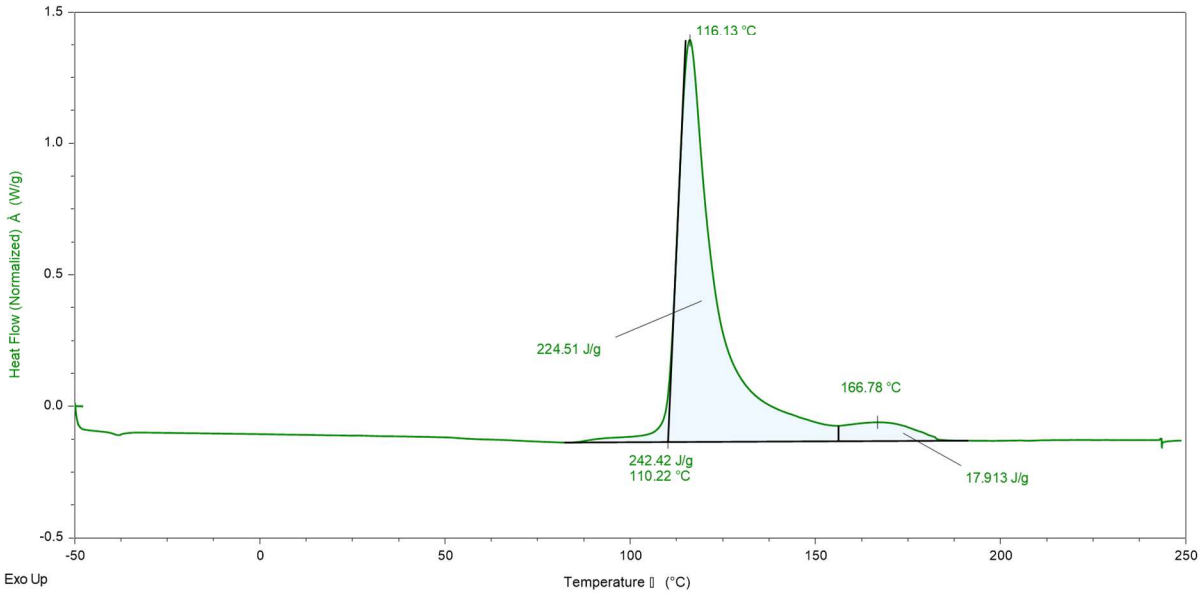

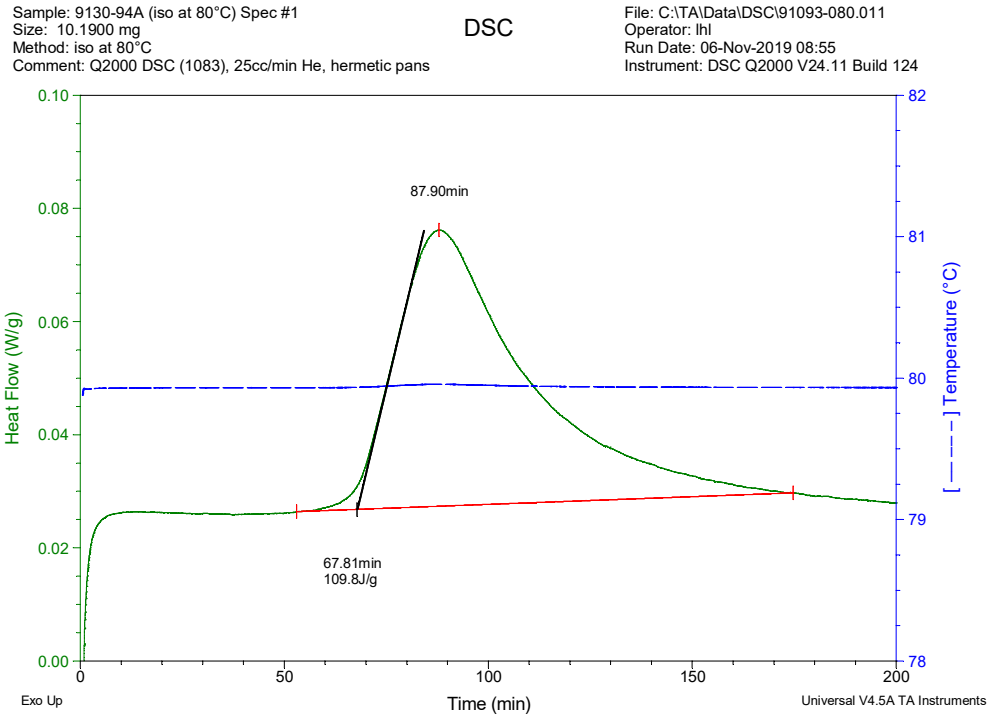
Sample: 9130-94A (iso at 80°C) Spec #1
Size: 10.1900 mg
Method: iso at 80°C
Comment: Q2000 DSC (1083), 25cc/min He, hermetic pans
DSC
File: C:\TA\Data\DSC\91093-080.011
Operator: lhl
Run Date: 06-Nov-2019 08:55
Instrument: DSC Q2000 V24.11 Build 124
87.90min
67.81min
109.8J/g
Heat Flow (W/g)
[— — —] Temperature (°C)
Time (min)
Exo Up
Universal V4.5A TA Instruments

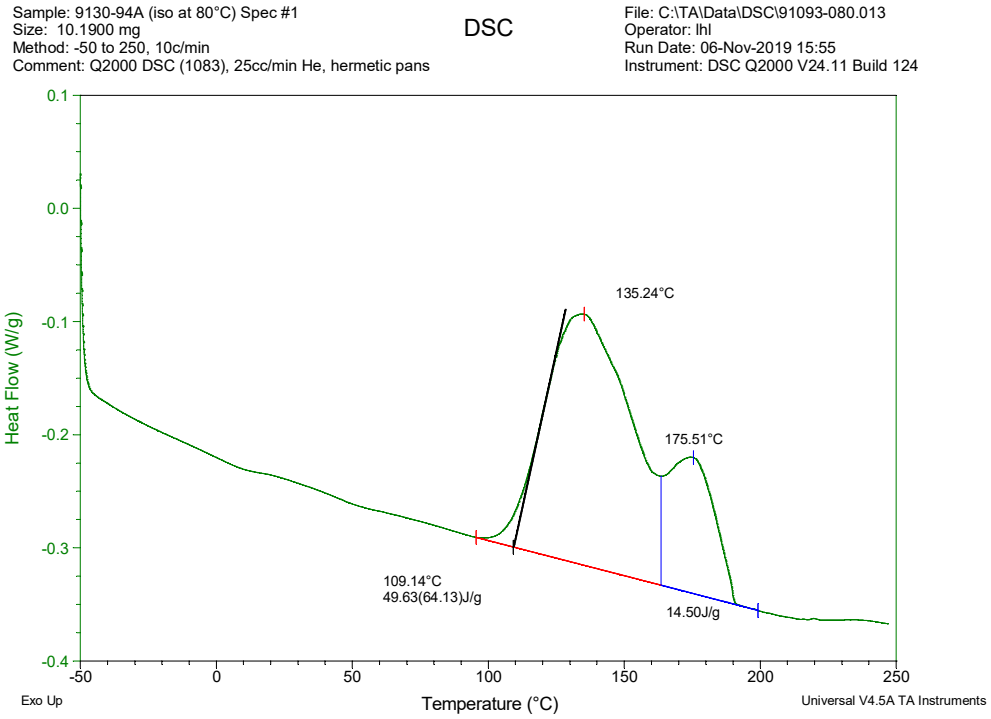
Sample: 9130-94A (iso at 80°C) Spec #1
Size: 10.1900 mg
Method: -50 to 250, 10c/min
Comment: Q2000 DSC (1083), 25cc/min He, hermetic pans
DSC
File: C:\TA\Data\DSC\91093-080.013
Operator: lhl
Run Date: 06-Nov-2019 15:55
Instrument: DSC Q2000 V24.11 Build 124
135.24°C
175.51°C
109.14°C
49.63(64.13)J/g
14.50J/g
Heat Flow (W/g)
Temperature (°C)
Exo Up
Universal V4.5A TA Instruments

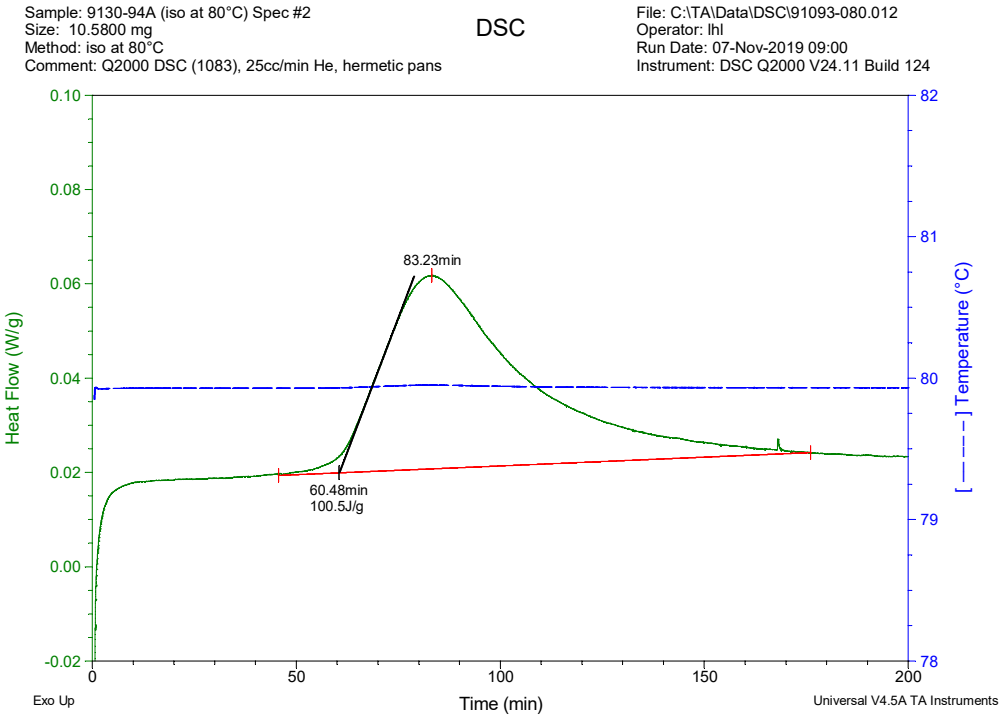
Sample: 9130-94A (iso at 80°C) Spec #2
Size: 10.5800 mg
Method: iso at 80°C
Comment: Q2000 DSC (1083), 25cc/min He, hermetic pans
DSC
File: C:\TA\Data\DSC\91093-080.012
Operator: lhl
Run Date: 07-Nov-2019 09:00
Instrument: DSC Q2000 V24.11 Build 124
83.23min
60.48min
100.5J/g
Heat Flow (W/g)
[— — —] Temperature (°C)
Time (min)
Exo Up
Universal V4.5A TA Instruments

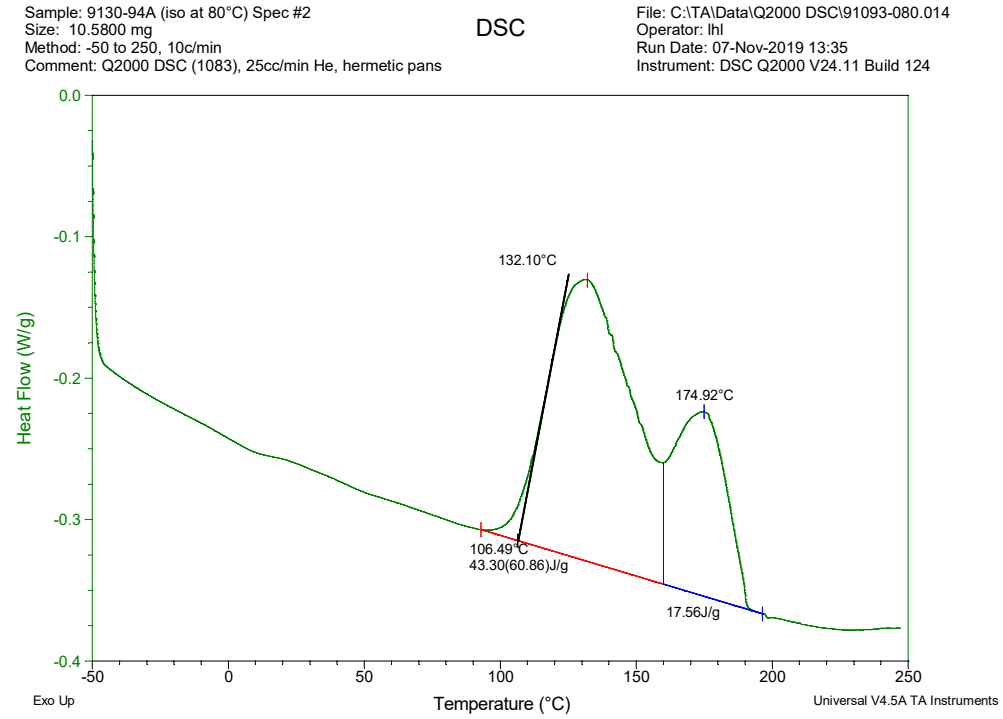
Sample: 9130-94A (iso at 80°C) Spec #2
Size: 10.5800 mg
Method: -50 to 250, 10c/min
Comment: Q2000 DSC (1083), 25cc/min He, hermetic pans
DSC
File: C:\TA\Data\Q2000 DSC\91093-080.014
Operator: lhl
Run Date: 07-Nov-2019 13:35
Instrument: DSC Q2000 V24.11 Build 124
132.10°C
174.92°C
106.49°C
43.30(60.86)J/g
17.56J/g
Heat Flow (W/g)
Temperature (°C)
Exo Up
Universal V4.5A TA Instruments

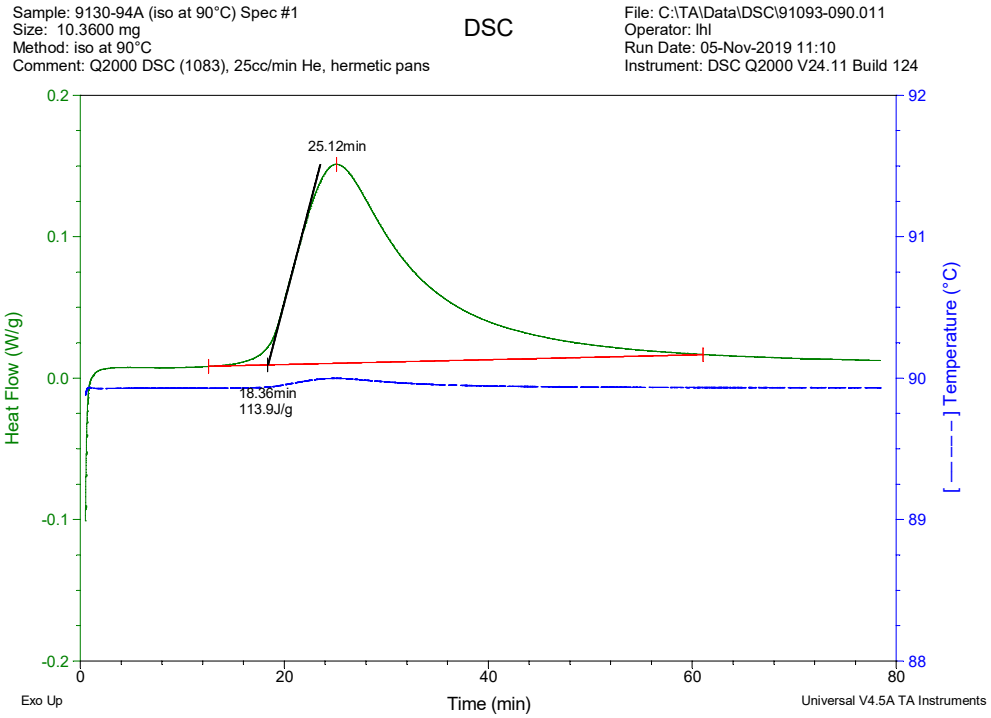
Sample: 9130-94A (iso at 90°C) Spec #1
Size: 10.3600 mg
Method: iso at 90°C
Comment: Q2000 DSC (1083), 25cc/min He, hermetic pans
DSC
File: C:\TA\Data\DSC\91093-090.011
Operator: lhl
Run Date: 05-Nov-2019 11:10
Instrument: DSC Q2000 V24.11 Build 124
25.12min
18.36min
113.9J/g
Heat Flow (W/g)
[— – –] Temperature (°C)
Time (min)
Exo Up
Universal V4.5A TA Instruments

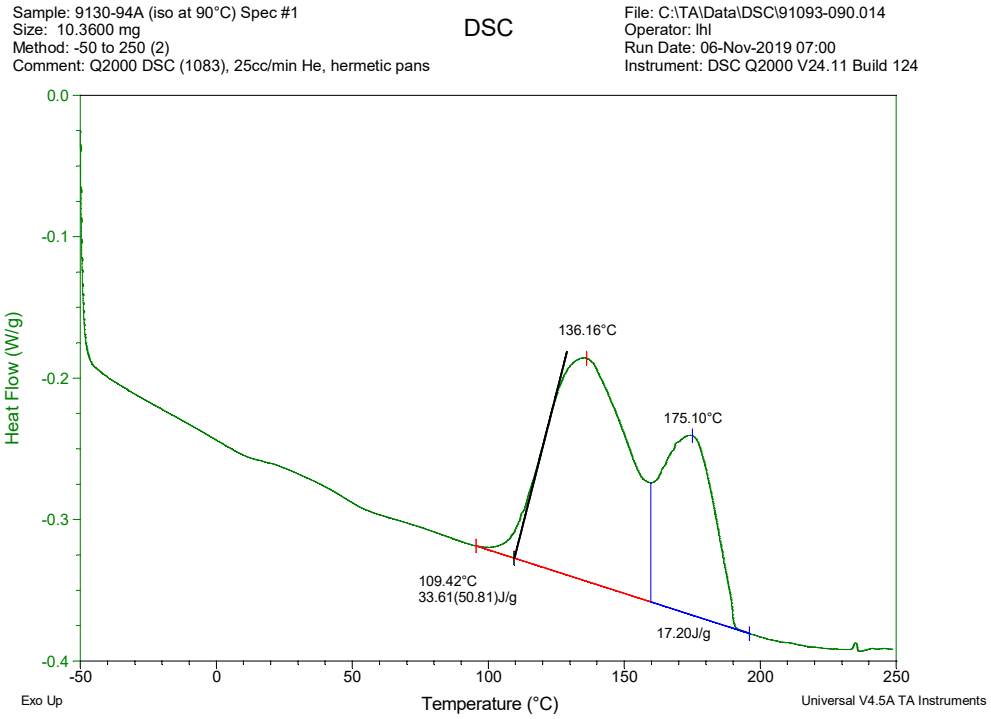
Sample: 9130-94A (iso at 90°C) Spec #1
Size: 10.3600 mg
Method: -50 to 250 (2)
Comment: Q2000 DSC (1083), 25cc/min He, hermetic pans
DSC
File: C:\TA\Data\DSC\91093-090.014
Operator: lhl
Run Date: 06-Nov-2019 07:00
Instrument: DSC Q2000 V24.11 Build 124
136.16°C
175.10°C
109.42°C
33.61(50.81)J/g
17.20J/g
Heat Flow (W/g)
Temperature (°C)
Exo Up
Universal V4.5A TA Instruments

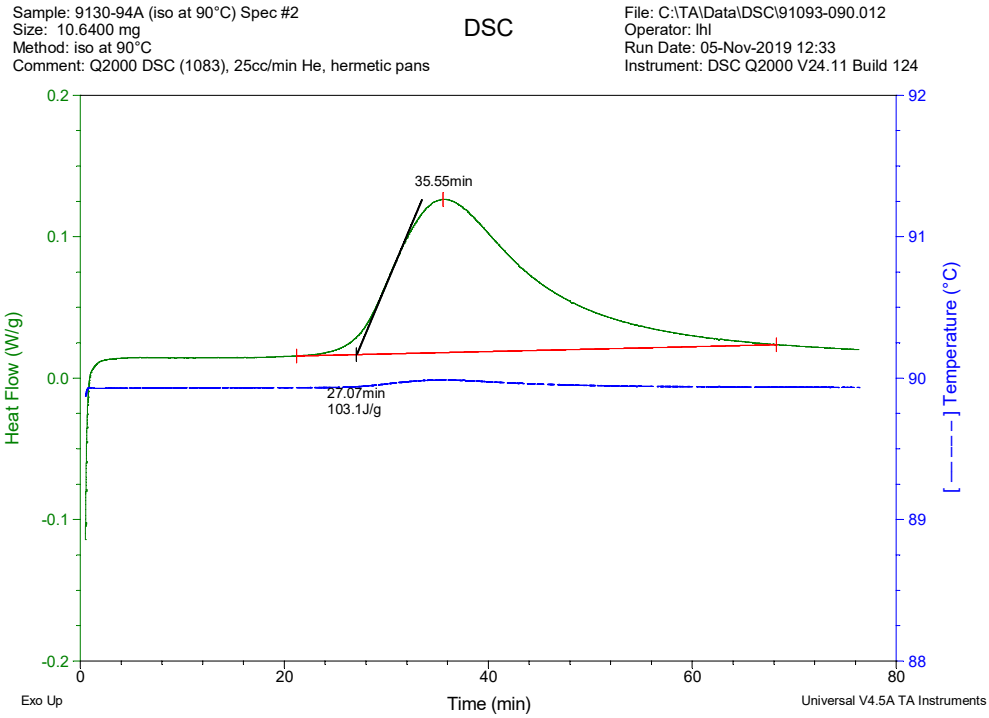
Sample: 9130-94A (iso at 90°C) Spec #2
Size: 10.6400 mg
Method: iso at 90°C
Comment: Q2000 DSC (1083), 25cc/min He, hermetic pans
DSC
File: C:\TA\Data\DSC\91093-090.012
Operator: lhl
Run Date: 05-Nov-2019 12:33
Instrument: DSC Q2000 V24.11 Build 124
35.55min
27.07min
103.1J/g
Heat Flow (W/g)
[— — –] Temperature (°C)
Time (min)
Exo Up
Universal V4.5A TA Instruments

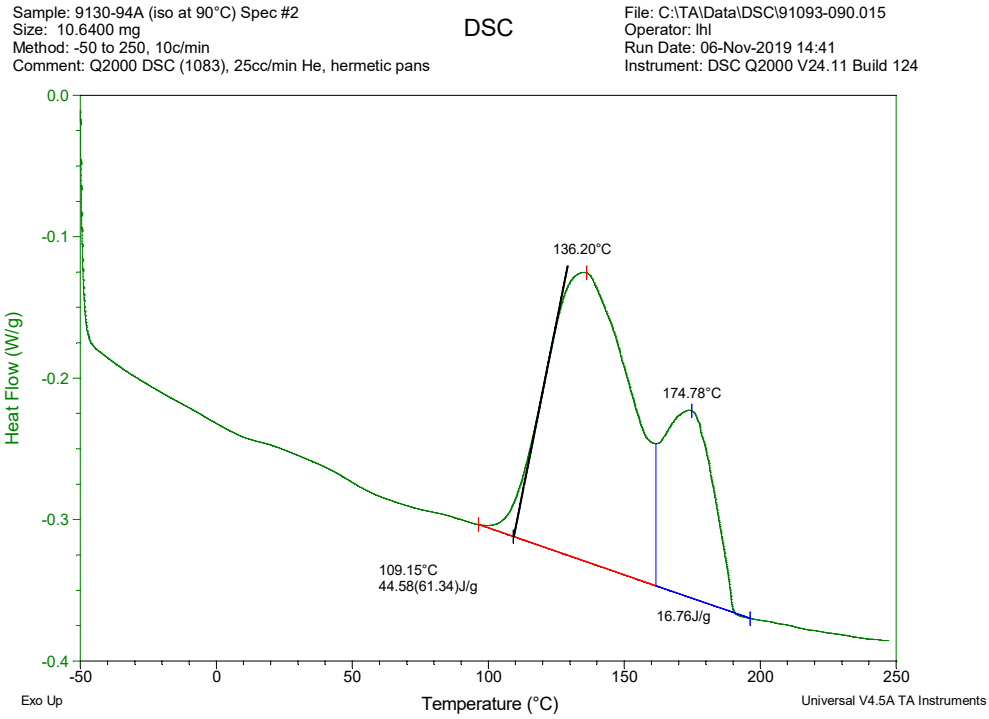
Sample: 9130-94A (iso at 90°C) Spec #2
Size: 10.6400 mg
Method: -50 to 250, 10c/min
Comment: Q2000 DSC (1083), 25cc/min He, hermetic pans
DSC
File: C:\TA\Data\DSC\91093-090.015
Operator: lhl
Run Date: 06-Nov-2019 14:41
Instrument: DSC Q2000 V24.11 Build 124
136.20°C
174.78°C
109.15°C
44.58(61.34)J/g
16.76J/g
Heat Flow (W/g)
Temperature (°C)
Exo Up
Universal V4.5A TA Instruments

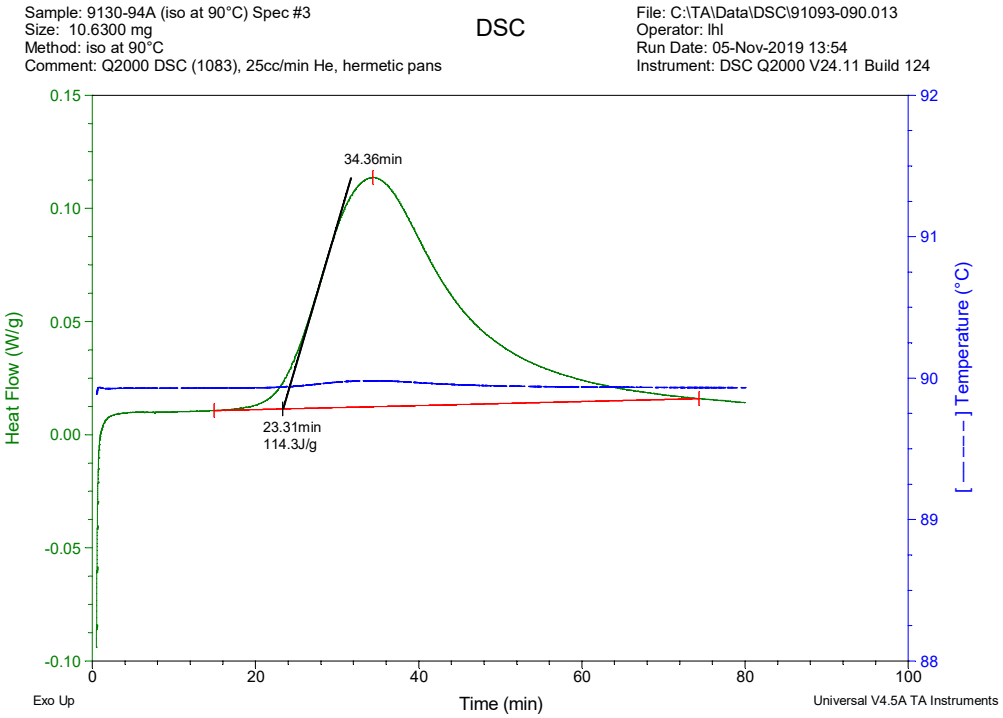
Sample: 9130-94A (iso at 90°C) Spec #3
Size: 10.6300 mg
Method: iso at 90°C
Comment: Q2000 DSC (1083), 25cc/min He, hermetic pans
DSC
File: C:\TA\Data\DSC\91093-090.013
Operator: lhl
Run Date: 05-Nov-2019 13:54
Instrument: DSC Q2000 V24.11 Build 124
34.36min
23.31min
114.3J/g
Heat Flow (W/g)
[— — —] Temperature (°C)
Time (min)
Exo Up
Universal V4.5A TA Instruments

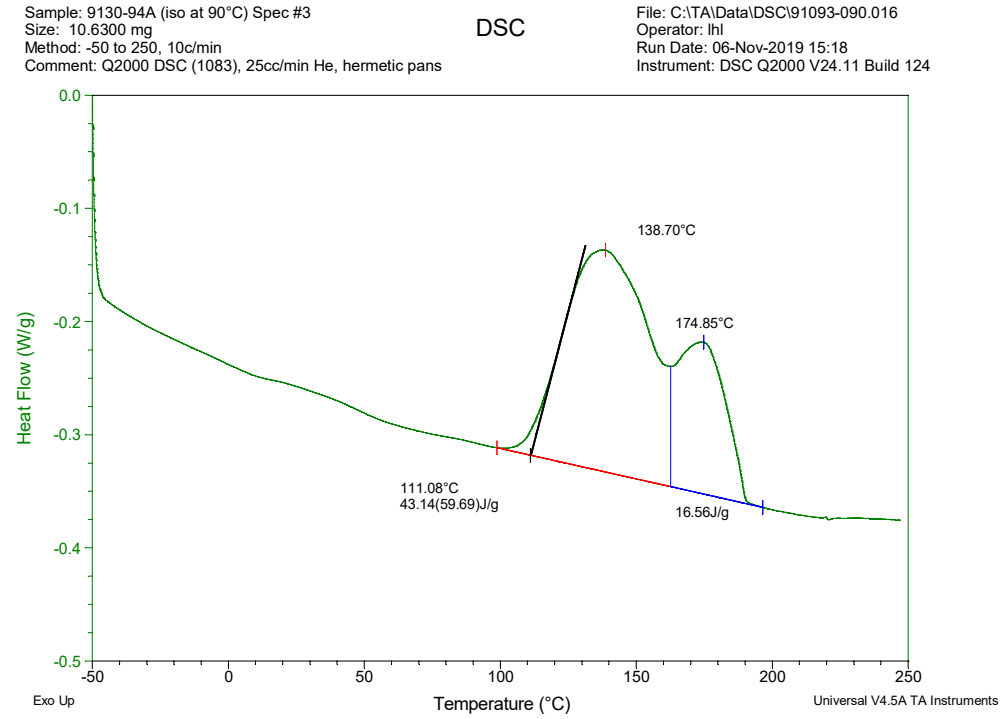
Sample: 9130-94A (iso at 90°C) Spec #3
Size: 10.6300 mg
Method: -50 to 250, 10c/min
Comment: Q2000 DSC (1083), 25cc/min He, hermetic pans
DSC
File: C:\TA\Data\DSC\91093-090.016
Operator: lhl
Run Date: 06-Nov-2019 15:18
Instrument: DSC Q2000 V24.11 Build 124
138.70°C
174.85°C
111.08°C
43.14(59.69)J/g
16.56J/g
Heat Flow (W/g)
Temperature (°C)
Exo Up
Universal V4.5A TA Instruments

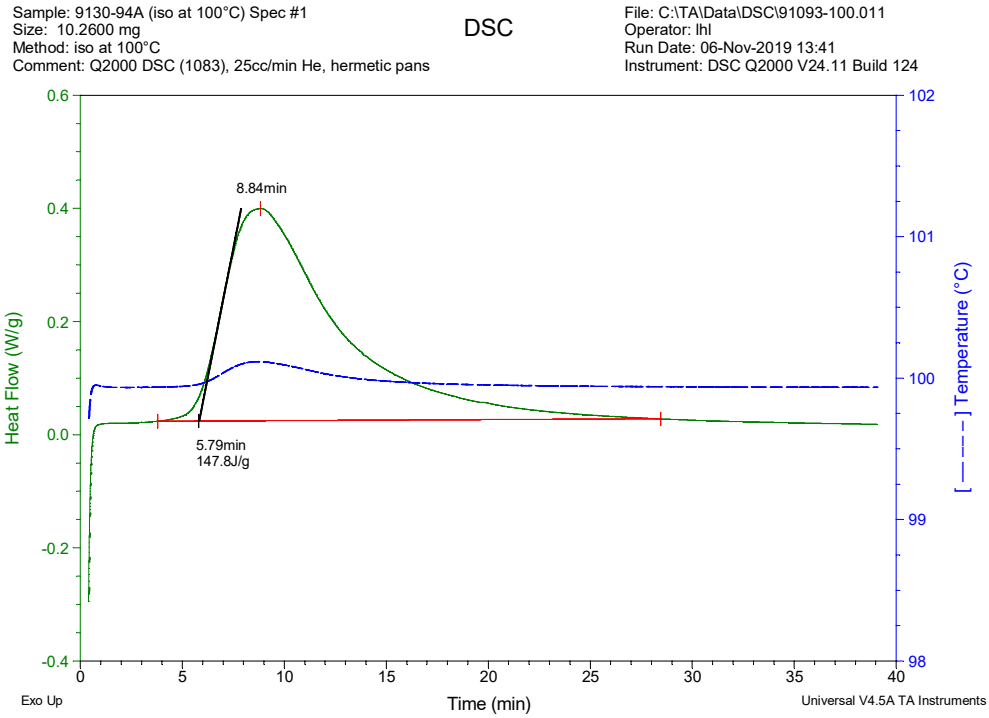
Sample: 9130-94A (iso at 100°C) Spec #1
Size: 10.2600 mg
Method: iso at 100°C
Comment: Q2000 DSC (1083), 25cc/min He, hermetic pans
DSC
File: C:\TA\Data\DSC\91093-100.011
Operator: lhl
Run Date: 06-Nov-2019 13:41
Instrument: DSC Q2000 V24.11 Build 124
8.84min
5.79min
147.8J/g
Heat Flow (W/g)
[— — –] Temperature (°C)
Time (min)
Exo Up
Universal V4.5A TA Instruments

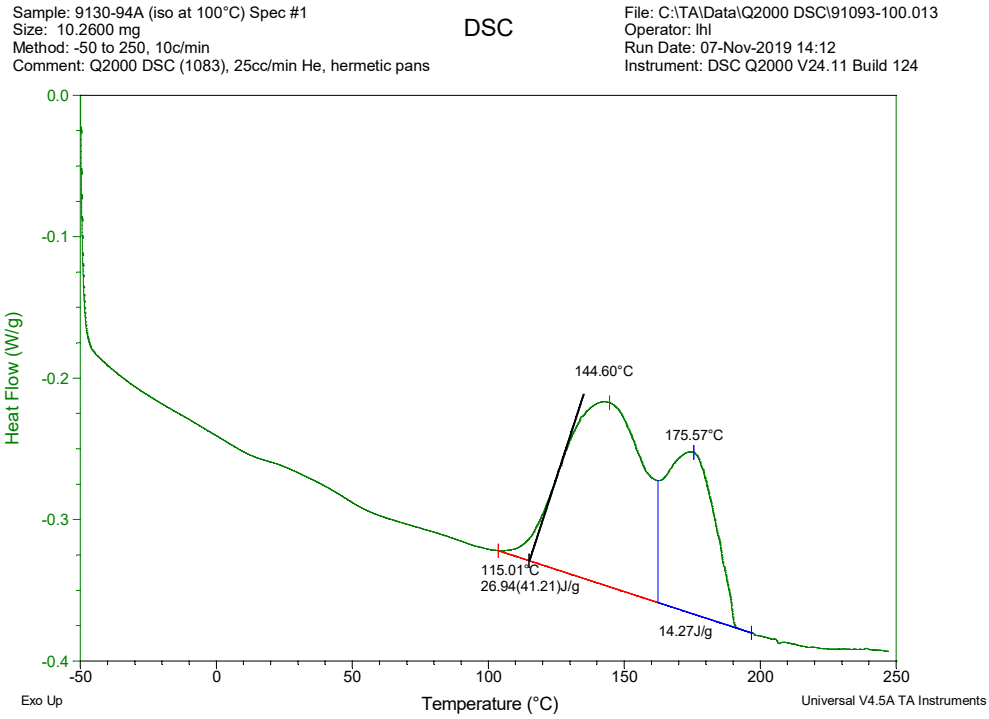
Sample: 9130-94A (iso at 100°C) Spec #1
Size: 10.2600 mg
Method: -50 to 250, 10c/min
Comment: Q2000 DSC (1083), 25cc/min He, hermetic pans
DSC
File: C:\TA\Data\Q2000 DSC\91093-100.013
Operator: lhl
Run Date: 07-Nov-2019 14:12
Instrument: DSC Q2000 V24.11 Build 124
144.60°C
175.57°C
115.01°C
26.94(41.21)J/g
14.27J/g
Heat Flow (W/g)
Temperature (°C)
Exo Up
Universal V4.5A TA Instruments

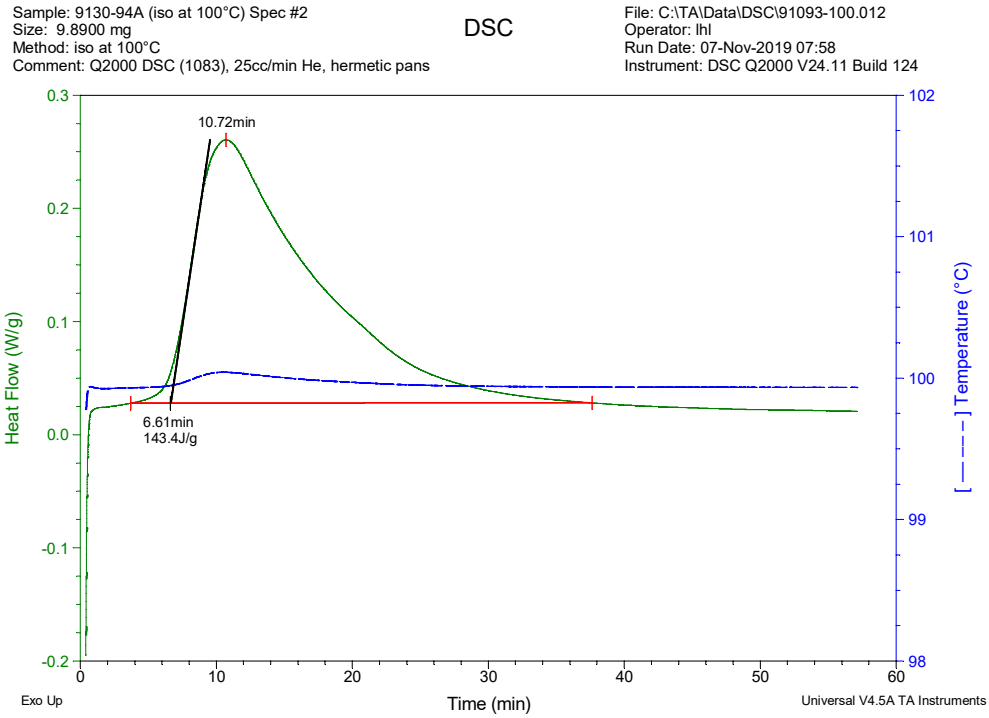
Sample: 9130-94A (iso at 100°C) Spec #2
Size: 9.8900 mg
Method: iso at 100°C
Comment: Q2000 DSC (1083), 25cc/min He, hermetic pans
DSC
File: C:\TA\Data\DSC\91093-100.012
Operator: lhl
Run Date: 07-Nov-2019 07:58
Instrument: DSC Q2000 V24.11 Build 124
10.72min
6.61min
143.4J/g
Heat Flow (W/g)
[— — —] Temperature (°C)
Time (min)
Exo Up
Universal V4.5A TA Instruments

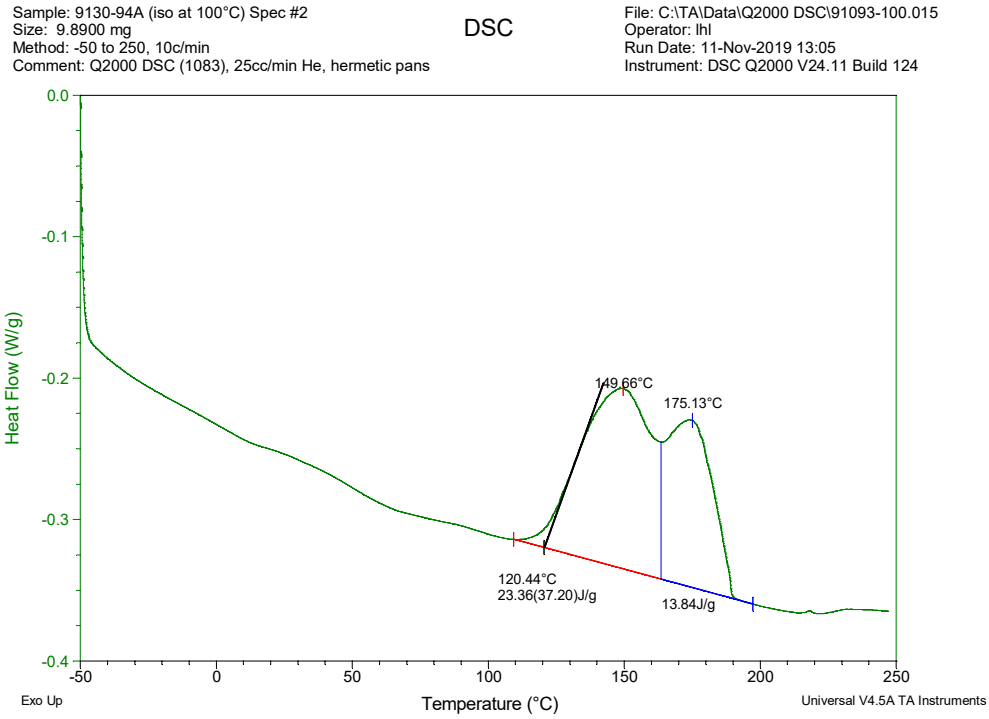
Sample: 9130-94A (iso at 100°C) Spec #2
Size: 9.8900 mg
Method: -50 to 250, 10c/min
Comment: Q2000 DSC (1083), 25cc/min He, hermetic pans
DSC
File: C:\TA\Data\Q2000 DSC\91093-100.015
Operator: lhl
Run Date: 11-Nov-2019 13:05
Instrument: DSC Q2000 V24.11 Build 124
149.66°C
175.13°C
120.44°C
23.36(37.20)J/g
13.84J/g
Heat Flow (W/g)
Temperature (°C)
Exo Up
Universal V4.5A TA Instruments

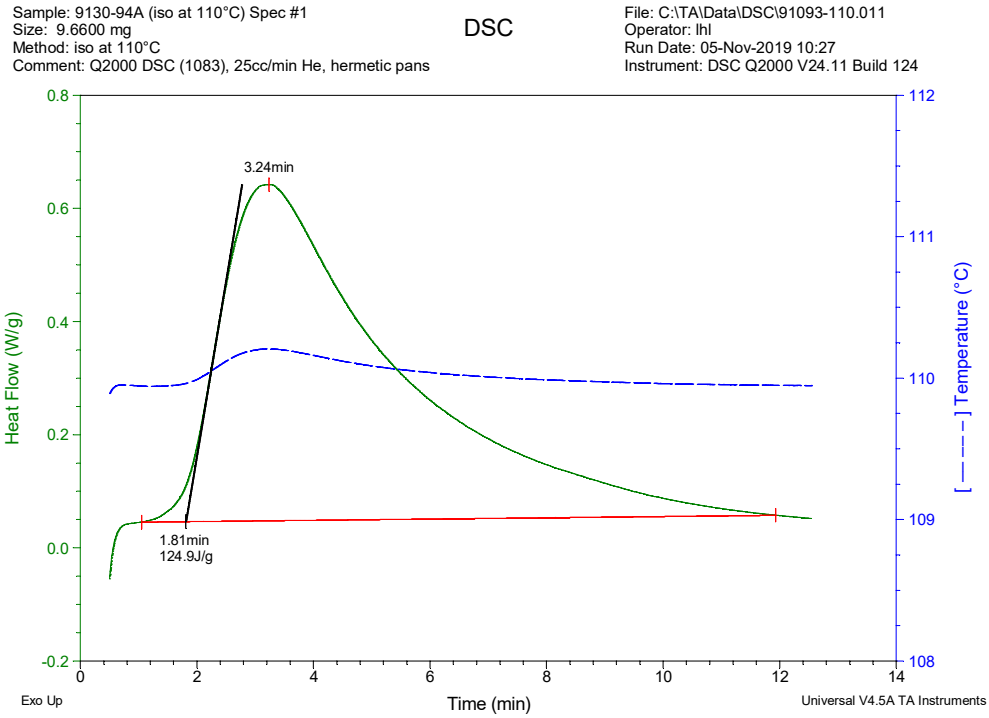
Sample: 9130-94A (iso at 110°C) Spec #1
Size: 9.6600 mg
Method: iso at 110°C
Comment: Q2000 DSC (1083), 25cc/min He, hermetic pans
DSC
File: C:\TA\Data\DSC\91093-110.011
Operator: lhl
Run Date: 05-Nov-2019 10:27
Instrument: DSC Q2000 V24.11 Build 124
3.24min
1.81min
124.9J/g
Heat Flow (W/g)
[— — —] Temperature (°C)
Time (min)
Exo Up
Universal V4.5A TA Instruments

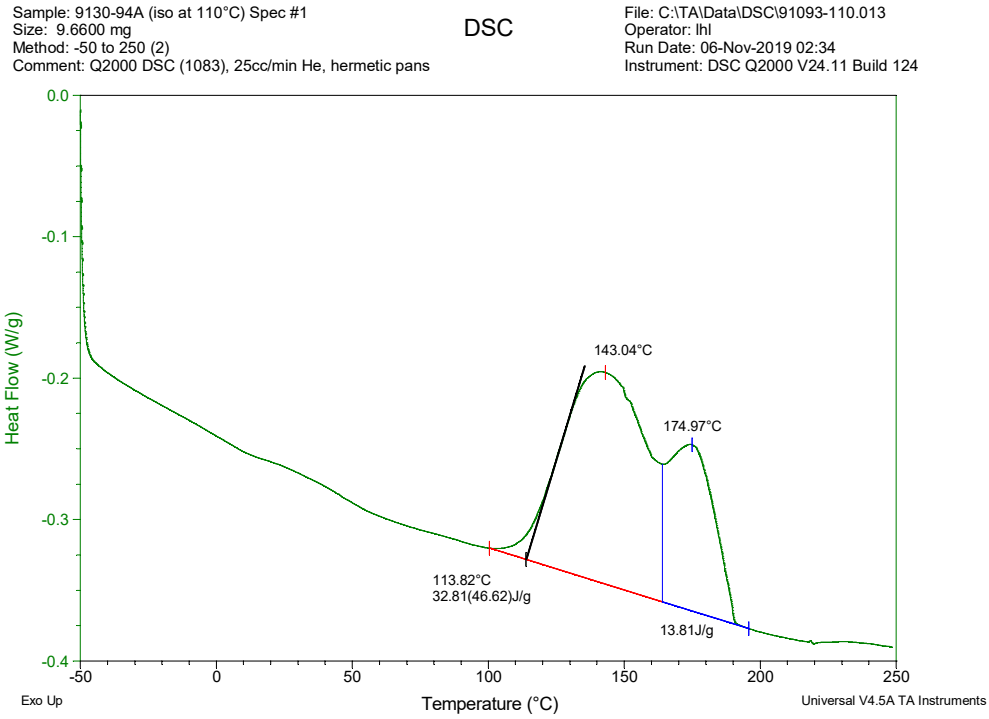
Sample: 9130-94A (iso at 110°C) Spec #1
Size: 9.6600 mg
Method: -50 to 250 (2)
Comment: Q2000 DSC (1083), 25cc/min He, hermetic pans
DSC
File: C:\TA\Data\DSC\91093-110.013
Operator: lhl
Run Date: 06-Nov-2019 02:34
Instrument: DSC Q2000 V24.11 Build 124
143.04°C
174.97°C
113.82°C
32.81(46.62)J/g
13.81J/g
Heat Flow (W/g)
Temperature (°C)
Exo Up
Universal V4.5A TA Instruments

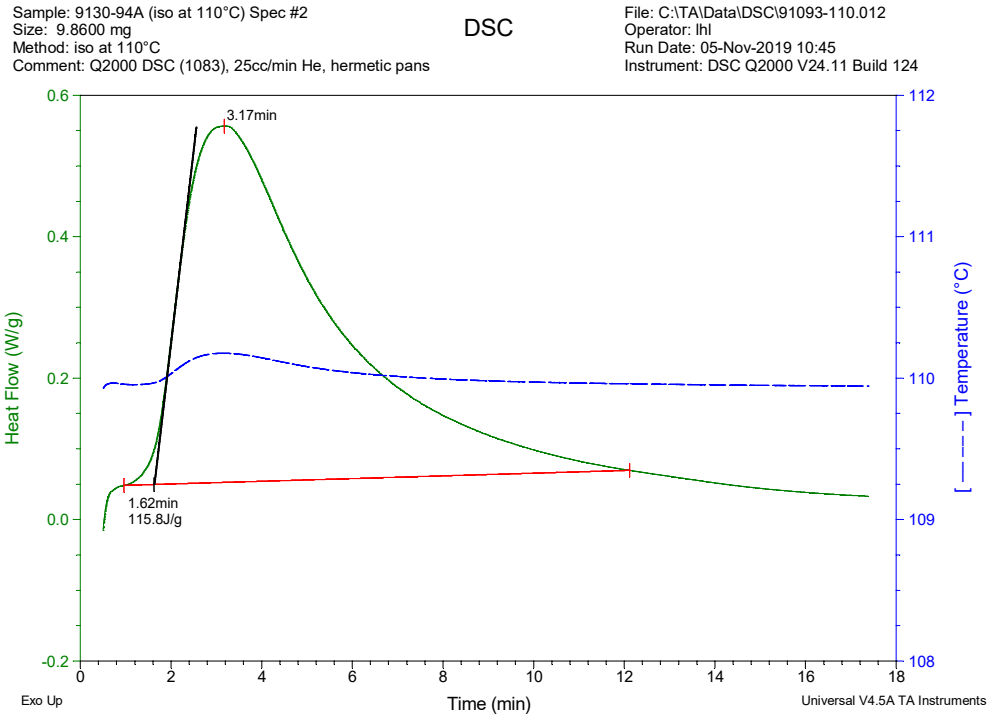
Sample: 9130-94A (iso at 110°C) Spec #2
Size: 9.8600 mg
Method: iso at 110°C
Comment: Q2000 DSC (1083), 25cc/min He, hermetic pans
DSC
File: C:\TA\Data\DSC\91093-110.012
Operator: lhl
Run Date: 05-Nov-2019 10:45
Instrument: DSC Q2000 V24.11 Build 124
3.17min
1.62min
115.8J/g
Heat Flow (W/g)
[— — —] Temperature (°C)
Time (min)
Exo Up
Universal V4.5A TA Instruments

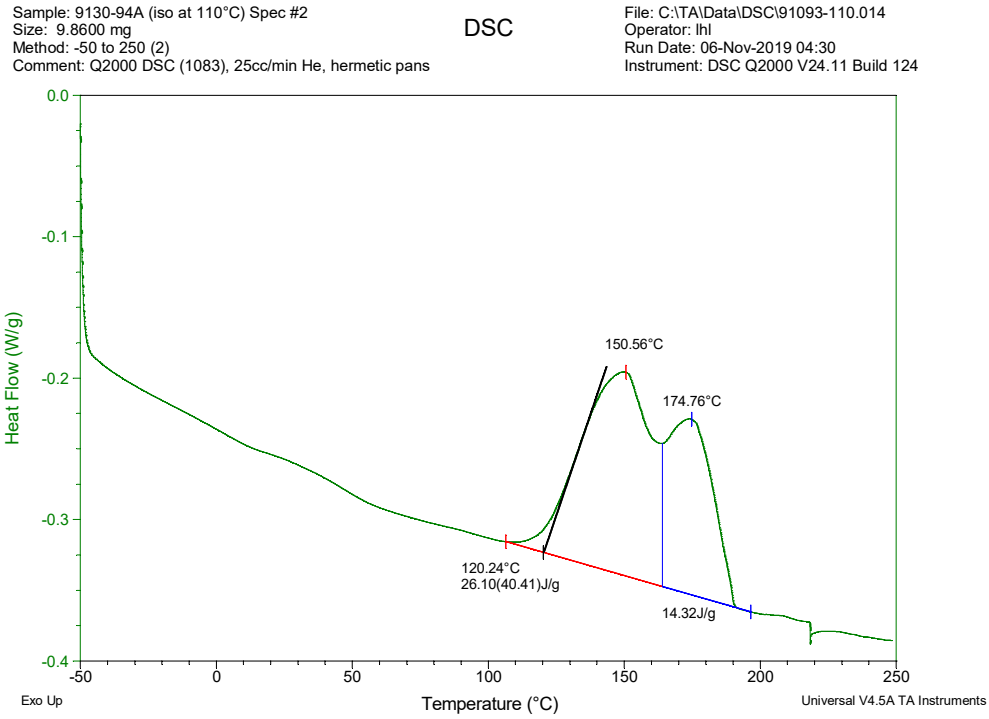
Sample: 9130-94A (iso at 110°C) Spec #2
Size: 9.8600 mg
Method: -50 to 250 (2)
Comment: Q2000 DSC (1083), 25cc/min He, hermetic pans
DSC
File: C:\TA\Data\DSC\91093-110.014
Operator: lhl
Run Date: 06-Nov-2019 04:30
Instrument: DSC Q2000 V24.11 Build 124
150.56°C
174.76°C
120.24°C
26.10(40.41)J/g
14.32J/g
Heat Flow (W/g)
Temperature (°C)
Exo Up
Universal V4.5A TA Instruments

Sample: 9130-94A (iso at 120°C) Spec #1
Size: 10.5900 mg
Method: iso at 120°C
Comment: Q2000 DSC (1083), 25cc/min He, hermetic pans

DSC

File: C:\TA\Data\DSC\91093-120.011
Operator: lhl
Run Date: 06-Nov-2019 12:39
Instrument: DSC Q2000 V24.11 Build 124

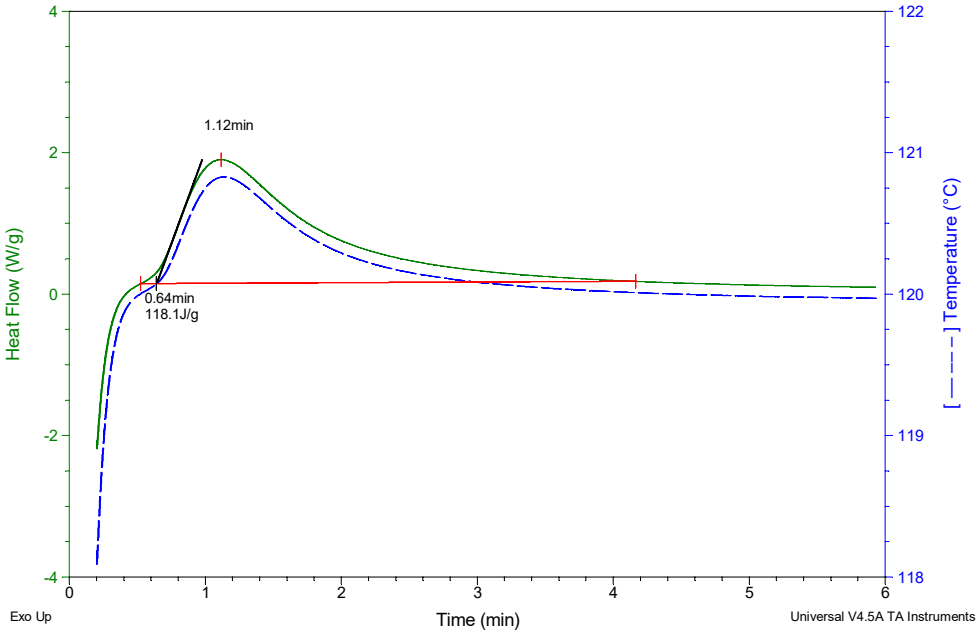

Sample: 9130-94A (iso at 120°C) Spec #1
Size: 10.5900 mg
Method: -50 to 250, 10c/min
Comment: Q2000 DSC (1083), 25cc/min He, hermetic pans

DSC

File: C:\TA\Data\DSC\91093-120.013
Operator: lhl
Run Date: 06-Nov-2019 16:32
Instrument: DSC Q2000 V24.11 Build 124

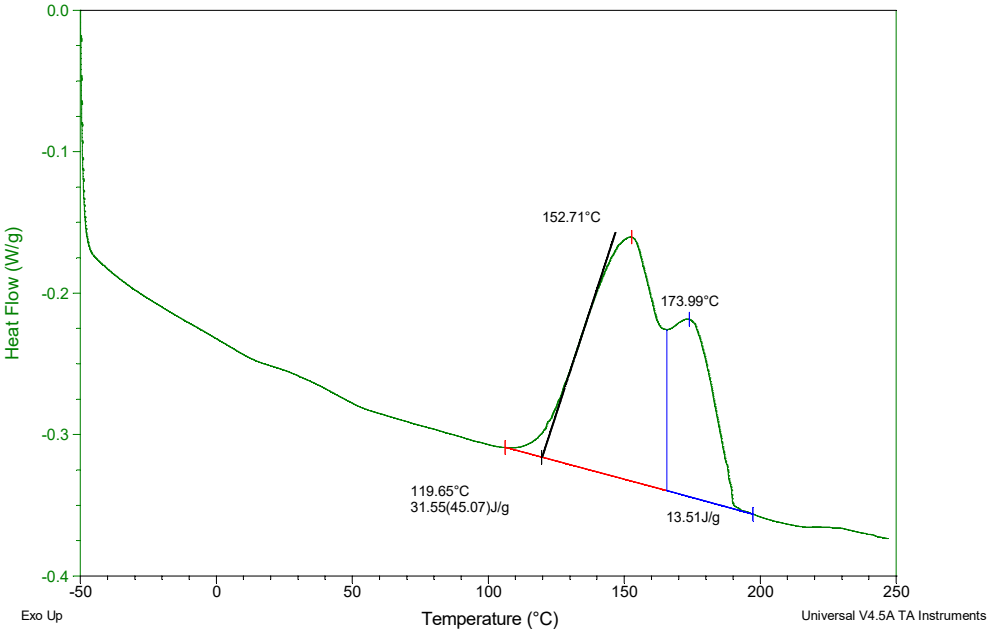

Sample: 9130-94A (iso at 120°C) Spec #2
Size: 9.3100 mg
Method: iso at 120°C
Comment: Q2000 DSC (1083), 25cc/min He, hermetic pans

DSC

File: C:\TA\Data\DSC\91093-120.012
Operator: lhl
Run Date: 06-Nov-2019 12:50
Instrument: DSC Q2000 V24.11 Build 124

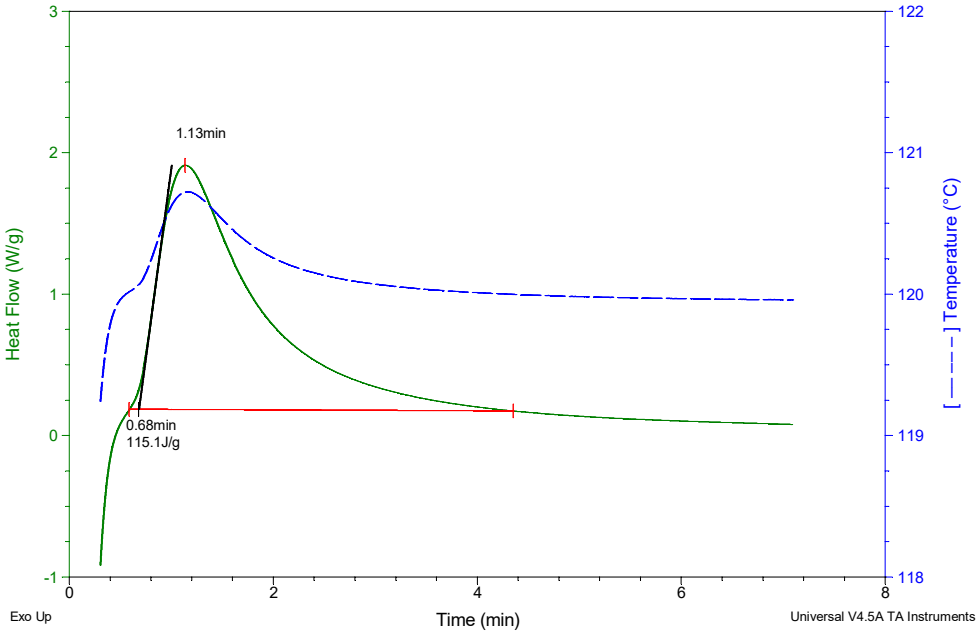

Sample: 9130-94A (iso at 120°C) Spec #2
Size: 9.3100 mg
Method: -50 to 250, 10c/min
Comment: Q2000 DSC (1083), 25cc/min He, hermetic pans

DSC

File: C:\TA\Data\DSC\91093-120.014
Operator: lhl
Run Date: 06-Nov-2019 17:09
Instrument: DSC Q2000 V24.11 Build 124

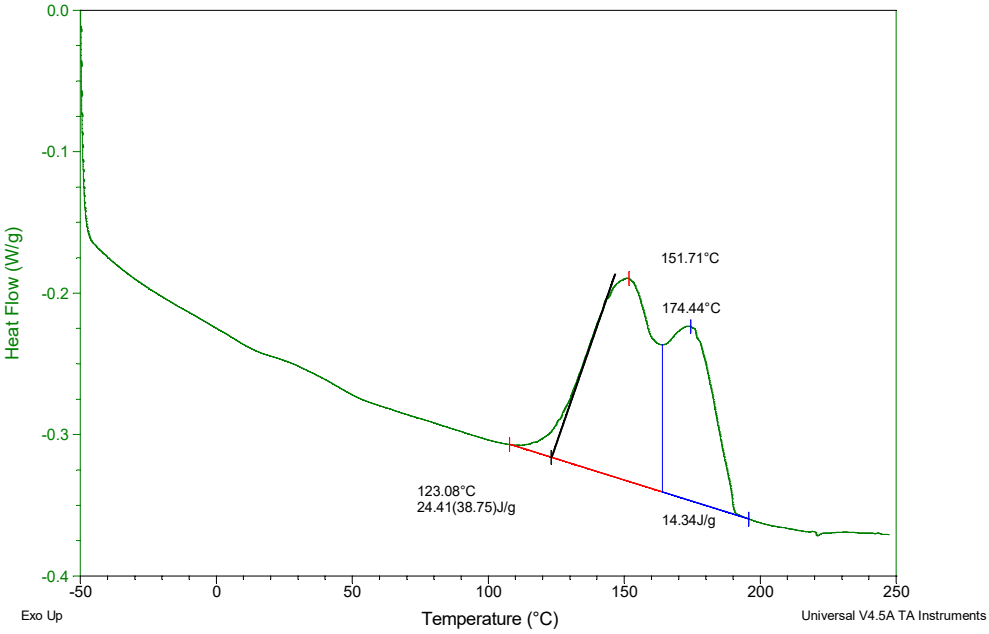

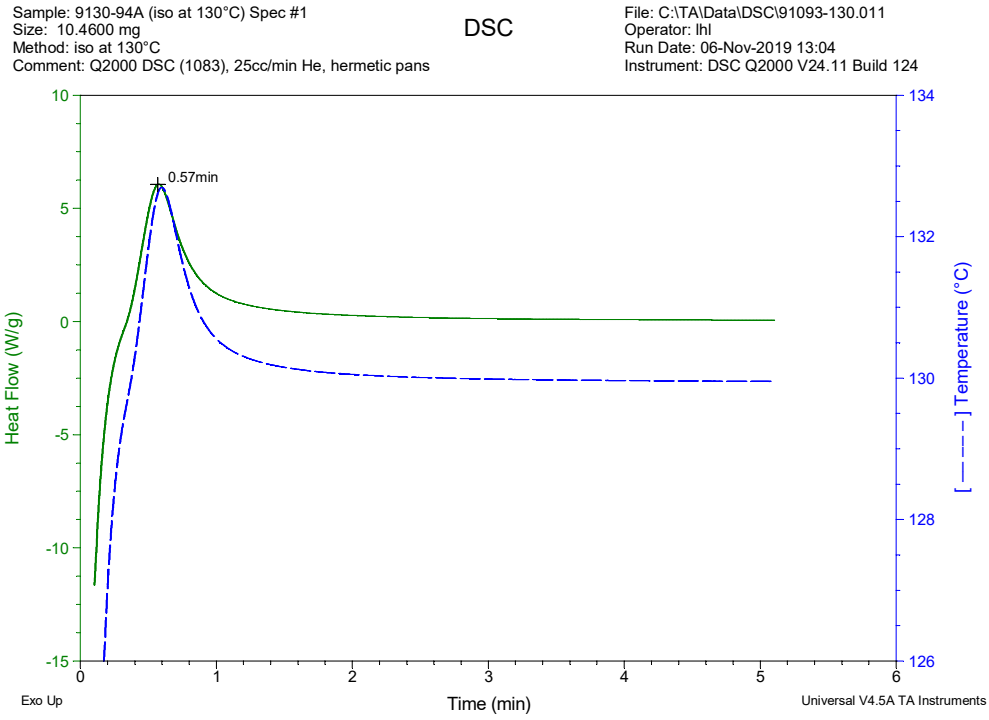
Sample: 9130-94A (iso at 130°C) Spec #1
Size: 10.4600 mg
Method: iso at 130°C
Comment: Q2000 DSC (1083), 25cc/min He, hermetic pans
DSC
File: C:\TA\Data\DSC\91093-130.011
Operator: lhl
Run Date: 06-Nov-2019 13:04
Instrument: DSC Q2000 V24.11 Build 124
0.57min
Heat Flow (W/g)
[— — —] Temperature (°C)
Time (min)
Exo Up
Universal V4.5A TA Instruments

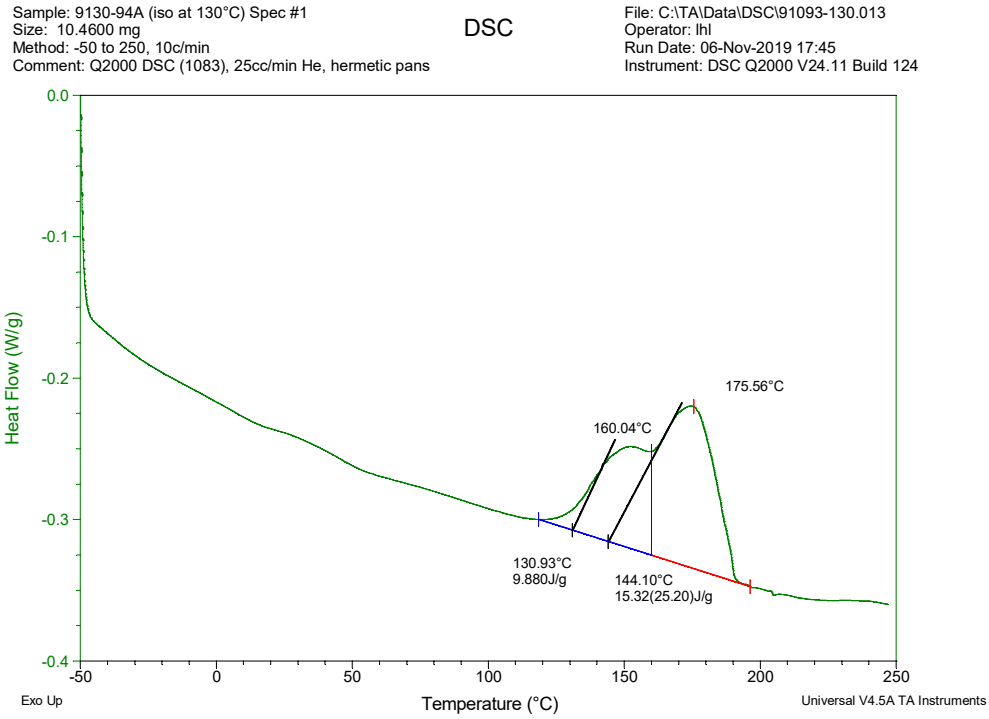
Sample: 9130-94A (iso at 130°C) Spec #1
Size: 10.4600 mg
Method: -50 to 250, 10c/min
Comment: Q2000 DSC (1083), 25cc/min He, hermetic pans
DSC
File: C:\TA\Data\DSC\91093-130.013
Operator: lhl
Run Date: 06-Nov-2019 17:45
Instrument: DSC Q2000 V24.11 Build 124
175.56°C
160.04°C
130.93°C
9.880J/g
144.10°C
15.32(25.20)J/g
Heat Flow (W/g)
Temperature (°C)
Exo Up
Universal V4.5A TA Instruments

Sample: 9130-94A (iso at 130°C) Spec #2
Size: 9.6000 mg
Method: iso at 130°C
Comment: Q2000 DSC (1083), 25cc/min He, hermetic pans

DSC

File: C:\TA\Data\DSC\91093-130.012
Operator: lhl
Run Date: 06-Nov-2019 13:18
Instrument: DSC Q2000 V24.11 Build 124

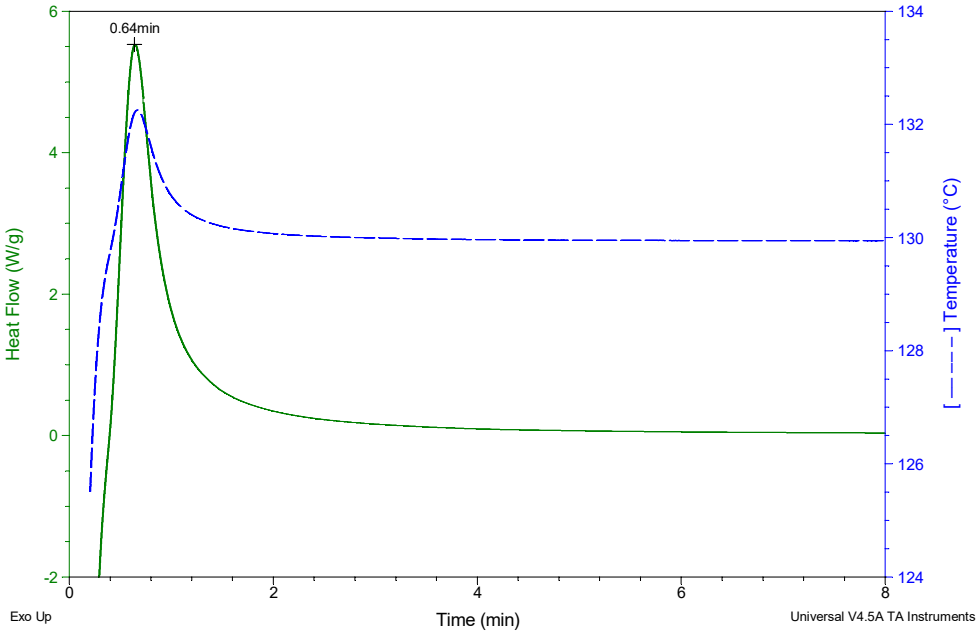

Sample: 9130-94A (iso at 130°C) Spec #2
Size: 9.6000 mg
Method: -50 to 250, 10c/min
Comment: Q2000 DSC (1083), 25cc/min He, hermetic pans

DSC

File: C:\TA\Data\DSC\91093-130.014
Operator: lhl
Run Date: 06-Nov-2019 18:22
Instrument: DSC Q2000 V24.11 Build 124

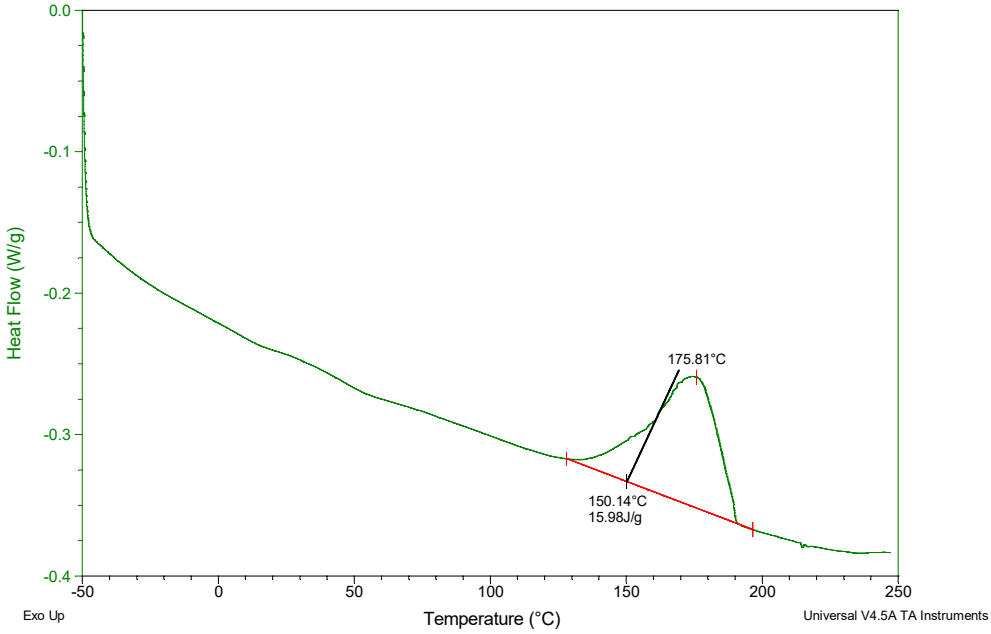

Sample: 9130-94B (Spec #1) 5°C/min 6 days
Comment: 50ml/minute nitrogen
Method: -50 to 250 (5°C/min)
Operator: lhl
File: C:\TA\Data\Discovery DSC\91093 9130-94B (Spec #1) 5°Cmin 6 days -50 to 250 (5°Cmin) .tri

Instrument/Date: DSC2500,10/7/2019 9:21:37 AM
Sample Mass: 10.0300 mg
Pan type: None
Project: 91093

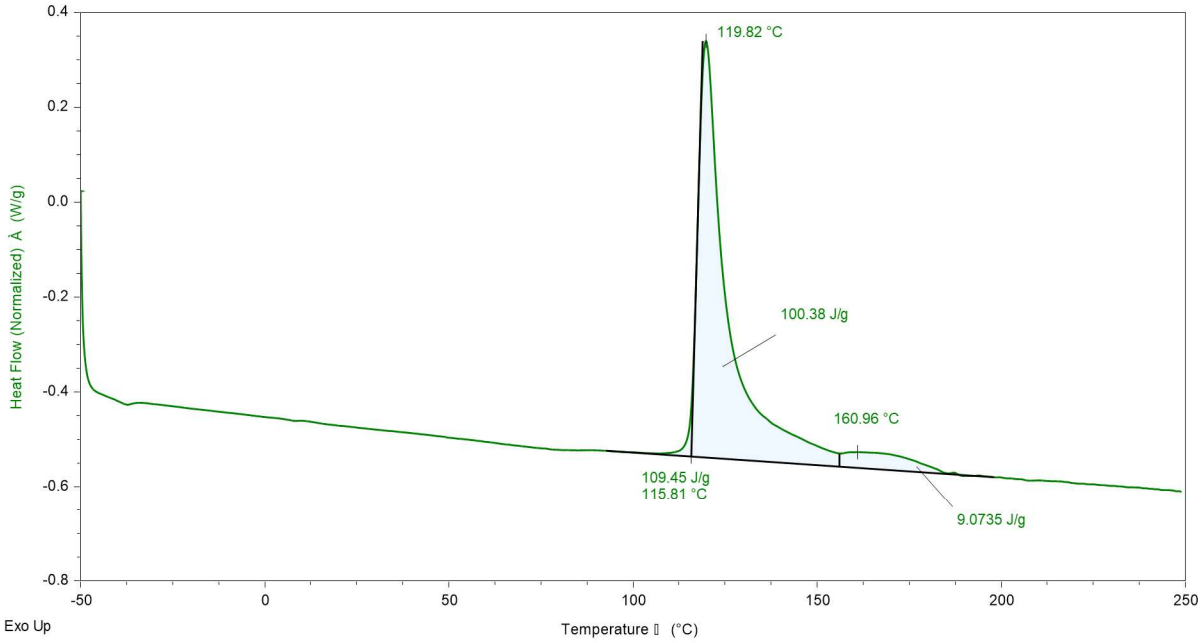

Sample: 9130-94B (Spec #2) 5°C/min 6 days
Comment: 50ml/minute nitrogen
Method: -50 to 250 (5°C/min)
Operator: lhl
File: C:\TA\Data\Discovery DSC\91093 9130-94B (Spec #2) 5°Cmin 6 days -50 to 250 (5°Cmin) .tri

Instrument/Date: DSC2500,10/7/2019 10:34:16 AM
Sample Mass: 10.5800 mg
Pan type: None
Project: 91093

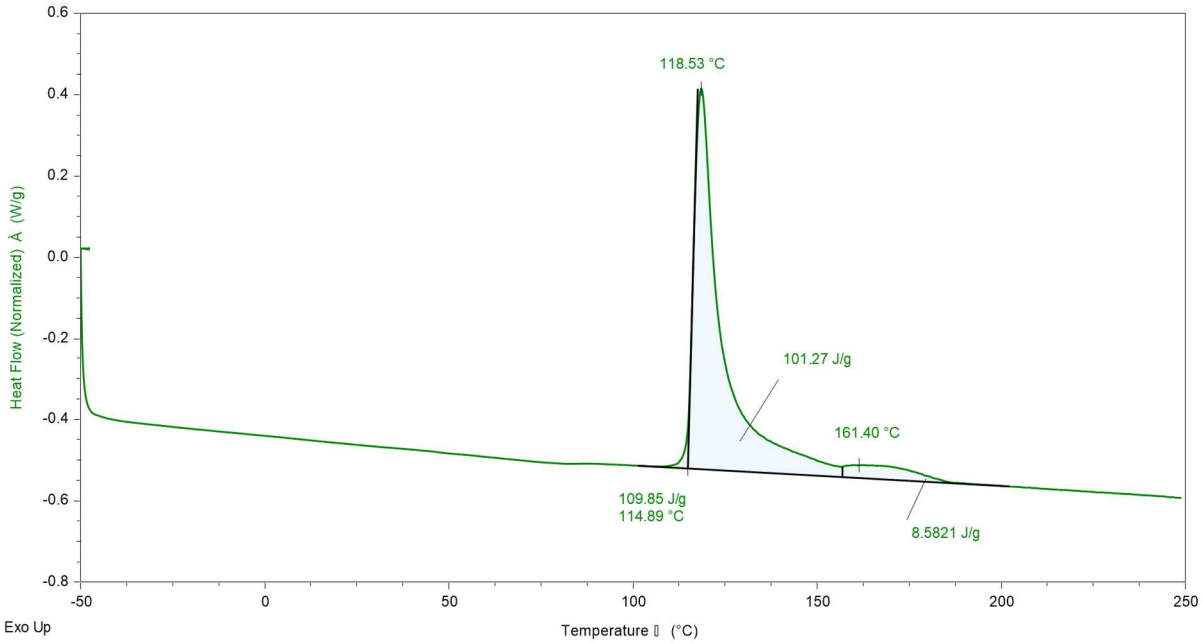

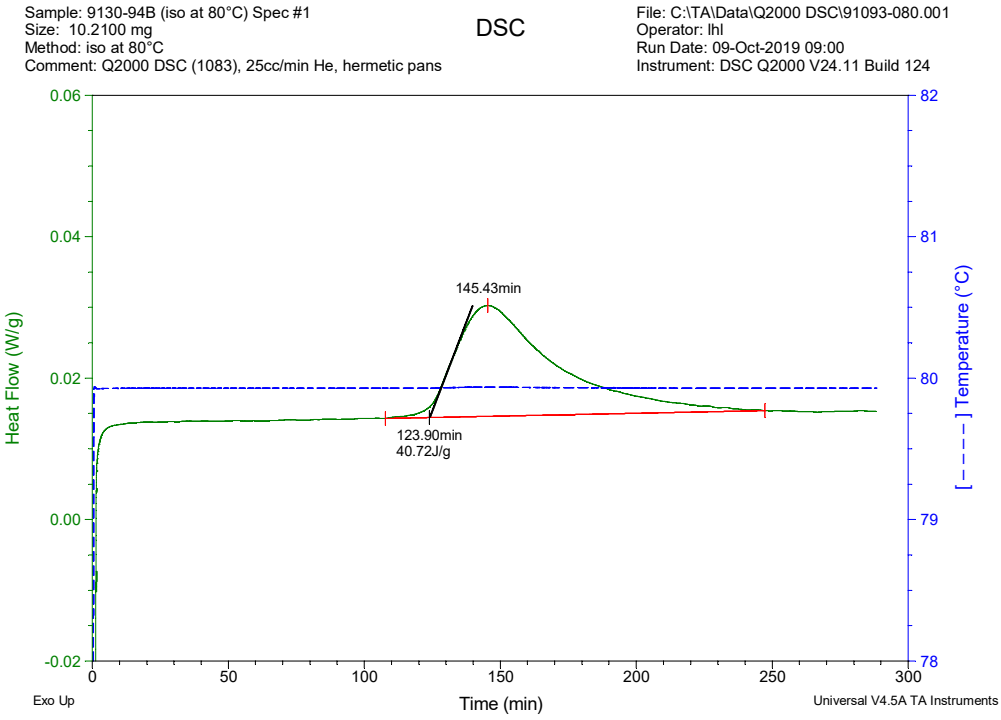
Sample: 9130-94B (iso at 80°C) Spec #1
Size: 10.2100 mg
Method: iso at 80°C
Comment: Q2000 DSC (1083), 25cc/min He, hermetic pans
DSC
File: C:\TA\Data\Q2000 DSC\91093-080.001
Operator: lhl
Run Date: 09-Oct-2019 09:00
Instrument: DSC Q2000 V24.11 Build 124
145.43min
123.90min
40.72J/g
Heat Flow (W/g)
[– – –] Temperature (°C)
Time (min)
Exo Up
Universal V4.5A TA Instruments

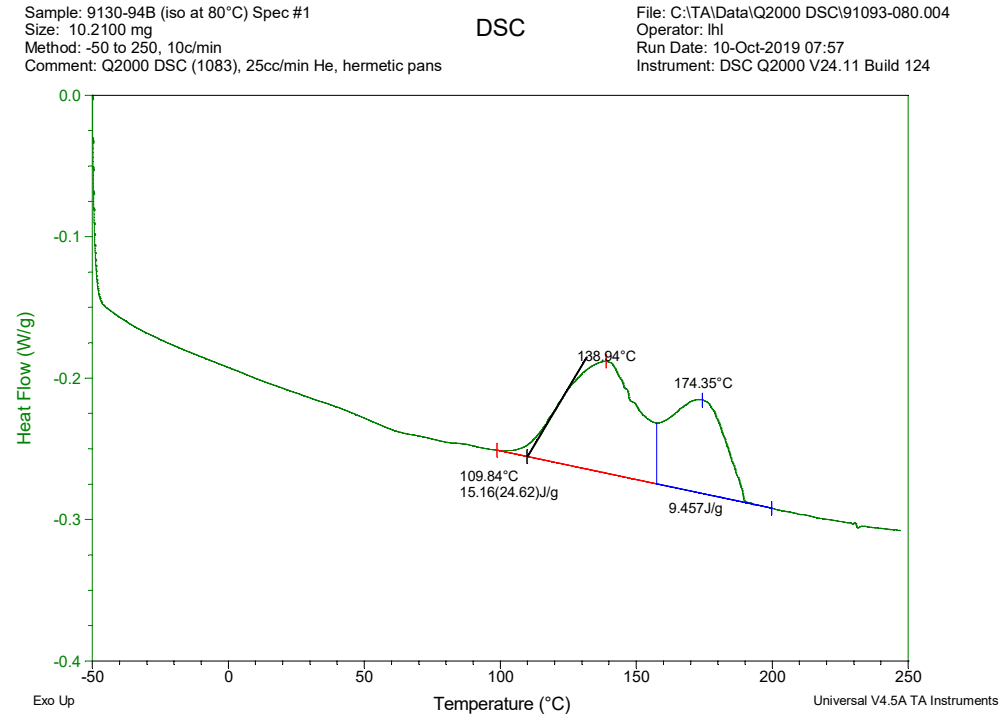
Sample: 9130-94B (iso at 80°C) Spec #1
Size: 10.2100 mg
Method: -50 to 250, 10c/min
Comment: Q2000 DSC (1083), 25cc/min He, hermetic pans
DSC
File: C:\TA\Data\Q2000 DSC\91093-080.004
Operator: lhl
Run Date: 10-Oct-2019 07:57
Instrument: DSC Q2000 V24.11 Build 124
138.94°C
174.35°C
109.84°C
15.16(24.62)J/g
9.457J/g
Heat Flow (W/g)
Temperature (°C)
Exo Up
Universal V4.5A TA Instruments

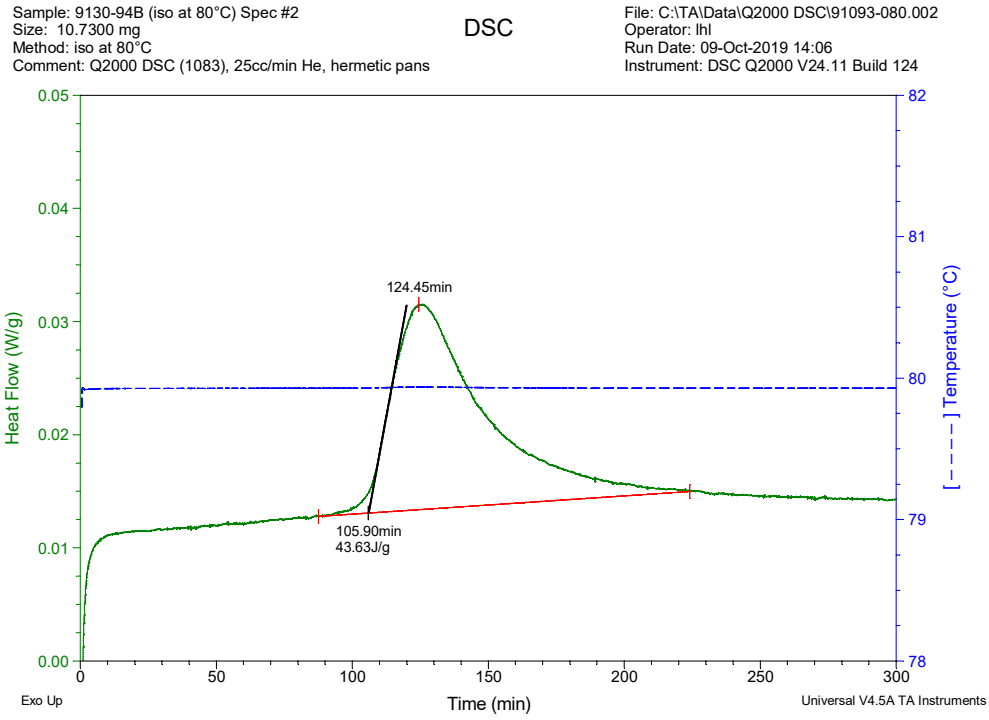
Sample: 9130-94B (iso at 80°C) Spec #2
Size: 10.7300 mg
Method: iso at 80°C
Comment: Q2000 DSC (1083), 25cc/min He, hermetic pans
DSC
File: C:\TA\Data\Q2000 DSC\91093-080.002
Operator: lhl
Run Date: 09-Oct-2019 14:06
Instrument: DSC Q2000 V24.11 Build 124
124.45min
105.90min
43.63J/g
Heat Flow (W/g)
[– – – –] Temperature (°C)
Time (min)
Exo Up
Universal V4.5A TA Instruments

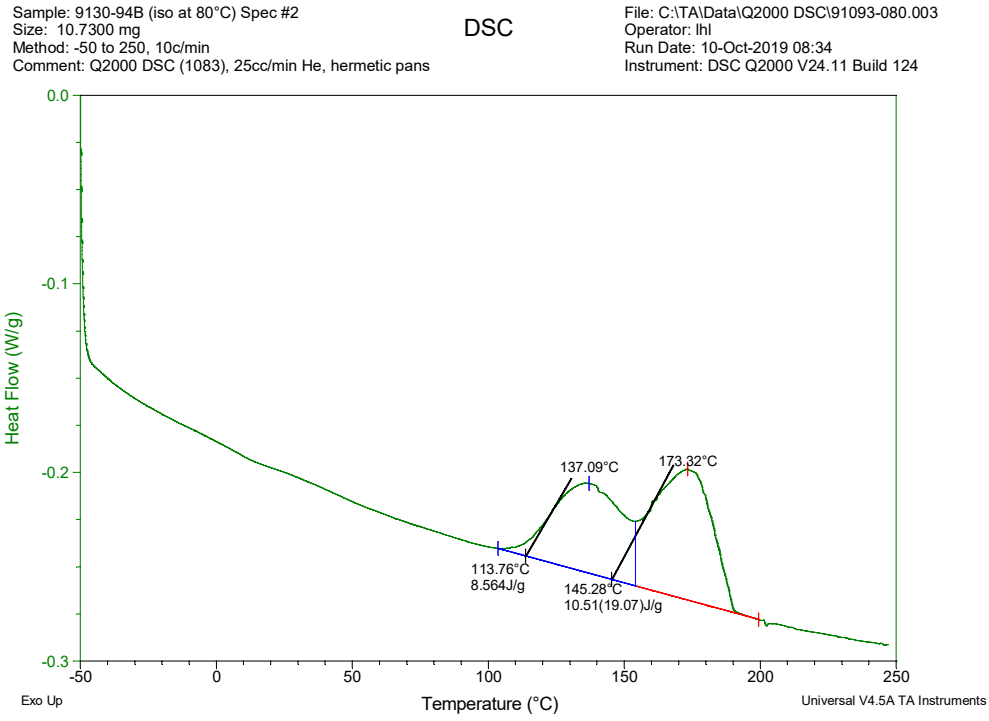
Sample: 9130-94B (iso at 80°C) Spec #2
Size: 10.7300 mg
Method: -50 to 250, 10c/min
Comment: Q2000 DSC (1083), 25cc/min He, hermetic pans
DSC
File: C:\TA\Data\Q2000 DSC\91093-080.003
Operator: lhl
Run Date: 10-Oct-2019 08:34
Instrument: DSC Q2000 V24.11 Build 124
137.09°C
173.32°C
113.76°C
8.564J/g
145.28°C
10.51(19.07)J/g
Heat Flow (W/g)
Temperature (°C)
Exo Up
Universal V4.5A TA Instruments

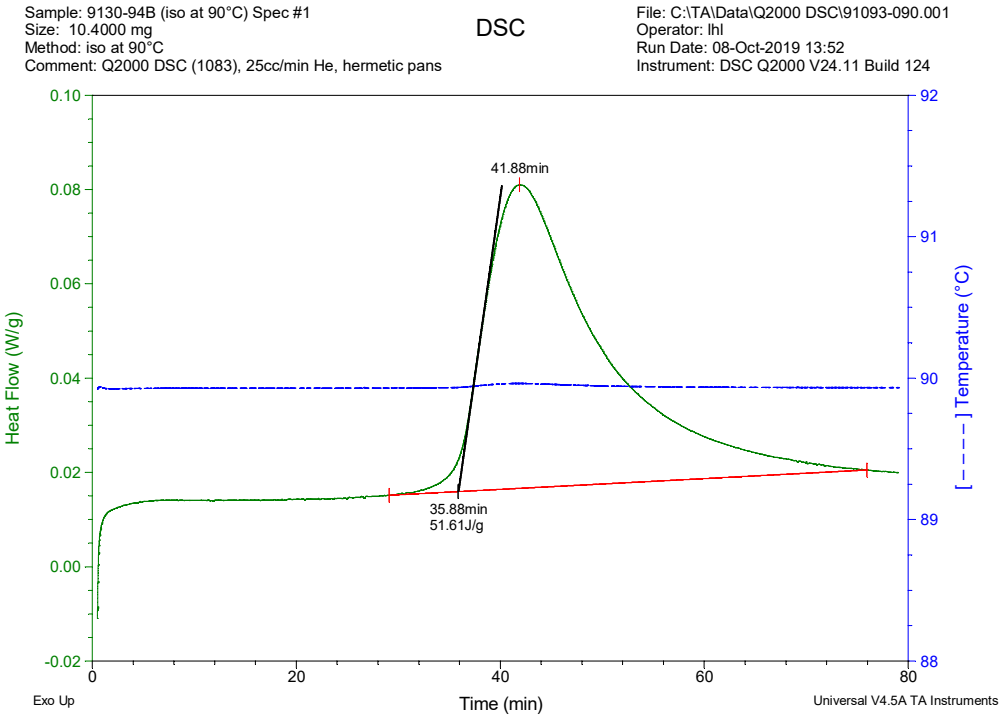
Sample: 9130-94B (iso at 90°C) Spec #1
Size: 10.4000 mg
Method: iso at 90°C
Comment: Q2000 DSC (1083), 25cc/min He, hermetic pans
DSC
File: C:\TA\Data\Q2000 DSC\91093-090.001
Operator: lhl
Run Date: 08-Oct-2019 13:52
Instrument: DSC Q2000 V24.11 Build 124
41.88min
35.88min
51.61J/g
Heat Flow (W/g)
[– – – –] Temperature (°C)
Time (min)
Exo Up
Universal V4.5A TA Instruments

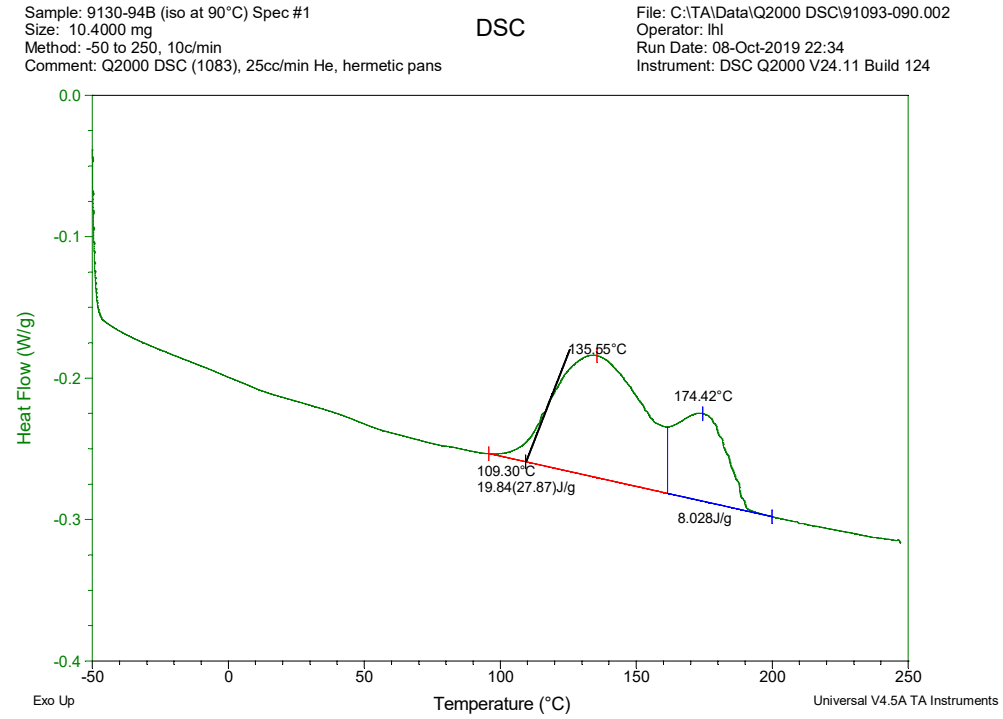
Sample: 9130-94B (iso at 90°C) Spec #1
Size: 10.4000 mg
Method: -50 to 250, 10c/min
Comment: Q2000 DSC (1083), 25cc/min He, hermetic pans
DSC
File: C:\TA\Data\Q2000 DSC\91093-090.002
Operator: lhl
Run Date: 08-Oct-2019 22:34
Instrument: DSC Q2000 V24.11 Build 124
135.55°C
174.42°C
109.30°C
19.84(27.87)J/g
8.028J/g
Heat Flow (W/g)
Temperature (°C)
Exo Up
Universal V4.5A TA Instruments

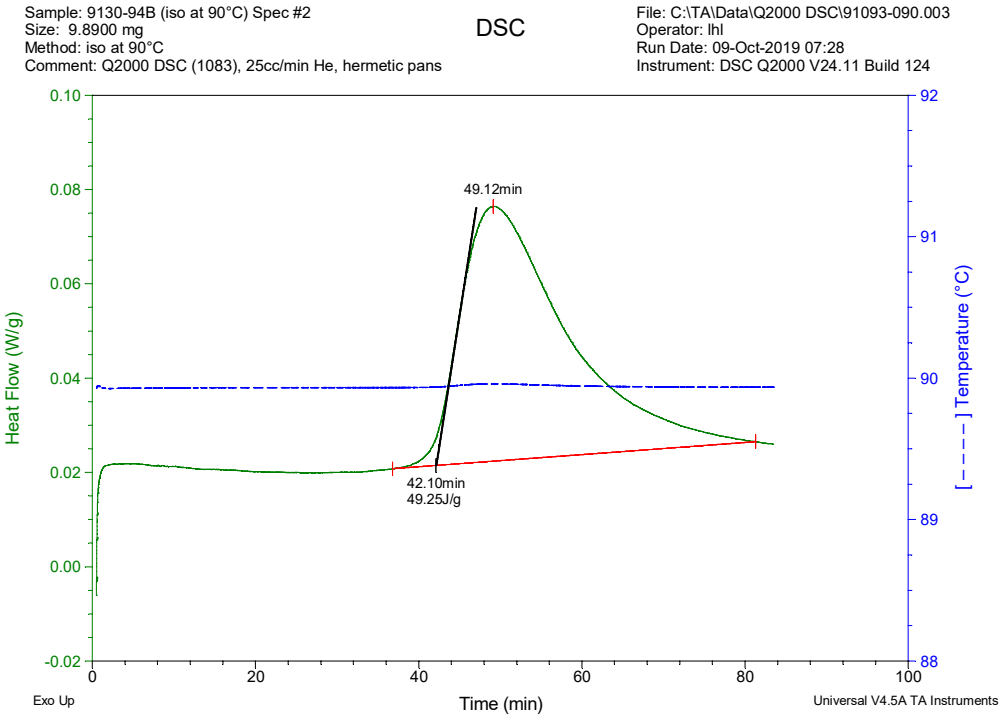
Sample: 9130-94B (iso at 90°C) Spec #2
Size: 9.8900 mg
Method: iso at 90°C
Comment: Q2000 DSC (1083), 25cc/min He, hermetic pans
DSC
File: C:\TA\Data\Q2000 DSC\91093-090.003
Operator: lhl
Run Date: 09-Oct-2019 07:28
Instrument: DSC Q2000 V24.11 Build 124
49.12min
42.10min
49.25J/g
Heat Flow (W/g)
[– – – –] Temperature (°C)
Time (min)
Exo Up
Universal V4.5A TA Instruments

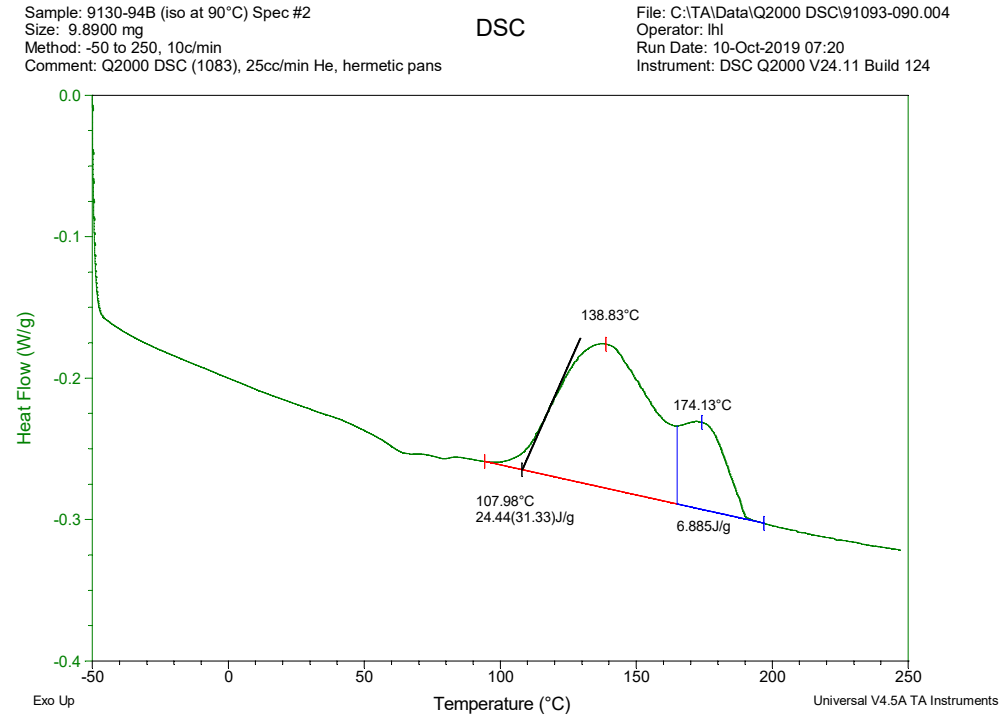
Sample: 9130-94B (iso at 90°C) Spec #2
Size: 9.8900 mg
Method: -50 to 250, 10c/min
Comment: Q2000 DSC (1083), 25cc/min He, hermetic pans
DSC
File: C:\TA\Data\Q2000 DSC\91093-090.004
Operator: lhl
Run Date: 10-Oct-2019 07:20
Instrument: DSC Q2000 V24.11 Build 124
138.83°C
174.13°C
107.98°C
24.44(31.33)J/g
6.885J/g
Heat Flow (W/g)
Temperature (°C)
Exo Up
Universal V4.5A TA Instruments

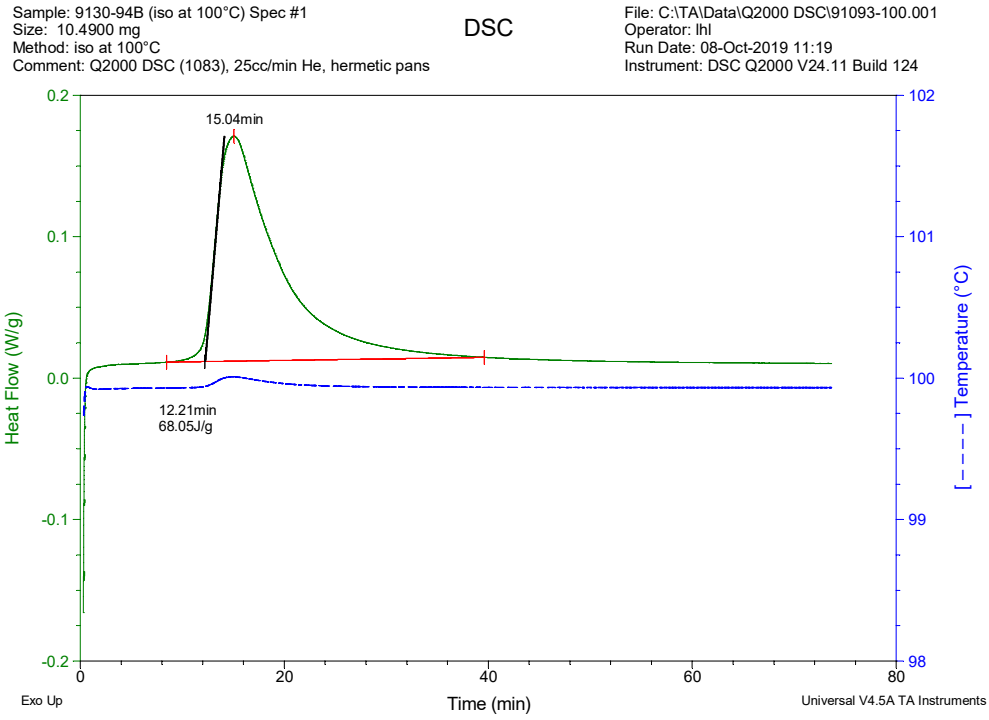
Sample: 9130-94B (iso at 100°C) Spec #1
Size: 10.4900 mg
Method: iso at 100°C
Comment: Q2000 DSC (1083), 25cc/min He, hermetic pans
DSC
File: C:\TA\Data\Q2000 DSC\91093-100.001
Operator: lhl
Run Date: 08-Oct-2019 11:19
Instrument: DSC Q2000 V24.11 Build 124
15.04min
12.21min
68.05J/g
Heat Flow (W/g)
[- - - -] Temperature (°C)
Time (min)
Exo Up
Universal V4.5A TA Instruments

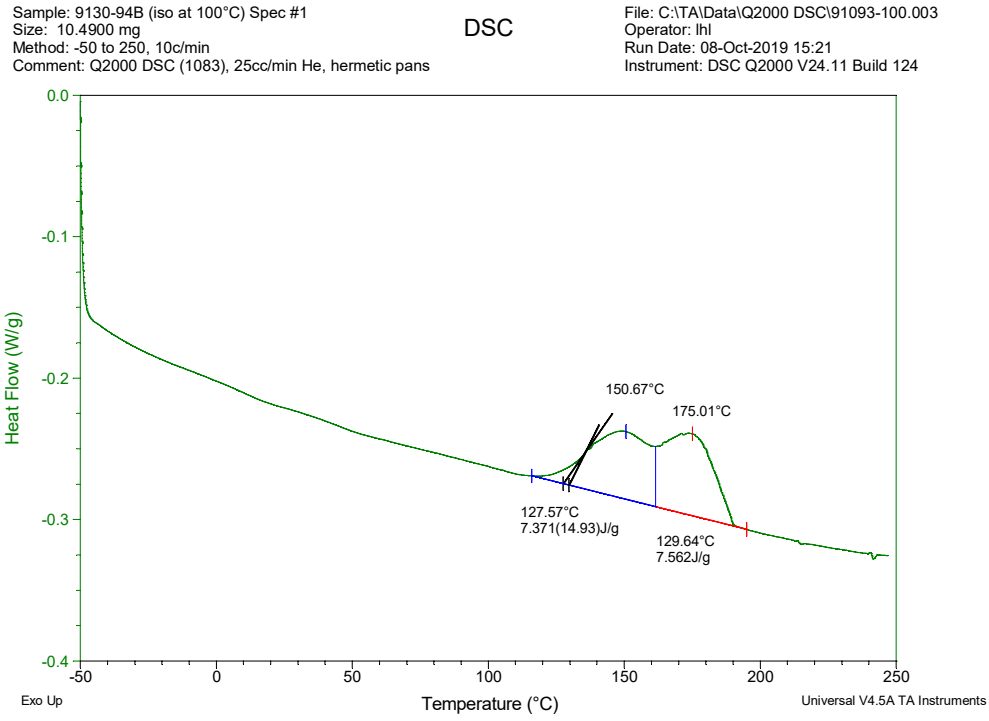
Sample: 9130-94B (iso at 100°C) Spec #1
Size: 10.4900 mg
Method: -50 to 250, 10c/min
Comment: Q2000 DSC (1083), 25cc/min He, hermetic pans
DSC
File: C:\TA\Data\Q2000 DSC\91093-100.003
Operator: lhl
Run Date: 08-Oct-2019 15:21
Instrument: DSC Q2000 V24.11 Build 124
150.67°C
175.01°C
127.57°C
7.371(14.93)J/g
129.64°C
7.562J/g
Heat Flow (W/g)
Temperature (°C)
Exo Up
Universal V4.5A TA Instruments

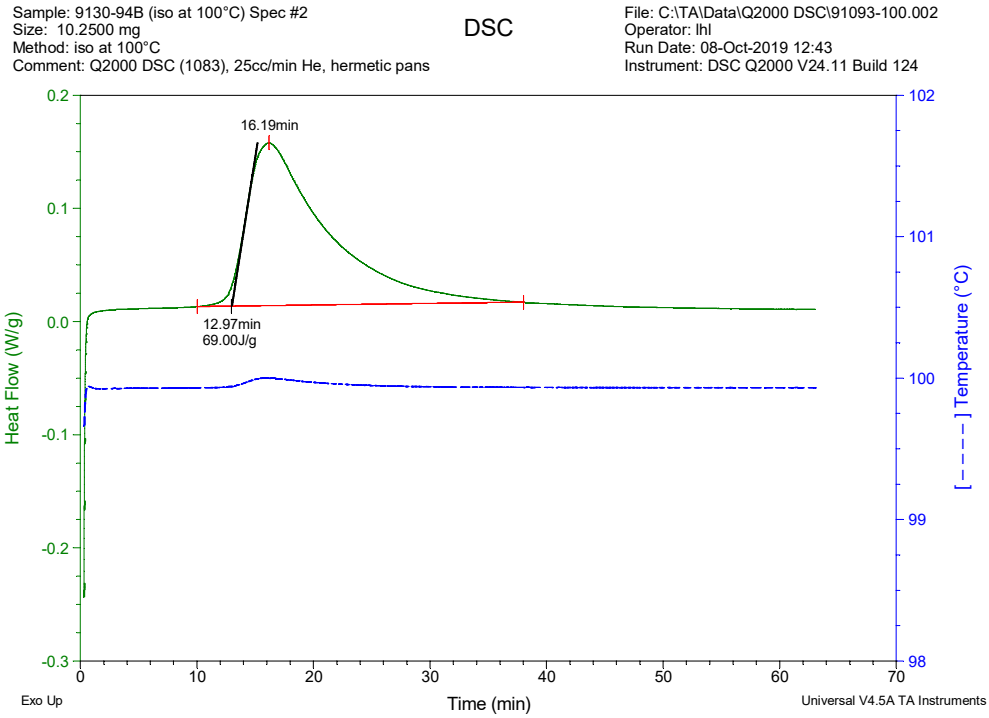
Sample: 9130-94B (iso at 100°C) Spec #2
Size: 10.2500 mg
Method: iso at 100°C
Comment: Q2000 DSC (1083), 25cc/min He, hermetic pans
DSC
File: C:\TA\Data\Q2000 DSC\91093-100.002
Operator: lhl
Run Date: 08-Oct-2019 12:43
Instrument: DSC Q2000 V24.11 Build 124
16.19min
12.97min
69.00J/g
Heat Flow (W/g)
[- - - -] Temperature (°C)
Time (min)
Exo Up
Universal V4.5A TA Instruments

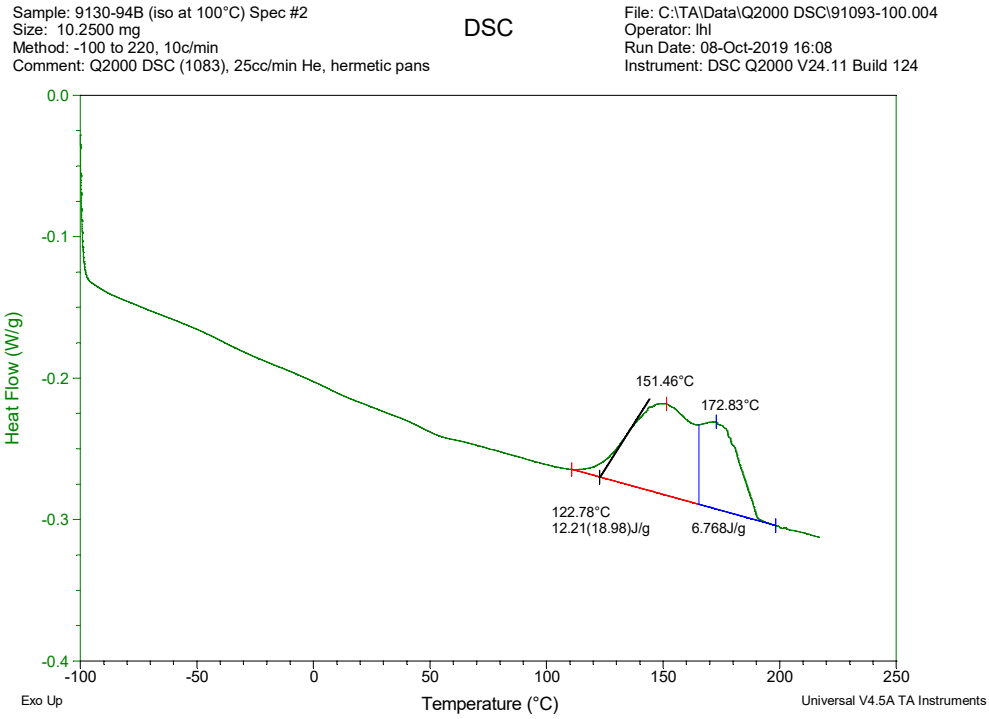
Sample: 9130-94B (iso at 100°C) Spec #2
Size: 10.2500 mg
Method: -100 to 220, 10c/min
Comment: Q2000 DSC (1083), 25cc/min He, hermetic pans
DSC
File: C:\TA\Data\Q2000 DSC\91093-100.004
Operator: lhl
Run Date: 08-Oct-2019 16:08
Instrument: DSC Q2000 V24.11 Build 124
151.46°C
172.83°C
122.78°C
12.21(18.98)J/g
6.768J/g
Heat Flow (W/g)
Temperature (°C)
Exo Up
Universal V4.5A TA Instruments

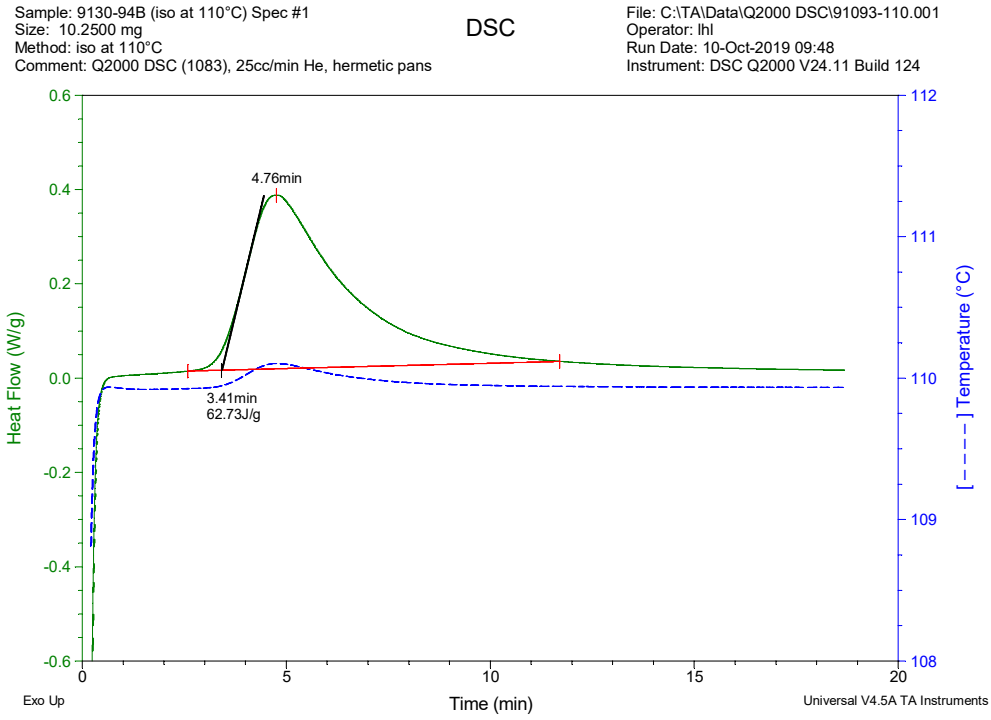
Sample: 9130-94B (iso at 110°C) Spec #1
Size: 10.2500 mg
Method: iso at 110°C
Comment: Q2000 DSC (1083), 25cc/min He, hermetic pans
DSC
File: C:\TA\Data\Q2000 DSC\91093-110.001
Operator: lhl
Run Date: 10-Oct-2019 09:48
Instrument: DSC Q2000 V24.11 Build 124
4.76min
3.41min
62.73J/g
Heat Flow (W/g)
[- - - -] Temperature (°C)
Time (min)
Exo Up
Universal V4.5A TA Instruments

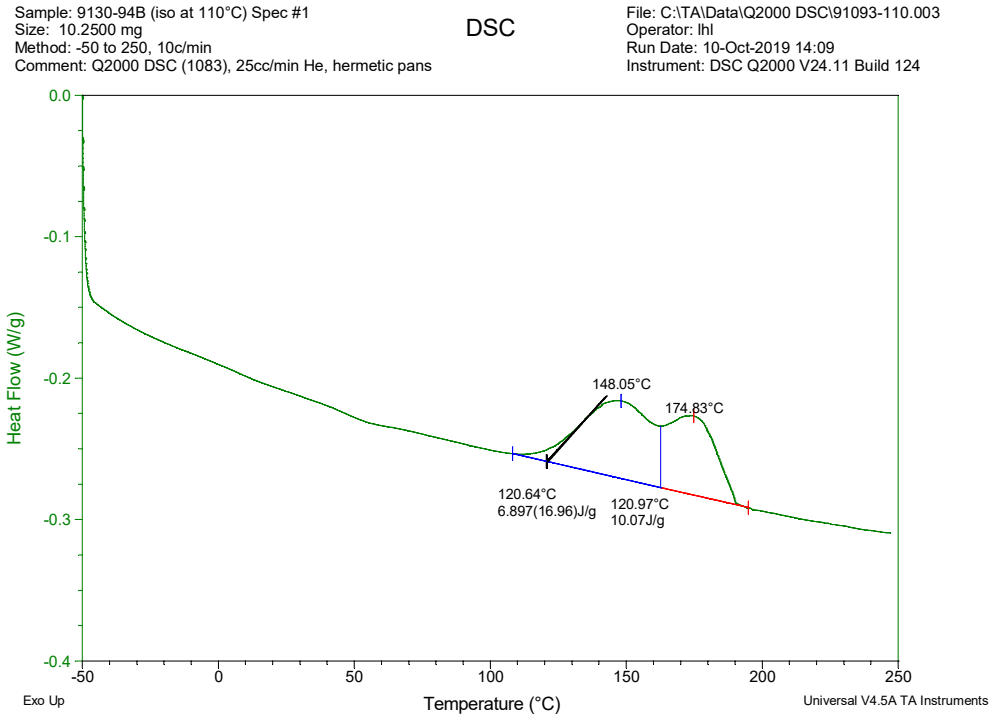
Sample: 9130-94B (iso at 110°C) Spec #1
Size: 10.2500 mg
Method: -50 to 250, 10c/min
Comment: Q2000 DSC (1083), 25cc/min He, hermetic pans
DSC
File: C:\TA\Data\Q2000 DSC\91093-110.003
Operator: lhl
Run Date: 10-Oct-2019 14:09
Instrument: DSC Q2000 V24.11 Build 124
148.05°C
174.83°C
120.64°C
6.897(16.96)J/g
120.97°C
10.07J/g
Heat Flow (W/g)
Temperature (°C)
Exo Up
Universal V4.5A TA Instruments

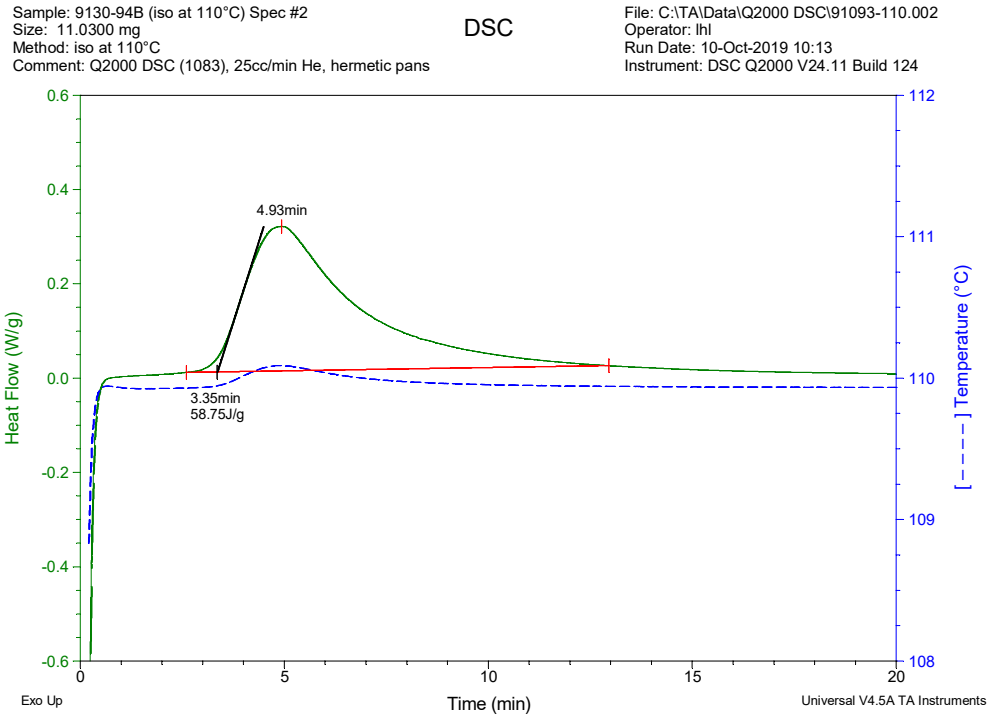
Sample: 9130-94B (iso at 110°C) Spec #2
Size: 11.0300 mg
Method: iso at 110°C
Comment: Q2000 DSC (1083), 25cc/min He, hermetic pans
DSC
File: C:\TA\Data\Q2000 DSC\91093-110.002
Operator: lhl
Run Date: 10-Oct-2019 10:13
Instrument: DSC Q2000 V24.11 Build 124
4.93min
3.35min
58.75J/g
Heat Flow (W/g)
[- - - -] Temperature (°C)
Time (min)
Exo Up
Universal V4.5A TA Instruments

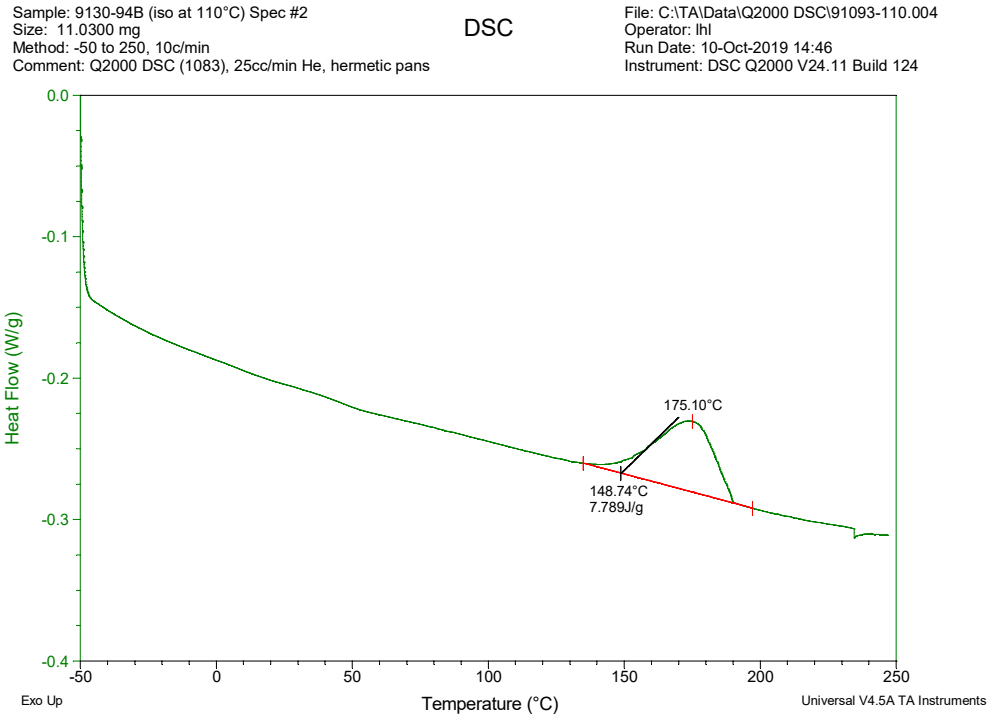
Sample: 9130-94B (iso at 110°C) Spec #2
Size: 11.0300 mg
Method: -50 to 250, 10c/min
Comment: Q2000 DSC (1083), 25cc/min He, hermetic pans
DSC
File: C:\TA\Data\Q2000 DSC\91093-110.004
Operator: lhl
Run Date: 10-Oct-2019 14:46
Instrument: DSC Q2000 V24.11 Build 124
175.10°C
148.74°C
7.789J/g
Heat Flow (W/g)
Temperature (°C)
Exo Up
Universal V4.5A TA Instruments

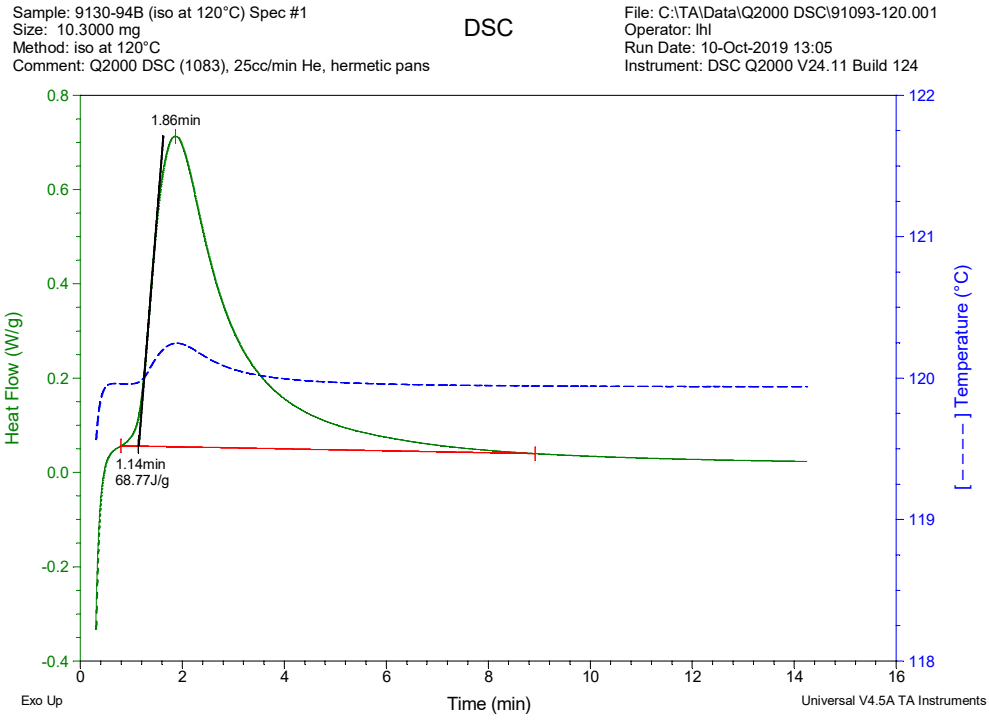
Sample: 9130-94B (iso at 120°C) Spec #1
Size: 10.3000 mg
Method: iso at 120°C
Comment: Q2000 DSC (1083), 25cc/min He, hermetic pans
DSC
File: C:\TA\Data\Q2000 DSC\91093-120.001
Operator: lhl
Run Date: 10-Oct-2019 13:05
Instrument: DSC Q2000 V24.11 Build 124
1.86min
1.14min
68.77J/g
Heat Flow (W/g)
[- - - -] Temperature (°C)
Time (min)
Exo Up
Universal V4.5A TA Instruments

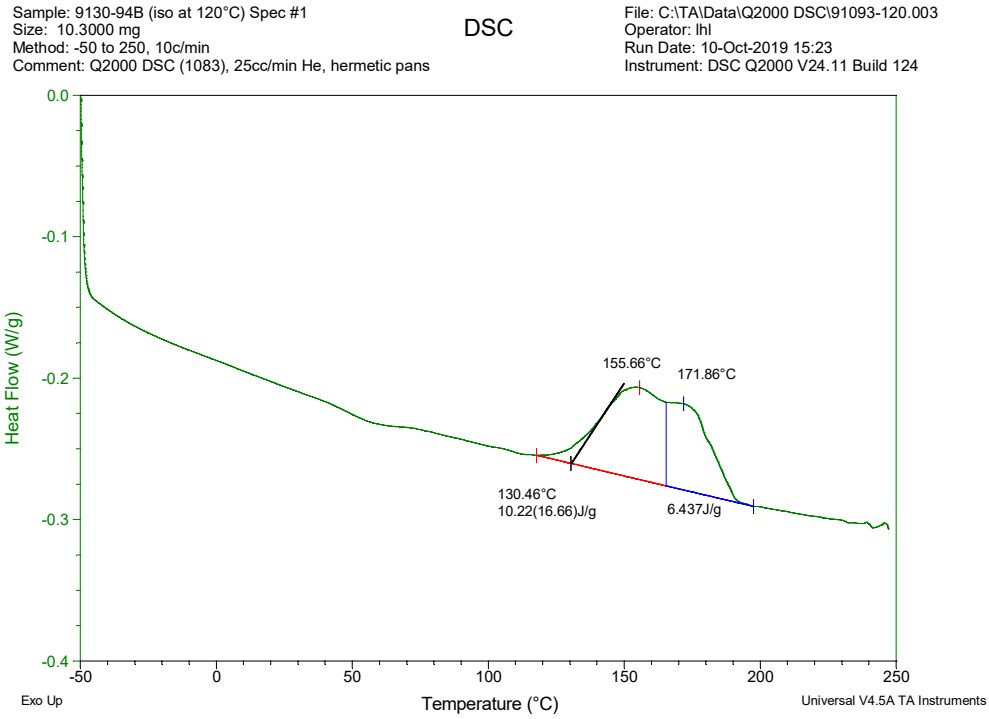
Sample: 9130-94B (iso at 120°C) Spec #1
Size: 10.3000 mg
Method: -50 to 250, 10c/min
Comment: Q2000 DSC (1083), 25cc/min He, hermetic pans
DSC
File: C:\TA\Data\Q2000 DSC\91093-120.003
Operator: lhl
Run Date: 10-Oct-2019 15:23
Instrument: DSC Q2000 V24.11 Build 124
155.66°C
171.86°C
130.46°C
10.22(16.66)J/g
6.437J/g
Heat Flow (W/g)
Temperature (°C)
Exo Up
Universal V4.5A TA Instruments

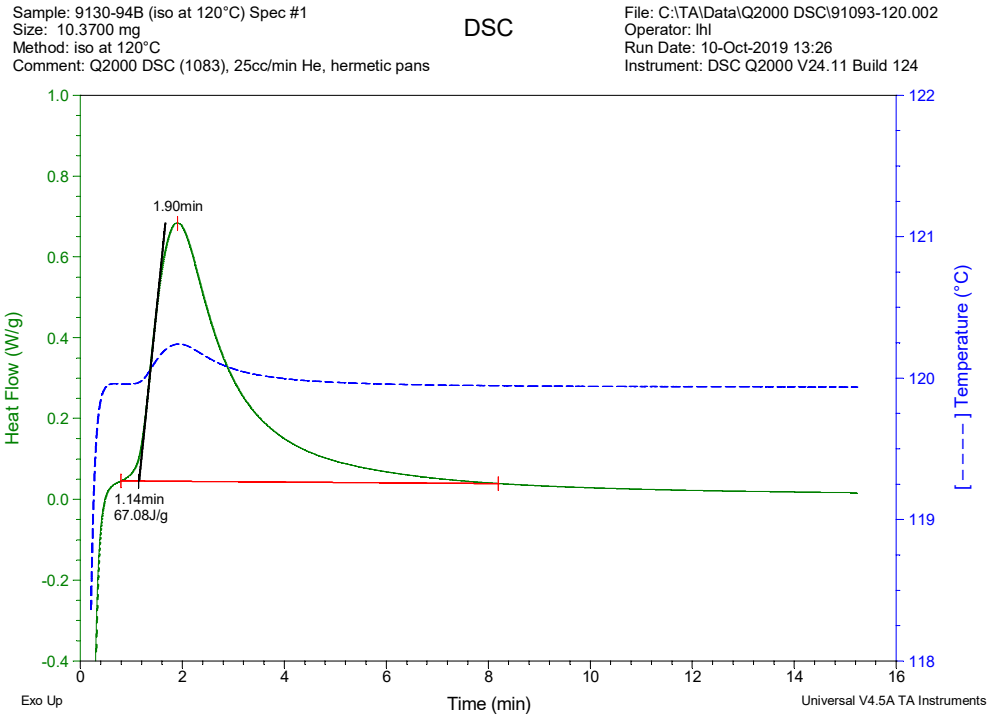
Sample: 9130-94B (iso at 120°C) Spec #1
Size: 10.3700 mg
Method: iso at 120°C
Comment: Q2000 DSC (1083), 25cc/min He, hermetic pans
DSC
File: C:\TA\Data\Q2000 DSC\91093-120.002
Operator: lhl
Run Date: 10-Oct-2019 13:26
Instrument: DSC Q2000 V24.11 Build 124
1.90min
1.14min
67.08J/g
Heat Flow (W/g)
[- - - -] Temperature (°C)
Time (min)
Exo Up
Universal V4.5A TA Instruments

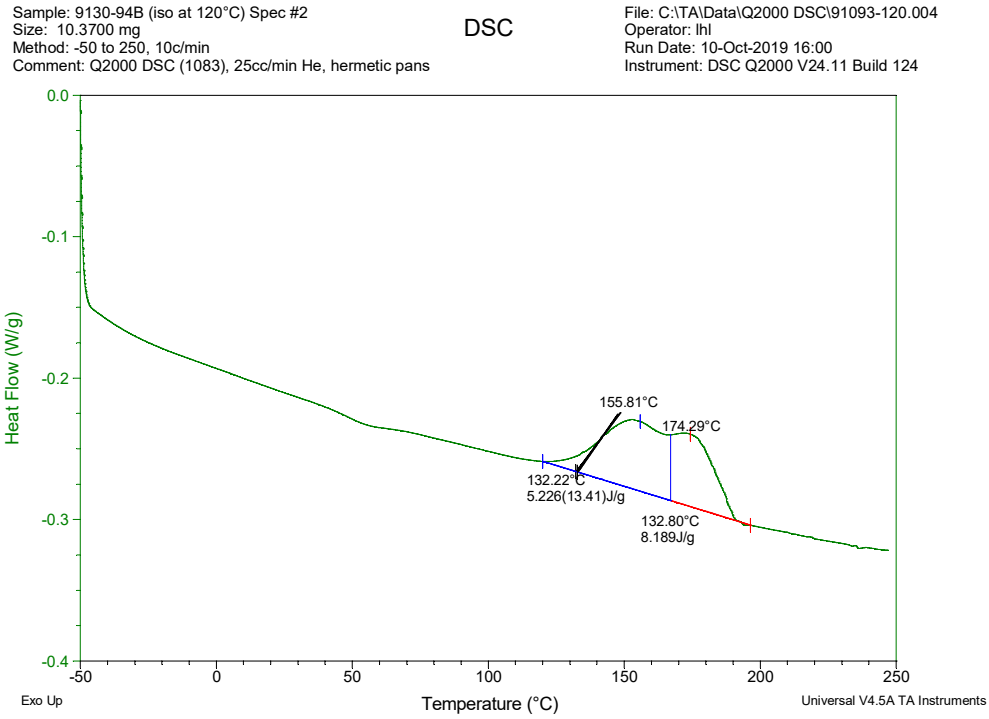
Sample: 9130-94B (iso at 120°C) Spec #2
Size: 10.3700 mg
Method: -50 to 250, 10c/min
Comment: Q2000 DSC (1083), 25cc/min He, hermetic pans
DSC
File: C:\TA\Data\Q2000 DSC\91093-120.004
Operator: lhl
Run Date: 10-Oct-2019 16:00
Instrument: DSC Q2000 V24.11 Build 124
155.81°C
174.29°C
132.22°C
5.226(13.41)J/g
132.80°C
8.189J/g
Heat Flow (W/g)
Temperature (°C)
Exo Up
Universal V4.5A TA Instruments

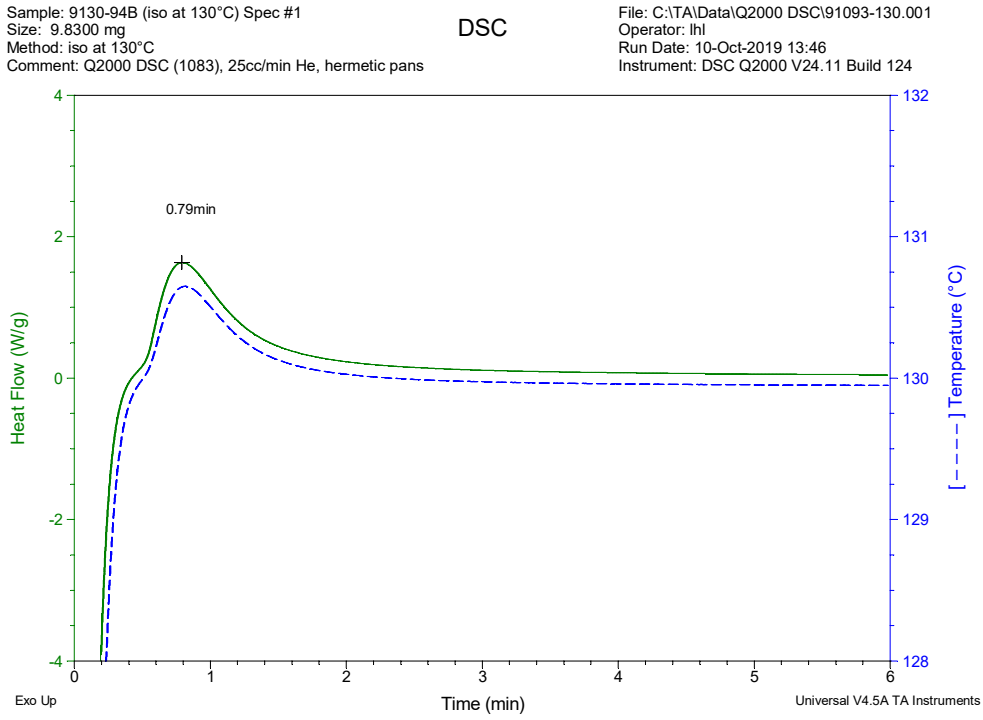
Sample: 9130-94B (iso at 130°C) Spec #1
Size: 9.8300 mg
Method: iso at 130°C
Comment: Q2000 DSC (1083), 25cc/min He, hermetic pans
DSC
File: C:\TA\Data\Q2000 DSC\91093-130.001
Operator: lhl
Run Date: 10-Oct-2019 13:46
Instrument: DSC Q2000 V24.11 Build 124
0.79min
Heat Flow (W/g)
[- - - -] Temperature (°C)
Time (min)
Exo Up
Universal V4.5A TA Instruments

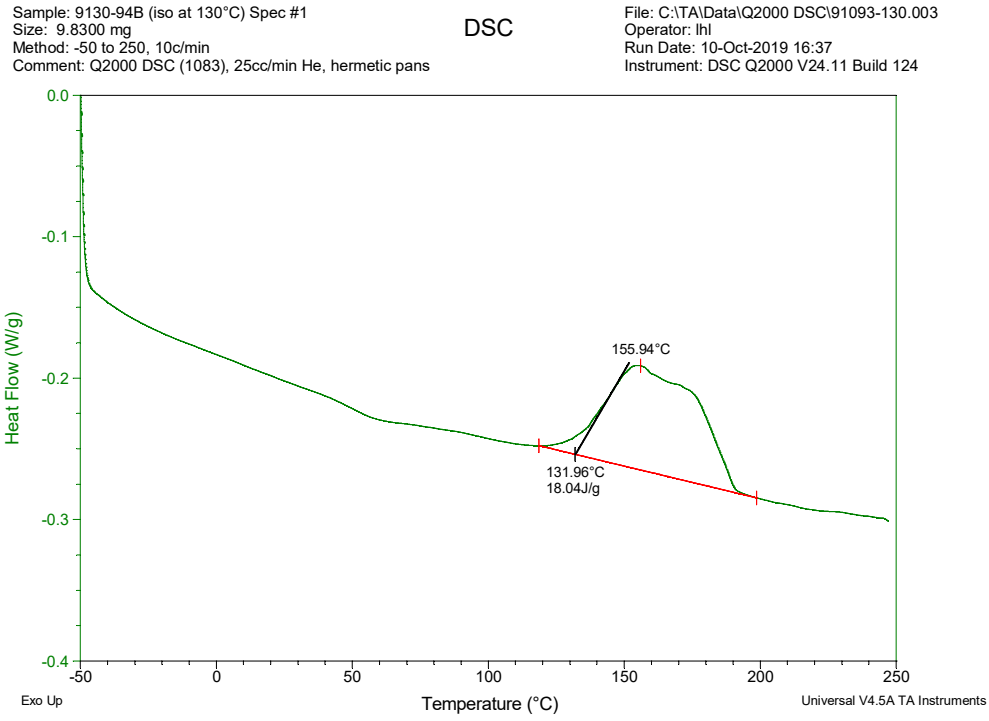
Sample: 9130-94B (iso at 130°C) Spec #1
Size: 9.8300 mg
Method: -50 to 250, 10c/min
Comment: Q2000 DSC (1083), 25cc/min He, hermetic pans
DSC
File: C:\TA\Data\Q2000 DSC\91093-130.003
Operator: lhl
Run Date: 10-Oct-2019 16:37
Instrument: DSC Q2000 V24.11 Build 124
155.94°C
131.96°C
18.04J/g
Heat Flow (W/g)
Temperature (°C)
Exo Up
Universal V4.5A TA Instruments

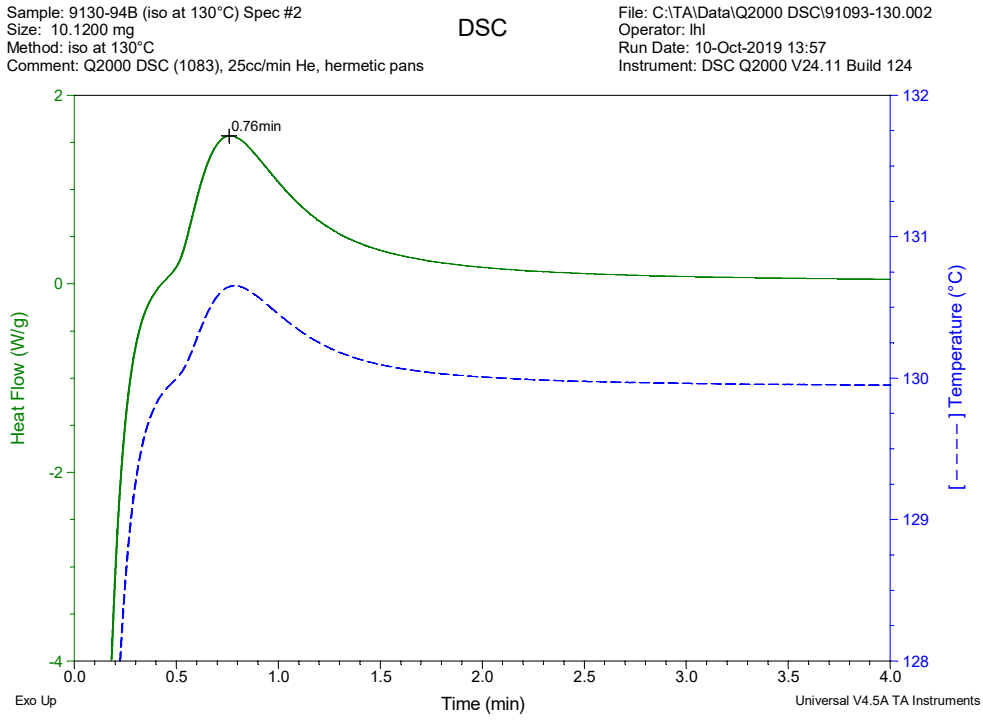
Sample: 9130-94B (iso at 130°C) Spec #2
Size: 10.1200 mg
Method: iso at 130°C
Comment: Q2000 DSC (1083), 25cc/min He, hermetic pans
DSC
File: C:\TA\Data\Q2000 DSC\91093-130.002
Operator: lhl
Run Date: 10-Oct-2019 13:57
Instrument: DSC Q2000 V24.11 Build 124
0.76min
Heat Flow (W/g)
[- - - -] Temperature (°C)
Time (min)
Exo Up
Universal V4.5A TA Instruments

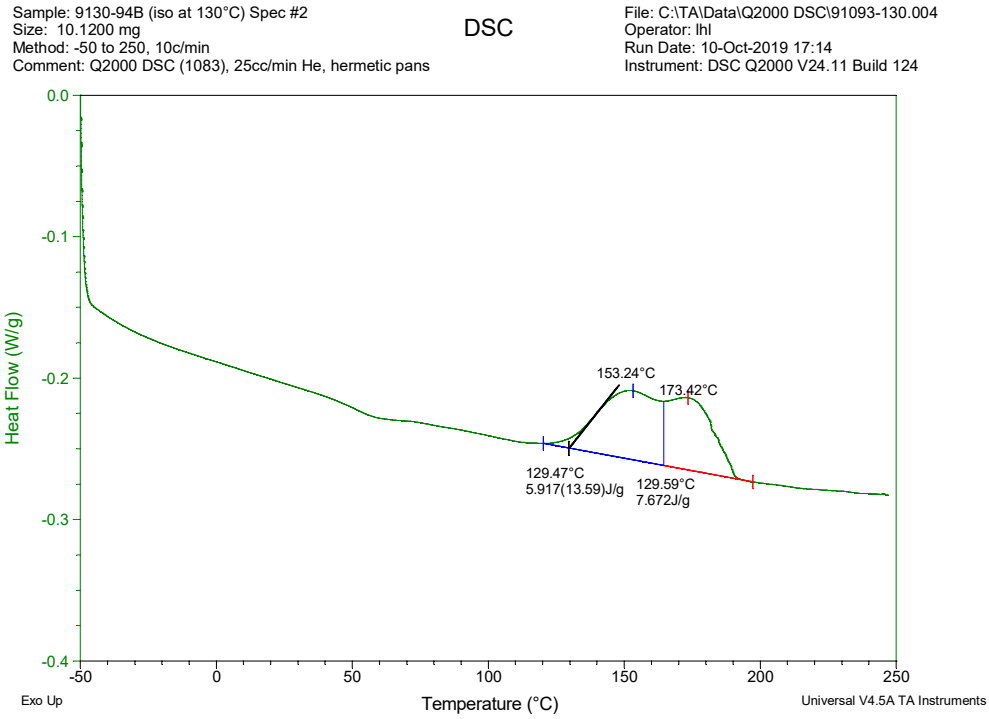
Sample: 9130-94B (iso at 130°C) Spec #2
Size: 10.1200 mg
Method: -50 to 250, 10c/min
Comment: Q2000 DSC (1083), 25cc/min He, hermetic pans
DSC
File: C:\TA\Data\Q2000 DSC\91093-130.004
Operator: lhl
Run Date: 10-Oct-2019 17:14
Instrument: DSC Q2000 V24.11 Build 124
153.24°C
173.42°C
129.47°C
5.917(13.59)J/g
129.59°C
7.672J/g
Heat Flow (W/g)
Temperature (°C)
Exo Up
Universal V4.5A TA Instruments

11.7. Tensile Test Results

1A:

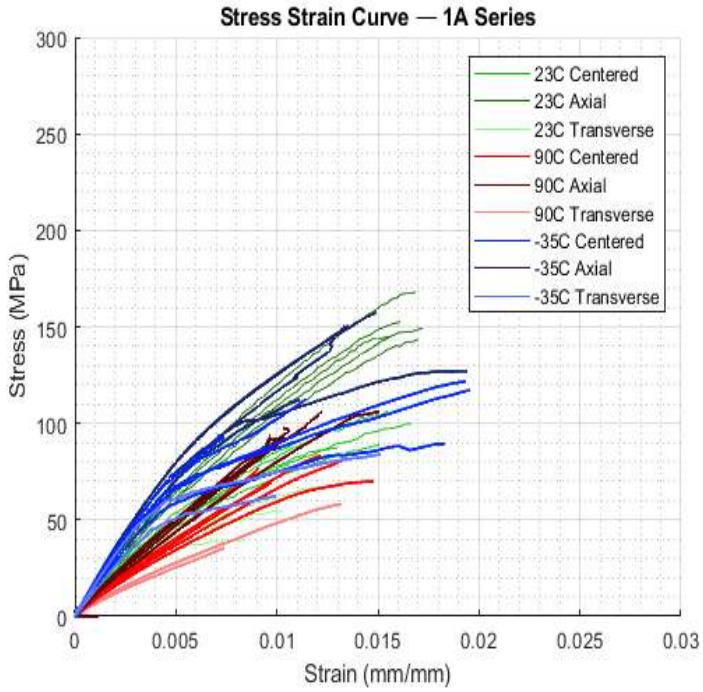

	Sample	Ultimate Stress (MPa)	Max Strain	Tensile Modulus (GPa)		Sample	Ultimate Stress (MPa)	Max Strain	Tensile Modulus (GPa)		Sample	Ultimate Stress (MPa)	Max Strain	Tensile Modulus (GPa)
23C Axial	1	168.3	0.017	14.6	90C Axial	7	106.1	0.012	15.9	-35 Axial	6	157.3	0.015	16.0
	2	145.1	0.016	12.6		8	106.2	0.015	8.4		7	127.0	0.019	15.8
	3	143.5	0.017	11.9		1	92.1	0.011	10.3		8	150.5	0.013	16.4
	4	152.7	0.016	13.9		2	92.4	0.010	10.3		9	112.0	0.011	14.9
	5	149.3	0.017	13.3		3	86.6	0.010	10.0		10	145.8	0.013	14.7
						4	97.5	0.010	10.1					
						5	94.0	0.010	10.1					
Average		**151.8**	**0.017**	**13.3**	**Average**		**96.4**	**0.011**	**10.7**	**Average**		**138.5**	**0.014**	**15.6**
St. Deviation		**8.9**	**0.001**	**0.9**	**St. Deviation**		**6.8**	**0.002**	**2.2**	**St. Deviation**		**16.6**	**0.003**	**0.7**
23C Centered	1	87.2	0.013	10.0	90C Centered	1	76.8	0.009	8.8	-35 Centered	6	93.4	0.007	15.4
	2	88.8	0.015	9.2		2	69.2	0.010	8.2		7	121.9	0.019	14.8
	3	97.6	0.013	11.0		3	81.4	0.013	7.5		8	89.5	0.018	13.2
	4	99.7	0.017	10.4		4	69.9	0.015	6.9		9	113.4	0.011	15.9
	5	106.6	0.015	10.6		5	83.1	0.012	7.7		10	117.0	0.020	14.9
	6	74.3	0.009	10.5										
Average		**92.4**	**0.014**	**10.3**	**Average**		**76.1**	**0.012**	**7.8**	**Average**		**107.1**	**0.015**	**14.8**
St. Deviation		**10.4**	**0.002**	**0.6**	**St. Deviation**		**5.7**	**0.002**	**0.6**	**St. Deviation**		**13.1**	**0.005**	**0.9**
23C Transverse	1	53.4	0.008	8.7	90C Transverse	7	36.3	0.007	5.1	-35 Transverse	9	62.4	0.010	11.7
	2	39.7	0.008	7.4		8	58.2	0.013	5.6		10	83.9	0.015	14.6
	3	67.5	0.012	8.9										
	4	55.2	0.010	8.6										
	5	39.0	0.005	8.9										
Average		**51.0**	**0.009**	**8.5**	**Average**		**47.2**	**0.010**	**5.3**	**Average**		**73.1**	**0.013**	**13.1**
St. Deviation		**10.7**	**0.002**	**0.5**	**St. Deviation**		**10.9**	**0.003**	**0.3**	**St. Deviation**		**10.7**	**0.003**	**1.4**

1B:

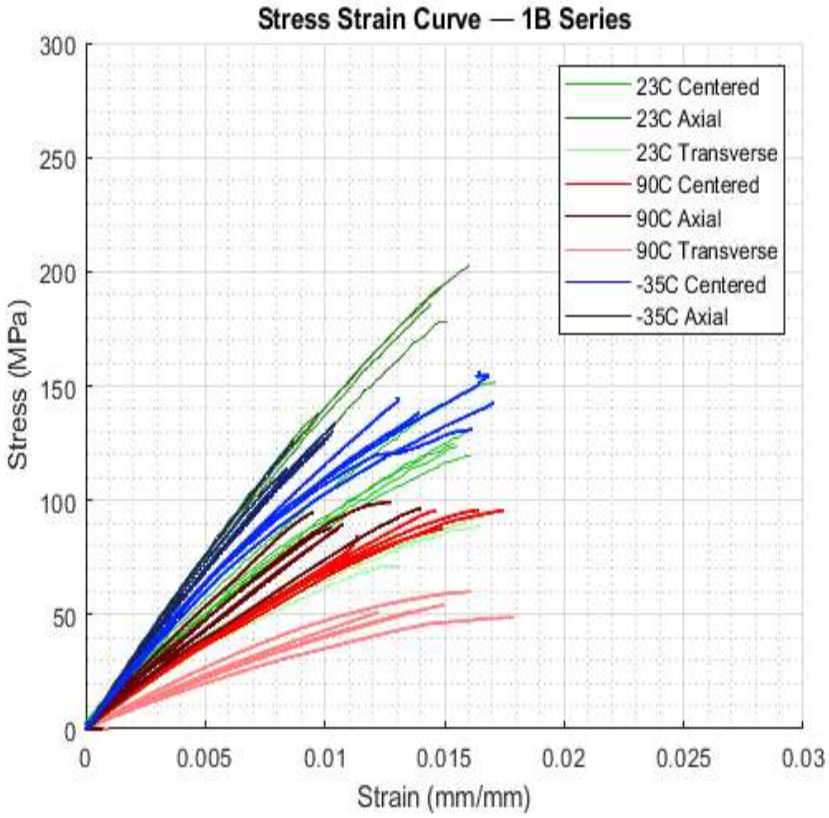

	Sample	Ultimate Stress (Mpa)	Max Strain	Tensile Modulus (Gpa)		Sample	Ultimate Stress (Mpa)	Max Strain	Tensile Modulus (Gpa)		Sample	Ultimate Stress (Mpa)	Max Strain	Tensile Modulus (Gpa)
	1	194.6	0.015	15.3		7	94.5	0.010	10.9		6	113.8	0.008	14.5
	2	202.8	0.016	15.2		8	90.7	0.008	12.7		7	126.5	0.009	15.5
23C Axial	3	138.7	0.010	15.7		1	88.1	0.010	10.0	-35 Axial	8	134.2	0.011	14.3
	4	186.0	0.014	15.1	90C Axial	2	87.8	0.011	9.2		9	130.2	0.010	14.0
	5	178.3	0.015	14.5		3	99.3	0.013	9.1		10	127.2	0.010	14.0
						4	89.3	0.011	8.1					
						5	96.4	0.014	8.3					
Average		180.1	0.014	15.2	Average		92.3	0.011	9.7	Average		126.4	0.010	14.5
St. Deviation		22.3	0.002	0.4	St. Deviation		4.1	0.002	1.5	St. Deviation		6.8	0.001	0.6
	1	129.2	0.016	10.9		1	95.1	0.015	8.2		6	142.5	0.017	12.3
	2	123.8	0.016	9.5		2	95.6	0.017	7.5		7	131.1	0.016	12.9
23C Centered	3	119.7	0.016	9.6	90C Centered	3	87.7	0.015	7.8	-35 Centered	8	138.2	0.014	13.0
	4	125.4	0.015	9.9		4	95.6	0.016	7.8		9	156.1	0.016	13.0
	5	151.5	0.017	11.0		5	84.0	0.011	7.6		10	145.5	0.013	13.1
Average		129.9	0.016	10.2	Average		91.6	0.015	7.8	Average		142.7	0.015	12.9
St. Deviation		11.2	0.001	0.6	St. Deviation		4.9	0.002	0.2	St. Deviation		8.3	0.002	0.3
	1	90.0	0.016	7.9		6	51.6	0.014	4.6					
	2	71.4	0.013	7.4		7	48.8	0.018	4.0					
23C Transverse	3	89.1	0.017	7.8	90C Transverse	8	51.3	0.012	4.8					
	4	92.7	0.017	7.7		9	54.1	0.015	4.4					
	5	85.6	0.013	8.3		10	60.0	0.016	5.5					
Average		85.8	0.015	7.8	Average		53.2	0.015	4.7					
St. Deviation		7.6	0.002	0.3	St. Deviation		3.8	0.002	0.5					

1C:

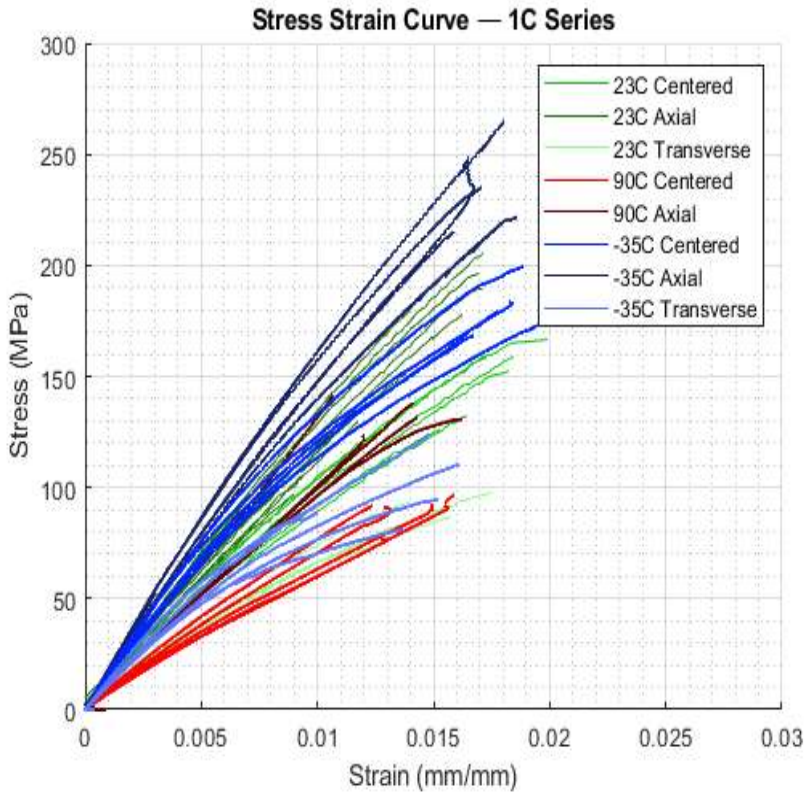

	Sample	Ultimate Stress (MPa)	Max Strain	Tensile Modulus (GPa)		Sample	Ultimate Stress (MPa)	Max Strain	Tensile Modulus (GPa)		Sample	Ultimate Stress (MPa)	Max Strain	Tensile Modulus (GPa)
23C Axial	1	205.5	0.017	14.4	90C Axial	1	142.6	0.011	13.7	-35 Axial	6	264.7	0.018	17.8
	2	97.2	0.009	11.3		2	131.8	0.014	10.9		7	248.5	0.016	15.9
	3	189.8	0.017	13.5		3	138.5	0.014	10.9		8	221.9	0.019	15.7
	4	151.2	0.014	11.8		4	123.8	0.012	10.8		9	235.1	0.017	17.1
	5	206.0	0.017	13.7		5	130.8	0.016	10.8		10	215.3	0.016	16.0
	6	128.8	0.011	12.3										
	7	196.4	0.017	13.8										
	8	104.9	0.009	11.5										
	9	178.3	0.016	12.8										
	10	129.7	0.012	12.0										
Average		**158.8**	**0.014**	**12.7**	**Average**		**133.5**	**0.013**	**11.4**	**Average**		**237.1**	**0.017**	**16.5**
St. Deviation		**39.6**	**0.003**	**1.0**	**St. Deviation**		**6.5**	**0.002**	**1.1**	**St. Deviation**		**17.9**	**0.001**	**0.8**
23C Centered	1	126.3	0.015	10.6	90C Centered	1	76.7	0.013	6.7	-35 Centered	6	183.6	0.018	15.5
	2	132.2	0.016	10.1		2	92.8	0.015	7.1		7	179.6	0.018	14.1
	3	152.5	0.018	10.8		3	96.9	0.016	6.6		8	168.6	0.017	14.0
	4	166.5	0.020	11.8		4	91.7	0.012	8.5		9	199.4	0.019	15.5
	5	158.5	0.017	11.5		5	91.0	0.013	7.7		10	193.1	0.024	13.3
	6	159.1	0.018	11.0										
Average		**149.2**	**0.018**	**11.0**	**Average**		**89.8**	**0.014**	**7.3**	**Average**		**184.8**	**0.019**	**14.4**
St. Deviation		**14.8**	**0.001**	**0.6**	**St. Deviation**		**6.9**	**0.001**	**0.7**	**St. Deviation**		**10.7**	**0.002**	**0.9**
23C Transverse	1	80.6	0.013	7.4						-35 Transverse	6	81.1	0.014	10.0
	2	86.6	0.016	7.2							7	89.0	0.010	12.3
	3	97.9	0.018	7.8							8	94.8	0.015	10.0
	4	89.2	0.015	7.6							9	110.5	0.016	10.4
	5	93.0	0.014	8.8							10	124.1	0.015	11.2
Average		**89.4**	**0.015**	**7.7**						**Average**		**99.9**	**0.014**	**10.8**
St. Deviation		**5.8**	**0.001**	**0.6**						**St. Deviation**		**15.5**	**0.002**	**0.9**

1D:

Once tows started to break, the extensometer data became useless as it bounced around

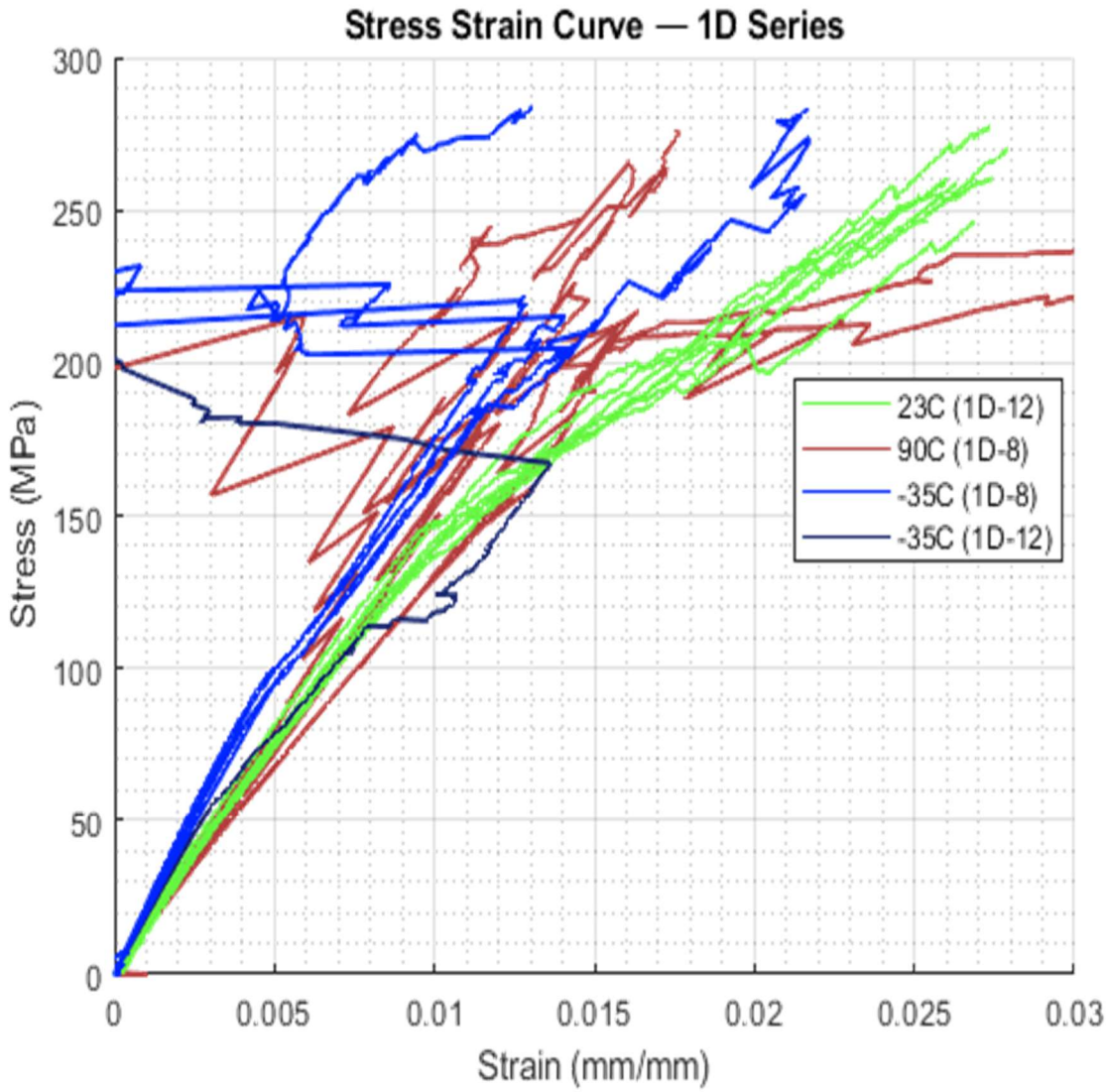

	Sample	Ultimate Stress (MPa)	Max Strain	Tensile Modulus (GPa)		Sample	Ultimate Stress (MPa)	Max Strain	Tensile Modulus (GPa)		Sample	Ultimate Stress (MPa)	Max Strain	Tensile Modulus (GPa)
23C (1D-12)	1	258.9	0.026	16.1	90C (1D-8)	1	245.1	0.036	20.3	-35C (1D-8)	6	283.2	0.022	21.39
23C (1D-12)	2	260.5	0.027	15.0	90C (1D-8)	2	231.7	0.044	13.5	-35C (1D-8)	7	284.1	0.013	20.74
23C (1D-12)	3	270.1	0.028	16.1	90C (1D-8)	3	249.1	-0.008	16.0	-35C (1D-8)	8	285.1	-0.003	21.08
23C (1D-12)	4	277.3	0.027	16.4	90C (1D-8)	4	246.9	0.015	14.4	-35C (1D-8)	9	284.6	-0.019	19.23
23C (1D-12)	5	260.5	0.026	15.3	90C (1D-8)	5	276.8	0.018	15.7	-35C (1D-12)	8	272.5	-0.026	17.79
23C (1D-12)	6	246.3	0.027	15.3										
23C (1D-12)	7	259.4	0.026	15.0										
Average		**261.8**	**0.027**	**15.6**	**Average**		**249.9**	**0.021**	**16.0**	**Average**		**281.9**	-0.003	**20.05**
St. Deviation		**9.0**	**0.001**	**0.5**	**St. Deviation**		**14.8**	**0.018**	**2.3**	**St. Deviation**		**4.8**	**0.018**	**1.35**

2A:

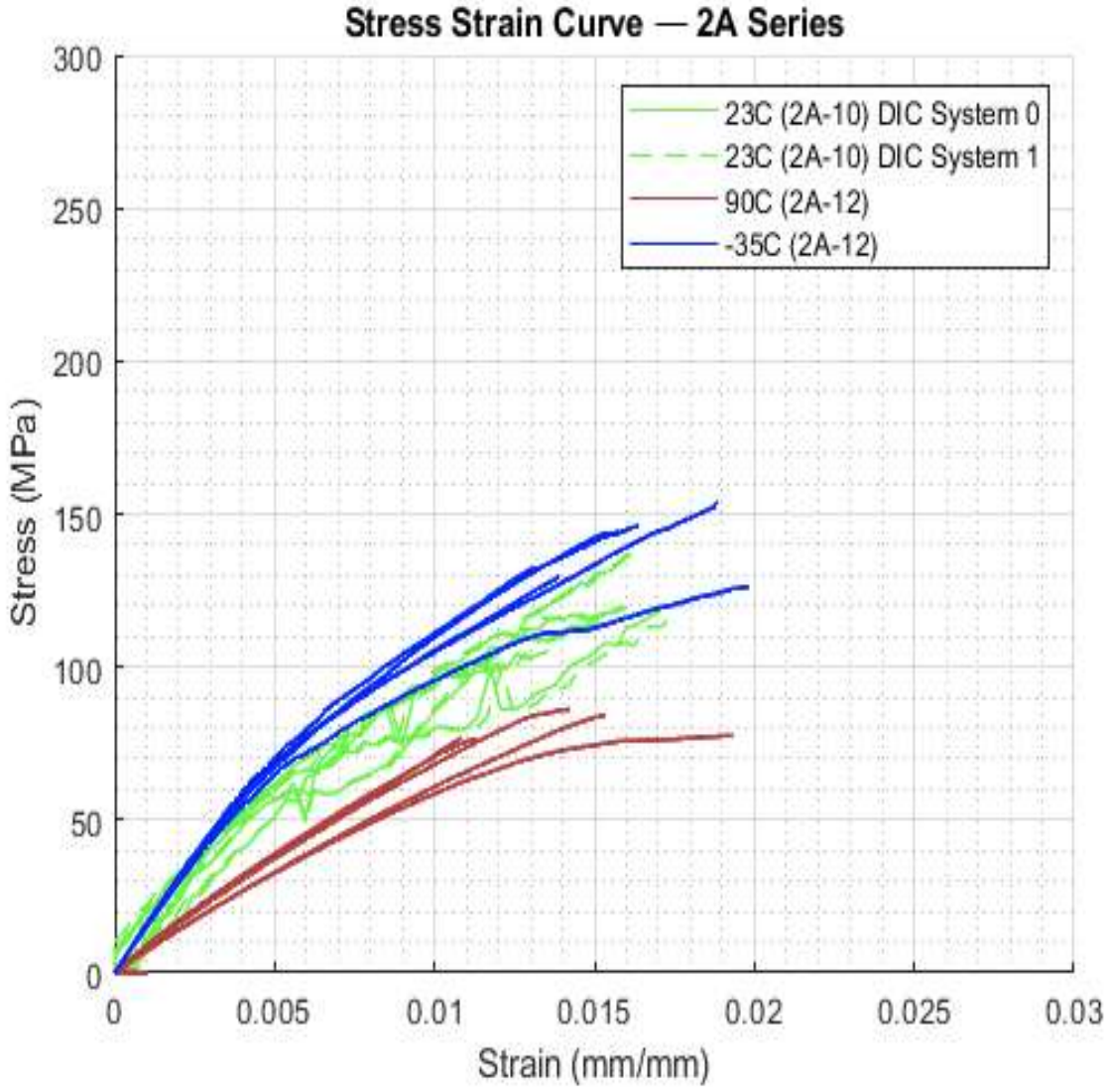

	Sample	Ultimate Stress (MPa)	Max Strain	Tensile Modulus (GPa)		Sample	Ultimate Stress (MPa)	Max Strain	Tensile Modulus (GPa)		Sample	Ultimate Stress (MPa)	Max Strain	Tensile Modulus (GPa)
23C (2A-10) DIC System 0	1	118.6	0.017	13.5	90C (2A-12)	1	76.5	0.011	7.9	-35C (2A-12)	6	129.6	0.014	14.7
23C (2A-10) DIC System 1	1	118.6	0.018	12.6	90C (2A-12)	2	76.8	0.011	9.9	-35C (2A-12)	7	126.2	0.020	13.9
23C (2A-10) DIC System 0	2	117.3	0.015	11.5	90C (2A-12)	3	77.4	0.019	6.6	-35C (2A-12)	8	144.2	0.016	15.0
23C (2A-10) DIC System 1	2	117.3	0.015	11.0	90C (2A-12)	4	84.1	0.015	6.6	-35C (2A-12)	9	146.0	0.016	14.3
23C (2A-10) DIC System 0	3	105.2	0.014	11.6	90C (2A-12)	5	86.2	0.014	7.5	-35C (2A-12)	10	153.8	0.019	14.8
23C (2A-10) DIC System 1	3	105.2	0.013	10.9										
23C (2A-10) DIC System 0	4	119.7	0.016	11.8										
23C (2A-10) DIC System 1	4	119.7	0.016	10.6										
23C (2A-10) DIC System 0	5	137.1	0.016	11.0										
23C (2A-10) DIC System 1	5	137.1	0.016	11.5										
Average		**119.6**	**0.016**	**11.6**	**Average**		**80.2**	**0.014**	**7.7**	**Average**		**140.0**	**0.017**	**14.5**
St. Deviation		**10.2**	**0.001**	**0.8**	**St. Deviation**		**4.1**	**0.003**	**1.2**	**St. Deviation**		**10.4**	**0.002**	**0.4**

2B:

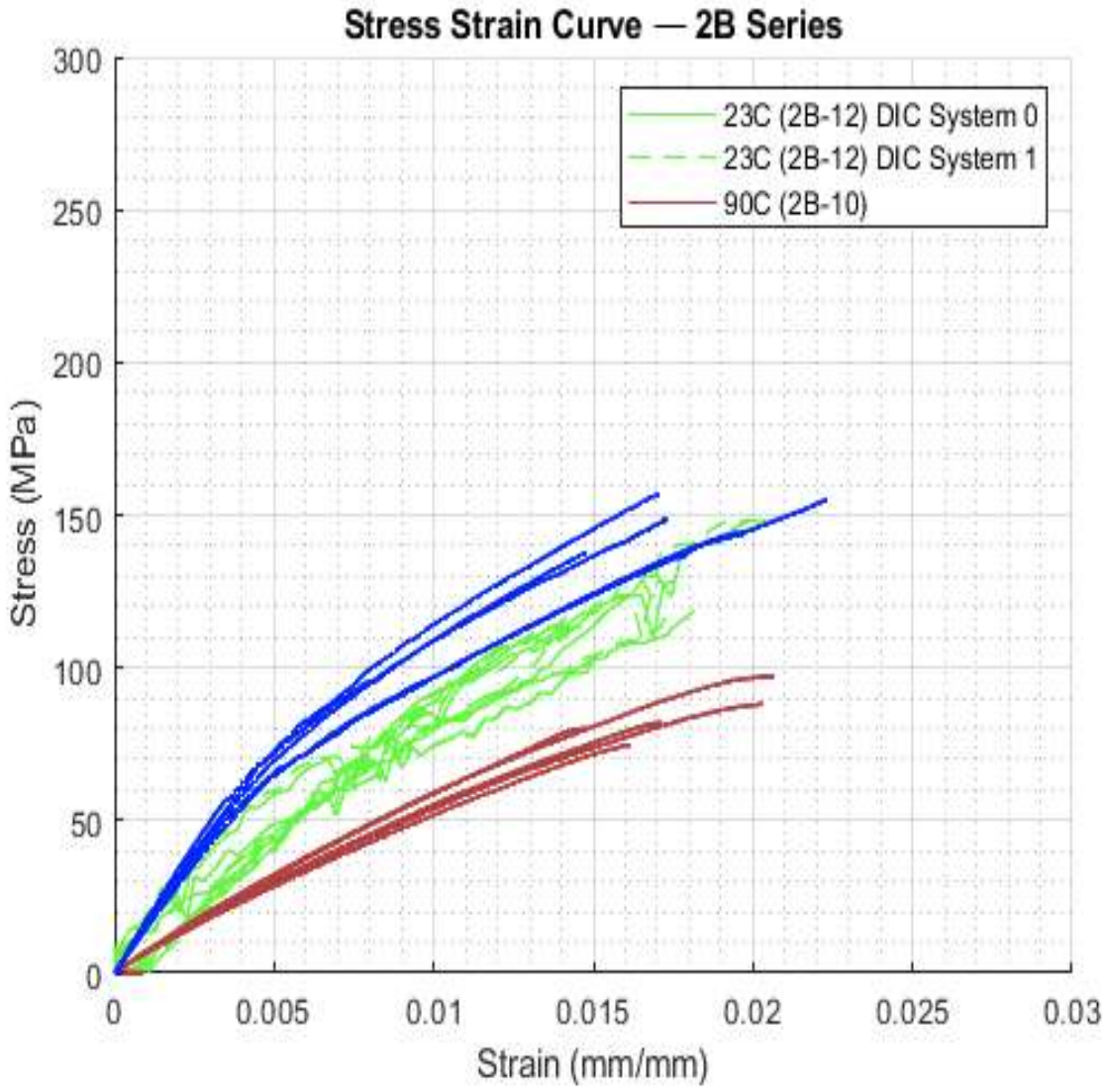

	Sample	Ultimate Stress (MPa)	Max Strain	Tensile Modulus (GPa)		Sample	Ultimate Stress (MPa)	Max Strain	Tensile Modulus (GPa)		Sample	Ultimate Stress (MPa)	Max Strain	Tensile Modulus (GPa)
23C (2B-12) DIC System 0	1	112.6	0.014	9.9	90C (2B-10)	1	74.7	0.016	5.7	35C (2B-10)	6	144.1	0.020	13.7
23C (2B-12) DIC System 1	1	112.6	0.014	8.9	90C (2B-10)	2	88.2	0.020	6.0	35C (2B-10)	7	137.8	0.015	14.7
23C (2B-12) DIC System 0	2	148.3	0.020	11.9	90C (2B-10)	3	97.1	0.021	6.4	35C (2B-10)	8	148.6	0.017	16.1
23C (2B-12) DIC System 1	2	148.3	0.020	12.1	90C (2B-10)	4	82.1	0.017	6.1	35C (2B-10)	9	156.5	0.017	15.1
23C (2B-12) DIC System 0	3	118.9	0.015	11.6	90C (2B-10)	5	80.1	0.015	6.5	35C (2B-10)	10	155.3	0.022	14.4
23C (2B-12) DIC System 1	3	118.9	0.015	10.7										
23C (2B-12) DIC System 0	4	128.5	0.018	7.0										
23C (2B-12) DIC System 1	4	128.5	0.017	7.5										
23C (2B-12) DIC System 0	5	118.7	0.018	11.0										
23C (2B-12) DIC System 1	5	118.7	0.017	10.8										
23C (2B-12) DIC System 0	6	103.3	0.015	6.7										
23C (2B-12) DIC System 1	6	103.3	0.015	7.2										
Average		**121.7**	**0.017**	**9.6**	**Average**		**84.5**	**0.018**	**6.1**	**Average**		**148.4**	**0.018**	**14.8**
St. Deviation		**14.1**	**0.002**	**2.0**	**St. Deviation**		**7.7**	**0.002**	**0.3**	**St. Deviation**		**7.0**	**0.003**	**0.8**

2C:

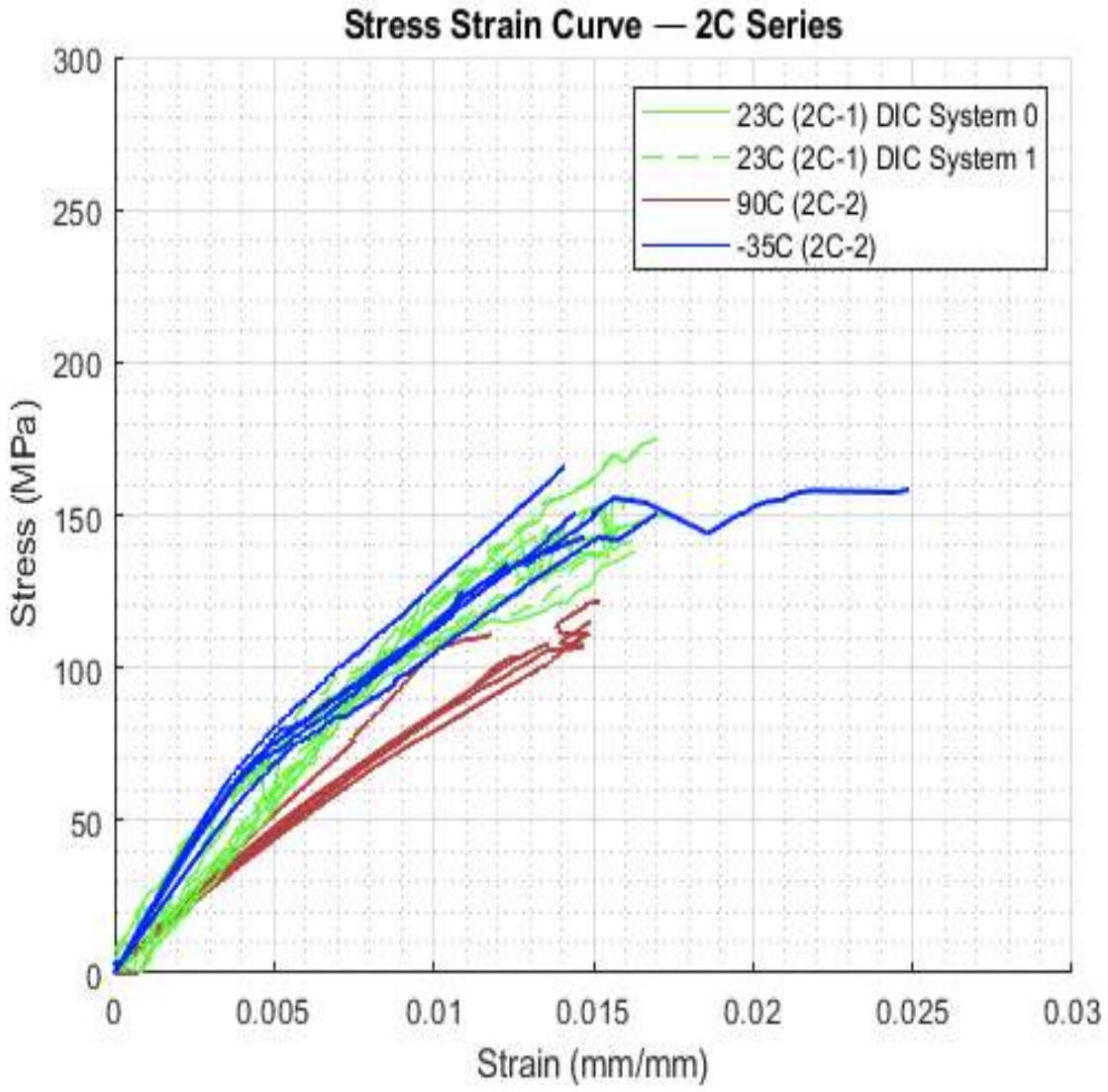

	Sample	Ultimate Stress (MPa)	Max Strain	Tensile Modulus (GPa)		Sample	Ultimate Stress (MPa)	Max Strain	Tensile Modulus (GPa)		Sample	Ultimate Stress (MPa)	Max Strain	Tensile Modulus (GPa)
23C (2C-1) DIC System 0	2	155.4	0.016	9.3	90C (2C-2)	1	103.6	0.013	9.7	-35C (2C-2)	6	150.4	0.017	14.5
23C (2C-1) DIC System 1	2	156.5	0.016	7.6	90C (2C-2)	2	107.6	0.014	9.5	-35C (2C-2)	7	150.7	0.014	16.6
23C (2C-1) DIC System 0	3	149.8	0.017	10.0	90C (2C-2)	3	121.6	0.015	8.8	-35C (2C-2)	8	142.9	0.015	16.5
23C (2C-1) DIC System 1	3	149.8	0.018	10.1	90C (2C-2)	4	115.1	0.015	9.1	-35C (2C-2)	9	158.4	0.025	16.5
23C (2C-1) DIC System 0	4	138.2	0.016	18.9	90C (2C-2)	5	110.8	0.012	10.5	-35C (2C-2)	10	166.2	0.014	17.5
23C (2C-1) DIC System 1	4	138.2	0.015	18.6										
23C (2C-1) DIC System 0	5	175.0	0.017	15.0										
23C (2C-1) DIC System 1	5	175.0	0.017	15.1										
23C (2C-1) DIC System 0	6	143.4	0.016	12.7										
23C (2C-1) DIC System 1	6	143.4	0.017	13.3										
Average		**152.5**	**0.017**	**13.0**	**Average**		**111.7**	**0.014**	**9.5**	**Average**		**153.7**	**0.017**	**16.3**
St. Deviation		**12.7**	**0.001**	**3.7**	**St. Deviation**		**6.2**	**0.001**	**0.6**	**St. Deviation**		**7.9**	**0.004**	**1.0**

3A:

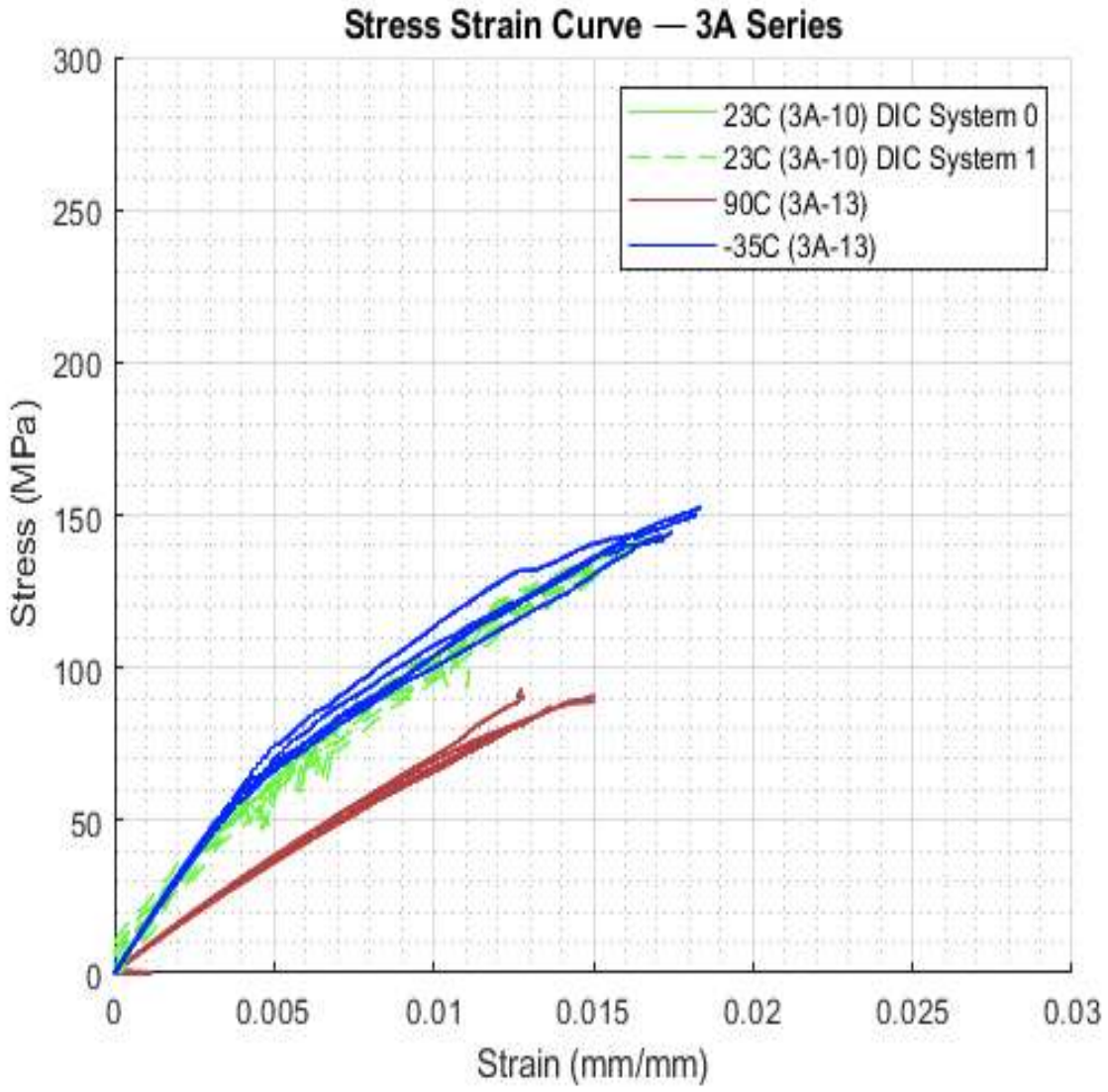

	Sample	Ultimate Stress (MPa)	Max Strain	Tensile Modulus (GPa)		Sample	Ultimate Stress (MPa)	Max Strain	Tensile Modulus (GPa)		Sample	Ultimate Stress (MPa)	Max Strain	Tensile Modulus (GPa)
23C (3A-10) DIC System 0	1	146.2	0.017	11.3	90C (3A-13)	1	78.9	0.012	11.5	-35 (3A-13)	6	144.7	0.018	14.7
23C (3A-10) DIC System 1	1	146.2	0.017	11.5	90C (3A-13)	2	92.6	0.013	7.7	-35 (3A-13)	7	152.8	0.018	14.5
23C (3A-10) DIC System 0	2	148.0	0.017	12.8	90C (3A-13)	3	87.2	0.014	7.3	-35 (3A-13)	8	139.5	0.016	15.1
23C (3A-10) DIC System 1	2	148.0	0.017	12.3	90C (3A-13)	4	89.0	0.015	7.8	-35 (3A-13)	9	150.1	0.018	15.4
23C (3A-10) DIC System 0	3	129.5	0.014	11.2	90C (3A-13)	5	90.8	0.015	7.3	-35 (3A-13)	10	142.0	0.017	15.0
23C (3A-10) DIC System 1	3	130.1	0.015	11.1										
23C (3A-10) DIC System 0	4	130.9	0.015	14.9										
23C (3A-10) DIC System 1	4	130.9	0.015	13.9										
23C (3A-10) DIC System 0	5	141.6	0.017	12.4										
23C (3A-10) DIC System 1	5	141.6	0.017	13.1										
Average		**139.3**	**0.016**	**12.4**	**Average**		**87.7**	**0.014**	**8.3**	**Average**		**145.8**	**0.017**	**15.0**
St. Deviation		**7.6**	**0.001**	**1.2**	**St. Deviation**		**4.8**	**0.001**	**1.6**	**St. Deviation**		**5.0**	**0.001**	**0.3**

3B:

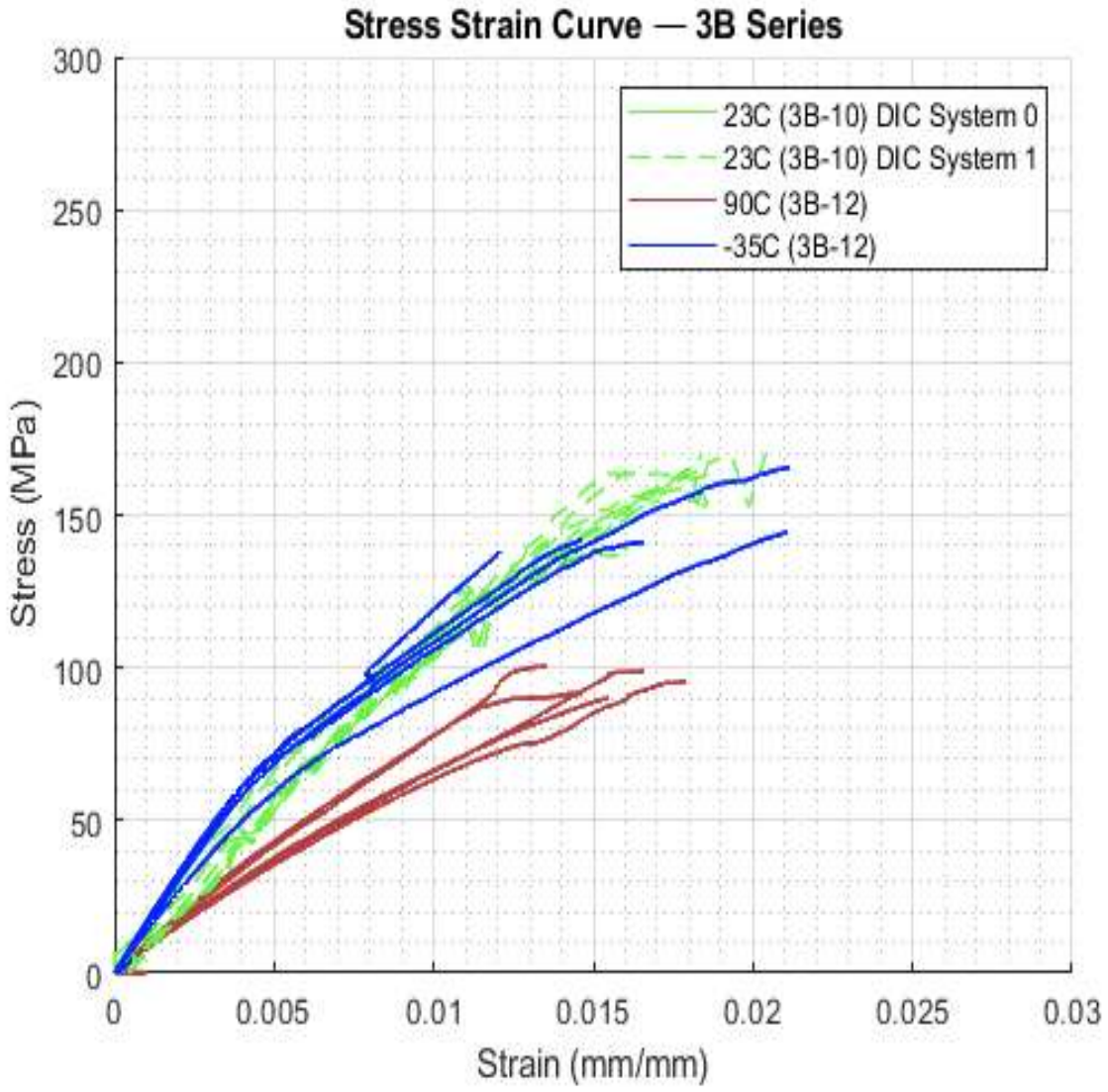

	Sample	Ultimate Stress (MPa)	Max Strain	Tensile Modulus (GPa)		Sample	Ultimate Stress (MPa)	Max Strain	Tensile Modulus (GPa)		Sample	Ultimate Stress (MPa)	Max Strain	Tensile Modulus (GPa)
23C (3B-10) DIC System 0	1	165.6	0.016	12.9	90C (3B-12)	1	100.5	0.014	8.5	-35C (3B-12)	6	144.7	0.021	12.5
23C (3B-10) DIC System 1	1	165.6	0.018	12.7	90C (3B-12)	2	92.3	0.014	8.9	-35C (3B-12)	7	141.2	0.017	15.1
23C (3B-10) DIC System 0	2	140.3	0.016	10.1	90C (3B-12)	3	95.6	0.018	7.2	-35C (3B-12)	8	165.6	0.021	14.8
23C (3B-10) DIC System 1	2	140.3	0.016	10.9	90C (3B-12)	4	99.0	0.017	7.5	-35C (3B-12)	9	138.4	0.012	15.4
23C (3B-10) DIC System 0	3	163.1	0.018	12.7	90C (3B-12)	5	89.9	0.015	7.7	-35C (3B-12)	10	142.0	0.015	15.5
23C (3B-10) DIC System 1	3	163.1	0.019	13.2										
23C (3B-10) DIC System 0	4	170.5	0.020	9.8										
23C (3B-10) DIC System 1	4	170.5	0.018	9.5										
23C (3B-10) DIC System 0	5	154.9	0.017	11.5										
23C (3B-10) DIC System 1	5	154.9	0.017	12.1										
Average		**158.9**	**0.018**	**11.5**	**Average**		**95.4**	**0.016**	**7.9**	**Average**		**146.4**	**0.017**	**14.7**
St. Deviation		**10.6**	**0.001**	**1.3**	**St. Deviation**		**4.0**	**0.002**	**0.6**	**St. Deviation**		**9.8**	**0.004**	**1.1**

11.8. Flexure (4-point Bending) Test Results

1A Flexure Results:

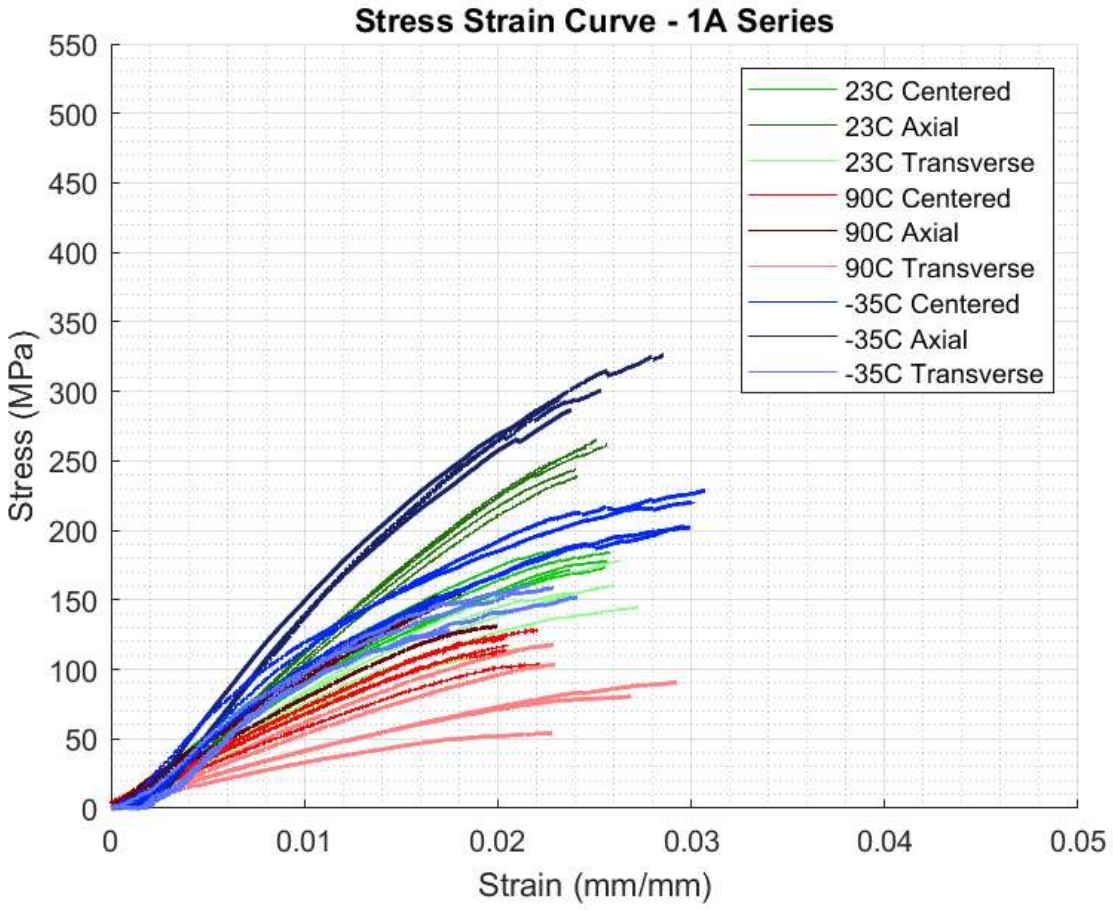

	Sample	Flexural Strength (Mpa)	Flexural Modulus (Gpa)	Thickness (mm)		Sample	Flexural Strength (Mpa)	Flexural Modulus (Gpa)	Thickness (mm)		Sample	Flexural Strength (Mpa)	Flexural Modulus (Gpa)	Thickness (mm)
23C Axial (1A-S3)	1	239.6	12.4	2.56	90C Axial (1A-S3)	6	154.9	9.8	2.76	-35C Axial (1A-S3)	12	311.1	18.37	2.849
23C Axial (1A-S3)	2	244.2	12.7	2.62	90C Axial (1A-S3)	7	152.7	10.1	2.79	-35C Axial (1A-S3)	13	286.7	17.28	2.877
23C Axial (1A-S3)	3	259.9	13.4	2.64	90C Axial (1A-S3)	8	148.0	9.4	2.85	-35C Axial (1A-S3)	14	326.8	16.94	2.928
23C Axial (1A-S3)	4	265.4	13.4	2.70	90C Axial (1A-S3)	9	131.4	8.0	2.74	-35C Axial (1A-S3)	15	300.5	17.53	2.948
23C Axial (1A-S3)	5	261.9	13.7	2.72	90C Axial (1A-S3)	10	142.1	9.5	2.76	-35C Axial (1A-S3)	16	297.3	17.99	2.992
Average		254.2	13.1	2.65	Average		145.8	9.4	2.78	Average		304.5	17.6	2.92
St. Deviation		10.3	0.5	0.06	St. Deviation		8.4	0.7	0.04	St. Deviation		13.6	0.5	0.05
23C Centered (1A-14)	1	186.7	11.3	3.18	90C Centered (1A-14)	6	113.9	7.1	3.01	-35C Centered (1A-14)	11	188.4	13.38	3.087
23C Centered (1A-14)	2	184.8	11.1	3.17	90C Centered (1A-14)	7	122.4	7.3	2.96	-35C Centered (1A-14)	12	202.8	13.21	3.06
23C Centered (1A-14)	3	173.8	11.3	3.14	90C Centered (1A-14)	8	104.1	5.7	2.95	-35C Centered (1A-14)	13	202.5	12.94	3.003
23C Centered (1A-14)	4	178.3	11.6	3.09	90C Centered (1A-14)	9	117.9	6.2	3.15	-35C Centered (1A-14)	14	220.5	14.11	2.953
23C Centered (1A-14)	5	171.5	11.2	3.05	90C Centered (1A-14)	10	128.5	7.1	3.11	-35C Centered (1A-14)	15	228.5	14.77	2.94
Average		179.0	11.3	3.13	Average		117.4	6.7	3.04	Average		208.5	13.7	3.01
St. Deviation		6.0	0.2	0.05	St. Deviation		8.2	0.6	0.08	St. Deviation		14.3	0.7	0.06
23C Transverse (1A-S5)	1	161.1	10.0	2.77	90C Transverse (1A-S5)	6	54.4	3.2	2.96	-35C Transverse (1A-S5)	11	211.5	14.08	2.686
23C Transverse (1A-S5)	2	179.2	10.5	2.80	90C Transverse (1A-S5)	7	91.1	4.0	3.01	-35C Transverse (1A-S5)	12	161	11.89	2.72
23C Transverse (1A-S5)	3	155.5	10.3	2.84	90C Transverse (1A-S5)	8	80.8	4.0	3.06	-35C Transverse (1A-S5)	13	153.5	11.39	2.781
23C Transverse (1A-S5)	4	145.2	9.7	2.88	90C Transverse (1A-S5)	9	118.6	6.7	2.59	-35C Transverse (1A-S5)	14	128.2	11.93	2.803
23C Transverse (1A-S5)	5	117.6	8.9	2.92	90C Transverse (1A-S5)	10	104.8	5.5	2.63	-35C Transverse (1A-S5)	15	158.9	12.78	2.85
Average		151.7	9.9	2.84	Average		89.9	4.7	2.85	Average		162.6	12.4	2.77
St. Deviation		20.3	0.6	0.06	St. Deviation		21.9	1.2	0.20	St. Deviation		27.1	0.9	0.06

1A Failure Modes:

First Character

Failure Mode	Code
Tension	T
Compression	C
Buckling	B
interlaminar Shear	S
Multi-mode	M(xyz)
Other	O

Second Character

Failure Area	Code
At loading nose	A
Between loading noses	B
at Support nose	S
between Load and support nose	L
Unknown	U

Third Character

Failure Location	Code
Top	T
Bottom	B
Left	L
Right	R
Middle	M
Various	V
Unknown	U

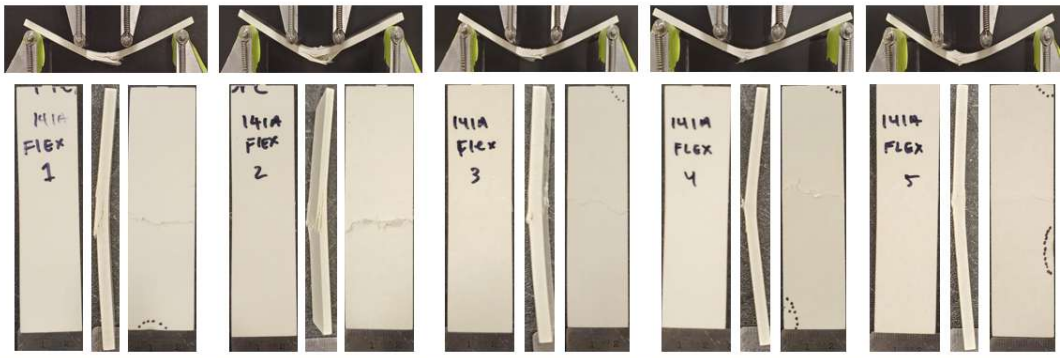

1A Centered	1	2	3	4	5
Failure Mode	TBB	MBV	TBB	TBB	MBV

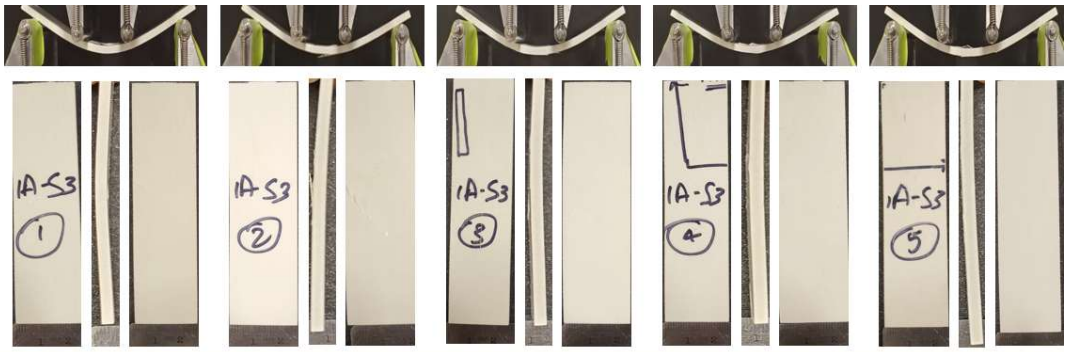

1A Axial	1	2	3	4	5
Failure Mode	CBT	MBV	CBT	CBT	CBT

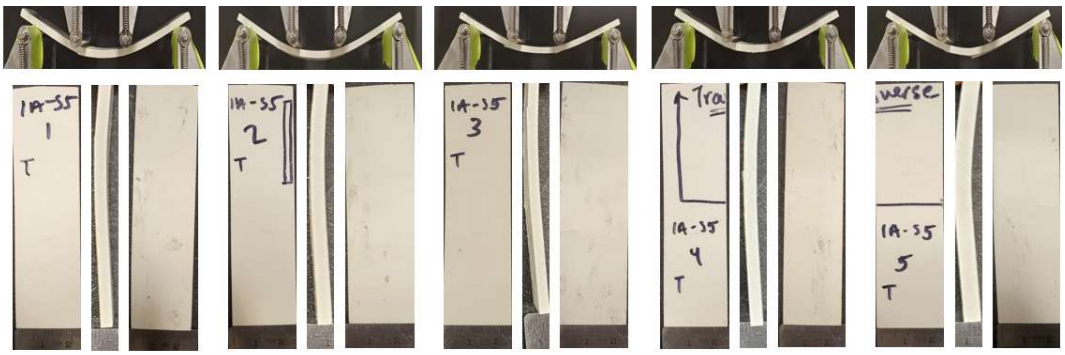

1A Axial	1	2	3	4	5
Failure Mode	TAB	SBB	TAB	TAB	MAB

1B Flexure Test Data:

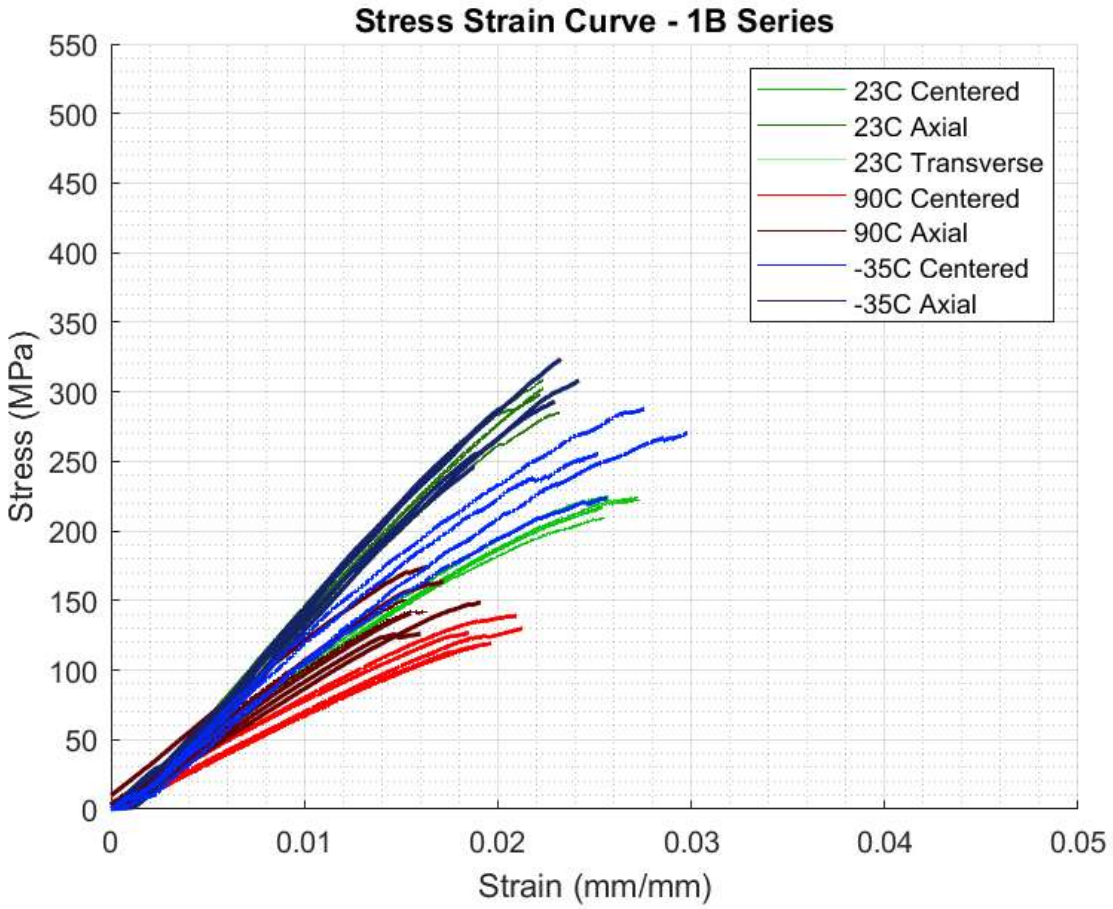

	Sample	Flexural Strength (Mpa)	Flexural Modulus (Gpa)	Thickness (mm)		Sample	Flexural Strength (Mpa)	Flexural Modulus (Gpa)	Thickness (mm)		Sample	Flexural Strength (Mpa)	Flexural Modulus (Gpa)	Thickness (mm)
23C Axial	1	297.2	15.9	3.43	90C Axial	6	174.4	11.3	3.27	Low Temp Axial	11	247.8	13.74	3.268
23C Axial	2	308.9	16.2	3.42	90C Axial	7	163.9	11.0	3.24	Low Temp Axial	12	246.3	13.98	3.227
23C Axial	3	302.7	15.5	3.41	90C Axial	8	148.8	9.2	3.19	Low Temp Axial	13	295.6	14.05	3.188
23C Axial	4	284.9	15.0	3.35	90C Axial	9	140.6	9.7	3.36	Low Temp Axial	14	308.1	13.64	3.153
23C Axial	5	298.2	15.8	3.32	90C Axial	10	126.3	9.5	3.29	Low Temp Axial	15	288	14.53	3.103
					90C Axial	15	142.4	9.6	3.38	Low Temp Axial	16	323.7	14.56	3.073
					90C Axial	16	150.7	10.4	3.42					
Average		**298.4**	**15.7**	**3.38**	**Average**		**149.6**	**10.1**	**3.31**	**Average**		**284.9**	**14.1**	**3.2**
St. Deviation		**7.9**	**0.4**	**0.04**	**St. Deviation**		**14.6**	**0.7**	**0.08**	**St. Deviation**		**28.9**	**0.4**	**0.1**
23C Centered	2	209.9	10.5	2.85	90C Centered	7	126.8	7.4	3.06	Low Temp Centered	12	230.3	12.21	2.972
23C Centered	3	227.1	10.9	2.94	90C Centered	8	139.3	7.9	3.11	Low Temp Centered	13	225.1	11.47	3.104
23C Centered	4	225.3	10.8	2.95	90C Centered	9	129.9	7.2	2.84	Low Temp Centered	14	270.5	12.36	3.057
23C Centered	5	216.7	10.7	2.99	90C Centered	10	119.2	7.0	2.91	Low Temp Centered	15	255.9	13.17	3.086
23C Centered	6	225.0	11.2	3.03	90C Centered	11	116.8	7.1	2.92	Low Temp Centered	16	287.9	13.95	3.12
Average		**220.8**	**10.8**	**2.95**	**Average**		**126.4**	**7.3**	**2.97**	**Average**		**253.9**	**12.6**	**3.07**
St. Deviation		**6.5**	**0.2**	**0.06**	**St. Deviation**		**8.0**	**0.3**	**0.10**	**St. Deviation**		**23.8**	**0.9**	**0.05**

1B Failure Modes:

First Character

Failure Mode	Code
Tension	T
Compression	C
Buckling	B
interlaminar Shear	S
Multi-mode	M(xyz)
Other	O

Second Character

Failure Area	Code
At loading nose	A
Between loading noses	B
at Support nose	S
between Load and support nose	L
Unknown	U

Third Character

Failure Location	Code
Top	T
Bottom	B
Left	L
Right	R
Middle	M
Various	V
Unknown	U

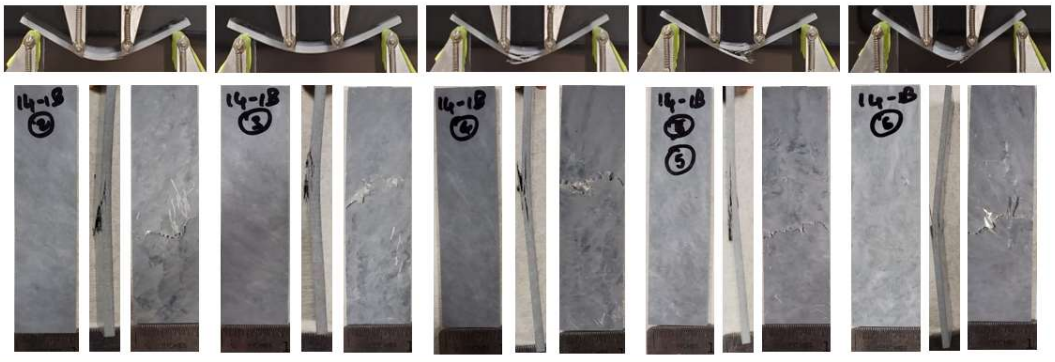

1B Centered	2	3	4	5	6
Failure Mode	TAB	TAB	MBB	MBV	MBV

1B Axial	1	2	3	4	5
Failure Mode	MUV	MUV	MUV	TBB	TBB

1C Flexure Test Data:

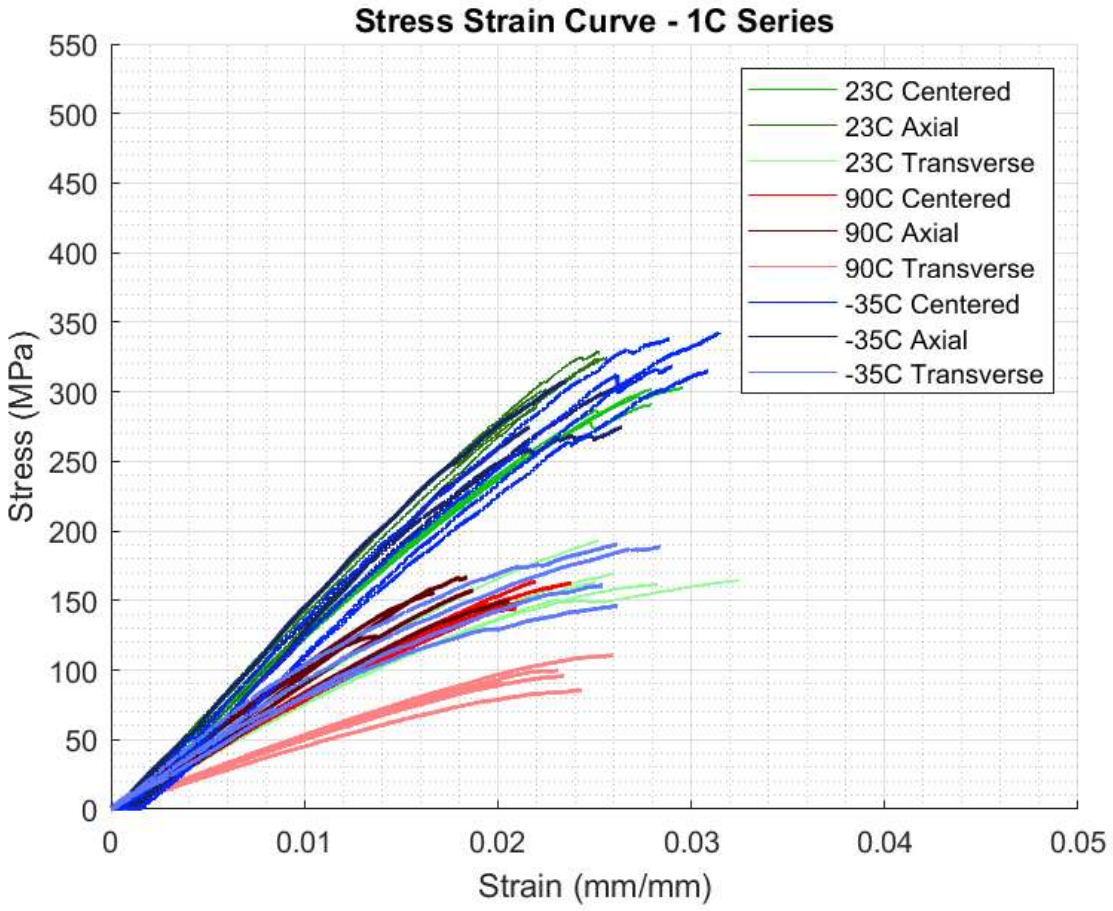

	Sample	Flexural Strength (Mpa)	Flexural Modulus (Gpa)	Thickness (mm)		Sample	Flexural Strength (Mpa)	Flexural Modulus (Gpa)	Thickness (mm)		Sample	Flexural Strength (Mpa)	Flexural Modulus (Gpa)	Thickness (mm)
23C Axial	1	289.4	14.4	3.31	90C Axial	6	166.9	10.4	3.14	Low Temp Axial	12	274.076	13.8	3.315
23C Axial	2	303.8	14.9	3.29	90C Axial	7	157.3	9.7	3.10	Low Temp Axial	13	274.634	13.1	3.294
23C Axial	3	324.1	14.9	3.26	90C Axial	8	149.7	9.1	3.07	Low Temp Axial	14	310.261	12.9	3.260
23C Axial	4	324.8	14.3	3.22	90C Axial	9	124.3	10.1	3.17	Low Temp Axial	15	274.438	13.6	3.210
23C Axial	5	329.2	14.9	3.17	90C Axial	10	155.8	10.4	3.13	Low Temp Axial	16	307.425	14.2	3.161
Average		**314.3**	**14.7**	**3.25**	**Average**		**150.8**	**9.9**	**3.12**	**Average**		**288.2**	**13.5**	**3.248**
St. Deviation		**15.2**	**0.3**	**0.05**	**St. Deviation**		**14.4**	**0.5**	**0.04**	**St. Deviation**		**16.9**	**0.5**	**0.056**
23C Centered	1	287.6	13.0	3.23	90C Centered	6	163.7	8.5	3.12	Low Temp Centered	12	325.3	13.1	3.101
23C Centered	2	277.0	12.9	3.24	90C Centered	7	144.6	8.1	3.09	Low Temp Centered	13	342.9	12.3	3.071
23C Centered	3	303.1	13.0	3.21	90C Centered	8	162.7	8.2	3.08	Low Temp Centered	14	315.1	11.8	3.042
23C Centered	4	291.0	13.0	3.16	90C Centered	9	149.4	7.8	3.04	Low Temp Centered	15	338.4	13.9	3.025
23C Centered	5	302.4	12.8	3.15	90C Centered	10	147.6	8.1	3.05	Low Temp Centered	16	319.1	12.6	2.996
					90C Centered	11	145.7	8.3	3.13					
Average		**292.2**	**13.0**	**3.20**	**Average**		**152.3**	**8.2**	**3.09**	**Average**		**328.2**	**12.7**	**3.047**
St. Deviation		**9.8**	**0.1**	**0.04**	**St. Deviation**		**7.8**	**0.2**	**0.03**	**St. Deviation**		**10.8**	**0.7**	**0.036**
23C Transverse	1	193.4	9.4	3.27	90C Transverse	6	96.2	5.0	3.08	Low Temp Transverse	12	172.9	10.1	3.315
23C Transverse	2	169.2	8.2	3.21	90C Transverse	7	85.8	4.5	3.05	Low Temp Transverse	13	146.5	8.3	3.294
23C Transverse	3	165.2	8.0	3.20	90C Transverse	8	90.7	5.1	3.02	Low Temp Transverse	14	188.8	9.9	3.260
23C Transverse	4	164.6	8.1	3.17	90C Transverse	9	110.6	5.2	3.43	Low Temp Transverse	15	160.8	8.7	3.210
23C Transverse	5	161.9	7.8	3.13	90C Transverse	10	99.8	5.1	3.38	Low Temp Transverse	16	190.5	10.9	3.161
Average		**170.9**	**8.3**	**3.20**	**Average**		**96.6**	**5.0**	**3.19**	**Average**		**171.9**	**9.6**	**3.248**
St. Deviation		**11.5**	**0.6**	**0.05**	**St. Deviation**		**8.5**	**0.2**	**0.18**	**St. Deviation**		**16.7**	**1.0**	**0.056**

1C Failure Modes:

First Character

Failure Mode	Code
Tension	T
Compression	C
Buckling	B
interlaminar Shear	S
Multi-mode	M(xyz)
Other	O

Second Character

Failure Area	Code
At loading nose	A
Between loading noses	B
at Support nose	S
between Load and support nose	L
Unknown	U

Third Character

Failure Location	Code
Top	T
Bottom	B
Left	L
Right	R
Middle	M
Various	V
Unknown	U

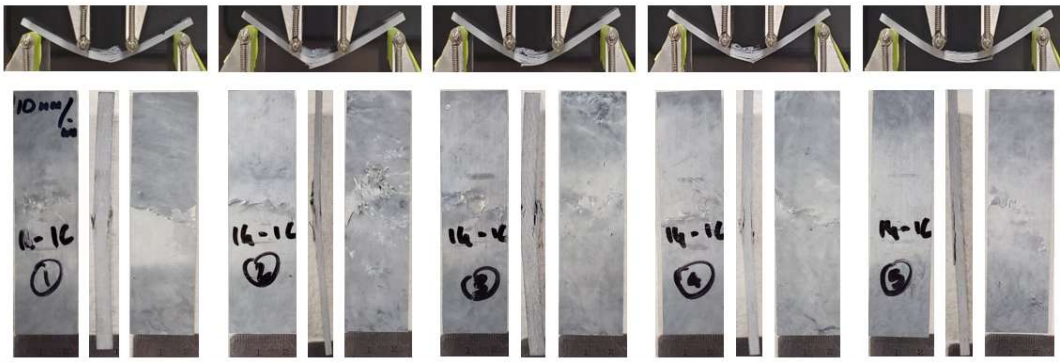

1C Centered	1	2	3	4	5
Failure Mode	MBV	MBV	MBV	MBV	MUV

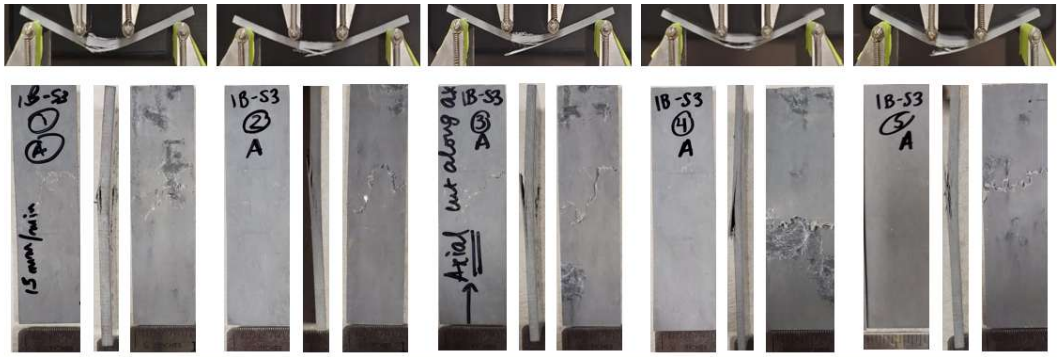

1C Axial	1	2	3	4	5
Failure Mode	MBV	MBB	MBV	TBB	TBB

1C Transverse	1	2	3	4	5
Failure Mode	MUV	TBB	MBV	MUV	MBV

1D:

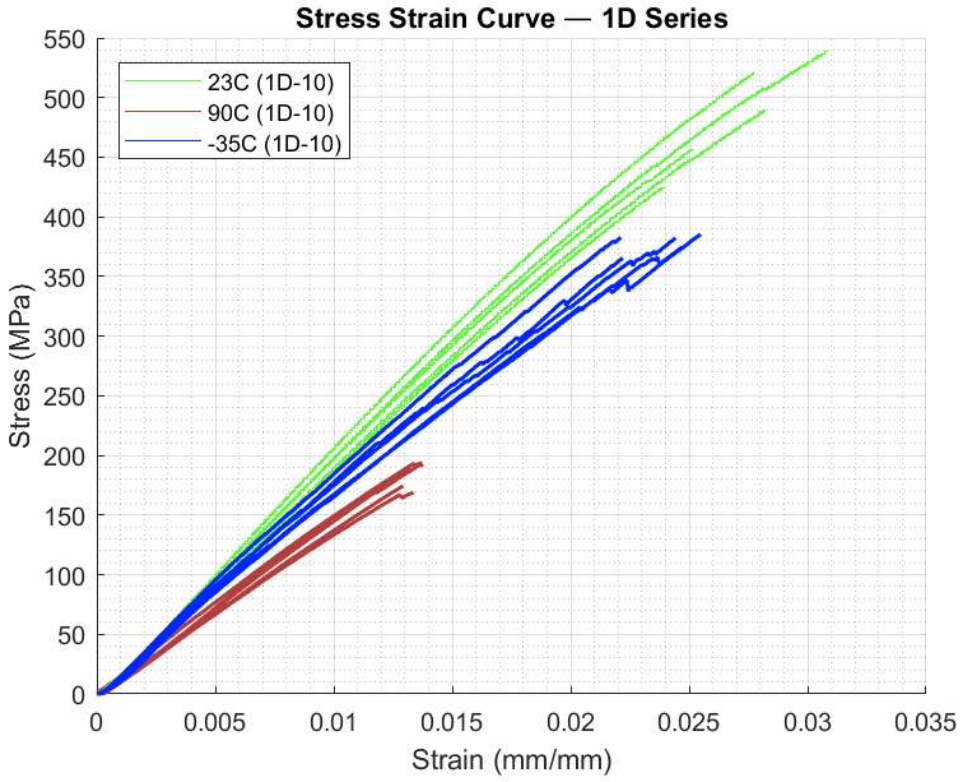

	Sample	Flexural Strength (MPa)	Flexural Modulus (GPa)	Thickness (mm)		Sample	Flexural Strength (MPa)	Flexural Modulus (GPa)	Thickness (mm)		Sample	Flexural Strength (MPa)	Flexural Modulus (GPa)	Thickness (mm)
23C (1D-10)	1	520.3	21.4	2.90	90C (1D-10)	6	174.5	14.4	3.00	-35C (1D-10)	12	382.7	19.5	3.067
23C (1D-10)	2	457.2	20.3	2.94	90C (1D-10)	7	192.2	15.7	2.98	-35C (1D-10)	13	382.5	18.4	3.100
23C (1D-10)	3	489.5	19.7	2.93	90C (1D-10)	8	188.3	15.2	3.01	-35C (1D-10)	14	374.6	18.0	3.154
23C (1D-10)	4	539.5	20.6	2.94	90C (1D-10)	9	193.6	15.0	2.99	-35C (1D-10)	15	365.8	19.3	3.094
23C (1D-10)	5	425.4	19.5	2.97	90C (1D-10)	10	169.0	13.8	3.07	-35C (1D-10)	16	385.5	17.3	3.182
Average		**486.4**	**20.3**	**2.94**	**Average**		**183.5**	**14.8**	**3.01**	**Average**		**378.2**	**18.5**	**3.12**
St. Deviation		**41.4**	**0.6**	**0.02**	**St. Deviation**		**9.9**	**0.7**	**0.03**	**St. Deviation**		**7.2**	**0.8**	**0.04**

First Character

Failure Mode	Code
Tension	T
Compression	C
Buckling	B
interlaminar Shear	S
Multi-mode	M(xyz)
Other	O

Second Character

Failure Area	Code
At loading nose	A
Between loading noses	B
at Support nose	S
between Load and support nose	L
Unknown	U

Third Character

Failure Location	Code
Top	T
Bottom	B
Left	L
Right	R
Middle	M
Various	V
Unknown	U

1D-10-C Sample	1	2	3	4	5
Failure Mode	CBT	CAT	CBT	CBT	CBT

2A:

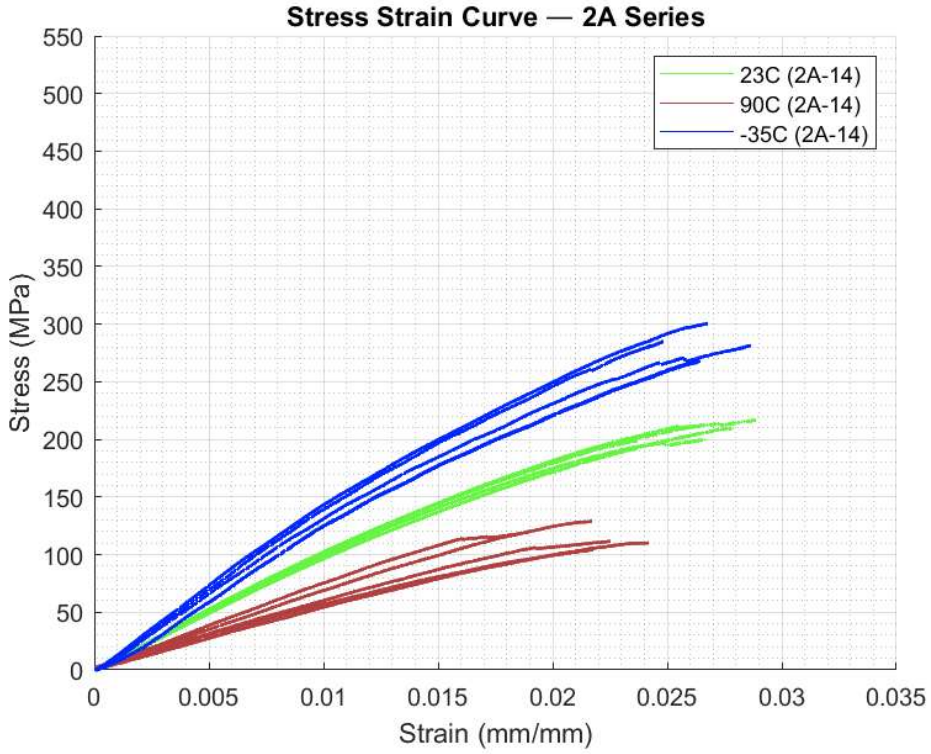

	Sample	Flexural Strength (MPa)	Flexural Modulus (GPa)	Thickness (mm)		Sample	Flexural Strength (MPa)	Flexural Modulus (GPa)	Thickness (mm)		Sample	Flexural Strength (MPa)	Flexural Modulus (GPa)	Thickness (mm)
23C (2A-14)	1	216.8	10.6	3.15	90C (2A-14)	6	111.9	6.0	3.18	-35C (2A-14)	12	300.4	14.95	3.022
23C (2A-14)	2	199.4	10.5	3.16	90C (2A-14)	7	110.4	5.7	3.17	-35C (2A-14)	13	285.1	14.64	3.024
23C (2A-14)	3	210.2	10.0	3.18	90C (2A-14)	8	104.5	5.6	3.17	-35C (2A-14)	14	268.5	13.61	3.026
23C (2A-14)	4	199.7	10.3	3.15	90C (2A-14)	9	129.1	6.9	3.00	-35C (2A-14)	15	267.9	13.56	3.031
23C (2A-14)	5	212.6	10.6	3.15	90C (2A-14)	10	118.4	7.6	3.01	-35C (2A-14)	16	281.4	13.59	3.047
Average		**207.7**	**10.4**	**3.16**	**Average**		**114.9**	**6.3**	**3.11**	**Average**		**280.6**	**14.1**	**3.03**
St. Deviation		**7.0**	**0.2**	**0.01**	**St. Deviation**		**8.4**	**0.8**	**0.08**	**St. Deviation**		**12.0**	**0.6**	**0.01**

First Character

Failure Mode	Code
Tension	T
Compression	C
Buckling	B
interlaminar Shear	S
Multi-mode	M(xyz)
Other	O

Second Character

Failure Area	Code
At loading nose	A
Between loading noses	B
at Support nose	S
between Load and support nose	L
Unknown	U

Third Character

Failure Location	Code
Top	T
Bottom	B
Left	L
Right	R
Middle	M
Various	V
Unknown	U

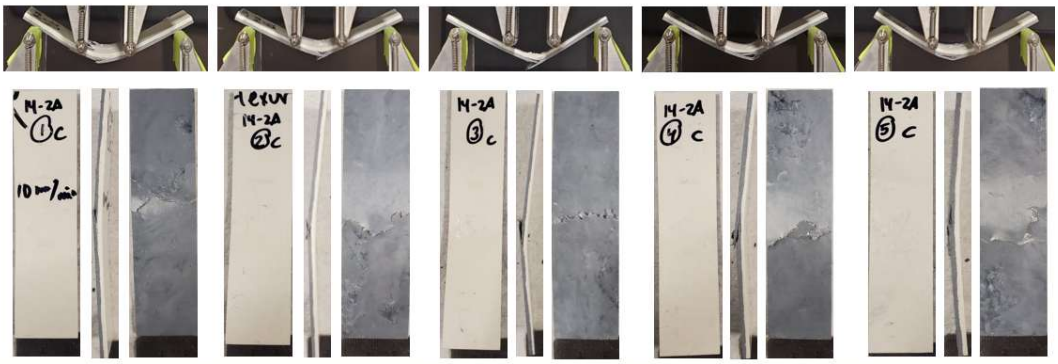

2A-14-C Sample	1	2	3	4	5
Failure Mode	MBV	MBV	MBV	MBV	MBV

2B:

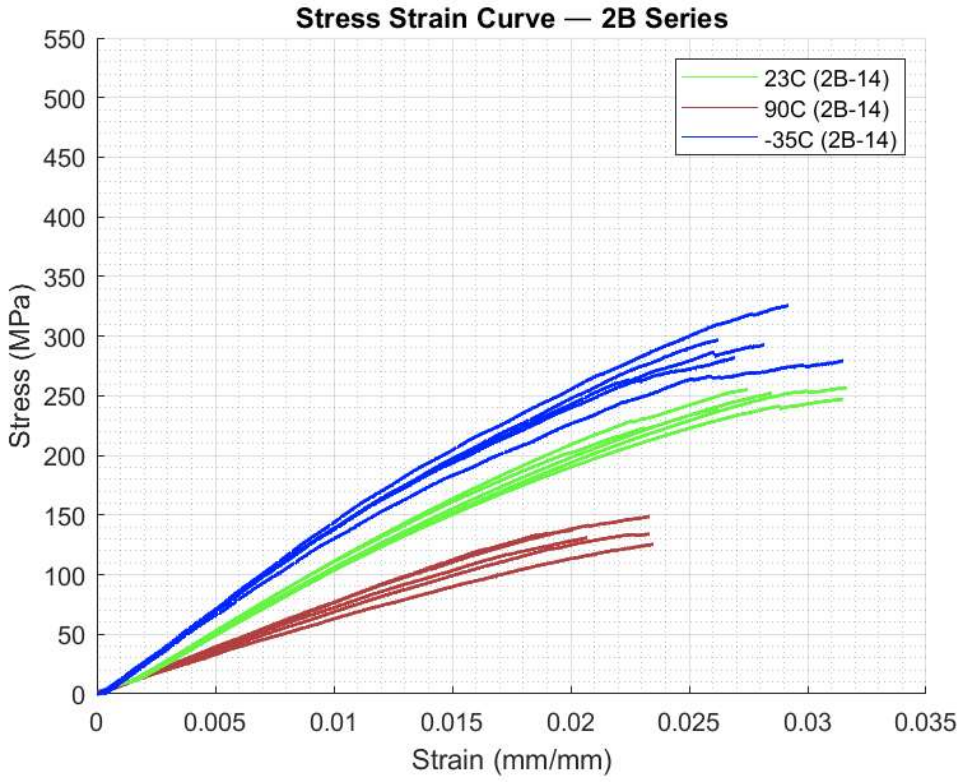

	Sample	Flexural Strength (MPa)	Flexural Modulus (GPa)	Thickness (mm)		Sample	Flexural Strength (MPa)	Flexural Modulus (GPa)	Thickness (mm)		Sample	Flexural Strength (MPa)	Flexural Modulus (GPa)	Thickness (mm)
23C (2B-14)	1	257.8	11.1	3.125	90C (2B-14)	6	137.5	7.9	2.955	-35C (2B-14)	12	329.6	15.38	3.017
23C (2B-14)	2	255.2	12.0	3.100	90C (2B-14)	7	131.2	7.1	2.900	-35C (2B-14)	13	299.9	14.34	2.991
23C (2B-14)	3	252.9	11.4	3.069	90C (2B-14)	8	125.5	6.3	2.858	-35C (2B-14)	14	282.4	14.67	2.945
23C (2B-14)	4	247.4	11.4	3.024	90C (2B-14)	9	134.2	6.9	3.142	-35C (2B-14)	15	298.2	14.63	2.907
23C (2B-14)	5	240.2	12.0	2.994	90C (2B-14)	10	149.0	7.8	3.118	-35C (2B-14)	16	280.5	13.64	2.849
Average		**250.7**	**11.6**	**3.062**	**Average**		**135.5**	**7.2**	**2.995**	**Average**		**298.1**	**14.5**	**2.942**
St. Deviation		**6.3**	**0.3**	**0.048**	**St. Deviation**		**7.8**	**0.6**	**0.115**	**St. Deviation**		**17.6**	**0.6**	**0.060**

First Character

Failure Mode	Code
Tension	T
Compression	C
Buckling	B
interlaminar Shear	S
Multi-mode	M(xyz)
Other	O

Second Character

Failure Area	Code
At loading nose	A
Between loading noses	B
at Support nose	S
between Load and support nose	L
Unknown	U

Third Character

Failure Location	Code
Top	T
Bottom	B
Left	L
Right	R
Middle	M
Various	V
Unknown	U

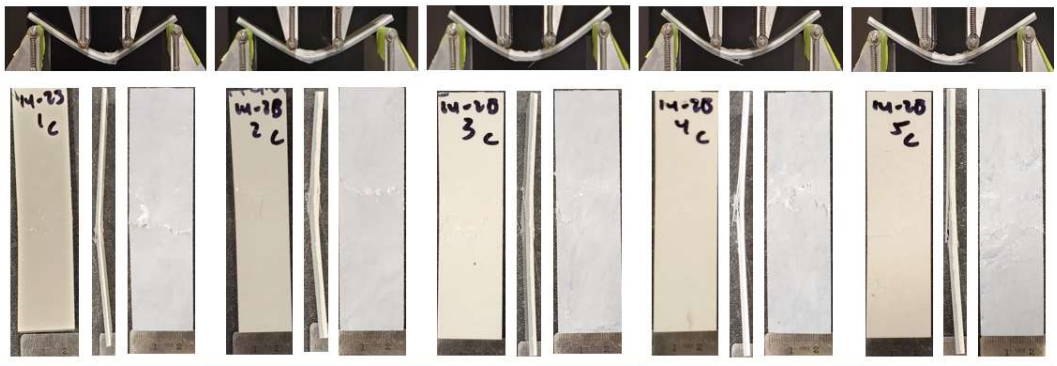

2A-14-C Sample	1	2	3	4	5
Failure Mode	MBV	MBV	MBV	MBV	MBV

2C:

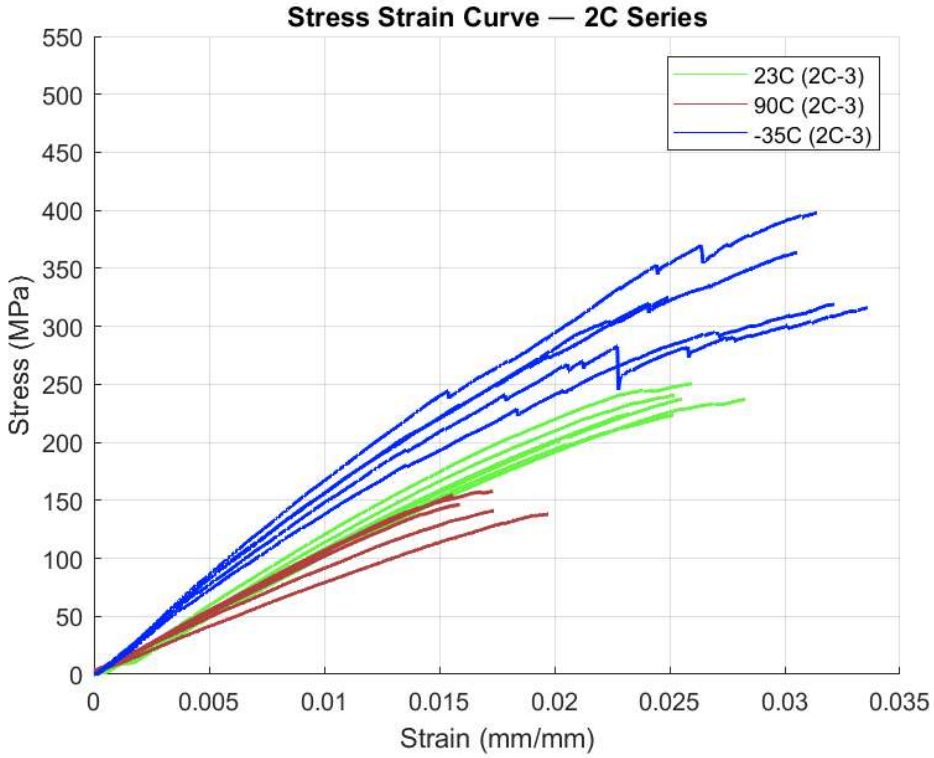

	Sample	Flexural Strength (MPa)	Flexural Modulus (GPa)	Thickness (mm)		Sample	Flexural Strength (MPa)	Flexural Modulus (GPa)	Thickness (mm)		Sample	Flexural Strength (MPa)	Flexural Modulus (GPa)	Thickness (mm)
23C (2C-3)	1	215.8	12.2	3.18	90C (2C-3)	7	141.5	9.0	2.94	-35C (2C-3)	11	398.4	17.38	3.19
23C (2C-3)	2	182.9	12.4	3.14	90C (2C-3)	8	138.4	7.8	2.89	-35C (2C-3)	12	316.1	15.02	3.159
23C (2C-3)	3	204.8	11.8	3.10	90C (2C-3)	9	154.5	10.7	3.26	-35C (2C-3)	13	325.3	16.38	3.112
23C (2C-3)	4	241.5	13.1	3.08	90C (2C-3)	10	146.3	10.3	3.23	-35C (2C-3)	14	364.1	16.23	3.074
23C (2C-3)	5	225.5	12.5	3.02	90C (2C-3)	11	157.8	10.7	3.19	-35C (2C-3)	15	320	14.15	3.034
Average		**214.1**	**12.4**	**3.10**	**Average**		**147.7**	**9.7**	**3.10**	**Average**		**344.8**	**15.8**	**3.11**
St. Deviation		**19.7**	**0.5**	**0.06**	**St. Deviation**		**7.4**	**1.1**	**0.15**	**St. Deviation**		**31.8**	**1.1**	**0.06**

First Character

Failure Mode	Code
Tension	T
Compression	C
Buckling	B
interlaminar Shear	S
Multi-mode	M(xyz)
Other	O

Second Character

Failure Area	Code
At loading nose	A
Between loading noses	B
at Support nose	S
between Load and support nose	L
Unknown	U

Third Character

Failure Location	Code
Top	T
Bottom	B
Left	L
Right	R
Middle	M
Various	V
Unknown	U

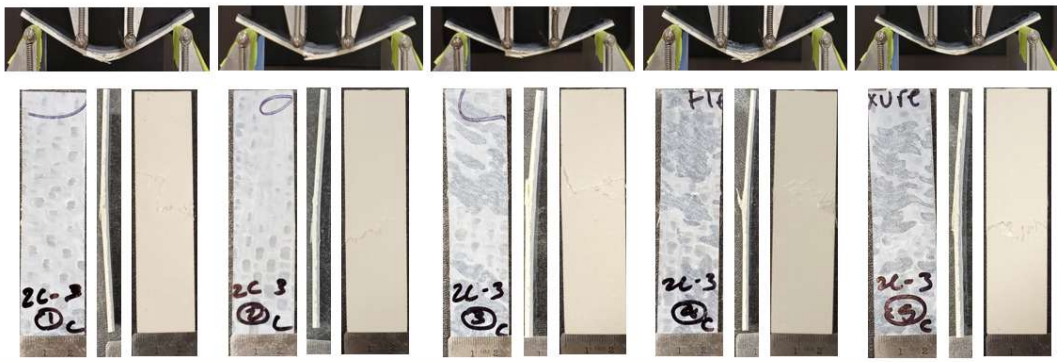

2C-3-C Sample	1	2	3	4	5
Failure Mode	MBV	MBV	TBB	MBV	SBB

3A:

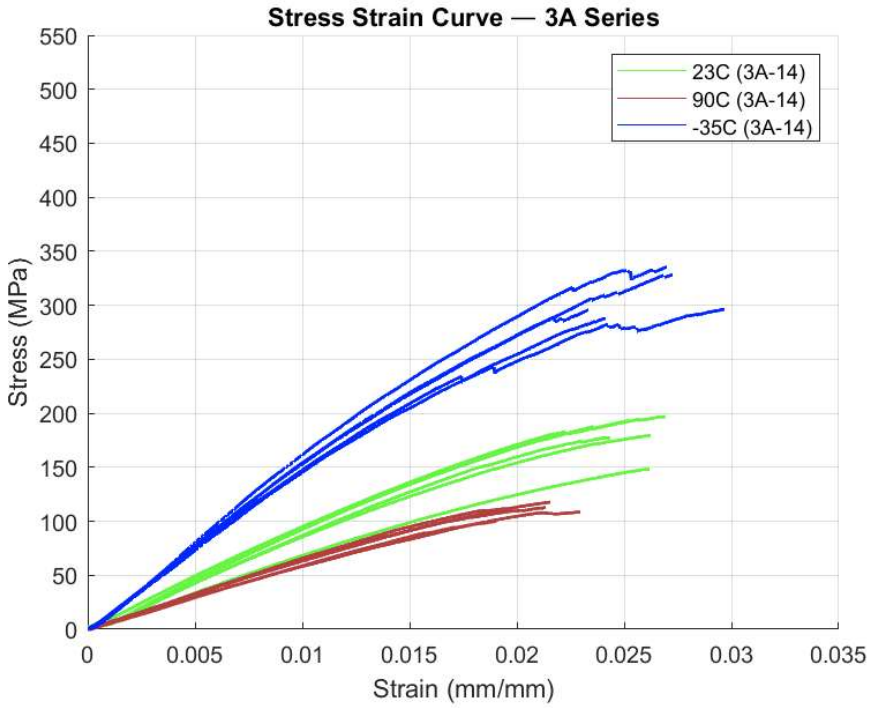

	Sample	Flexural Strength (MPa)	Flexural Modulus (GPa)	Thickness (mm)		Sample	Flexural Strength (MPa)	Flexural Modulus (GPa)	Thickness (mm)		Sample	Flexural Strength (MPa)	Flexural Modulus (GPa)	Thickness (mm)
23C (3A-14)	1	200.3	10.0	3.64	90C (3A-14)	6	117.8	6.3	3.58	-35C (3A-14)	11	329.0	16.1	3.458
23C (3A-14)	2	208.8	10.5	3.61	90C (3A-14)	7	112.8	6.5	3.58	-35C (3A-14)	12	335.6	17.2	3.469
23C (3A-14)	3	198.0	9.9	3.62	90C (3A-14)	8	108.7	5.8	3.50	-35C (3A-14)	13	287.8	15.3	3.461
23C (3A-14)	4	211.1	10.4	3.62	90C (3A-14)	9	100.0	6.1	3.50	-35C (3A-14)	14	295.5	15.9	3.423
23C (3A-14)	5	180.5	9.8	3.61	90C (3A-14)	10	111.8	6.8	3.48	-35C (3A-14)	15	296.4	15.0	3.431
Average		**199.7**	**10.1**	**3.62**	**Average**		**110.2**	**6.3**	**3.53**	**Average**		**308.9**	**15.9**	**3.448**
St. Deviation		**10.8**	**0.3**	**0.01**	**St. Deviation**		**5.9**	**0.3**	**0.04**	**St. Deviation**		**19.5**	**0.8**	**0.018**

First Character

Failure Mode	Code
Tension	T
Compression	C
Buckling	B
interlaminar Shear	S
Multi-mode	M(xyz)
Other	O

Second Character

Failure Area	Code
At loading nose	A
Between loading noses	B
at Support nose	S
between Load and support nose	L
Unknown	U

Third Character

Failure Location	Code
Top	T
Bottom	B
Left	L
Right	R
Middle	M
Various	V
Unknown	U

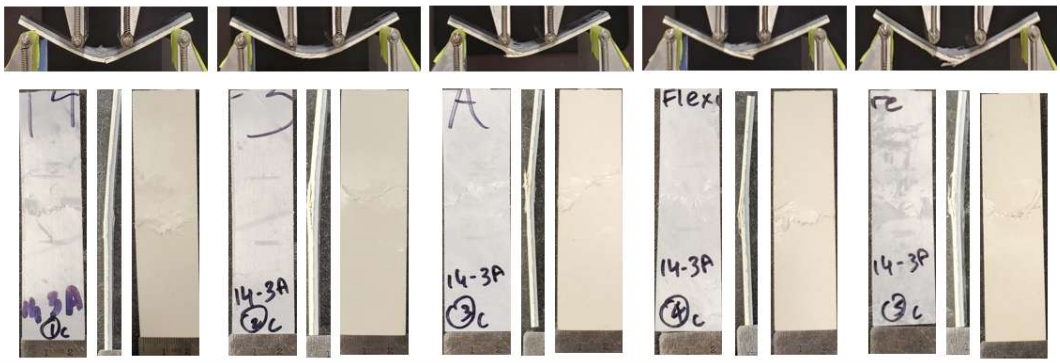

3A-14-C Sample	1	2	3	4	5
Failure Mode	MBV	TBB	MBV	MBV	MBV

3B:

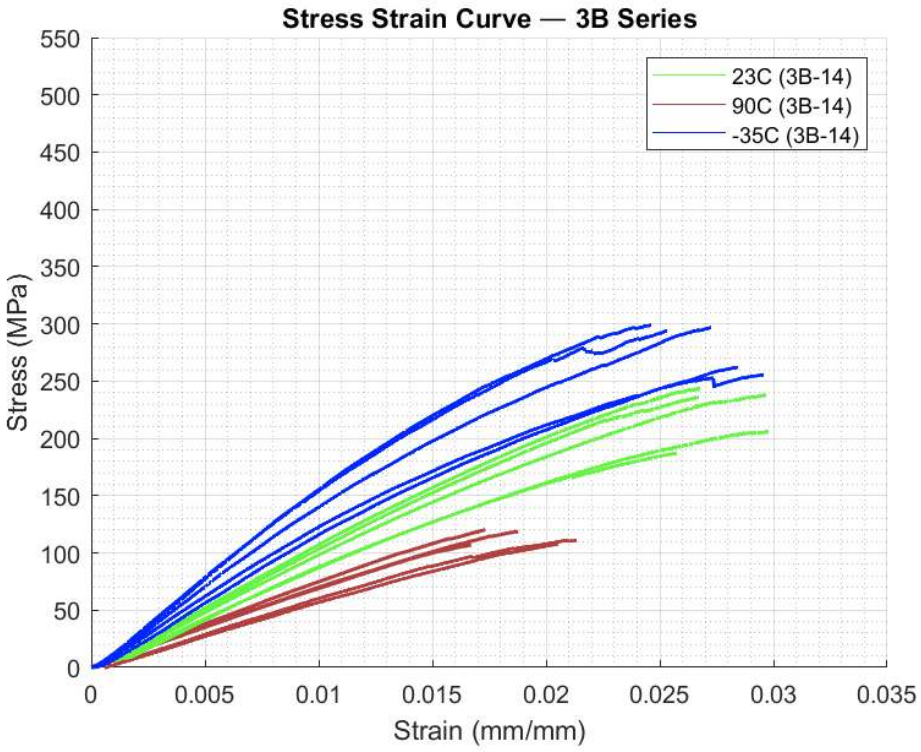

	Sample	Flexural Strength (MPa)	Flexural Modulus (GPa)	Thickness (mm)		Sample	Flexural Strength (MPa)	Flexural Modulus (GPa)	Thickness (mm)		Sample	Flexural Strength (MPa)	Flexural Modulus (GPa)	Thickness (mm)
23C (3B-14)	1	238.0	10.5	3.35	90C (3B-14)	6	118.7	7.0	3.60	-35C (3B-14)	12	262.1	12.41	3.590
23C (3B-14)	2	206.5	9.3	3.39	90C (3B-14)	7	106.9	6.9	3.65	-35C (3B-14)	13	255.6	12.79	3.529
23C (3B-14)	3	187.7	9.8	3.46	90C (3B-14)	8	120.3	7.5	3.68	-35C (3B-14)	14	297.1	14.76	3.480
23C (3B-14)	4	243.7	11.4	3.50	90C (3B-14)	9	111.2	6.5	3.27	-35C (3B-14)	15	293.9	16.08	3.437
23C (3B-14)	5	236.1	11.0	3.55	90C (3B-14)	10	108.1	6.2	3.32	-35C (3B-14)	16	299.1	16.66	3.384
Average		**222.4**	**10.4**	**3.45**	**Average**		**113.0**	**6.8**	**3.50**	**Average**		**281.6**	**14.5**	**3.484**
St. Deviation		**21.6**	**0.8**	**0.07**	**St. Deviation**		**5.5**	**0.4**	**0.17**	**St. Deviation**		**18.7**	**1.7**	**0.072**

First Character

Failure Mode	Code
Tension	T
Compression	C
Buckling	B
interlaminar Shear	S
Multi-mode	M(xyz)
Other	O

Second Character

Failure Area	Code
At loading nose	A
Between loading noses	B
at Support nose	S
between Load and support nose	L
Unknown	U

Third Character

Failure Location	Code
Top	T
Bottom	B
Left	L
Right	R
Middle	M
Various	V
Unknown	U

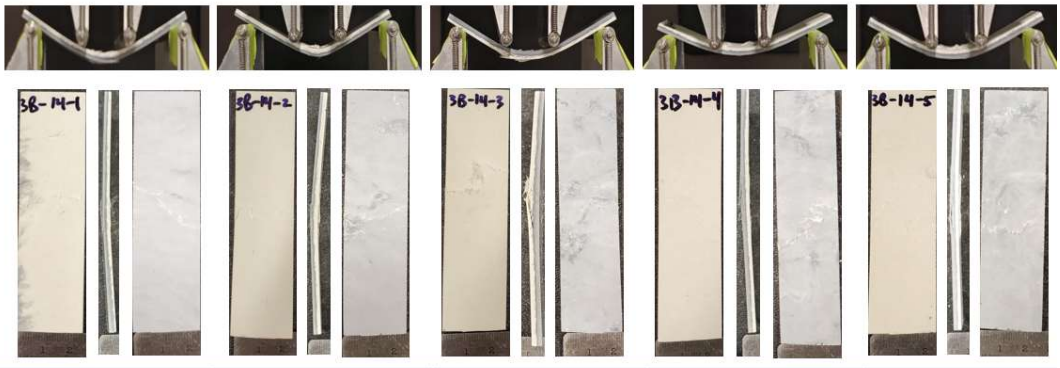

3A-14-C Sample	1	2	3	4	5
Failure Mode	MBV	MBV	MBV	MBV	MBV

11.9. Interlaminar Shear (3-point bend) Test Data

1A:

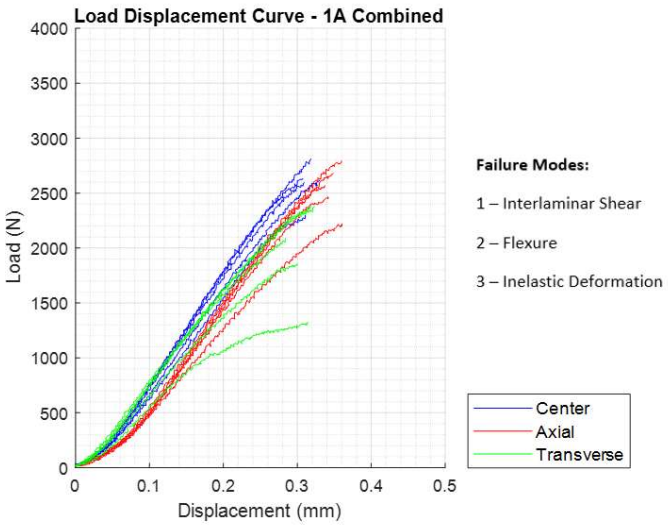

Sample	ILSS (MPa)	Thickness (mm)	Failure Mode
1A-12-C_1	31.4	3.10	2
1A-12-C_2	27.4	3.12	2
1A-12-C_3	31.4	3.12	2
1A-12-C_4	30.1	3.48	2
1A-12-C_5	30.6	3.15	2
Average	**30.2**	**3.19**	
Standard Deviation	**1.5**		
1A-S1-A_1	33.7	3.09	3
1A-S1-A_2	32.8	3.05	3
1A-S1-A_3	32.0	2.99	3
1A-S1-A_4	31.5	2.93	3
1A-S1-A_5	29.1	2.85	3
Average	**31.8**	**2.98**	
Standard Deviation	**1.6**		
1A-S4-T_1	17.4	2.84	3
1A-S4-T_2	23.8	2.91	3
1A-S4-T_3	29.9	2.96	3
1A-S4-T_4	29.2	3.04	3
1A-S4-T_5	25.0	3.09	3
Average	**25.1**	**2.97**	
Standard Deviation	**4.5**		

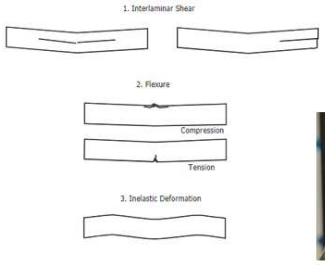

1A Axial	6	7	8	9	10
Failure Mode	2 - Flexure	2 - Flexure	2 - Flexure	2 - Flexure	2 - Flexure

1A Axial	6	7	8	9	10
Failure Mode	3 – Inelastic Deformation	3 – Inelastic Deformation	3 – Inelastic Deformation	3 – Inelastic Deformation	3 – Inelastic Deformation

1A-S4-T Sample	6	7	8	9	10
Failure Mode	3 – Inelastic Deformation	3 – Inelastic Deformation	3 – Inelastic Deformation	3 – Inelastic Deformation	3 – Inelastic Deformation

1B:

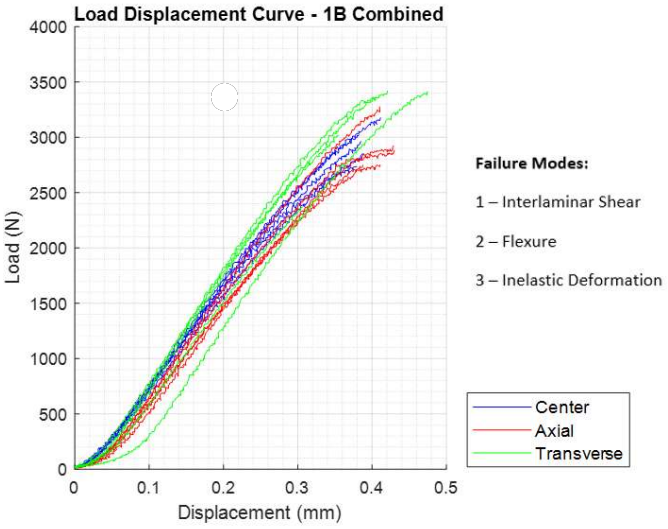

Sample	ILSS (MPa)	Thickness (mm)	Failure Mode
1B-15-C_1	34.3	2.81	3
1B-15-C_2	34.7	2.85	3
1B-15-C_3	35.3	2.94	3
1B-15-C_4	35.4	2.95	3
1B-15-C_5	36.4	2.99	3
Average	**35.2**	**2.91**	
Standard Deviation	**0.7**		
1B-S1-A_1	28.6	3.43	3
1B-S1-A_2	26.1	3.37	2
1B-S1-A_3	26.2	3.29	2
1B-S1-A_4	25.6	3.22	2
1B-S1-A_5	26.0	3.17	2
Average	**26.5**	**3.30**	
Standard Deviation	**1.1**		
1B-S4-T_1	28.7	3.52	3
1B-S4-T_2	29.4	3.47	3
1B-S4-T_3	30.0	3.42	3
1B-S4-T_4	27.1	3.34	3
1B-S4-T_5	21.8	3.26	3
Average	**27.4**	**3.40**	
Standard Deviation	**3.0**		

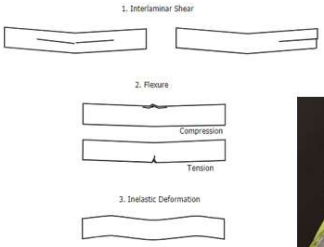

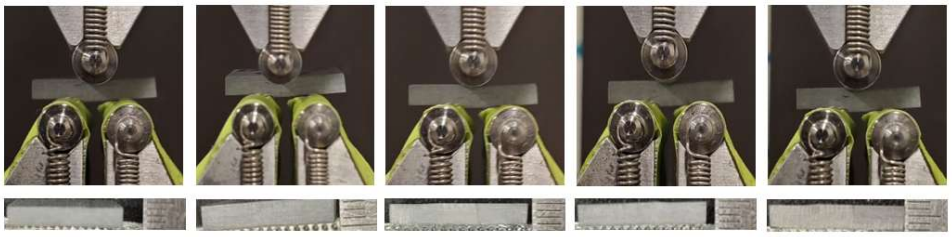

1B Centered	1	2	3	4	5
Failure Mode	3 – Inelastic Deformation	3 – Inelastic Deformation	3 – Inelastic Deformation	3 – Inelastic Deformation	3 – Inelastic Deformation

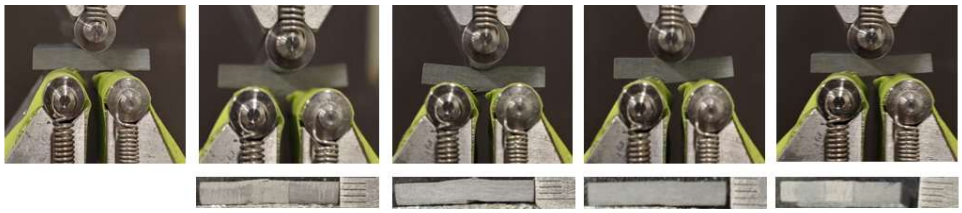

1B Axial	1	2	3	4	5
Failure Mode	3 – Inelastic Deformation	2 - Flexure	2 - Flexure	2 - Flexure	2 - Flexure

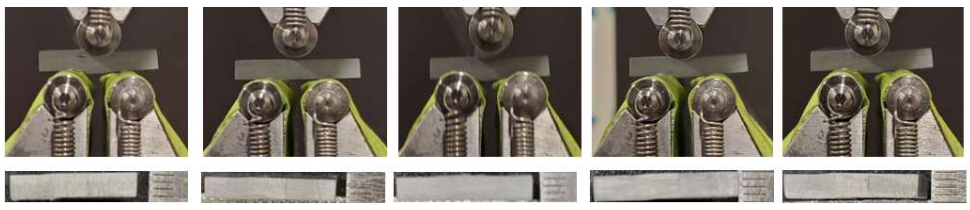

1B Transverse	1	2	3	4	5
Failure Mode	3 – Inelastic Deformation	3 – Inelastic Deformation	3 – Inelastic Deformation	3 – Inelastic Deformation	3 – Inelastic Deformation

1C:

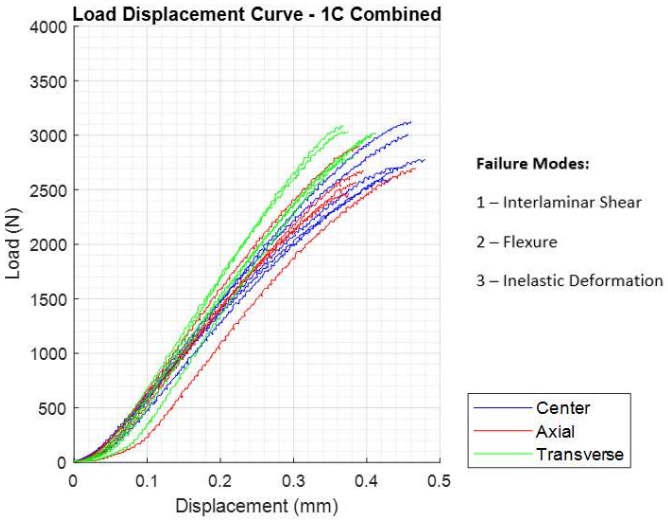

Sample	ILSS (MPa)	Thickness (mm)	Failure Mode
1C-10-C_1	29.9	2.72	3
1C-10-C_2	27.9	2.82	3
1C-10-C_3	31.3	2.88	3
1C-10-C_4	28.2	2.96	2
1C-10-C_5	31.1	3.03	3
Average	**29.7**	**2.88**	
Standard Deviation	**1.4**		
1C-S2-A_1	24.2	3.06	2
1C-S2-A_2	24.6	3.13	2
1C-S2-A_3	25.0	3.20	2
1C-S2-A_4	26.5	3.28	2
1C-S2-A_5	24.1	3.35	3
Average	**24.8**	**3.21**	
Standard Deviation	**0.9**		
1C-S4-T_1	28.6	3.24	3
1C-S4-T_2	28.6	3.17	3
1C-S4-T_3	28.8	3.11	3
1C-S4-T_4	29.6	3.05	3
1C-S4-T_5	28.1	2.99	3
Average	**28.7**	**3.11**	
Standard Deviation	**0.5**		

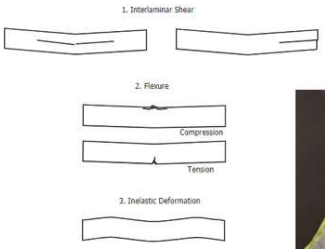

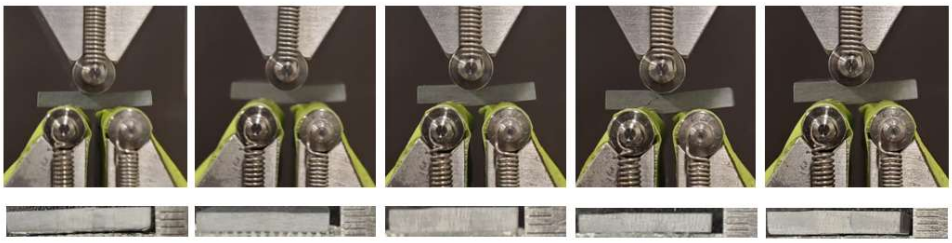

1C Centered	1	2	3	4	5
Failure Mode	3 – Inelastic Deformation	3 – Inelastic Deformation	3 – Inelastic Deformation	2 - Flexure	3 – Inelastic Deformation

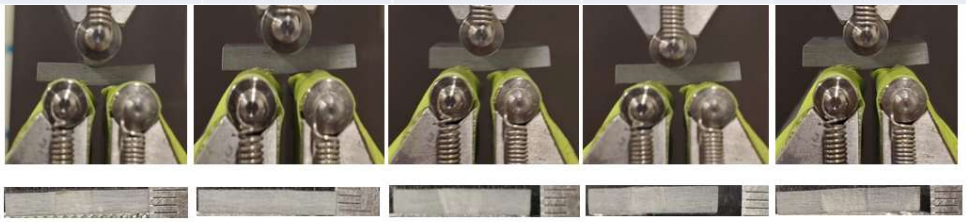

1C Axial	1	2	3	4	5
Failure Mode	2 Flexure	2 - Flexure	2 - Flexure	2 - Flexure	3 – Inelastic Deformation

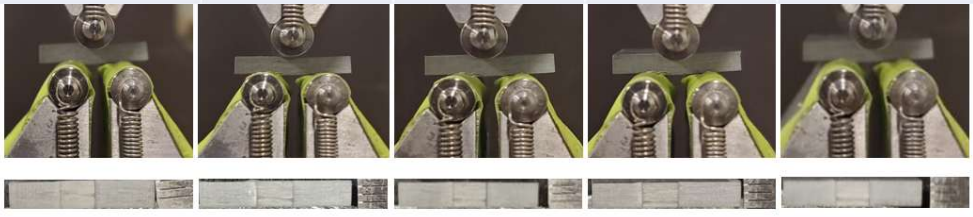

1C Transverse	1	2	3	4	5
Failure Mode	3 – Inelastic Deformation	3 – Inelastic Deformation	3 – Inelastic Deformation	3 – Inelastic Deformation	3 – Inelastic Deformation

1D:

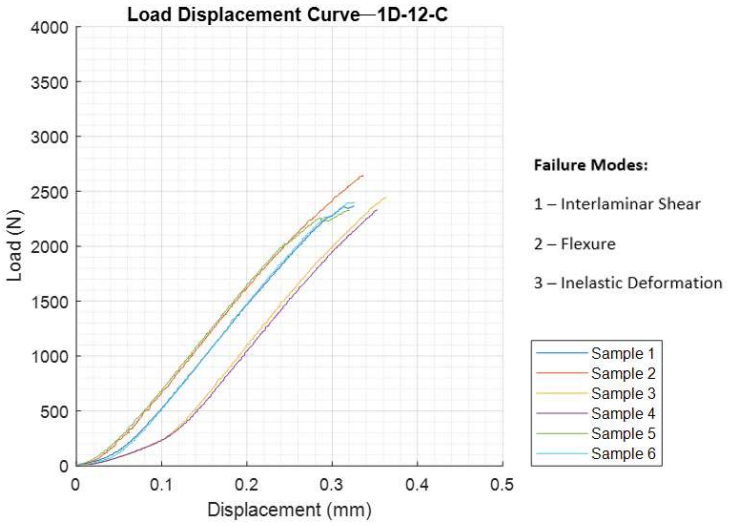

Sample	ILSS (Mpa)	Thickness (mm)	Failure Mode
1D-12-C_1	23.6	2.99	3
1D-12-C_2	26.7	2.96	3
1D-12-C_3	24.7	2.95	3
1D-12-C_4	23.6	2.95	1
1D-12-C_5	23.5	2.95	1
1D-12-C_6	24.4	2.94	1
Average	**24.4**	**2.96**	
Standard Deviation	**1.1**		

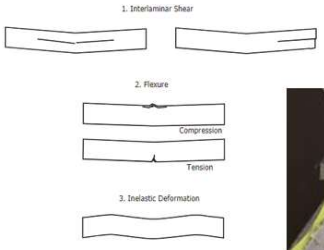

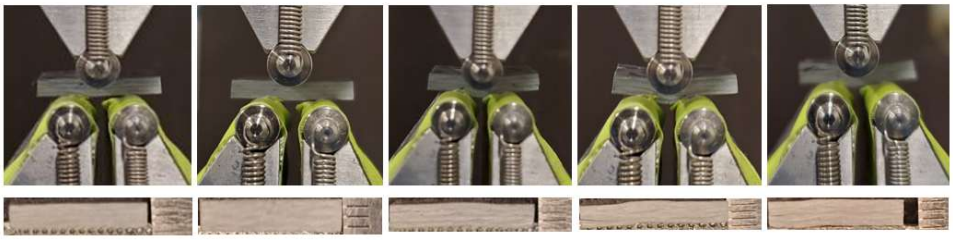

1D-12-C Sample	2	3	4	5	6
Failure Mode	3 – Inelastic Deformation	3 – Inelastic Deformation	1 – Interlaminar Shear	1 – Interlaminar Shear	1 – Interlaminar Shear

2A:

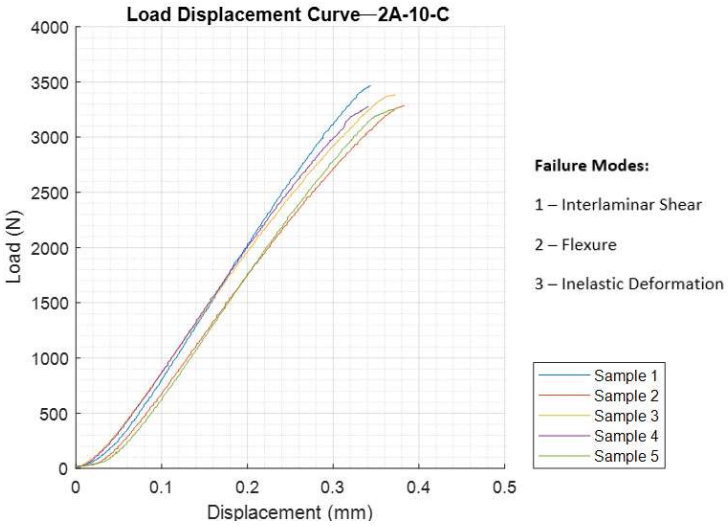

Sample	ILSS (Mpa)	Thickness (mm)	Failure Mode
2A-10-C_1	32.1	3.24	3
2A-10-C_2	30.7	3.21	1
2A-10-C_3	32.0	3.16	1
2A-10-C_4	31.9	3.08	3
2A-10-C_5	32.1	3.04	1
Average	**31.8**	**3.15**	
Standard Deviation	**0.5**		

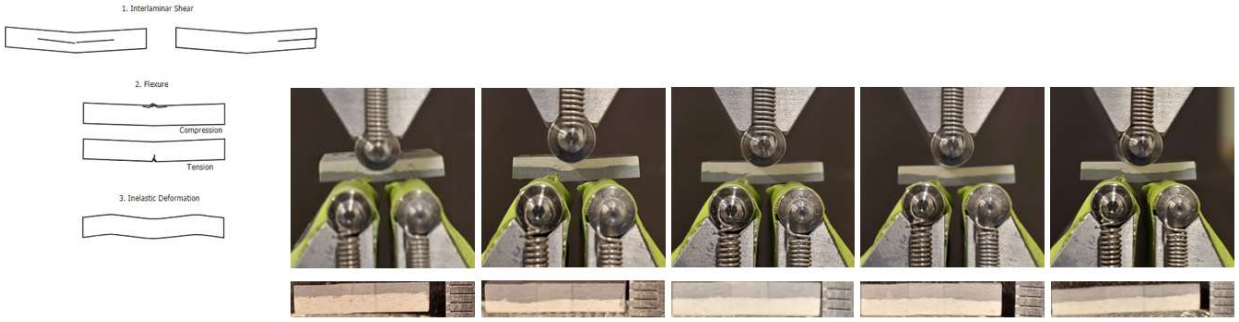

2A-10-C Sample	1	2	3	4	5
Failure Mode	3 – Inelastic Deformation	1 – Interlaminar Shear	1 – Interlaminar Shear	3 – Inelastic Deformation	1 – Interlaminar Shear

2B:

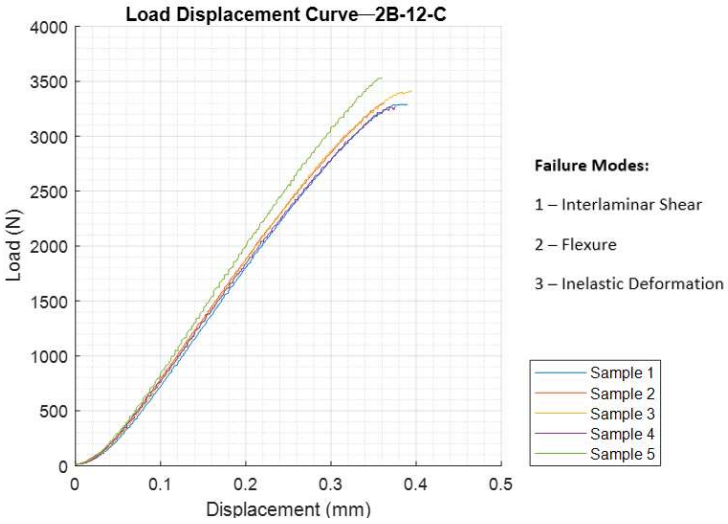

Sample	ILSS (Mpa)	Thickness (mm)	Failure Mode
2B-12-C_1	31.2	3.17	1
2B-12-C_2	31.1	3.18	1
2B-12-C_3	32.2	3.18	1
2B-12-C_4	30.7	3.19	1
2B-12-C_5	33.1	3.20	1
Average	**31.7**	**3.18**	
Standard Deviation	**0.9**		

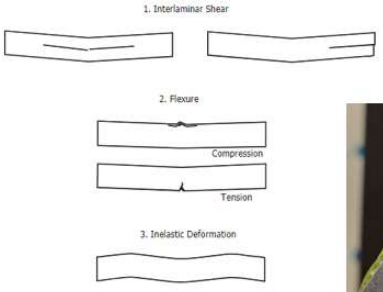

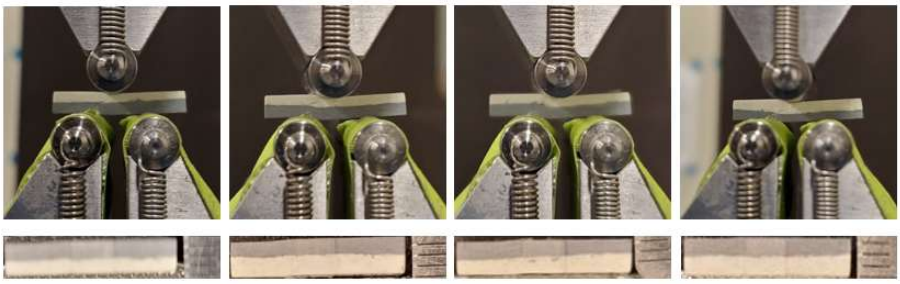

2B-12-C Sample	2	3	4	5
Failure Mode	1 – Interlaminar Shear	1 – Interlaminar Shear	1 – Interlaminar Shear	1 – Interlaminar Shear

2C:

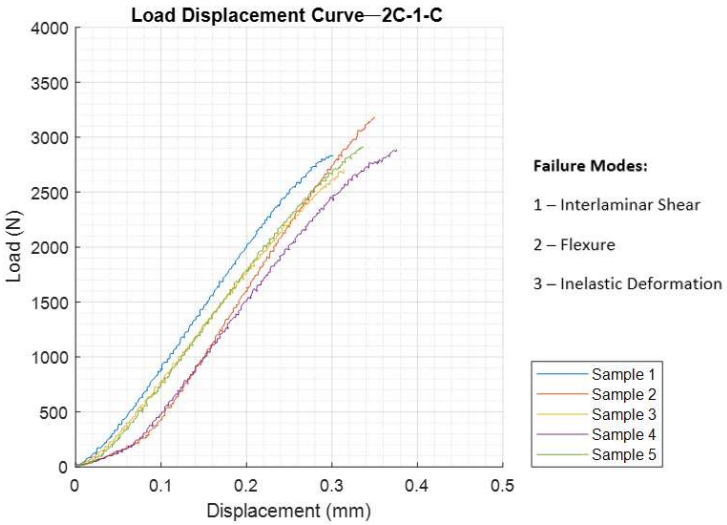

Sample	ILSS (Mpa)	Thickness (mm)	Failure Mode
2C-1-C_1	28.5	2.98	1
2C-1-C_2	32.7	2.91	1
2C-1-C_3	28.4	2.85	1
2C-1-C_4	31.2	2.77	1
2C-1-C_5	32.3	2.70	1
Average	**30.6**	**2.84**	
Standard Deviation	**1.8**		

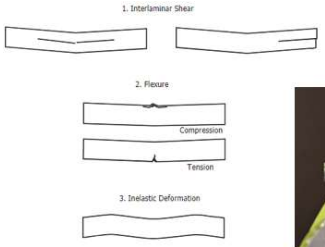

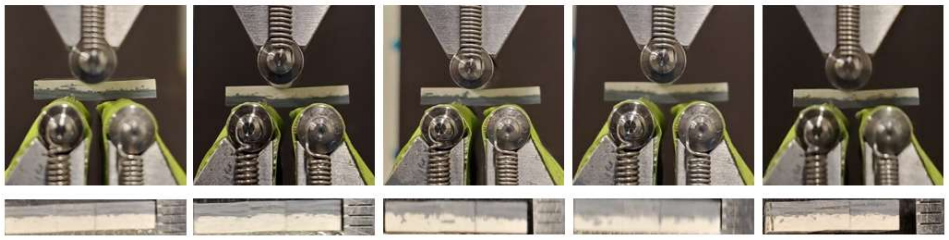

2B-12-C Sample	1	2	3	4	5
Failure Mode	1 – Interlaminar Shear	1 – Interlaminar Shear	1 – Interlaminar Shear	1 – Interlaminar Shear	1 – Interlaminar Shear

2C:

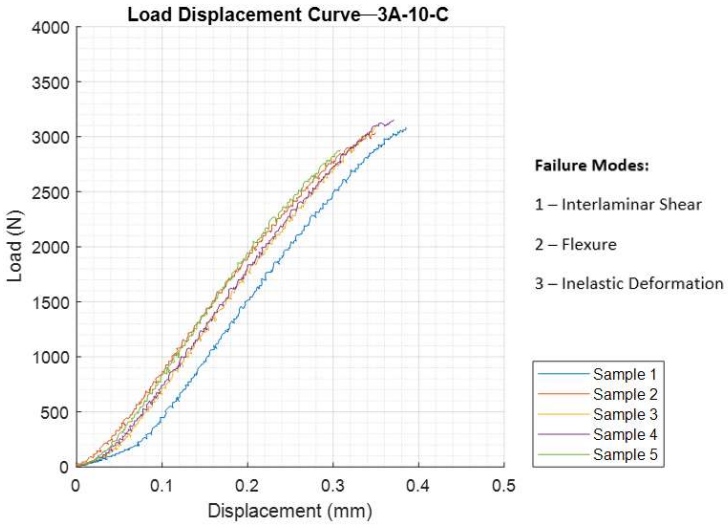

Sample	ILSS (Mpa)	Thickness (mm)	Failure Mode
3A-10-C_1	26.2	3.53	1
3A-10-C_2	25.8	3.51	1
3A-10-C_3	26.5	3.48	3
3A-10-C_4	27.2	3.47	1
3A-10-C_5	25.0	3.44	1
Average	**26.1**	**3.49**	
Standard Deviation	**0.7**		

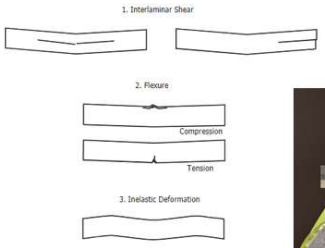

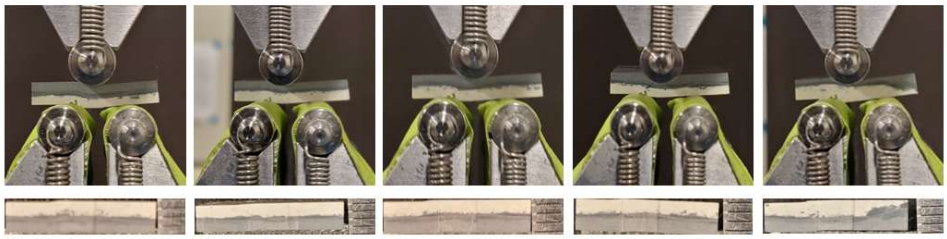

3A-10-C Sample	1	2	3	4	5
Failure Mode	1 – Interlaminar Shear	1 – Interlaminar Shear	3 – Inelastic Deformation	1 – Interlaminar Shear	1 – Interlaminar Shear

3B:

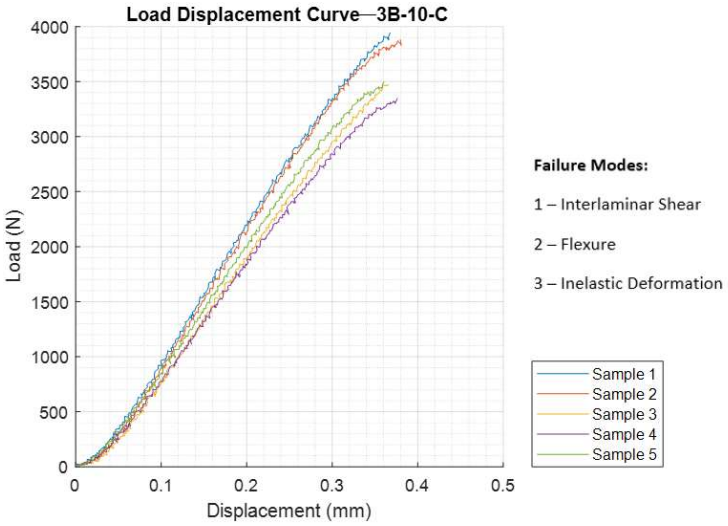

Sample	ILSS (Mpa)	Thickness (mm)	Failure Mode
3B-10-C_1	32.0	3.69	1
3B-10-C_2	32.6	3.57	1
3B-10-C_3	29.9	3.49	1
3B-10-C_4	29.5	3.41	1
3B-10-C_5	29.0	3.62	1
Average	**30.6**	**3.56**	
Standard Deviation	**1.5**		

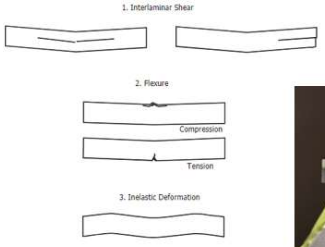

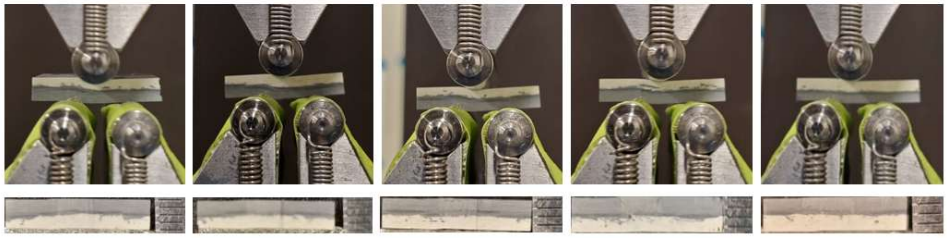

3B-10-C Sample	1	2	3	4	5
Failure Mode	1 – Interlaminar Shear	1 – Interlaminar Shear	1 – Interlaminar Shear	1 – Interlaminar Shear	1 – Interlaminar Shear

11.10. Microscopy Results

1A 30%

Regional A_{ij}		
A_{xx}	A_{yy}	A_{zz}
0.43	0.52	0.05

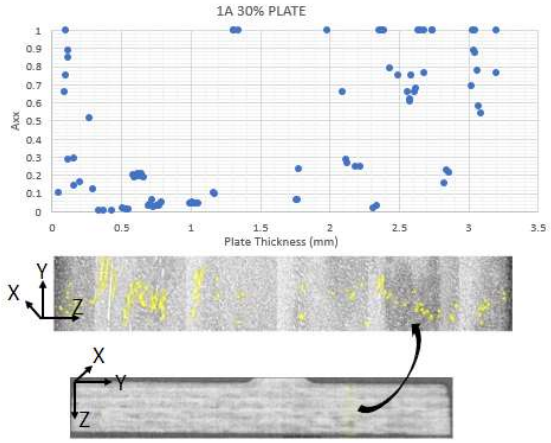

Regional A_{ij}		
A_{xx}	A_{yy}	A_{zz}
0.41	0.06	0.53

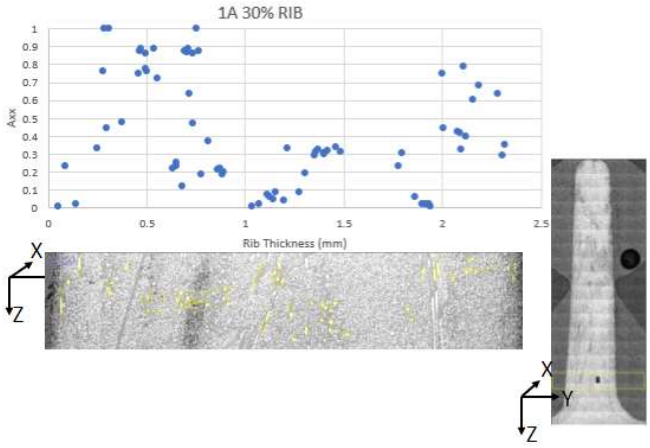

1A 60%

Regional A_{ij}		
A_{xx}	A_{yy}	A_{zz}
0.26	0.70	0.03

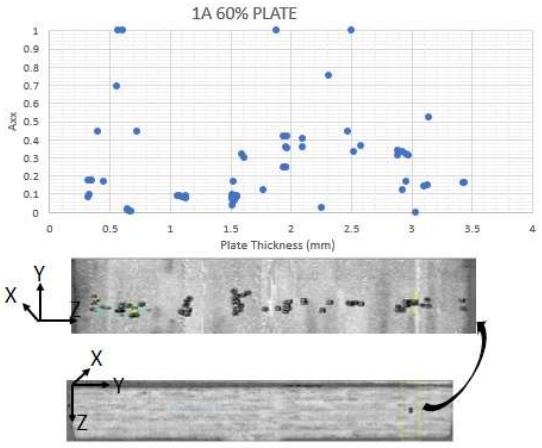

Regional A_{ij}		
A_{xx}	A_{yy}	A_{zz}
0.43	0.11	0.46

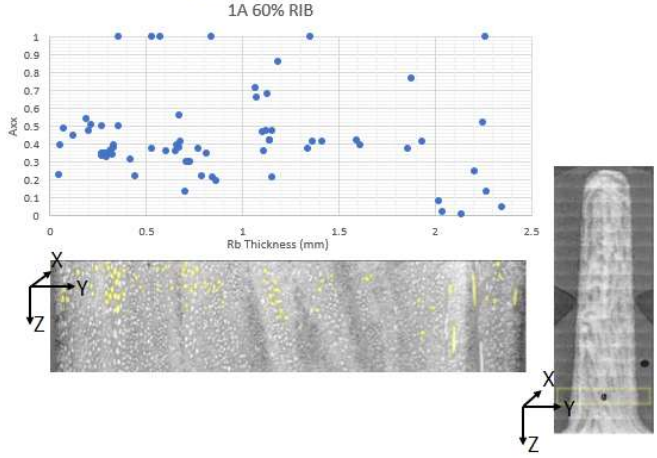

1A DIRF Section 2

Regional A_{ij}		
A_{xx}	A_{yy}	A_{zz}
0.36	0.51	0.14

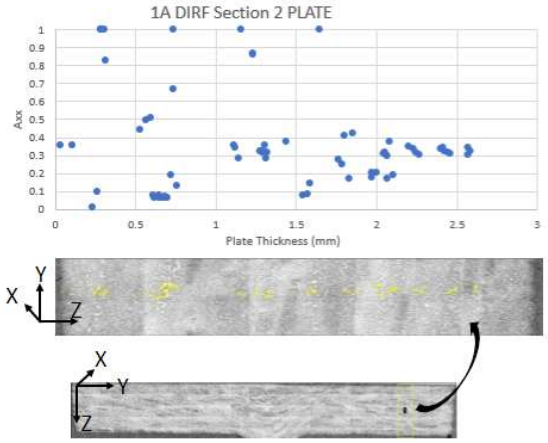

Regional A_{ij}		
A_{xx}	A_{yy}	A_{zz}
0.32	0.03	0.65

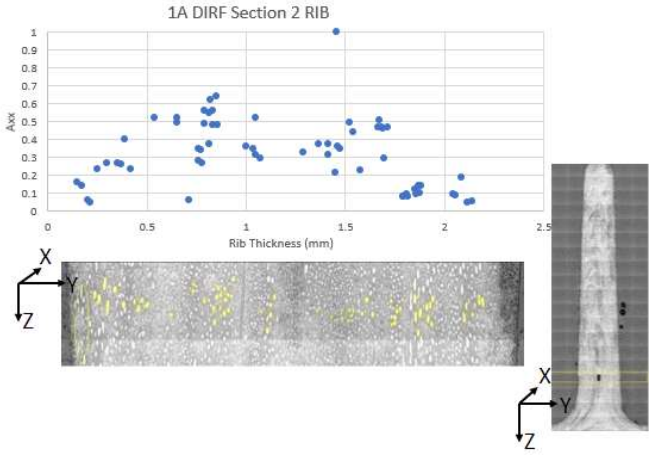

1A DIRF Section 3

Regional A_{ij}		
A_{xx}	A_{yy}	A_{zz}
0.35	0.51	0.14

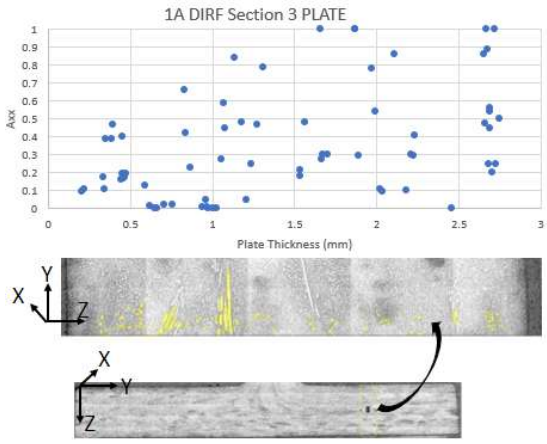

Regional A_{ij}		
A_{xx}	A_{yy}	A_{zz}
0.34	0.05	0.61

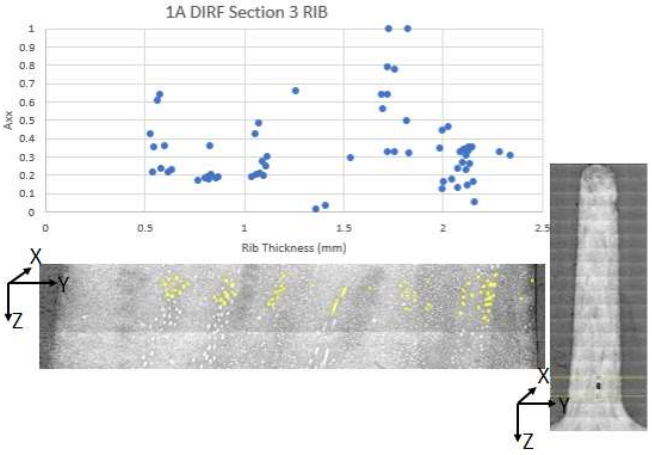

2A 30%

Regional A_{ij}		
A_{xx}	A_{yy}	A_{zz}
0.27	0.67	0.06

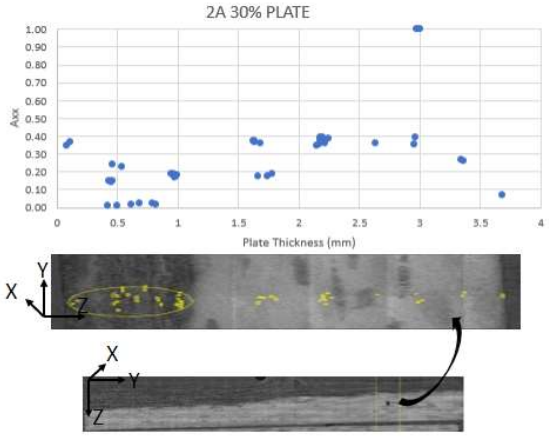

Regional A_{ij}		
A_{xx}	A_{yy}	A_{zz}
0.30	0.06	0.65

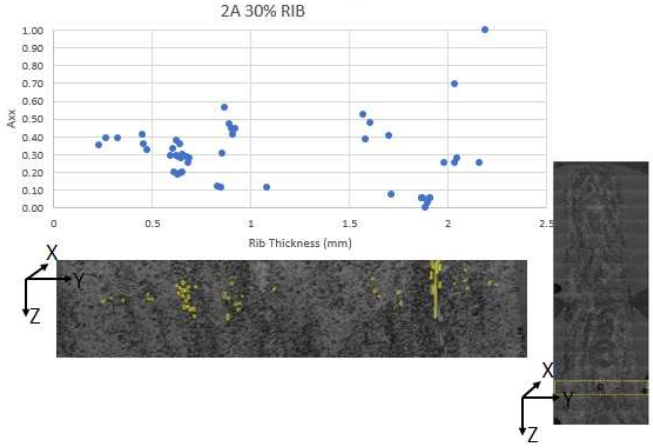

2A 60%

Regional A_{ij}		
A_{xx}	A_{yy}	A_{zz}
0.35	0.58	0.06

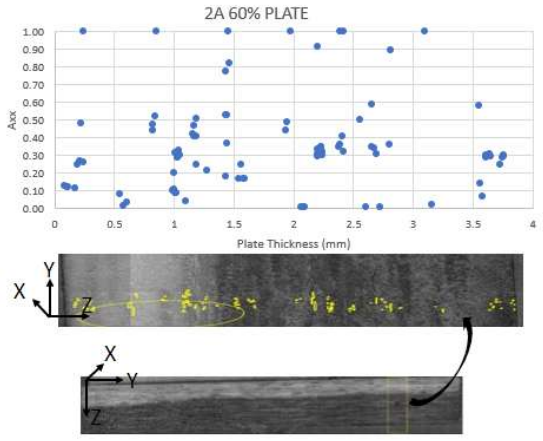

Regional A_{ij}		
A_{xx}	A_{yy}	A_{zz}
0.33	0.20	0.46

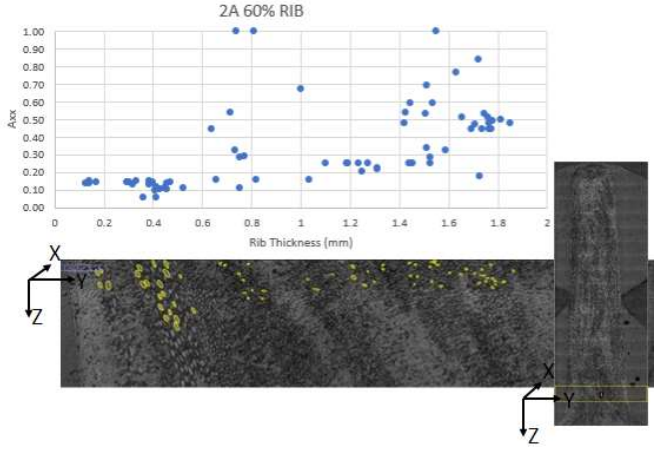

2A DIRF Section 2

Regional A_{ij}		
A_{xx}	A_{yy}	A_{zz}
0.35	0.56	0.10

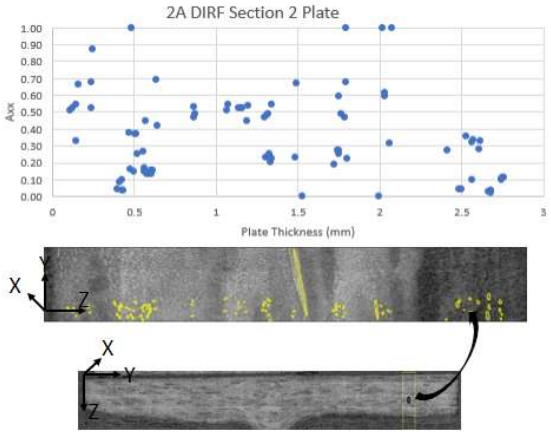

Regional A_{ij}		
A_{xx}	A_{yy}	A_{zz}
0.42	0.08	0.50

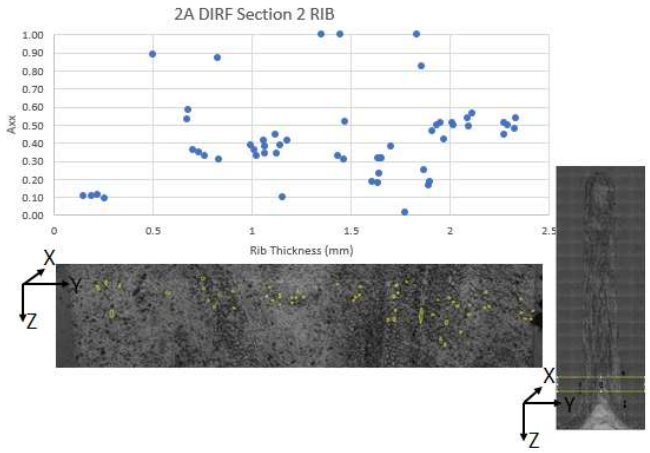

2A DIRF Section 3

Regional A_{ij}		
A_{xx}	A_{yy}	A_{zz}
0.39	0.46	0.15

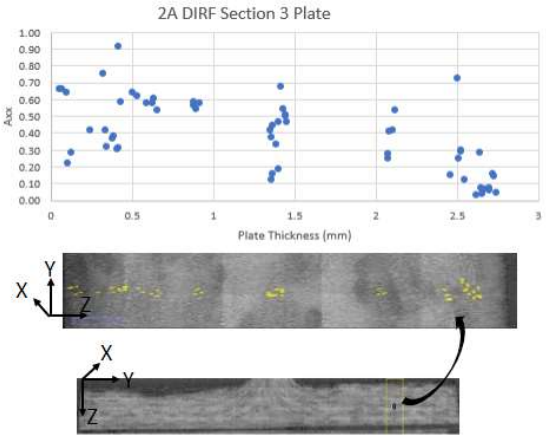

Regional A_{ij}		
A_{xx}	A_{yy}	A_{zz}
0.31	0.06	0.64

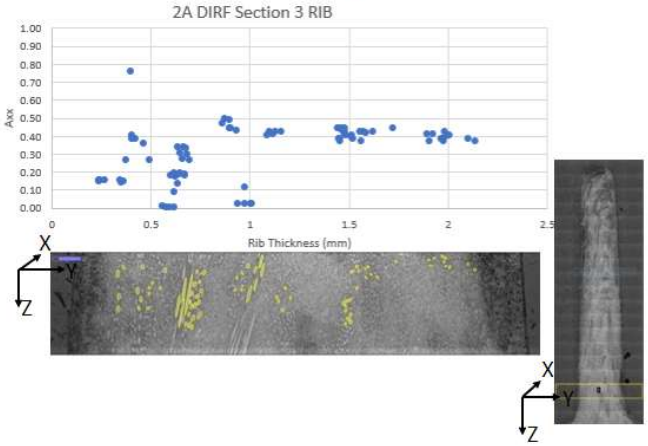

2B 30%

Regional A_{ij}		
A_{xx}	A_{yy}	A_{zz}
0.28	0.69	0.03

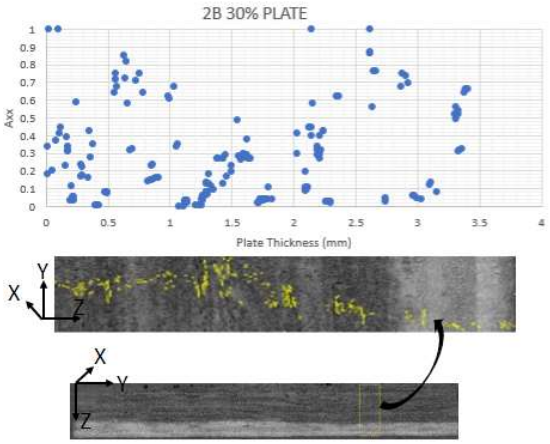

Regional A_{ij}		
A_{xx}	A_{yy}	A_{zz}
0.38	0.06	0.56

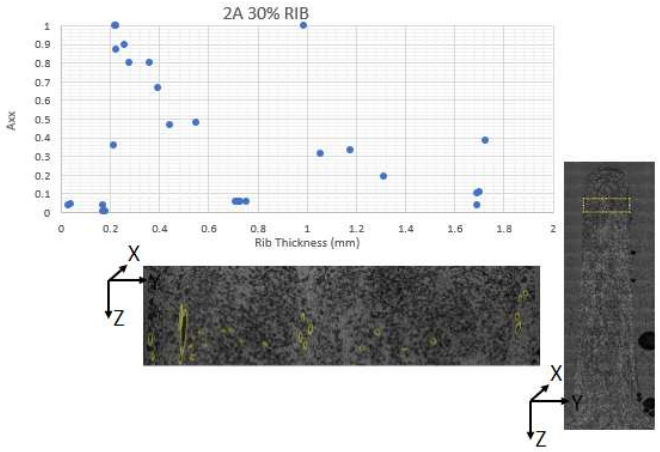

2B 60%

Regional A_{ij}		
A_{xx}	A_{yy}	A_{zz}
0.20	0.79	0.02

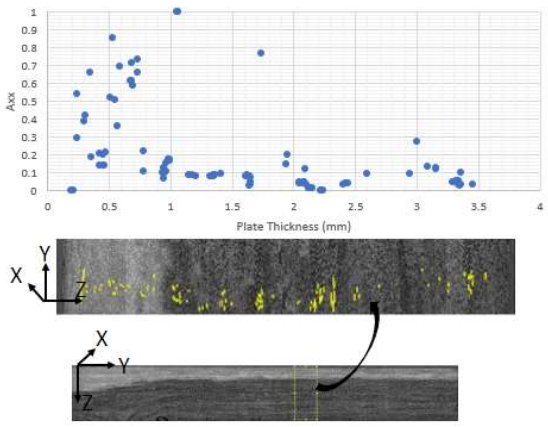

Regional A_{ij}		
A_{xx}	A_{yy}	A_{zz}
0.44	0.06	0.51

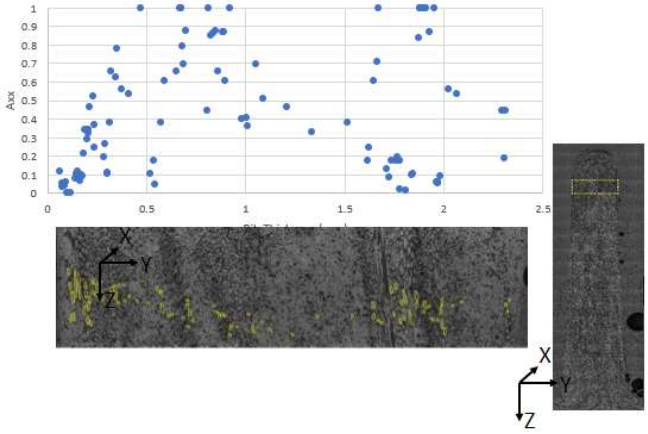

2B DIRF Section 2

Regional A_{ij}		
A_{xx}	A_{YY}	A_{zz}
0.48	0.44	0.08

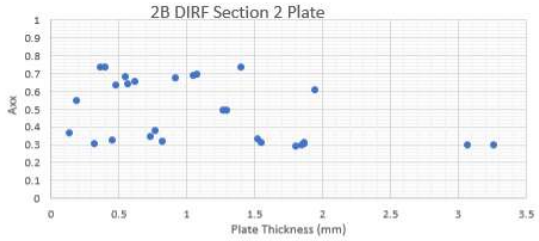

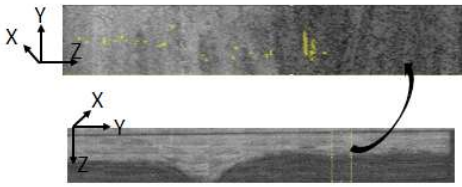

Regional A_{ij}		
A_{xx}	A_{YY}	A_{zz}
0.39	0.06	0.55

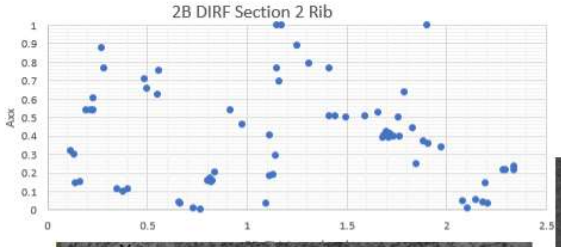

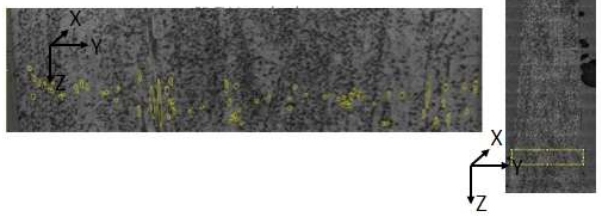

2B DIRF Section 3

Regional A_{ij}		
A_{xx}	A_{YY}	A_{zz}
0.48	0.49	0.03

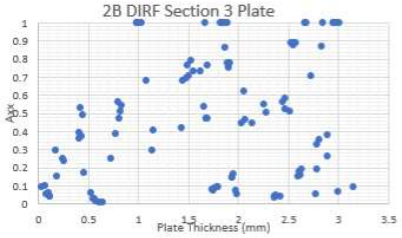

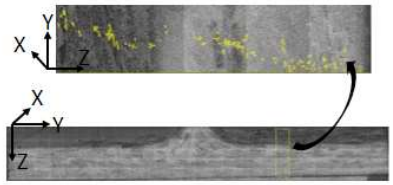

Regional A_{ij}		
A_{xx}	A_{YY}	A_{zz}
0.22	0.05	0.73

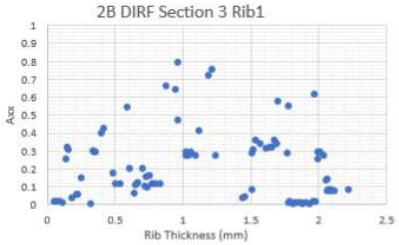

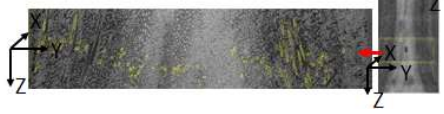

Regional A_{ij}		
A_{xx}	A_{YY}	A_{zz}
0.38	0.03	0.60

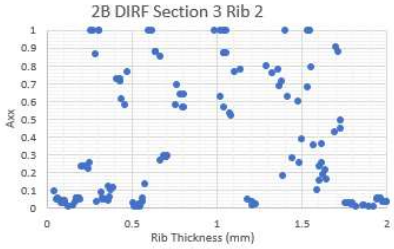

3A 30%

Regional A_{ij}		
A_{xx}	A_{yy}	A_{zz}
0.49	0.19	0.32

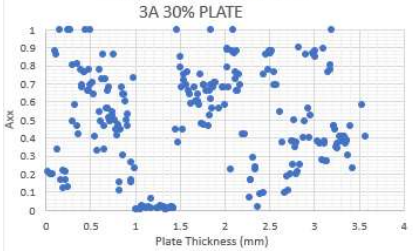

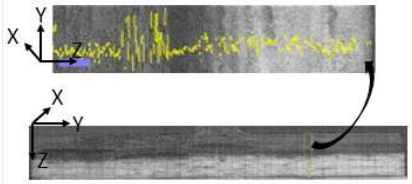

Regional A_{ij}		
A_{xx}	A_{yy}	A_{zz}
0.61	0.17	0.22

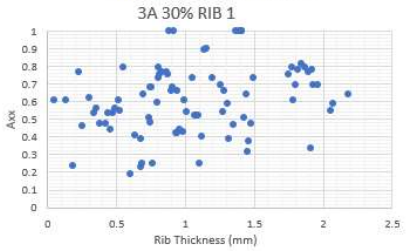

Regional A_{ij}		
A_{xx}	A_{yy}	A_{zz}
0.60	0.14	0.26

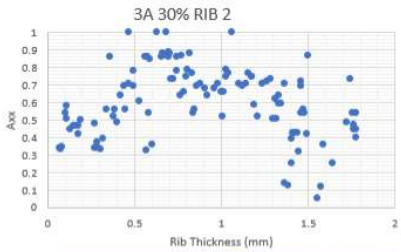

3A 60%

Regional A_{ij}		
A_{xx}	A_{yy}	A_{zz}
0.52	0.43	0.05

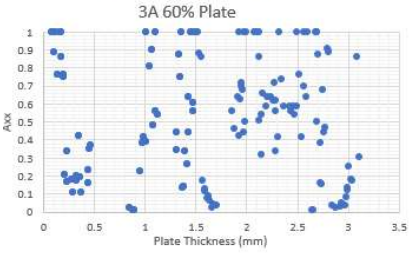

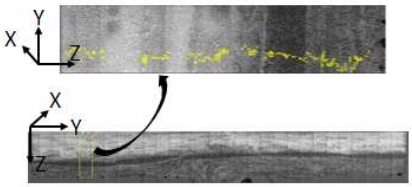

Regional A_{ij}		
A_{xx}	A_{yy}	A_{zz}
0.57	0.09	0.35

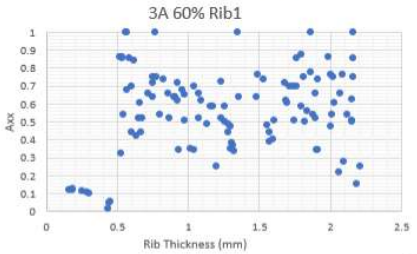

Regional A_{ij}		
A_{xx}	A_{yy}	A_{zz}
0.47	0.09	0.44

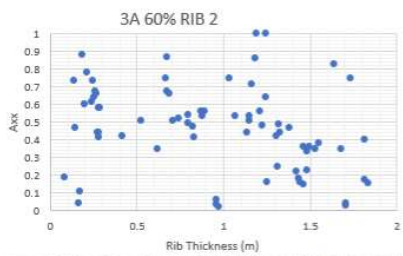

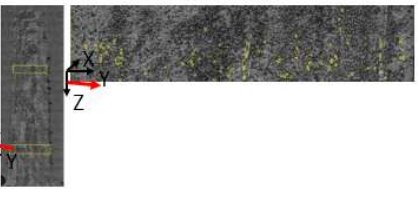

3A DIRF Section 2

Regional A_{ij}		
A_{xx}	A_{yy}	A_{zz}
0.66	0.25	0.09

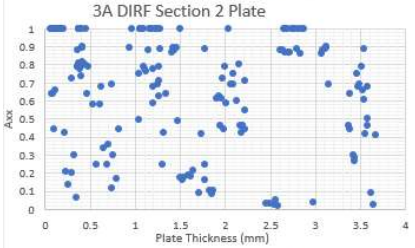

Regional A_{ij}		
A_{xx}	A_{yy}	A_{zz}
0.64	0.03	0.34

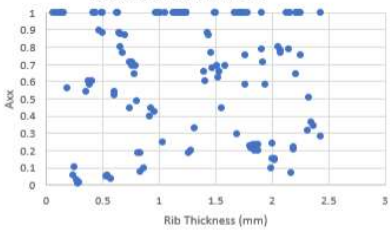

Regional A_{ij}		
A_{xx}	A_{yy}	A_{zz}
0.74	0.04	0.21

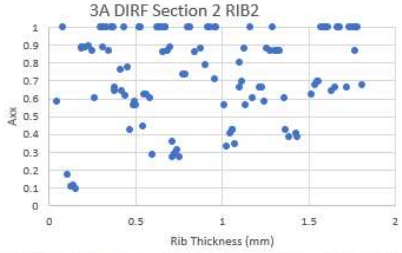

3A DIRF Section 3

Regional A_{ij}		
A_{xx}	A_{yy}	A_{zz}
0.46	0.48	0.07

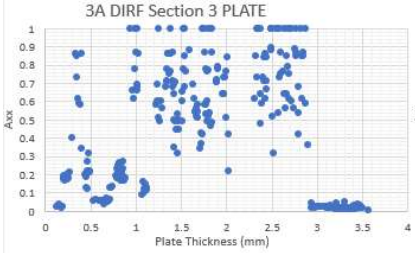

Regional A_{ij}		
A_{xx}	A_{yy}	A_{zz}
0.56	0.04	0.40

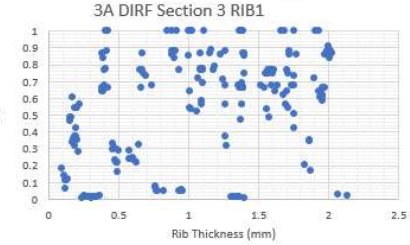

Regional A_{ij}		
A_{xx}	A_{yy}	A_{zz}
0.67	0.04	0.29

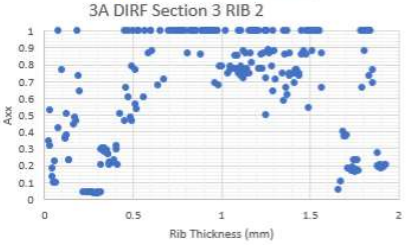

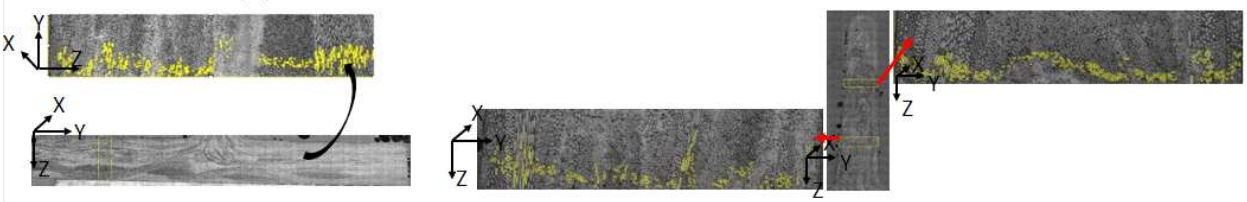

3B 30%

Regional A_{ij}		
A_{xx}	A_{YY}	A_{zz}
0.44	0.52	0.04

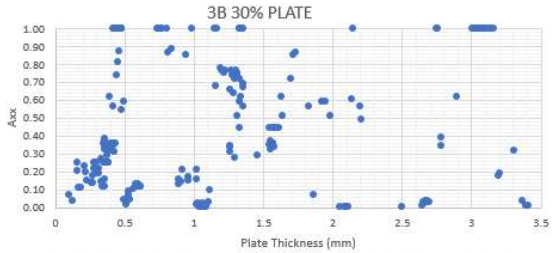

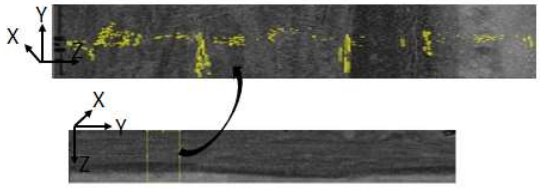

Regional A_{ij}		
A_{xx}	A_{YY}	A_{zz}
0.55	0.08	0.38

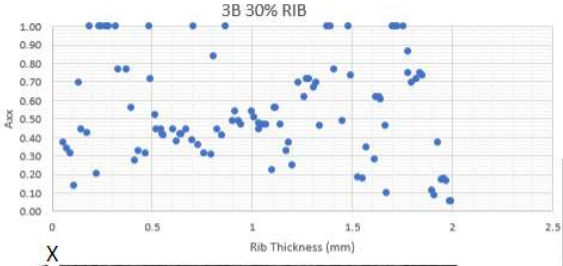

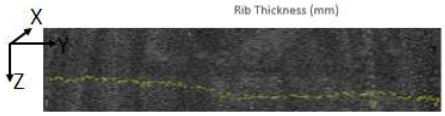

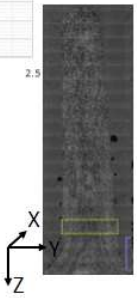

3B 60%

Regional A_{ij}		
A_{xx}	A_{YY}	A_{zz}
0.61	0.36	0.03

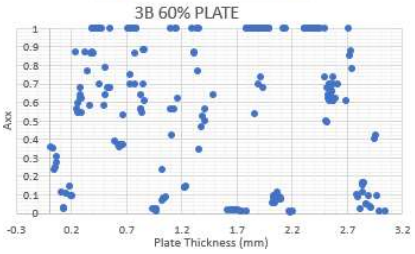

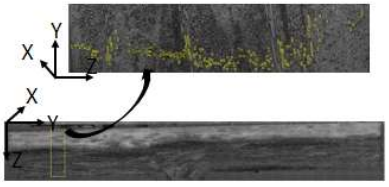

Regional A_{ij}		
A_{xx}	A_{YY}	A_{zz}
0.50	0.03	0.48

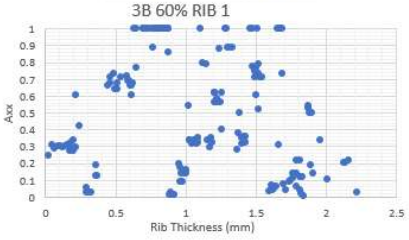

Regional A_{ij}		
A_{xx}	A_{YY}	A_{zz}
0.58	0.03	0.39

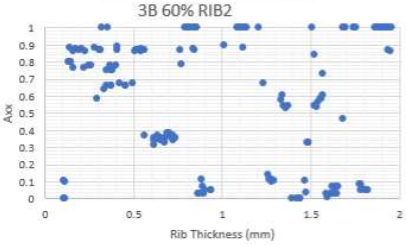

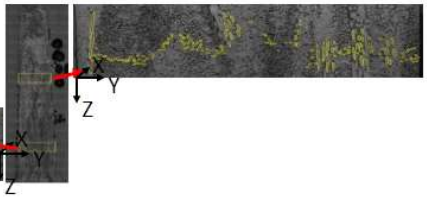

3B DIRF Section2

Regional A_{ij}		
A_{xx}	A_{yy}	A_{zz}
0.64	0.33	0.03

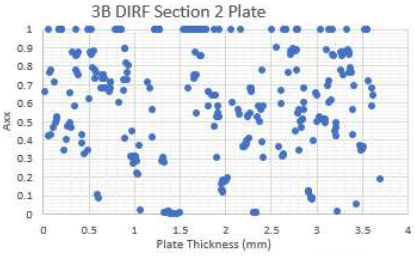

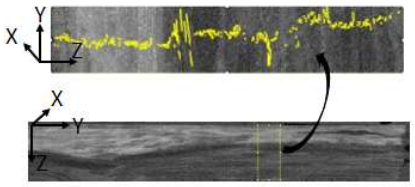

Regional A_{ij}		
A_{xx}	A_{yy}	A_{zz}
0.47	0.03	0.50

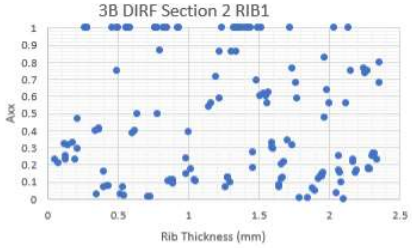

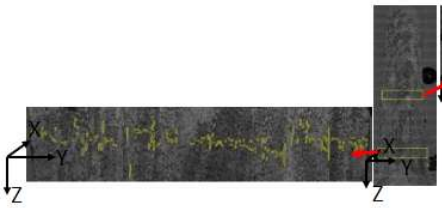

Regional A_{ij}		
A_{xx}	A_{yy}	A_{zz}
0.60	0.03	0.37

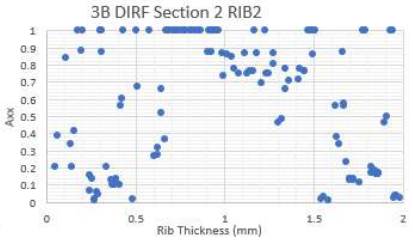

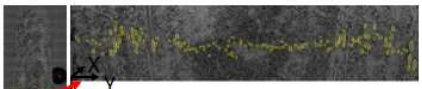

3B DIRF Section 3

Regional A_{ij}		
A_{xx}	A_{yy}	A_{zz}
0.40	0.57	0.03

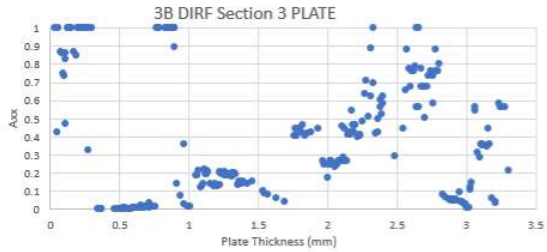

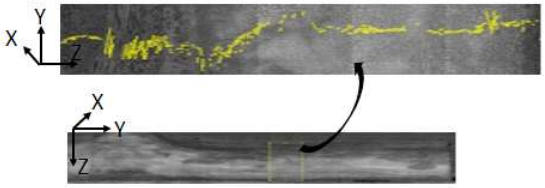

Regional A_{ij}		
A_{xx}	A_{yy}	A_{zz}
0.56	0.07	0.37